Fabrication of Transparent Nanocellulose Paper from Plant Sources for Energy Devices

by

Rajeswari Sen

A thesis
presented to the University Of Waterloo
in fulfilment of the
thesis requirement for the degree of
Master of Applied Science
in
Chemical Engineering

Waterloo, Ontario, Canada, 2023

© Rajeswari Sen 2023

Author’s Declaration

I hereby declare that I am the sole author of this thesis. This is the true copy of the thesis, including any required final revisions, as accepted by my examiners.

I understand that my thesis may be electronically available to the public.

Abstract

Over the past decades, electronic waste has accumulated and has increased by 21% in the last five years. Recently, a UN report found that the world dumped a gross record of 53.6 million tonnes of e-waste across last year. In the past, electronics had limitations due to their size constraint but with technological growth, electronics have now become a prominent part of the waste stream. Plastic substrates such as polyethylene (PET) and polycarbonate (PC) has been used pervasively in electronic devices. But due to their low co-efficient of thermal expansion (CTE), low recyclability and immense levels of pollution, a new state-of-art technology the cellulose nanopaper (CNP) has shown immense potential to replace plastic as a substrate in optoelectronics. Bio-derived decomposable electronics have exhibited great prospective to reduce the environmental footprint and avoid the surplus amounts of plastic based waste.

This project reports about a nanopaper fabricated from self-assembled network structure from nanoscale building blocks known as cellulose nanofibers (CNF). Nanofibers from two distinct sources were tested – (a) *Cannabis sativa* - Hemp (b) *Softwood* – Pine. Hemp CNFs provided by IND Hemp, United States in association with Tangho Green Inc., Canada was prepared via alkaline and acid hydrolysis along with high compression grinding and a cellulose purity of 97% was obtained. Pine CNFs were purchased from Forestry Department of University of Maine, USA had a >98% purity spectrum. A comprehensive study of CNP's structure-property relationship has been established under different processing conditions such as temperature of drying and CNF grammage, through characterization analyses. Two main nanopaper fabrication techniques of Solution Casting and Vacuum Filtration were studied in detail. Secondary objective comprised of optimizing optical properties of CNPs by adding polymers like Poly (vinyl alcohol) (PVA) and Polymethyl methacrylate (PMMA). Both PVA and PMMA showed considerable compatibility with CNF as a way of making them transparent.

The project was rounded off by incorporating Silver Nanowires (AgNWs) which was chosen as a conductive nano-filler due to its well-expressed aspect ratio. AgNWs showed high conductivity with increasing its loading density (mg/cm^2) or grammage. The films showed a resistivity as low as 9.45 ohm.µm with higher grammage of nanowire added. The results showed that nanocellulose changed their nature from insulator to conductor after addition of conductive materials. Moreover,

the highest conductivity around 1.05 kS/cm was obtained with maximum amounts of nanowire deposited.

This work solely presents a trend for the application of this conductive nanopaper in foldable or flexible electronics such as solar cells, OLEDS, electrodes or electronic skin for electrophysiological monitoring.

Acknowledgement

I sincerely express my gratitude towards my supervisor, Professor Leonardo Simon for choosing me as his graduate candidate and for his unwavering support and constant guidance during my thesis at the University of Waterloo. I am thankful of his assistance who stood by my side during challenging days, offering invaluable encouragement throughout my educational journey in this project.

I would like to thank Dr. Franciele Turbiani for encouraging me and guiding me through this journey of research. It would have been difficult without her advice and expertise and Douglas Casetta for supporting this project in collaboration with Tangho Green Inc. and Mitacs, Canada. I am immensely appreciative of Dr. Chong Meng whose generous advice significantly enriched the quality of my research.

I extend my appreciation for Prof. Boxin Zhao who have let me use their facility for material analysis and testing. I would also want to thank Prof. Ting Tsui for lending me his lab equipment. The completion of this thesis wouldn't be possible without the help of Charles Dal Castel and Nina Heinig who have helped me carry out multiple experiments in their labs. I would also thank our lab Research Assistant Sarah Jankhani for her time and assistance.

I am immensely thankful to Prof. Vivek Maheshwari and his student Saikiran Khamgaonkar for their generous support in facilitating access to equipment which played a pivotal role in the success of my project. I was fortunate to have such wonderful lab mates like Gulzeb Khan Khakwani and Yasaman Yasoubi who kept me motivated during my bad days.

Lastly, I would like to express my gratitude towards my partner Shoubhik Pandit for being an anchor of support who has kept me from falling during daunting days. I want to thank my mother Sunanda Sen and father Binayok Broto Sen for their sustenance from miles away without whose care I would not be here today.

Table of Contents

Author's Declaration ..... **ii**

Abstract ..... **iii**

Acknowledgement ..... **v**

List of Figures ..... **vii**

List of Tables ..... **x**

List of Abbreviations ..... **xvi**

Chapter 1: Introduction **1**

1.1 Overview and Background 1

1.2. Objective & Aim of the Project 4

1.3. Experimental Plan 5

1.4. Thesis Layout: **5**

Chapter 2: Literature Review **7**

2.1. Cellulose 7

2.2. Plant Cell 8

2.3. Structure of Cellulose 10

2.3. Types of Nanocellulose 11

2.4. Features of NFC/CNF 12

2.5. Sources of CNF 14

2.7. Applications of Nano-fibrillated cellulose (CNF): 27

2.8. Porosity and Concepts of Porosity through Percolation of Nanofibers during Nanopaper formation 46

2.9. Polymer Infusion to Enhance Optical Properties of CNP – Thin film composites. 49

2.10. Conductive Nano paper and Deposition of Silver Nanowire as a conductive filler on CNP 53

Chapter 3 Materials and Methods **59**

3.1. Materials 59

3.2. Methodology: 65

3.2.1. Methodology to Extract Nanocellulose Fibers (CNF) to produce Nanopaper: 65

3.2.2. Masuko Sangyo – Supermass Collider/ Refining of Cellulose to Nanoscale Slurry 69

3.3. Methodology to Fabricate Nanopaper -Solution Casting and Vacuum Filtration 70

3.4. Addition of Polymer to fabricate thin film composites. 71

3.5. Cellulose Nanofiber (CNF) Characterization Methodology 72
3.6. Cellulose Nanopaper Characterization 74
3.7. Polymer Combination to Produce Thin-Films 76
3.8. Electrical Characterization of Conductive Nanopaper 76
Chapter 4 Results and Discussion 79
4.1. Bast Fibers and Fiber Characterization 79
4.1.1. Mechanical Disintegration 79
4.1.2.Morphology 79
4.2. Chemical Pre-Treatment 81
4.2.1.Sodium Hydroxide Pre-Treatment 83
4.2.2. Acid Hydrolysis of One-Step Treated Fibers 83
4.2.3. 2nd Alkali Treatment 84
4.2.4.Oxidation and Bleaching H_2O_2 85
4.3. Process Flow Diagram of Extraction of CNF and Preparation of CNP 88
4.4. De-Fibrillation through Masuko Sangyo or "Super Mass Collider" – Grinding 89
4.5. Characterization of Fiber 91
4.5.1., 4.5.2., Transmission Electron Microscopy (TEM) 91
4.5.3. FTIR (Fourier Transform Infra-Red Characterization) 95
4.6. Fabrication of Cellulose-nano paper (CNP) through Solution Casting: 98
4.6.1. Solution Casted Cellulose Nano-paper (CNP) Characterization 104
4.6.2.Mechanical Properties of Solution Casted Nanopaper from Hemp (Bast) UW-CNF and Softwood UM-CNF 104
4.7. Fabrication of Cellulose-nano paper (CNP) through Vacuum Filtration: 107
4.7.1.Comparing Results of Different Flow of Filtration(mL/s) of Nanopaper Formation. 110
4.8. Nanopaper Characterization 119
4.8.1. Mechanical Properties 119
4.8.2. Surface Characterization Analyses 123
4.8.3. Surface Energy of UM, UW 100% CNF Films 123
4.8.4. Surface Morphology 126
4.9. Percolation of Fibrils and Porosity Effecting the Strength, and Characteristics of Nanopaper. 132
4.9.1. Calculating Porosity of Filtered UM Nanopapers Dried at Variable Temperature ... 132
4.10. Addition of Synthetic Polymers to Cellulose Nanofiber Films to Enhance Optical

Properties 134
4.10.1. Poly vinyl Alcohol (PVA) with UW, UM CNF Films – A Hydrophilic Alternative 134
Characteristic Analysis 136
4.10.1.1. Mechanical Properties 136
4.10.1.2. Optical Properties 138
4.10.1.3.Surface Morphology 142
4.10.2. Polymethyl methacrylate and CNF Films (UM, UW) – Hydrophobic Alternative 143
4.10.2.1. Optical Properties 145
4.10.2.2. Surface Morphology – Scanning Electron Microscopy 147
4.10.2.3. Surface Wettability and Contact Angle Measurements 149
4.11. Conductive Nanopaper for Flexible & Wearable Electronics Application 151
4.11.1. Integrating Silver Nanowire as Conductive filler and layer on Cellulose Nanopaper 151
4.11.2. Electrical Conductivity 155
4.11.3. Surface and Cross-Sectional Morphology: FE-SEM 159
Chapter 5 Conclusion 163
5.1. Summary and Contributions 163
5.2. Main Conclusion 164
5.3. Recommendations and Future Work 166
References 168
Appendix A – Letter of Copyright Permission 179
Appendix B- Material Specification Sheet 187

List of Figures

Chapter 1: Introduction 1
Figure 1.1. Showing a schematic of Nanocellulose based publications over a decade 2
Figure 1.2. Displaying different applications of Nanocellulose (NC) 3
Figure 1.3. Overview of strategies of using CNF as a film in electronics 5
Chapter 2: Literature Review 8
Figure 2.1. Depicting the Market growth of NC from years 2020 to 2024 8
Figure 2.2. Sources of Cellulose Material 9
Figure 2.3. Has outlined the variety of plant sources of NC 9
Figure 2.4. Illustration of hierarchical structure of plant-derived nanocellulose 10
Figure 2.5. A) Repeating cellulose unit, with 1-4 linkage and hydrogen bonding in dotted line, (B) cellulose microfibril with crystalline and amorphous regions, and (C) disordered cellulose nanocrystal regions dissolved after acid hydrolysis 11
Figure 2.6. Mechanism of chemical and mechanical methods for producing CNC and CNF 13
Figure 2.7. Bast and Hurd fibers of Hemp plant respectively 16
Figure 2.8. Displaying different compositions of Hemp Bast Fiber 17
Figure 2.9. Assumed formation of lamellar geometry and alignment of fine fibers during lyophilization 19
Figure 2.10. Quantification of the most used pretreatment used for CNF production 20
Figure 2.11. A two-stone grinder “Masuko Sangyo” 21
Figure 2.12. Mechanism of Acid Hydrolysis in Cellulose 25
Figure 2.13. Schematic of CNF Synthesis by TEMPO-mediated oxidation 26
Figure 2.14. A reaction mechanism where per hydroxyl ion oxidizes cellulose at C_2 and C_3 position 27
Figure 2.15. Schematic of cellulase impacting cellulose 28
Figure 2.16. Different Applications of Nanocellulose. 29
Figure 2.17. Schematic to show the different sectors of packaging industry. 31
Figure 2.18. Observing plastic trade over the world taken from Our World in Data,2020. 33
Figure 2.19. Various nanopapers showing their transparency 35
Figure 2.20. Casting Method 37
Figure 2.21. Preparation of Nanopaper (left) solvent casting (right) vacuum filtration. 37
Figure 2.22. Representation of hydrogen bonding between CNF and Glycerol during Heat Treatment 38

Figure 2.23. Basic Relationship between contact angle and surface energy taken from Ossila Equipments 40
Figure 2.24. The fibrils form a network 44
Figure 2.25. Nanopaper in contact with substrate underneath indicate its transparent properties.. 51
Figure 2.26. Linking of PVA and CNF at an elevated temperature 52
Figure 2.27. Showing polymerization of Methyl Methacrylate to Polymethyl methacrylate. 53
Figure 2.28. UV crosslinking of acrylic resin coated Nanopaper under UV irradiation. 54
Figure 2.29. Integrating nanopaper and nanocellulose in optoelectronics 55
Figure 2.30. Representing a method of filtration to deposit nanowire suspension on CNP. 56
Chapter 3 Materials and Methods 60
Figure 3.1. Typical sieve with 3.1mm opening 62
Figure 3.2. A bleed valve 64
Figure 3.3. Press provided with the Sheet Former machine. 65
Figure 3.4. Parallel Hot Press 66
Figure 3.5. Standard Thomas Scientific Wiley Mill Model 4. 67
Figure 3.6. Schematic flow diagram of Acid hydrolysis Fibers 68
Figure 3.7. Schematic Flow Diagram of Acid Treated Fibers after NaOH treatment. 69
Figure 3.8. Masuko Sangyo Super Mass collider MKCA6-5J ® used in lab 71
Figure 3.9. Schematic diagram showing the method of image configuration in bright-field imaging mode in TEM 74
Figure 3.10. Dog-bone shaped films were moulded in compliance to ASTM D882-12 75
Chapter 4 Results and Discussion 79
Figure 4.1: Working Mechanism of Thomas Wiley Mill 79
Figure 4.2. Bast fibers after dis-integration under optical microscope 81
Figure 4.3. Histogram of Aspect ratio (L/D) after mechanical breakdown in the Mill 81
Figure 4.4. Reaction of NaOH on cellulose compounds 82
Figure 4.5. FTIR plots 83
Figure 4.6. Molecular representation of hydronium attack on cellulose 83
Figure 4.7. FTIR plots 84
Figure 4.8. a.) Alkali-acid-alkali treated, b.) 3 Step Treated and Bleached, c.) Bleached Pulp rinsed through sieve, d.) UP-100% Bast, e.) 3-Step treated, f.) Bleached 84
Figure 4.9. All chemically treated pulp showcasing the loss of colour and fiber size 87

Figure 4.10. PFD for Extracting, refining nanocellulose and fabricating UW (Bast) nanopaper through 2 broad methodologies. 87
Figure 4.11. A Typical Masuko Grinder..... 88
Figure 4.12.: (left) After masuko 2 % (w/w) (right) after masuko 3.1%(w/w)..... 88
Figure 4.13. Images of fibrillated cellulose fibers 89
Figure 4.14. TEM graph (a) 12^{th} Pass in Masuko (b)15^{th} Pass in Masuko 89
Figure 4.15. Defining higher surface area of nanofibers due to flattening 90
Figure 4.16. Histograms depict the Frequency of Repeating Fibers in 12^{th} Pass. 90
Figure 4.17. Histograms depict the Frequency of Repeating Fibers in 15^{th} Pass. 91
Figure 4.18. TEM micrograph of dispersed UM fibers 92
Figure 4.19. UW CNF through FTIR Analysis. 93
Figure 4.20. UM CNF through FTIR Analysis. 93
Figure 4.21 Solution casted CNF slurry, Glass Fiber reinforced Teflon sheets 94
Figure 4.22. Visual representation of agglomerates that form during un-even humidity drying of nanopaper via Solution Casting 95
Figure 4.23. Casted CNPs under different conditions. 97
Figure 4.24. Tensile Modulus (MPa) of Solution Casted UW and UM CNF respectively 98
Figure 4.25. Tensile Strength (MPa) of Solution Casted UW and UM CNF respectively 99
Figure 4.26. Exhibits the filtration and pressing of nanopapers. 101
Figure 4.28. Representation of Nanopaper manufacturing from Freeze-dried UM CNF..... 105
Figure 4.29. Shows UM Nanopapers at varied drying temperature..... 105
Figures 4.30. Show increase in opacity and light scattering from (left) Pressed at 25 ^{o}C , 50 ^{o}C (middle) and 110 ^{o}C (right)..... 106
Figure 4.31. Bar charts, show the Effect of Drying Nanopaper with Varying Temperature on Young's modulus (MPa)..... 106
Figure 4.32. Bar charts, show the Effect of Drying Nanopaper with Varying Temperature on Tensile Strength (MPa)..... 113
Figure 4.33. Logarithmic relationship of Tensile Modulus and Strength as a function of Temperature 115
Figure 4.34. Characteristic Water drop after 12 seconds of immersion on UM (left) and UW (right), respectively. 118
Figure 4.35. Dynamic contact angle of 25^{o}C dried nanopapers from (top) Grammage 3.7g/cm^2 (below) Grammage 5.8mg/cm^2 119
Figure 4.36. UM Nanopaper dried at 25°C prepared through Filtration..... 120

Figure 4.37. SEM micrographs of UM CNP fabricated at (a)25 °C, (b) 50 °C and (c) 110 °C. .. 122

Figure 4.38. Shows CNPs dried at 25° C (a) Filtered Nanopaper 0.1g CNF (by weight) both from UM CNF (b) Solution Casted 0.3g CNF (by weight) 124

Figure 4.39. SEM micrographs of the fracture surface of the cellulose nanopapers dried at 25°C (top left), 50°C (top right) and 110°C (below) 125

Figure 4.40. UW filtered nanopaper dried at 25°C (A), and UW filtered nanopaper dried at 110°C (B), Cross-Sectional view of Casted UW nanopaper (C), 110°C dried Filtered UW nanopaper (D). 126

Figure 4.41. Fiber fraction as a function of Modulus of Nanopapers dried at different temperatures, Increasing strength at lower porosities with variation in drying temperature 127

Figure 4.42. Graphical Representation of Decreasing Porosities with Increasing Temperature 128

Figure 4.43. Illustration showing Hydrogen bonding between PVA + CNF, arrows show 'H' bonding. 129

Figure 4.44. Different Proportions of PVA and CNF were casted (A) 100% PVA, (B) 50%PVA/50%CNF (C),10%PVA/90%CNF (D) 5% PVA/ 95% CNF all samples were made from UW CNF 131

Figure 4.45. Tensile Modulus of Solution Casted Films with decreasing concentration of UW CNF 134

Figure 4.46. Strength of Solution Casted Films with decreasing concentration of UW CNF 135

Figure 4.47. Transmittance of 100% PVA Film 136

Figure 4.48. Transmittance of Casted films from UW CNF 137

Figure 4.49. Tr. Values of filtered nanocellulose films from UW slurry 138

Figure 4.50. Shows graphical representation of PVA and UW CNF thin films 139

Figure 4.51. SEM graph for (left) 5PVA/95CNF, (right) 10PVA/90CNF, ... 140

Figure 4.52. SEM graph for 50PVA/50CNF 141

Figure 4.53. Exhibiting the coating of nanopaper with AR using a frosted microscopic glass slide 144

Figure 4.54. (a) Comparing UM 25°C dried CNP, coated and un-coated (b) UW 25°C dried AR coated CNP (c) UM 25°C coated AR with optimum grammage (d) & (e) depict difference in visibility of the coated and uncoated CNPs. 144

Figure 4.55. Depicts the comparison between AR coated and neat CNF Films from UW and UM respectively. 145

Figure 4.56.UM CNP coated with AR at 5000x and (right) 1000x (left) 147

Figure 4.57. SEM image of fractured cross-sectional area of AR coated CNP, coated with (left) Dr. Blade (right) Microscopic glass slide. 148

Figure 4.58. WCA imagery of PMMA coated UM CNP (left) and PMMA coated UW CNP (right) 149

Figure 4.59. Show contact angle physical characteristics after 30 secs on substrates UW (top) and UM (bottom) 150

Figure 4.60. Distribution of Nanowire embedded on CNF Matrix..... 151

Figure 4.61. Demonstrating the deposition of Silver through Filtration (top), with PET Mask (bottom) without PET Mask. 152

Figure 4.62. Conductive nanopapers with differing nanowire grammage (mg/cm^2)..... 153

Figure 4.63. Putative process of formation of AgNW networks on nanopaper..... 154

Figure 4.64. Graph of conductivity (S/cm) according to AgNW grammage (mg/cm^2)..... 156

Figure 4.65. Demonstrating measurement of resistance via 2 Probe along the diameter of the nanopaper. 157

Figure 4.66. Demonstrating a typical 4 Probe Resistivity Measurement set-up adapted from Ossila Equipment. 158

Figure 4.67. Graph of increasing conductance by increasing volume of AgNWs..... 158

Figure 4.68. Top-view SEM micrographs of AgNW mixed nanopaper substrates 160

Figure 4.69. Network of AgNW rods well connected with each other (left) and the same network on nanopaper as a layered assembly (right). 161

Figure 4.70. SEM image of AgNW films on nanopaper as bi-layered arrangement with grammage(mg/cm^2) (a) 32mg/cm^2, (b) 64mg/cm^2 & (c) 400mg/cm^2, respectively. Percolated nanowires are expressed in red dotted line 162

Figure 4.71. Cross-sectional SEM of bi-layered structure with AgNW and CNF with increasing volume of nanowire solution from (a) 32mg/cm2, (b) 64mg/cm2 & (c) 400mg/cm2. 163

Chapter 5 Conclusion..... 164

Figure 5.1. Comparing nanopapers made from UM CNF (left) Casting (right) Filtration 167

List of Tables

Chapter 1: Introduction 1
Table 1 Comparison of Nanopaper, traditional paper and plastics 2
Chapter 2: Literature Review 8
Table 2 Parameters used to refine cellulose to produce CNF through mechanical equipment 20
Table 3 Different Processing conditions used for Producing CNF 23
Table 4 A discussion table with their product and permeability, shell life and materials used has been given for comparison 31
Chapter 3 Materials and Methods 60
Chapter 4 Results and Discussion 79
Table 5 Lengths of fibers after Milling and their respective aspect ratio 80
Table 6 Steps of Chemical Treatment and Oxidation with their Respective Appearance 85
Table 7 Reaction time, temperature, and their corresponding appearance for Bleaching 86
Table 8 Different Processing Conditions used to obtain CNF – Gap according to no. of passes through the masuko of 5 wt.% treated pulp. 90
Table 9 Some expected FTIR Peaks associated with Nanocellulose Extraction and Freeze-dried CNF 96
Table 10 Different Modes of Drying undertaken to find the optimum condition for Drying 100
Table 11 below shows the aspect, visuals, and thickness of nano-paper fabricated from a dilute slurry of UW CNF 103
Table 12 Mechanical Properties for Solution Casted Nano-papers from UM & UW CNF 107
Table 13 Sources and Physical Phase of CNF from UM, UW, respectively 108
Table 14 shows Nanopapers from CNF UW and UM of different Grammage (mg/cm^2) 109
Table 15. 6cm Diameter PVDF membrane filtering 0.1wt% UM CNF soln., 100mL. 111
Table 16. 4cm Diametric PVDF Membrane filtering 0.1wt% UW CNF soln., 100mL. 111
Table 17 Showing Nanopapers (CNP) Properties from UMaine CNF Pressed at Different Temperatures 114
Table 18 Demonstrates Properties of Nanopapers from UW Pressed at Different Temperatures. 117
Table 19 Tensile Modulus and Strength of UM, UW CNPs Dried at Different Temperatures 121
Table 20 Tensile Properties and their Statistical Analysis to compare Significant Changes in their Mean. 121
Table 21 Surface Tension of dispersed and polar components of Two Liquids Used 123

Table 22 Surface Tension and Thickness Data for Uncoated Room Dried Nanopapers from UM, UW 124

Table 23 Dynamic Contact Angle, UM and UW Room Dried Nanopapers 126

Table 24 Pore Diameters with respect to Drying Temperature of UM CNPs 128

Table 25 below outlines average distance between adjacent layers of CNPs produced at different temperature ranges and their packing density (g/cm^3). 130

Table 26 Pore Diameters with respect to Drying Temperature of UM CNPs 130

Table 27 Thickness Effecting Packing Density of Nanopapers 132

Table 28 Porosity and Mechanical Properties According to their Respective Drying Temperatures 132

Table 29 Outlines the thin film composites with different proportions of PVA and CNF 133

Table 30 Tensile Modulus (E) and Strength (σ) 136

Table 31 Light Transmittance (%) of different films with combination of PVA and UW CNF 137

Table 32 Light Transmittance (%) of filtered UW CNPs dried at increasing temperature (°C) 142

Table 33 Different Modes of Coating and Thickness of AR coated CNPs (UW, UM) 143

Table 34 Layers, Thickness and Grammage of Nanowire and CNF (UW) film composites fabricated 146

Table 35: 2 Probe Measurement show Varying values of resistivity (ρ) and conductivity (S/cm) 155

Table 36- 4 Probe Measurement show Varying values of resistivity (ρ) and conductivity (S/cm) 156

List of Abbreviations

%	Percentage
CNF/NFC	Cellulose nanofiber / Nano-fibrillated cellulose
BC	Bacterial Cellulose
CNC	Cellulose nano crystals
NC	Nanocellulose
MCC	Micro-crystalline cellulose
UM	University of Maine, USA
UW	University of Waterloo, Canada
wt.%	Weight Percentage
nm	Nanometers
µm	Micrometers
PMMA	Poly methyl methacrylate
PVA	Poly Vinyl Alcohol
AR	Acrylic Resin
CNP	Cellulose nanopaper
WCA	Water contact angle
$\rho_{cellulose}$	Density of cellulose (g/cm^3)
rpm	Rotations per minute
ASTM	American Society for Testing and Materials
N_2	Nitrogen
WVTR	Water Vapour Transmittance Rate
SEM	Scanning Electron Microscopy
TEM	Transmission Electron Microscopy

Chapter 1: Introduction

This chapter explores the research topic and encompasses the motivation and objective behind undertaking this project.

1.1 Overview and Background

With immense development of technology and especially nanotechnology on electronic devices such as mobile phones, smart electronics including health monitors Li (2020) and artificial electronic skin, the demand for sustainable and stable alternatives have sky rocketed.

Researchers have associated increase of greenhouse gases due to radical climate changes and incineration of humongous amounts of plastic and electronic waste Plotnikoff (2004). The emergence of green electronics that naturally degrade in various physiochemical environment, different nature based resources have been explored through economically efficient routes Irimia-Vladu (2012). A new source of bio-derived material such as cellulose has received a lot of traction due to its non-toxicity, biodegradability, and immaculate properties. Paper made from cellulosic materials are flexible, lightweight, and economical. Regular paper have often a higher diametric fiber around 20-50 μm plus their coarseness and roughness make them difficult to be integrated into electronics Dinesh and Kandasubramanian, (2022). Hence paper products have been re-invented to meet requirements for lightweight, economical, and flexible substrate for optoelectronics.

Cellulose is one such bio-based material derived from both plant and non-plant sources. Cellulose was first discovered around 1800s by scientist Anselme Payen in a laboratory. Due to its non-toxicity, biodegradability, modifiable characteristics make it highly beneficial. Regular paper has been obtained from cellulosic material for decades from fibers ranging between 20 to 30 μm. Cellulose has been used to produce paper for years, where the fibers are isolated during pulp forming processes followed by a paper-making process. But they often lack favourability due to their roughness, porosity, and opacity. Table 1.1. draws a comparison among Regular paper, nanopaper and plastic.

Table 1 Comparison of Nanopaper, traditional paper and plastics (Dinesh and Kandasubramanian, 2022)

Characteristics	Nanopaper	Traditional Paper	Plastics
Surface Roughness (nm)	5	5000-10000	55
Optical Transparency at 550nm (%)	90	20	90
Max loading Stress (MPa)	200-400	6	50
Young's Modulus (GPa)	7.4-1.4	0.5	2.7

A more bottom-up approach has been undertaken to produce a new kind of material which is known as nanocellulose. Nanocellulose has received significant attraction due to their high mechanical and tunable optical properties. As displayed in figure 1.1. there has been a growing trend of citing nanocellulose based papers in the last one decade. Cellulose fibers are disintegrated through mechanical as well as chemical treatments to attain fiber diameters ranging between several to several tens of nanometers. Nanocellulose fibrils could be similarly used as building blocks for paper as it is feasible due to the presence of numerous hydroxyl groups as well as high surface area and aspect ratio. This type of paper is named as nanopaper due to their smaller diametric fibers. Using traditional paper making processes, nanopaper can be formed in similar manner through inter and intra hydrogen bonding. The cellulose fibers consist of a bunch of microfibrils (5 nm to 50nm in diameter). These microfibrils themselves are made of self-assembled elementary fibers.

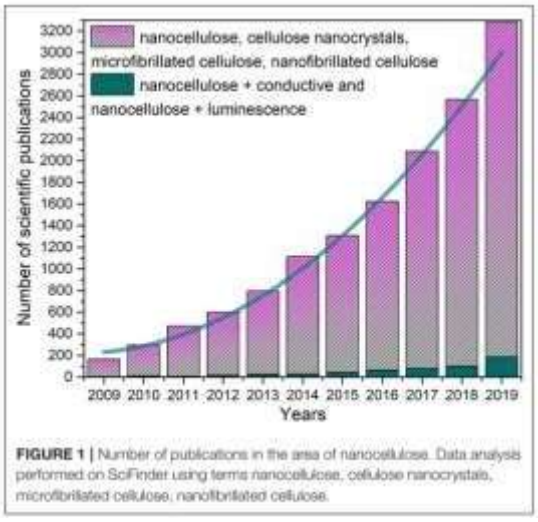


Figure 1.1. Showing a schematic of Nanocellulose based publications over a decade(Dias et al., 2020).

Cellulose nanopapers have shown great strength, flexibility mostly governed by pulping and extraction mechanisms and sources of cellulose. The maximum strength reported was 200MPa and Young's moduli over 10GPa (Kafy, 2017a). Besides mechanical properties and transmittance, nanopapers also exhibit good oxygen barrier properties (Aulin, 2010) and low thermal expansion. The idea of fabricating a nanopaper with good strength and considerable transparency would make it viable to replace plastic based or petroleum derived substrates in optoelectronics.

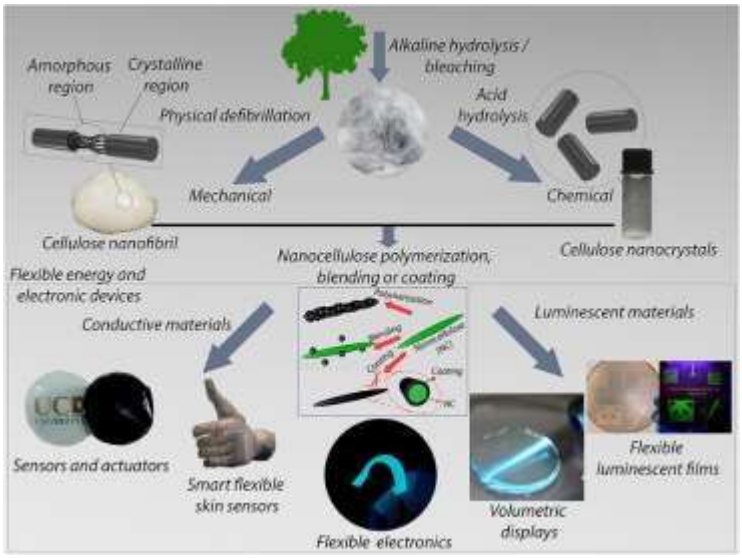


Figure 1.2. Displaying different applications of Nanocellulose (NC), by Otavio 2020

According to treatment procedures and defibrillation, nanocellulose can be classified in broad groups – Cellulose Nanofibers (CNF), Cellulose nano crystals (CNC) Bacterial Nanocellulose (BC).

Nanocellulose's tunable surface chemistry allows surface modification by physio-chemical interactions or through covalently bonded molecules being introduced during chemical modifications (Nechyporchuk,2016). Chemical treatments such as TEMPO (2,2,6,6-tetramethylpiperidine-N-oxyl) and Sulfonation, help introduce different functional groups on the surface of nanocellulose depending on its end application. However, nanocellulose fibrils still face some adversities and large-scale production because of its limiting parameters such as hydrophilicity and meso-porous nature which leads to degradation and light scattering respectively. The purpose of this thesis was to obtain nanopaper of thinnest width and highest structural properties by regulating their processing parameters, such as temperature, grammage

and nanopaper formation mechanism for applications in energy devices and smart flexible devices, see figure 1.2.

1.2. Objective & Aim of the Project

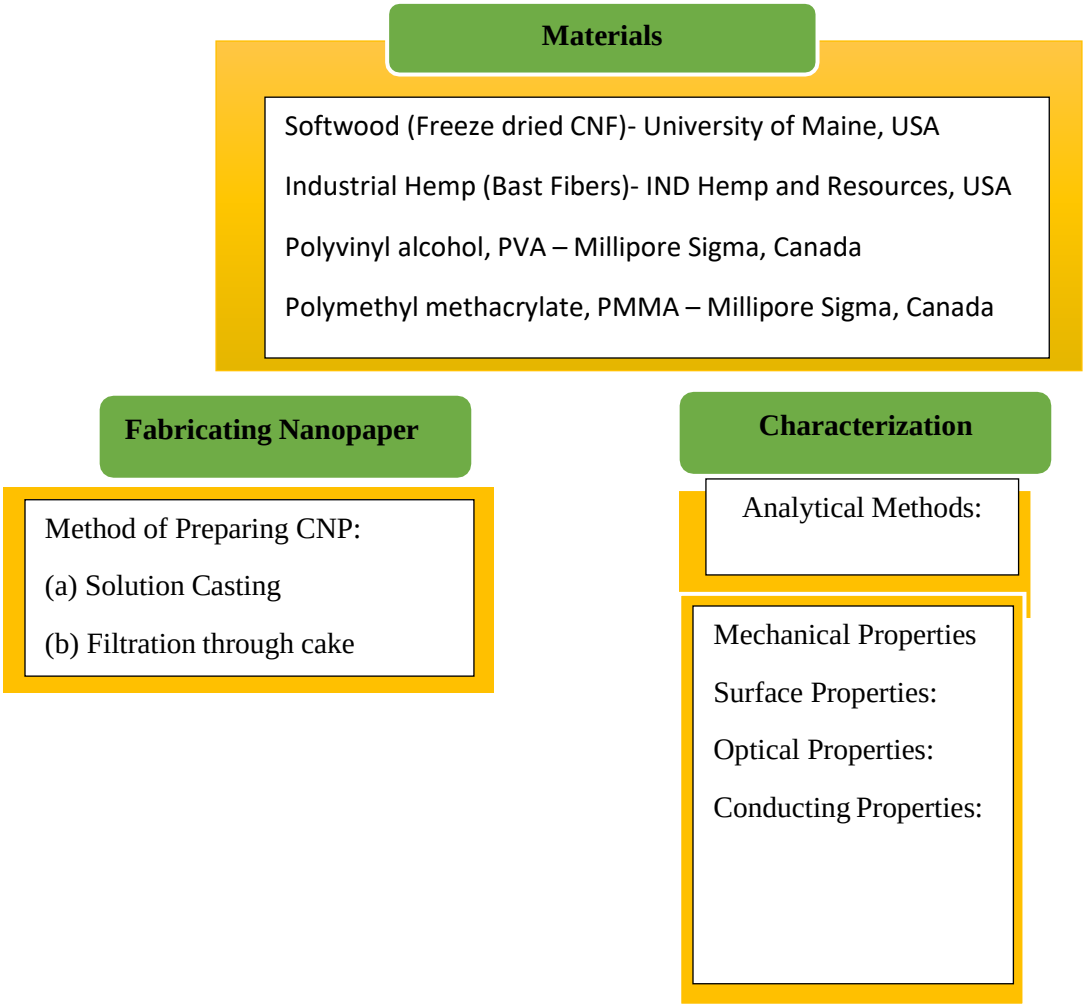
This thesis project focuses on three main hypotheses (a) Extraction of nanocellulose from – *Hemp* (b) Fabricating nanopaper through two broad techniques (Casting and Filtration) from Hemp CNF and Softwood CNF from University of Maine, c) Enhancing optical properties and conductivity by incorporating additives.

The work thus shown, proposes a thorough understanding of structural and transmitting properties of nanopapers derived from two different CNF sources. Systematic experimental approach was undertaken. The research aims are listed below:

1) To understand the composition of nanofibers with series of chemical treatments and to elucidate the properties controlling nano fibrillation and pulping of the fibers.
    - Optimise different levels of chemical treatment by regulating their concentrations and reaction parameters.
    - Pursue in-depth evaluation of fiber diameters through microscopy.
    - Collect morphological information of fibrillar size according to different stages and cycles of fibrillation.
2) To investigate two main methods of nanopaper making – Casting and Filtration.
    - Apply different techniques to fabricate nanopaper by controlling drying methodologies.
    - Notice and report data of analyses to determine good mechanical and surface properties.
3) To enhance the optical properties of nanopaper by adding compatible polymers either as an additive filler or a coating.
4) To produce conductive nanopaper with incorporation of Silver Nanowires in order produce a flexible conducting substrate.
    - Incorporate AgNW solution at varying loading density to understand conductivity as a function of density.

1.3. Experimental Plan

The schematic figure defines the experimental plan proposed and commenced in this research project.



1.4. Thesis Layout:



Chapter 2: Literature Review

2.1. Cellulose

The need to switch to environmentally friendly biodegradable products from fossil-oil based ones is urgent right now.

Worldwide the usage of green, renewable as well as sustainable substances with lowest environmental impacts have drawn attention. With increasing amounts of plastic waste every year, scientists have developed bio-derived naturally occurring products like cellulose, starch, chitin. Among which, cellulose has been by far the most promising candidate due to its abundant availability.

According to market research nanocellulose market is expected to reach a turnover of around USD 783 million by the year 2025 according to official ‘businesswire’ website.

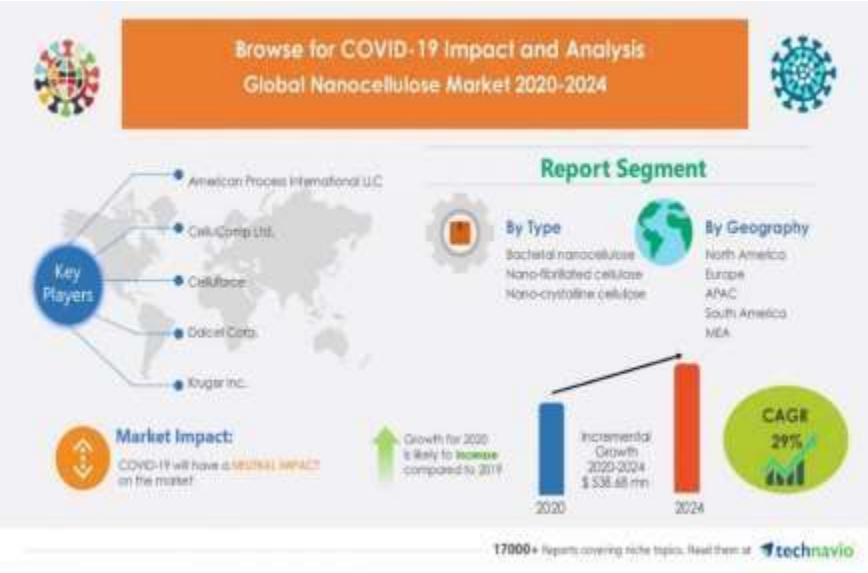


Figure 2.1. Depicting the Market growth of NC from years 2020 to 2024. (Businesswire open)

Yearly production of NC is estimated to be between 1010 to 1011 tons, even though a very small proportion of which is utilised in several industries such as textile, chemical, paper and pulp and material industries. Various raw sources like wood, plants, grass, as well as animal sources like tunicates, bacterial sources are major raw goods to produce nanocellulose displayed in figure 2.2. presented by (Dinesh and Kandasubramanian, 2022).

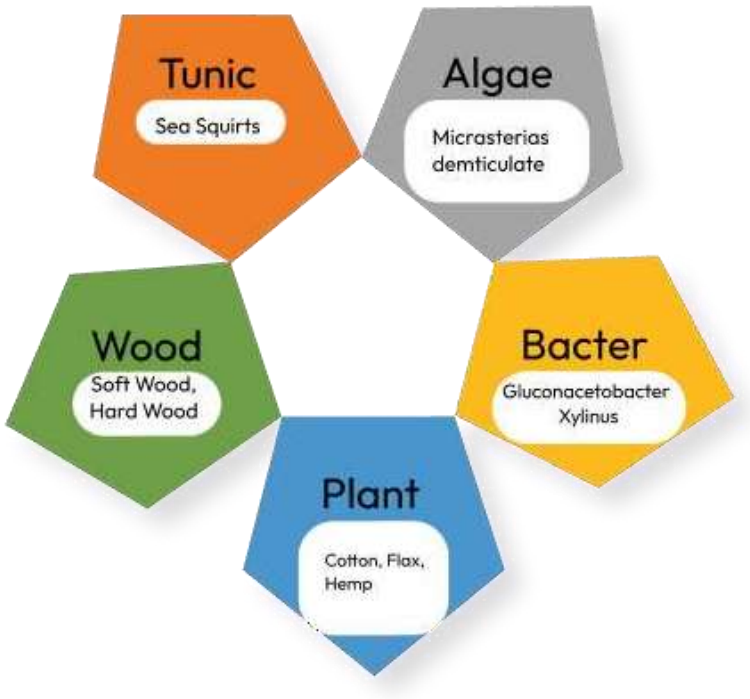


Figure 2.2. Sources of Cellulose Material.

2.2. Plant Cell

Due to its unique qualities (Trache, 2020) (surface chemistry), such as abundance, high aspect ratio, improved mechanical properties, renewability, and biocompatibility, cellulosic materials have attracted increasing interest.

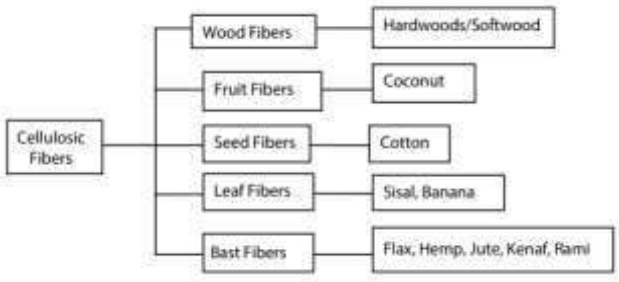


Figure 2.3. Variety of plant sources of NC.

The main component of a cell wall is cellulose Nasir (2017), which can be obtained from a range of sources including wood, bast fibre, grasses, and seed fibres etc., outlined in figure 2.3. The plant cell also includes lignin, hemicellulose, and trace levels of extractives. Even though wood species remain the primary source of cellulose, non-wood plants are gaining popularity due to their low

cost and low lignin concentration. This has been used for years to manufacture materials for a variety of commodities in the food, pharmaceutical, and paint industries.

The structure of plant cell walls is intricate and made up of various interlocking polysaccharides Nechyporchuk et al., (2016). There are several layers that make up the cell wall, as shown in figure 2.4: the primary wall (P), the middle lamella (ML), the outer (S1), middle (S2), and inner (S3) layers of the secondary wall, and the warty layer (W). The middle lamella is responsible for connecting adjacent cells and contains high levels of lignin. The primary and secondary walls are composed of three primary constituents: cellulose, hemicellulose, and a matrix, which is typically made up of pectin in the primary wall and lignin in the secondary wall. The thickness of the secondary cell wall, which contains most of the cellulose, ranges from 100 nm (in cotton) to 300 nm (in spruce wood).

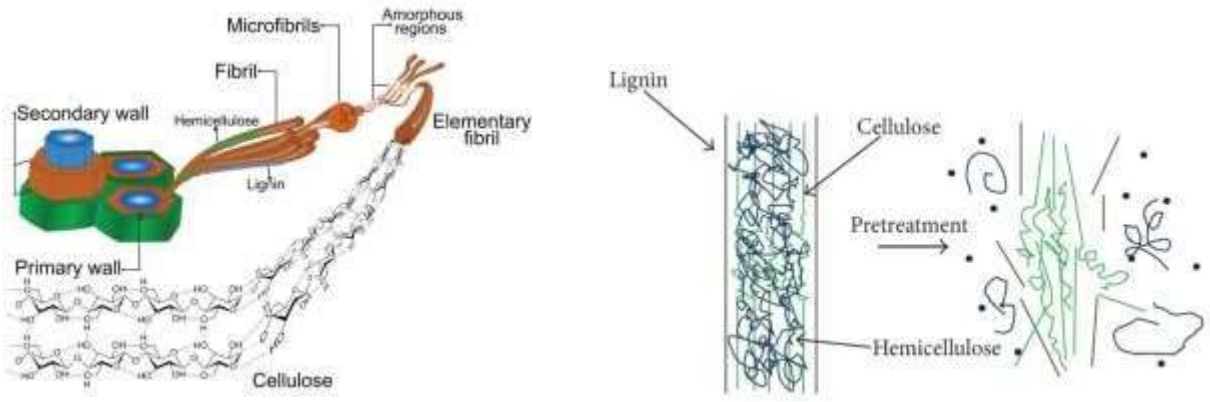


Figure 2.4. Graphical illustration of hierarchical structure of plant-derived nanocellulose (Wajid et. al., 2021) & (Naik et. al., 2020).

The abundant hydroxyl groups (-OH) allow a wide range of functionalization via chemical reactions, leading to the growth of various tunable features. Cellulose could be made more useful if the cellulosic chains are wrapped together giving rise to highly ordered structures, which can be subsequently isolated as nanomaterials known as cellulose nanomaterial or nanocellulose. This is classified as a group of bio friendly futuristic materials.

Typically, nanocellulose can be divided into two major classes, (1) micro structured materials (cellulose microcrystals and cellulose microfibrils) (2) nanoscale materials (Cellulose nanocrystals and cellulose nanofibers. The extraction procedure, chemical pre- and post-treatments define the

characteristics of cellulose, surface morphology, crystallinity, and class Trache, (2017). The broad classification of cellulose has been standardised by the TAPPI WI 3021.

2.3. Structure of Cellulose

Micro cellulose is a semi-crystalline poly-carbohydrate and consists of anhydrous glucose units (AGUs) linked by the b-1,4 glycosidic chemical bond (Mohammed, 2021).

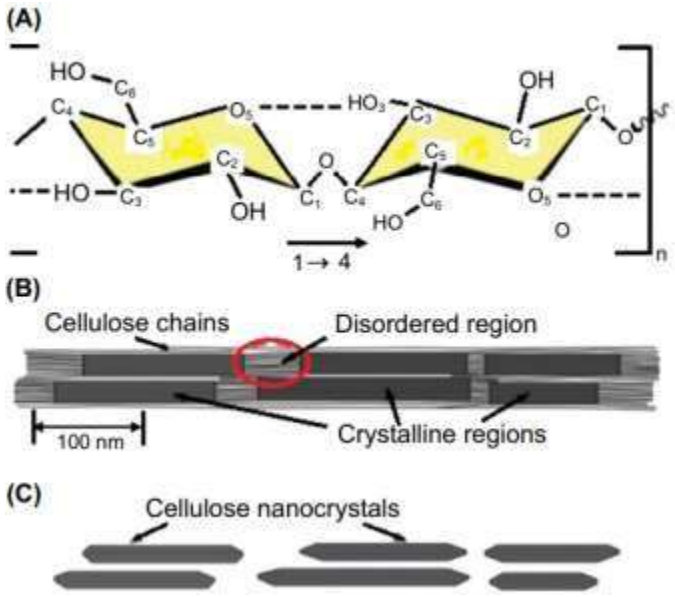


Figure 2.5. A) Repeating cellulose unit, with 1-4 linkage and hydrogen bonding in dotted line, (B) cellulose microfibril with crystalline and amorphous regions, and (C) disordered cellulose nanocrystal regions dissolved after acid hydrolysis, adapted from Nevin 2015 (opensource).

Figure 2.5. shows the conformation of two repeating AGU units via carbon atom numbering system. With the hydroxyls group at the equatorial position, each AGU unit forms internal hydrogen bonding between the oxygen atom in the ring of the adjacent AGU unit and the hydrogen atom of the C-3 hydroxyl group. A strong system of crystallite intermolecular and intramolecular hydrogen bonding renders them highly rigid, ordered, lower accessibility toward water and certain chemical reagents, which strengthens and stabilizes the cellulose. On the other hand, in the amorphous domains, very weak hydrogen bonding increases the hydrophilicity and water accessibility of the cellulose materials.

2.3.1. Lignified and Non-Lignified Nanocellulose

Non-lignified nanocellulose contains lignin and aromatic compounds and carbohydrate polymers and cellulosic materials. Cellulose is hydrophilic and is used in excellent water absorbing

applications such as in tissue and hygiene products applications. Whereas lignin is reasonably hydrophobic and cannot absorb water. Researchers found out that a lignin removed hull absorbs around 53% more water than non treated hulls. (Liu, 2017).

To build a nanopaper, getting rid of colour imparting chromophores are important. One of the main reasons of the pulping process is to split up the cellulose fibers from the lignin and other non-cellulosic resources such as hemicelluloses. Presence of lignin in paper pulp reduces paper permanence and contributes to the yellowing of paper over time. Oliaei (2020) was successful in fabricating nanopapers with three different kinds of MFC having separate colours. CNPs with less amounts of lignin demonstrated higher values of tensile strength and modulus whereas films with higher percentage of lignin showed lower mechanical properties along with lower density.

2.3. Types of Nanocellulose

NFC are cellulosic fibers that have been obtained from high fibrillation or shear forces with a range of pretreatments; NFCs have diameters ranging less than 100nm to a few hundreds and their length being a few micrometers. There are several denominations displayed for these fibers such as Nano fibrillated cellulose/Cellulose nano fibers (NFC/CNF). The Technical Association of the Pulp and Paper industry (TAPPI) have established NFC to be the widely accepted term defining nano ranged cellulose fibers. NCC or nanocellulose crystals, which is extracted from cellulose fibrils with strong acid hydrolysis and Bacterial Nano-cellulose (BNC) is widely produced from bacteria and enzymatic treatments.

2.3.1. Structure of Nanocellulose

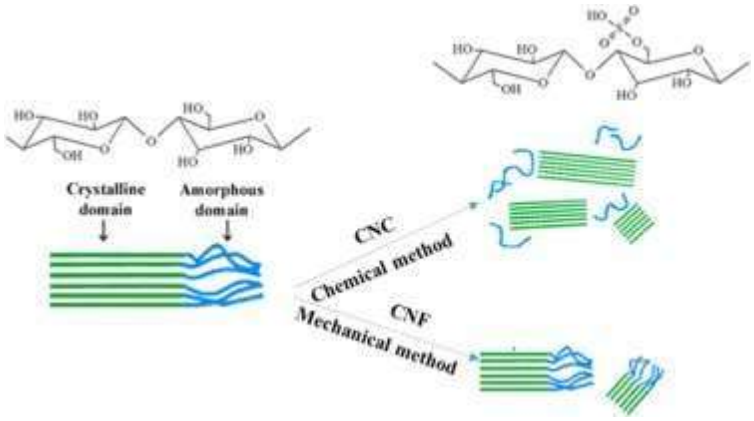


Figure 2.6. Mechanism of chemical and mechanical methods for producing CNC and CNF by Maryam et al., 2016.

Nanocellulose from plant cells can be extracted from different sources. Cellulose hydrolysis could help in extraction of nanocrystals, crystalline nanoparticles, and nano whiskers, as depicted in figure 2.6. The isolated CNP from different feedstocks is usually rod-shaped particles. Cellulose with one of its dimensions ranging between (1-100) nm is considered to be nano.

Depending on production process, which highly influence the physical, composition and properties, nanocellulose can be divided into two main categories: (i) CNC (ii) CNF (Mohammed, 2021). Nanocrystalline cellulose a.k.a cellulose nanocrystals, are nanocellulose of high strength. Their appearance is short rod like, or whisker shaped with 2-20nm in diameter and around 100-500 nm in length. These crystals mainly consist of NC with high crystallinity index (%) that is around 54-88%.

Bacterial nanocellulose (BNC) is manufactured via a bottom-up process unlike both CNF and CNCs (top-down approach). BNC can be extracted from different species of bacteria such as *Acetobacter, Azotobacter, Pseudomonas,* and *Sarcina ventriculi.*

CNF as nanosized was first introduced by Turbak (2015) and Herrick (1983), who manufactured cellulose with lateral dimension in nanometer range by passing softwood through a high-pressure homogenizer. During this process, intensely entangled arrangements of nanofibrils having both crystalline and amorphous domains were produced due to high shear forces. They acquire high aspect ratio and form gels in water with shear-thinning and thixotropic behavior. Cellulose fibers can be transformed into flexible cellulose nanofibers (CNF) with varying lateral dimensions, depending on the processing conditions. These dimensions range from approximately 5 nm, representing elementary fibrils, to several tens of nanometers, which correspond to single microfibrils and their bundles.

2.4. Features of NFC/CNF

NFC has widely gained its popularity due to some outstanding features like their high specific surface area, aspect ratio, tunable surface properties.

2.4.1. Specific Surface Area

The specific surface area of nanocellulose fibers refers to the total surface area (m^2/cm^2) per unit mass (g/mg) of the nanocellulosic material. The small diameter of the fibers lead to a greater extent of the surface area that is exposed. Some techniques such as the Brunauer-Emmett-Teller (BET)

method, which involves measuring the amount of gas molecules adsorbed on the fiber surface, can provide us with an overview of the available surface area (Sehaqui, 2011). The high surface area of NFC facilitates higher contact with surrounding materials, enhancing reactivity in chemical interactions. It also plays a significant role in increasing strength of composites by interfacial bonding between fibers and additional polymers, if added. Specific Surface Area of NFC has been reported to be as high as 153–284 $m^2 g^{-1}$.

2.4.2. Aspect Ratio

The aspect ratio of NFC is an important factor to determine its characteristic features. The ratio of length of a fiber to its diameter is the effective aspect ratio. Aspect ratio significantly increases interfibrillar bonding during nanocellulose composite formation imparting tensile strength to it. This is because, longer fibers provide more reinforcement, improving overall performance. Various analytical techniques can be used to determine aspect ratio of fibers among which Scanning Transmission Electron Microscopy (TEM) and Scanning Probe Microscopy (SPM/AFM) are most popular.

2.4.3. Abundance of Hydroxyl Groups

Cellulose has a backbone structure comprising of glucose units repeating itself over a chain of length. The hydrophilicity of cellulose arises from the abundance of hydroxyl groups (-OH) on its surface. Hydrogen bonding is a strong intermolecular bond between the positive hydrogen atoms (+H) and negative oxygen atoms (O^-) of another molecule. This hydrophilic or “water loving” cellulose enables it to readily interact with water and other polar solvents. Cellulose when fibrillated under high shear (T), has hydroxyl groups expressed on its surface. Each glucose unit in cellulose has three hydroxyl groups: two on the C_2 and C_3 carbons and one on the C_6 carbon. (Moon, 2011).

2.4.4. Particle Morphology and Size of NFC

CNF recognised as cellulose nanofibril, is the entangled long and flexible nanocellulose that can be produced from cellulose fibers through mechanical disintegration. Both shear and impact forces play a major role in breaking down the cellulosic fibers.

The standard characteristic of NFC is their width ranges within 100 nm whereas, their lengths vary to a few micrometers in length. The most used mechanical techniques used to produce CNFs include micro fluidisation, grinding, ultrasonication, high-pressure homogenisation, and ball milling (Moon, 2023). However, one major drawback is the high-energy spent in obtaining CNFs, where the production of fine particles sizes down to the range of nanometers was transformed by high-energy ball milling by increasing rotational speed up to 1100 rpm for a couple of hours. To overcome this limitation, the mechanical processes are merged with chemical pre-treatment to reduce the energy consumption, since pre-treated cellulose fibers are easily fibrillated and prevent clogging.

These fibers exhibit a unique minute nano structure, leading to denser and closer packing networks within the film, making it highly robust. This research project centers around the selection of industrial hemp as one of the primary sources of nanocellulose fibers for the fabrication of nanopaper. Throughout this next part of the thesis, we will extensively explore the prolific use of hemp and thoroughly discuss the extraction of cellulose nanofibrils (CNF) from various bast fibers, providing a comprehensive analysis of the process.

2.5. Sources of CNF

The two sources of CNF used in this study to produce nanopaper, has been cited below.

- Nanocellulose from hemp was extracted through a sequence of chemical and mechanical treatments. The fibers were initially grounded to a suitable size for chemical hydrolysis and subjected to high-speed centrifugation in a two-stone grinder which uses shear force to break down the fibrils to their nanoscale.
- The already dried nanofibers acquired from University of Maine, USA were obtained via a series of lyophilization where the bleached and refined fibers were dried in two step procedure.

2.5.1. Hemp and Structure of Hemp:

Current research has focused on crops or biomass to produce chemicals, plastics, and textiles. This also contributes vastly to the decrease of natural resources being used for paper industry. Industrial hemp is one of the many crops being explored during recent times. (Ranalli and Venturi, 2004). The main hindrance that let researchers grow hemp is the THC (delta-9-tetrahydrocannabinol)

level in the plant. THC is the primary psychoactive constituent in the female cannabis plant which stimulates euphoric or psychotropic effects on the user (Liu, 2017a). Cannabis plants with their THC margins more than '0.3%' are considered as Marijuana plants. Whereas plants containing less than '0.3%' can be used for their benefits.



Figure 2.7. Bast and Hurd fibers of Hemp plant respectively.

Hemp being a multi-purpose crop can be widely used in different sectors of industries. Their fibers were recognised as sturdy and durable and were used in paper and textile industry. Hemp seeds have been processed to produce oil for cooking and food applications. Shorter fibers known as "hurd" were widely used for composites to be applied in car manufacturing or even paper boards for packaging, whereas bast fibers are longer and more flexible in figure 2.7.

Physical and Chemical Structure

Stems of hemp plants are around 1.5-2.5 m tall and 5-15 mm in thickness. Fiber content is about 30-40% w/w and the fibers are organized in layers: (i) primary wall (ii) secondary wall. (Ming, 2017).

For paper and textile industries, fiber length is an important aspect to investigate while extracting cellulose from it. A length anywhere higher than 15mm and less than 30-60mm is dominant (Liu, 2017b). Additionally, smoothness of these fibers defines the percentage content of impurities such

as non cellulosic components including hemi-cellulose and lignin, as shown in the pyramidal structure 2.8. (Ranalli and Venturi, 2004).

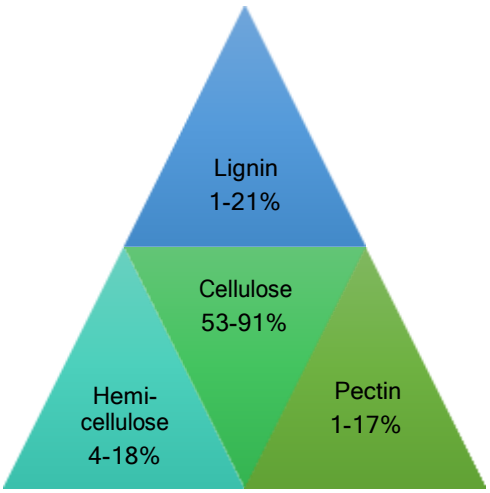


Figure 2.8. Displaying different compositions of Hemp Bast Fiber.

Cellulose - Cellulose is the most abundant naturally occurring biopolymer in plant cells. Hemp fibers have a cellulose content of about 53-91% in general. The chemical composition even though varies according to harvest time, fiber pretreatments and processing as well as position of fibers within their stems. The C_4 and C_1 atoms form covalent bonding through elimination of water (Ming, 2017).

Hemicellulose- Hemicellulose is a complex polysaccharide that makes up an integral part of the cell wall. Hemicellulose provides structural strength to the plant cell wall and contributes to its load-bearing capacity. It interacts with other components of the plant such as enzymes, to save it from external forces (Ming, 2017).

Aromatic Components –Lignin is an aromatic compound with ether and C-C linkages with different units. The hemicellulose and lignin linkages comprise of hydroxycinnamic acids.

2.5.2. Freeze-Dried Cellulose Nanofiber (University of Maine CNF)

Freeze drying or lyophilization is widely used in food, pharmaceutical and laboratory scale. This procedure is split into two steps – (i) freezing by refrigeration (solidification of the CNF) (ii) sublimation of the water molecules under reduced pressure (Peng, 2012). The NC is frozen to a

temperature below the triple point following a decrease in the pressure below the vapour pressure of the solvent which results in the solid to change its physical state from solid to gas (Sinquefield, 2020a). The product which resembles a 3D network can be easily fragmented into fine pieces with minimal shear. The fibers obtained have an average diameter in the nanoscale (UMaine NC Data sheet). Figure 2.9. portrays arrangement of fibers during lyophilization. The freeze-dried fibers were noticed to lose their crystallinity with an increasing freezing rate and longer drying times. Moreover, dilute suspension sometimes lacks proper bonding and need flash freezing in liquid nitrogen instead to keep the fibers individualised.

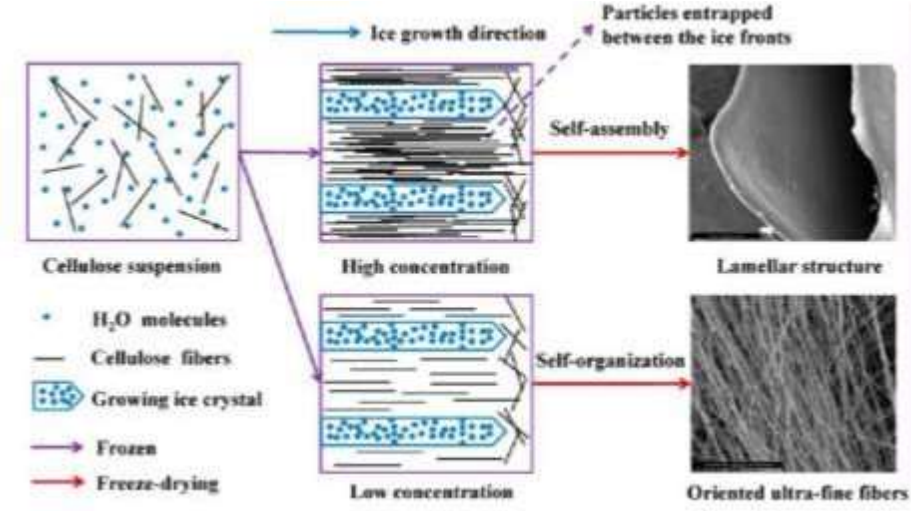


Figure 2.9. Assumed formation of lamellar geometry and alignment of fine fibers during lyophilization. Reprinted with permission from Han et al. 2013, copyright ACS.

2.6. Manufacturing of Cellulose nanofiber (CNF)

2.6.1. Mechanical Disintegration

Cellulose pulp can be shredded and disintegrated to smaller fragments. However, this leads to shredding of fibers instead of delamination of each elementary fibrils. Eventually, it will lead to CNF with low polymerization degree, crystallinity and aspect ratio which would lead to low quality nanoparticles/materials. To obtain optimum quality nanoparticles, the interfibrillar hydrogen bonding energy should be outdone to delaminate nanofibrils (Nechyporchuk, 2016).

Moreover, to use this fibrillated nanocellulose, counter aggregation should be prevented. For this reason, CNF is commonly produced in aqueous medium, which loosens the interfibrillar hydrogen

bonding. Typically, this nanocellulose is dispersed at concentrations as low as (<5 wt.%) due to its hydrophilic nature, which forms very high viscous solutions/suspensions. Some widely used mechanical disintegration method is homogenization, refining and grinding. These methods are most popular for extracting nano-fibrillated cellulose from cell wall and CNF isolation.

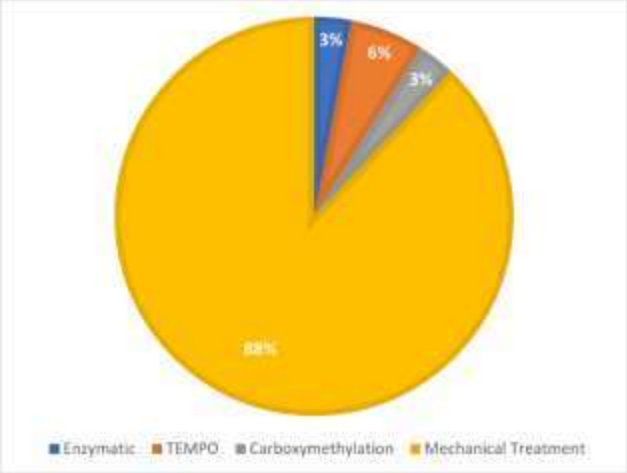


Figure 2.10. Quantification of the most frequently used pretreatment used for CNF production (Lavoine et al. 2012).

2.6.1.1. Homogenization

High pressure homogenization is used to obtain CNF from cellulosic fibers, mechanically (Nechyporchuk, 2016). Homogenization works on high pressure; pressure drop and shear/impact forces against the wall. The extent of fibrillation depends on homogenization cycle and the working pressure.

Table 2 Parameters used to refine cellulose to produce CNF through mechanical equipment (Nechyporchuk et. al., 2016)

Processing Method	Pretreatment	Speed (Rpm)	Number of Cycles	Total Energy (kWh/t)
Homogenizer	Refining	55	20	21888
Grinder (Masuko)	Chemical treatment	1300	40	1.5
Micro-grinder	Refining	1500	9	1550
Microfluidizer	Refining	69	20	3199

2.6.1.2. Microfluidizer

The principle of this technique is to pass the cellulose suspension to pass through a thin lined chamber with a specific geometry e.g., Z- or Y- shaped with an opening width of 100-400 um. It works at a high specific pressure of about 40,000x (Zimmermann, 2004).

The product is a gel like material, and the microfluidizer consists of a series of check valves allowing the recirculation of cellulose/water slurry. Microfluidizers are used in paper/pulp and food packaging industries. Micro-fluidizer works through a small nozzle which may entangle the fiber inside making the equipment less efficient.

2.6.1.3. Obtaining CNF via Grinding (Masuko Sangyo)

Ultra fine grinding is another widely used technique used to produce CNF. Super mass colliders are commonly used for this treatment. (Taniguchi and Okamura, 1998) have described this procedure by passing 5-10 wt.% cellulosic fibers several times (10 times) and obtained CNF of diameter 20-90 nm.

The process involves passing the pulp several times through a static and rotating grindstone with demarcations, revolving at around 1500-1800 rpm. Shearing force, rolling friction and attrition disrupts the cell structure, hydrogen bonds and individualizes nano scale fibers.

The two plates could be adjusted to various measurements and allows different shears as the gap increases. The various gaps used could range between 0 mm to 1.4mm, “zero” position being the two plates are in contact with each other.

Some drawbacks of grinding would be clogging of material in between plates if there is not much force while pouring the cellulose slurry in the grinder (Nechyporchuk, 2016).

Nanocellulose pulp is fabricated through 5-10 cycles of grinding, although after a while of refining the size of the nanocellulose is not brought down any further, report suggests.



Figure 2.11. A two-stone grinder "Masuko Sangyo"

Shear stress (τ) is the force per unit area acting parallel to a surface, while shear rate (γ) represents the rate of deformation per unit time.

The shear-rate inside the Masuko uses a formula of: $\boldsymbol{\tau = \mu\,\gamma}$

where**:**

τ = Shear stress (Pa or N/m^2)

μ = Viscosity of the material being processed (Pa·s or $N \cdot s/m^2$)

γ = Shear rate (1/s or s^{-1})

Besides this conventional mode of mechanical disintegration of cellulose in nanoscale, there are various non-conventional methods been used widely. Some of these techniques are Ultrasonication and steam explosion ball milling.

2.6.1.4. Ultrasonication:

Ultrasonication consists of subjecting the CNF slurry to ultrasonic waves, which causes the formation and implosion of vacuum gas bubbles. These hydrodynamic forces, causes the delamination of cellulosic fibers, to multiple fibrils. Largely used in laboratories and industries for well dispersion of nanoparticles. Researchers vastly use sonication after biochemical or chemical treatments. Low sonication power breaks the weak, and high power breaks the strong bond.

Depending on the size scale, the sonicated solution/dispersion is exposed to centrifugation from which the supernatant is recovered.

2.6.2. Chemical Pre-Treatment for Extraction of Nanocellulose Fiber:

Extracting CNF using mainly mechanical disintegration which requires very high energy costs. Moreover, using mechanical methods alone leaves behind traces of lignin, hemicellulose and other aromatic impurities as stated by (Spence, 2011). Chemical pre-treatments help in releasing individualised fibrils by preventing additional passes through grinders to reach desired fibrillation. Different chemicals are responsible for the alteration of cellulose structure, crystallinity influencing greatly the properties of CNF.

Some of the chemical treatments discussed in the result & discussion section of this thesis are mentioned below. The optimum amount of treatment would depend on the initial cellulose morphology.

Table 3 Different Processing conditions used for Producing CNF.

Raw Material	Chemical Pulping	Mechanical Treatment on Pulp	Chemical Pre-treatment on Pulp	Mechanical Methods for CNF Production	Reference
Softwood	Sulfite/Kraft Pulping	Refining (PFI Mill)	No	Homogenization	(Turbak 2015)
Softwood/ hardwood	Bleaching	Refining (disk refiner)	No	Homogenization	(Stelte and Sanadi, 2009)
Soybean pods	Sodium Hydroxide, Sodium Chlorite	Refining	No	Grinding/ Homogenization	(Wang and Sain, 2007)
Hemp (Bast)	Acid Treatment, Bleaching	Blending, refining	Yes	Grinding	(Ranalli and Venturi, 2004)
Sisal Fibers (Hardwood)	Sodium Hydroxide, chlorite treatment	Blending	Enzymatic	Cyro-crushing and Refining	Siqueiral 2010 Qing. (2013)
Kenaf Bast	Acid Treatment	Grinding	No	Homogenization	Sulaiman, (2016)
Regenerated Cellulose	No	Blending	-	Ultrasonication	Chen (2011)

2.6.2.1. Alkaline Treatment

Alkaline treatment or treating the fibers with Sodium Hydroxide plays a significant role in removing lignin by cleavage of the ether bonds present in the lignin half of the fibers. This leads to the disruption of the lignin structure and separates the links between cellulose and lignin. The

total internal surface area is also considerably increased due to solubilisation of various components such as lignin and hemicellulose. Additionally, depending on their concentration, time and temperature of reaction, sodium hydroxide (NaOH) or potassium hydroxide the two chemicals popularly used for alkaline treatment can be classified into high and low concentration processes (Mirahmadi, 2010).

The alkaline treatment ionizes pectin carboxylic groups (-COOH) and forms sodium carboxylate (COONa).

$$\text{Fiber-OH} + \text{NaOH} \rightarrow \text{Fiber -O-Na+ } H_2O$$

It is important to note that alkaline treatment maybe carried out by avoiding undesirable cellulose degradation and ensuring the reaction of acid hydrolysis to be performed only on their surface.

2.6.2.2. Acid Hydrolysis

Alkali treatments are further advanced by a step of acidification. Acids such as H_2SO_4 and HCl cause hydrolytic cleavage of the glycosidic bonds in the cellulose (Stamatelatou, 2014). Acid molecules donate protons, which attack the glycosidic bonds and cleave them. This is performed to break down polysaccharides and sugar. This is one of the simplest methods for preparation of CNF from lignocellulosic biomass. Even though strong acids have tendency to dissolve the amorphous regions of the cellulose as they have more hydroxyl group concentration providing more reactive sites for protonation, controlling conditions such as concentration of acid, time and temperature of the reaction might stop this from happening. The cellulose is arranged in ordered (crystalline) and dis-ordered (amorphous) regions in the plant cell. The disordered region can be easily hydrolyzed through acid reaction and the ordered parts are unhindered. This could be a drawback for production of cellulose nano fibers which contain both amorphous and crystalline domains. Hence, to mitigate this issue, the main controlling factors which are reaction time, temperature and concentration of acid are to be moderated before reaction.

The acid generates an H+ ion which protonates the hemicellulose molecule. The acid reacts with the protonated hemicellulose which undergoes hydrolytic cleavage of its glycosidic bonds until the sugar units are fragmented.

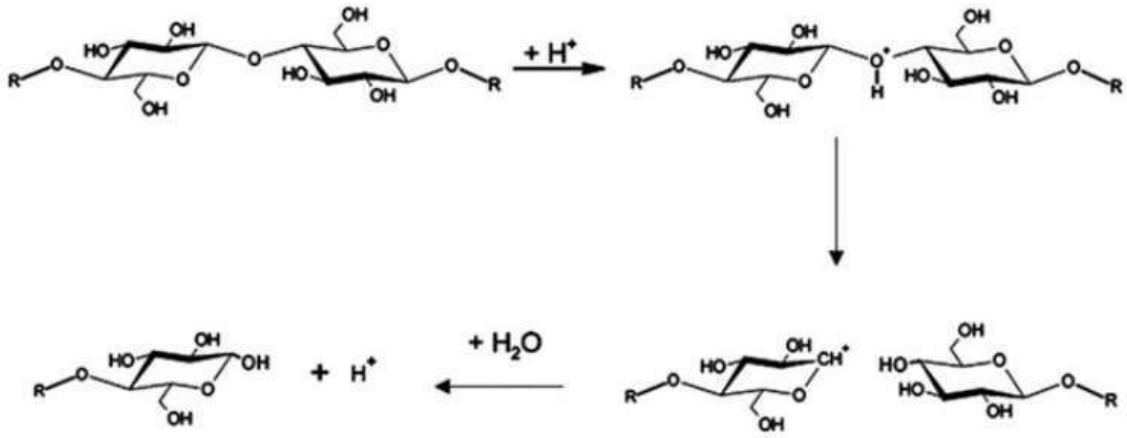


Figure 2.12. Mechanism of Acid Hydrolysis in Cellulose adapted from "Pretreatment of Lignocellulosic Biomass Toward Biofuel Production."

2.6.2.3. Carboxylation via TEMPO mediated oxidation

TEMPO-2,2,6,6-tetramethylpiperidine-1-oxyl radial (TEMPO) is predominantly used to delignify cellulosic material. This is the most effective chemical treatment to obtain a transparent nanocellulose fiber suspension. At this stage, delignification is carried out to eliminate lignin and hemicellulose. TEMPO (which is a stable organic nitrosyl radical) helps in catalyzing the oxidation of primary alcohol groups in aqueous media. The outcome of obtaining aldehydes or carboxylates from primary and secondary alcohols depends entirely on the specific reaction conditions and the nature of the substrate involved (De Nooy, 1995).

Oxidation is a fundamental tool in extracting nanocellulose fibers. It can inter convert functional groups (eg.: alcohols to aldehydes/carboxyls), activation and even oxidative cleavage (Mercadante, 2013).

The TEMPO mediated reaction is a surface modification, where the reaction proceeds through the fibers, but the surface becomes negatively charged. Different oxidants are used to oxide the nitroxyl radical to obtain the nitrosonium ion which is the actual oxidant. The procedure includes TEMPO and NaClO in an aqueous medium in presence of NaBr in room temperature (pH-10-11) (De Nooy , 1995). The degree of polymerization (DP) is controlled by the amount of NaClO used. Higher the amount of NaClO, lower the DP. The oxidation helps in: (i) Adding repulsive charge (ii) adding different groups on the surface (iii)hydration and swelling.

Carboxymethylation occurs when a carboxymethyl group is initiated or introduced in the surface chemistry of cellulose in alkali medium (KOH, NaOH). TEMPO oxidation also prevents any aggregation of CNF in a solvent due to the presence of -OH groups and -COOH (carboxylic) groups imparting enough negative charge to stabilise the colloid (figure 2.13.).

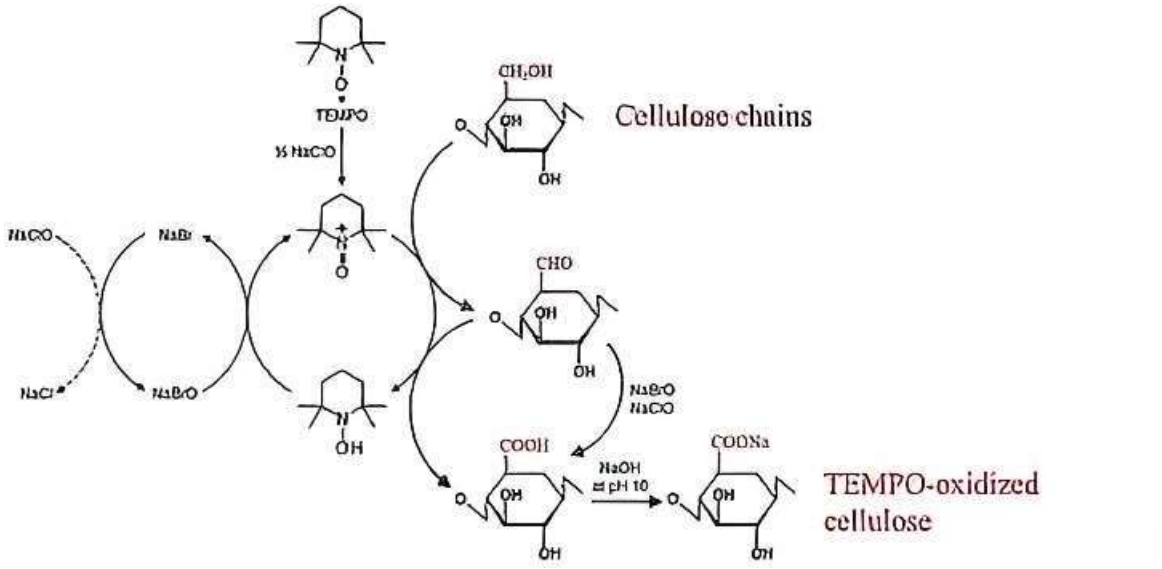


Figure 2.13. Schematic of CNF Synthesis by TEMPO-mediated oxidation (Isogai et al., 2011)

2.6.2.4. Oxidation or Bleaching with Hydrogen Peroxide

To get rid of the excessive lignin and to dissolve the conjugated chromophoric sites bleaching with hydrogen peroxide has become a popular alternative for cellulose oxidation. This mitigates the usage of chlorine and chlorine-based compounds such as NaCl and NaClO (sodium chlorite & hypochlorite, respectively). Bleaching takes place when the coloured substance is solubilized by altering their chemical properties. Oxidation occurs from the dissociated perhydroxyl ions of hydrogen peroxide in aqueous medium, as seen in equation (i).

$$H_2O_2 \rightleftharpoons H^+ + HO_2^- \ldots. \text{(i)}$$

In experiments, NaOH and Na_2SiO_3 are used as the stabilizers and wetting agents for peroxide bleaching. Stabilizing agents are incorporated to minimize the degradation of peroxide by forming complex compounds with heavy metals present in water. The most common stabilizers are sodium silicate and phosphonic acid. Stabilizers are thought to act as buffering agents to prevent the pH increasing too high (Li, 2011).

So, HO. Or $HO_{2.}$ might demobilise the mobile electrons in these conjugated double bonds in chromophores, hence decolorizing them. Figure 2.14. shows the reaction mechanism for cellulose oxidation. The extent of bleaching is largely dominated by the reacting pH and temperature. The process is henceforth quenched by water washing until the pH has been neutralised (Mussatto, 2008).

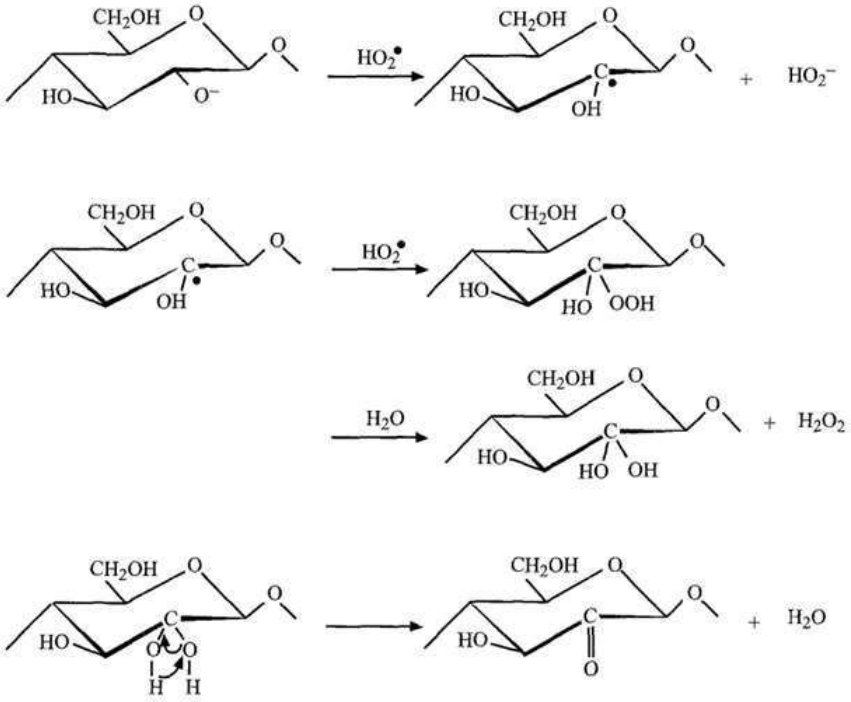


Figure 2.14. A reaction mechanism suggested by Ney (1982) where per hydroxyl ion oxidizes cellulose at C2 and C3 position.

2.6.2.5. Enzymatic Pre-Treatment

Enzymatic hydrolysis is a well-known fibrillation treatment. A widely popular enzyme called cellulase is used to breakdown cellulose. There are several patents which have used this enzyme in papermaking industry. From milder treatments, where enzyme helps in defibrillation to harsher environments where cellulase is used to convert cellulose to glucose for bioethanol production (Tangnu,1982). Depending on reaction conditions the cellulose formed is derived from two subdivisions of cellulases, β-1,4-endoglucanases and cellobiohydrolases (Dufresne, 2013).

Prolonged enzymatic action generally modifies the cellulose instead of degrading it. Both the above mentioned cellulases cause a synergistic effect during cellulose fibrillation. (Pääkkö, 2007),

came up with a method to degrade cellulose with cellulase with the following steps mentioned (i) refining, to expose the internal surface area of the cellulose (ii) enzymatic hydrolysis, for degrading the cellulose (iii) washing to stop reaction (iv) homogenization of 2-5 wt.% suspension through a microfluidizer to decrease their spatial diameters.

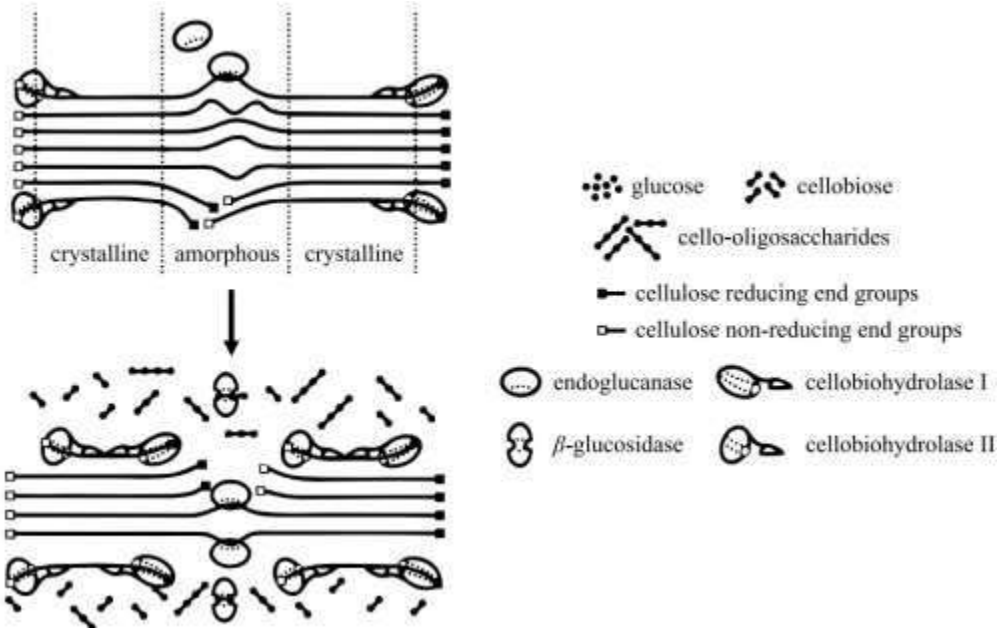


Figure 2.15. Schematic of cellulase impacting cellulose. Adapted from Lynd et al. 2002, printed with permission from American Society of Microbiology and the authors.

2.7. Applications of Nano-fibrillated cellulose (CNF):

Nanocellulose, has found its applications in different aspects and industries. Due to its tunable optical properties and surface functional groups, plus eco-friendliness it has been highly regarded in the field of polymers.



Figure 2.16. Different Applications of Nanocellulose.

Cellulose and nanocellulose fibers (CNF) being the most abundant biopolymer, has grown due to interest among scientists corroborating to its mechanical, physiochemical, and biological properties in companion with being eco-friendly. Many authors such as, researchers have commented on rheological structures, crystal ordering and colloidal behaviour.

Nanocellulose and their morphological dimensions depend on various factors:

- Origin of the cellulose or source- Based on the source of nanocellulose, their structure may differ from multi-fibrillated with repeating units of amorphous and crystalline domains (plant derived) whereas, bacterial sources show a unique 3D network like entanglement upon fermentation.
- Extraction and Treatment methods- Treating the original source material with different chemicals and refining the samples lead to formation of new functional groups on their surface.

Owing to its high tunable characteristics, nanocellulose is used in food and packaging, cement industries, paper.

Due to such profound characteristics, there are wide range of applications in fields of industry, paper and pulp, electronics and flexible opto-electronics, pharmaceuticals, food and packaging and composites (De Amorim, 2020) (Klemm, 2018).

Some several applications of CNF have been depicted below:

1. It possesses the capability to serve as a reinforcing element during the manufacturing of paper and cardboard. Due to its high mechanical strength bearing properties. (Shukla, 2020).
2. Likewise, when integrated into coatings for food packaging, it exhibits potential as a safeguard against oxygen, water vapor, grease, and oil.
3. Beyond this, there are prospective applications across diverse domains such as pharmaceuticals, military, design, and electronics. For instance, it holds promise in shaping flexible OLED displays, fabricating aerial vehicles, and even crafting military attire. (Nanografi Nanotechnology).

2.7.1. Food and Packaging Industries

Food industry is increasingly demanding to develop new age sustainable packaging materials. They require to be mechanically strong, with good physical and chemical barrier properties. Moreover, the most important aspect of packaging substances is their non-reactivity with the food materials. Food packaging takes up the largest chunk of market in the field of packaging about (85%) (Silva, 2020).

Packaging plays a major role in the food and edibles industry (food chain supply). They protect, handle and store food until it reaches the final customer (Silva, 2020). The basic requirements of packaging intended for fresh, frozen, dehydrated, thermal or aseptic processed foods depends on-

a) Intrinsic property of food materials such as water and oxidation reactivity.

b) External factors such as storage temperature, relative humidity, and light exposure.

c) Required shell-life of the food.

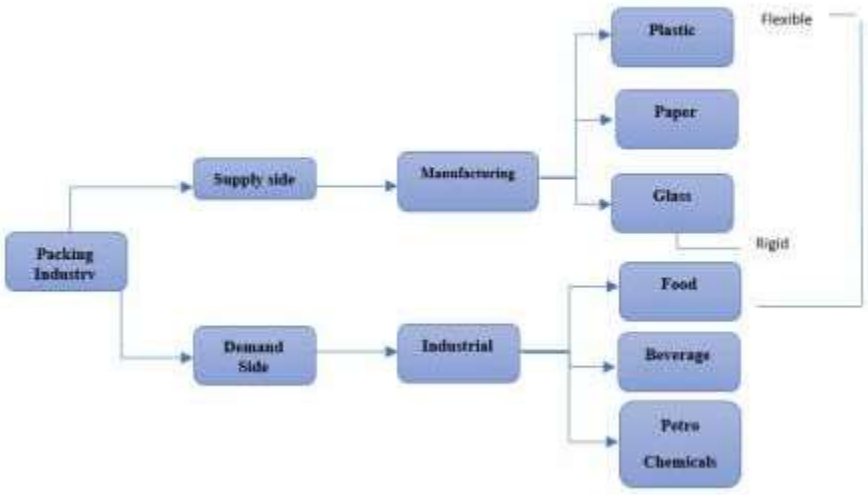


Figure 2.17. Schematic to show the different sectors of packaging industry.

NC could form hydrogen bonds both inter/intra and with other biopolymers that gives rise to a dense network. This improves the film's ability to permeate gases. Permeability of gas depends on diffusion rate and dissolution of the gas (Wang, 2018). By forming secondary bonds with a particular polymer, NC increases the path length for diffusion of these gases diffusing through the surface as shown by Mascheroni (2016) and Ahankari (2021)in their works.

Table 4 A discussion table with their product and permeability (oxygen and water vapour), shell life and materials used has been given for comparison (Mascheroni et al., 2016)

Product	**WVTR ($g/m^2.day$)**	**Shelf Life (Months)**
Nuts, snacks, chips	0.093-3.0	3-12
Coffee	0.61-1.1	12-18
Fruits, vegetables	10-4000	0.25
Meat	2-100	0.5
Dairy	0.2-8	0.5

Nanocellulose can be modified to (i) enhance interaction between the matrix phase (ii) enhance intrinsic properties of the fibers (iii) provide unique functions specific to the food or material getting packed (Tomé, 2011; Lee, 2011).

2.7.2. Nanocellulose in Cement and Concrete Industries

Growing concerns over the environment and pollution awareness have motivate innovators/constructors to take up sustainable materials instead of synthetic fibers as a reinforcement agent in the building industry. In another study, by Hisseine, 2019, a nano-engineering approach was taken to produce cement composites with nanocellulose materials (NCM) to measure their properties. Their research incorporated nanocellulose filaments (NCF) to cement systems and study their macroscale mechanisms with a top-down multiscale outlook. All these experiments led to an improvement in the performance of structural properties such as compressive strength, modulus of elasticity and strength. Results were outstanding as cellulose and other renewable non-fibrous materials along with nanoengineering was used to manufacture foams.

2.7.3. Nanocellulose in Cosmetic and Beauty Industry and Products

Nanocellulose fibers due to their moisture absorbing capacity and thickening effect are used in bio-based cosmetics or beautifying products. Bacterial cellulosic fibers in nanoscale are very common due to their high purity, less energy consumption during isolation or extraction methods when compared to plant cellulose. During fermentation, the microorganisms freely float in the medium or are attached to the fibrils stated by Dufresne (2013) in their research, producing a very gel like structure through swelling.

The process of purification needs killing the microorganisms and removing cell waste and growth media from the cellulose matrix. This is an essential step in ensuring the quality of the bacterial cellulose and can be accomplished by repeatedly washing with a hot sodium hydroxide solution, followed by water until the pH reaches a neutral level or by other techniques such gamma radiation (Pacheco, 2018). Bacterial cellulose fibers have also been used in drug delivery and they have showed considerable efficiency in case of hydrophilic and hydrophobic drug purposes. According to Pacheco (2018), propolis extract was added to bacterial cellulose film made in a modified medium so that it could be used as anti-inflammatory sheet mask for skin that is prone to acne and inflammation.

This thesis research concentrates on the preparation of such a state-of-art technology known as the nanopaper and optimising its characteristic parameters. The following portion presents a vivid and extensive review of their features and pre-established work related to the topic.

2.7.4. Nano paper from NC

Over the years, plastic waste has been a rather threatening issue being faced by the world. Every year worldwide, about 350 million metric tons of plastic waste is generated. Most of which gets incinerated or transported to other countries. About as less as 2% is transported to other countries.

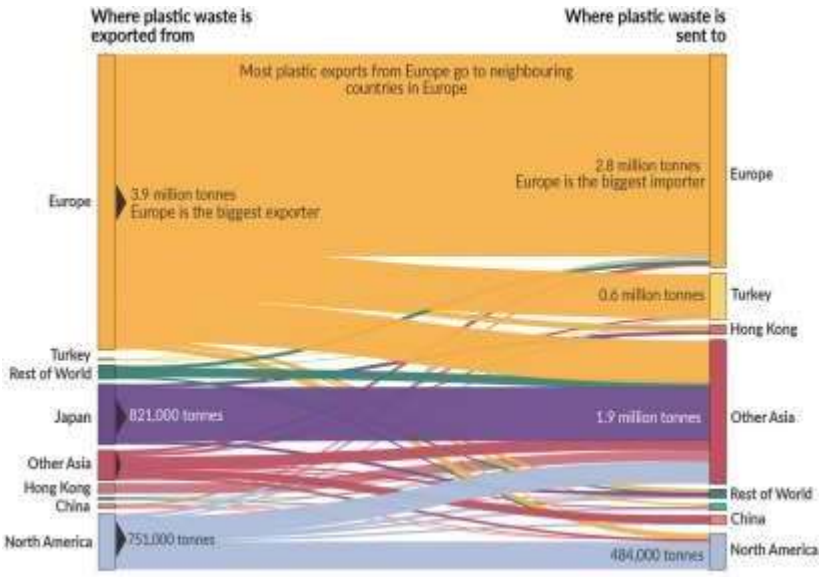


Figure 2.18. Observing plastic trade over the world taken from Our World in Data,2020.

A considerable part of this plastic waste is contributed from electronics and other electronic landfills. Researchers worldwide have found various green alternatives to mitigate this problem with a dip in gross plastic consumption. Cellulose nano paper is such a substitute which has displayed significant promise across a wide range of fields, including optoelectronic devices, food packaging, and biomedical applications. This is attributed to its numerous advantages, such as excellent flexibility, adjustable light transmission, remarkable thermal stability, minimal thermal expansion, and exceptional mechanical properties.

In the last three decades, a new type of nanomaterial known as nanocellulose has surfaced, involving cellulose nanocrystals or nano whiskers, nano fibrillated cellulose (NFC), and bacterial

cellulose (BC). The characteristics of nanocellulose have been evaluated both as individual nanofibers dispersed within a polymer matrix, as well as in the form of papers, coatings, and laminated composites. Unfortunately, realising the utmost potential of nanocellulose is still an obstacle at the moment. According to Nishino (2004) the critical study of the optical features of paper-based composites fabricated using nanocellulose demonstrated the potential to produce materials ranging from translucent to highly optically transparent, analogous to the transparency of some thermoplastic and thermoset polymers, including glass. Moreover, nanocellulose exhibited a thermal expansion coefficient of approximately 0.1 ppm/K, like that of quartz glass, which in turn promoted the replacement of glass and other plastic/petroleum-based substrates.

This part of the thesaurus is going to mainly focus on the fabrication of an optically transparent and their established results. Paper as we all know is a flexible sheet which is composed of cellulosic fibers intertwined with each other to form a continuous mat/network of these fiber. When cellulose is subjected to stress or mechanical forces, the amorphous regions can absorb and dissipate the stress more effectively due to their flexibility. As stress is applied, the amorphous regions can undergo deformation, bending, and stretching without easily breaking. This prevents the propagation of cracks or fractures that could weaken the material. Essentially, amorphous regions act as energy-absorbing zones, helping to distribute the stress throughout the material and preventing localized failure. Multiple factors have been identified as critical to produce nanocellulose papers with exceptional optical transparency, commonly known as cellulose nanopapers. Essential characteristics that significantly influence the control of optical transparency include fiber diameter, refractive index, packing density, surface roughness, and pore size of nanocellulose papers in figure 2.19.

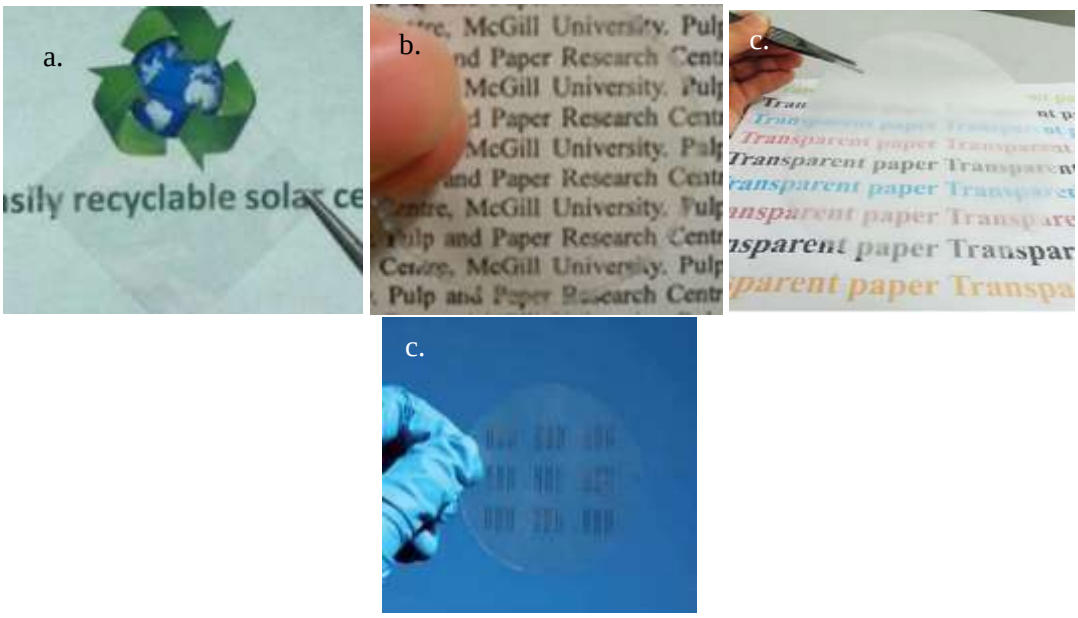


Figure 2.19. Various nanopapers showing their transparency (a) CNP made from NCC and glycerol (b)CNP using only NCCs (c) CNP prepared from TEMPO-oxidized wood fibers (d) Array of phototransistor by Shahoui et al., 2017.

Revol, (1992) fabricated a nanopaper by simply using evaporation methodology by evaporating water from different CNC suspension liquids. They showed observations how the positioning of fibers followed a nematic chiral crystalline phase and intertwined fibrillar layers formed from CNC. Other authors, over time have used different methodologies to fabricate CNP from plant sources such as sugar beet CNFs (Dufresne, 2013), The average thickness of these films turned out to be between 3-100 µm possessing good mechanical strength with a translucent appearance.

Cellulose is present in both plant and non-plant sources with a combination of hemicellulose and lignin. The later are some impurities that need to be eliminated before obtaining the nanocellulose fibrils optimum for nano-paper production. Since production of nanocellulose fibers without any treatment has been expensive, different cooking and bleaching methods are undertaken by researchers across the globe amongst which, acid hydrolysis and bleaching are two most common pre-treatments.

2.7.4.1. Preparation of Nanopaper:

Nano-papers are a fibrillar network like conventional paper which consists of cellulose nanofibers (10^{-9} of a meter) instead of fibers in micro scale (10^{-6} of a meter). The formation of nano-paper can be classified into two sub-processes: a) The formation of a CNF gel like pulp through a series of

chemical treatments and mechanical disintegration and b) Dewatering and hornification of this suspended pulp to form a complex structure through hydrogen bonding and inter-fiber entanglement. Different approaches like solution casting, filtration with a vacuum, using a Rapid-Kothen machine (paper forming machine), roll-2-roll production in industries followed by pressing and drying in a hot press or oven drying are often incorporated to fabricate nano-papers. Preparation methods, drying method, filter media are some of the many aspects that effect the physiochemical properties of the nanopaper in context.

Filtration Method: This method has been widely used as a technique for producing nanopaper in laboratory scale setup. The process mainly consists of diluting the pretreated and refined fiber slurry to a concentration typically close to 0.1-1.0 wt.%. Followed by thorough mixing, the CNF solution is poured onto a filtration column with a micron pore sized filtering membrane such as poly-vinyl di-fluoride and mixed-cellulose ester are used, at room conditions. (Liu, 2017b). The filtration is carried out with an assisted vacuum pump that draws the water out leaving behind a dense packing layer/wet filter cake with very little free water (Quero, 2018). The choice of filtration membrane is a crucial step towards retaining most of the nanofibers. Authors like Wetterling et.al. developed an electro assisted filtration which facilitates cellulose dewatering by inducing an electroosmotic flow (Wetterling, 2017)

The filtration process is followed by a step of hot pressing/drying which deals with removing the bound water. The filtered wet cake is subjected to a cumulative pressure and temperature cycles. A semi-automatic paper machine or a hot press can be used for this purpose. This results in increasing the packing density of the nanocellulose filter cake.

Solution Casting/Drop casting: Unlike filtration, casting retains 100% of the nanofibers even though this is a more complex methodology to attain nanopaper. By controlling the rates of evaporation and atmospheric conditions, the nanopaper may possess specific microstructures. Scientists have come up with a similar industrial roll-to-roll technique reaching a large scale production of these though Casting is fundamentally different from filtration (Vartiainen, 2014). Due to increase in concentration during evaporation, casting often results in in-homogenous aggregation if the evaporation parameters such as relative humidity (%) and temperature are not constant; making this a less viable method to manufacture nanopapers. Casting is a simple but comparatively slower process (Sehaqui, 2010).

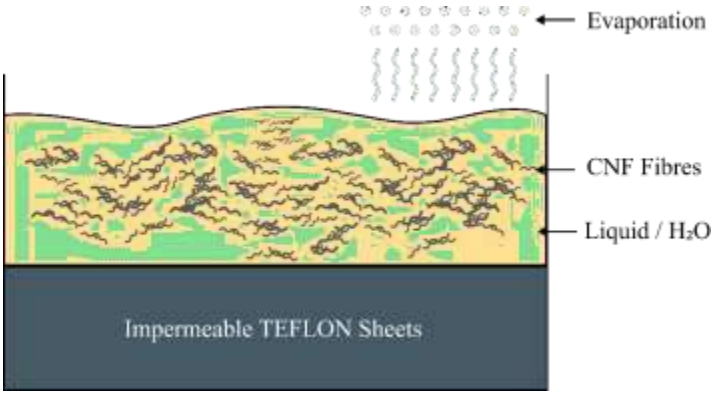


Figure 2.20. Casting Method

In both processes, during drying the internal structure of the nanocellulose collapses and capillary forces help dragging the nanofibrils closer to one another forming hydrogen bonds. In CNF, the 3D networks amongst these hydrogen bonding has a huge impact on the rigidity that show on their mechanical characteristics. Consequently, due to these hydroxyl groups present on the surface of nanofibrils interact with each other to form a dense structure.

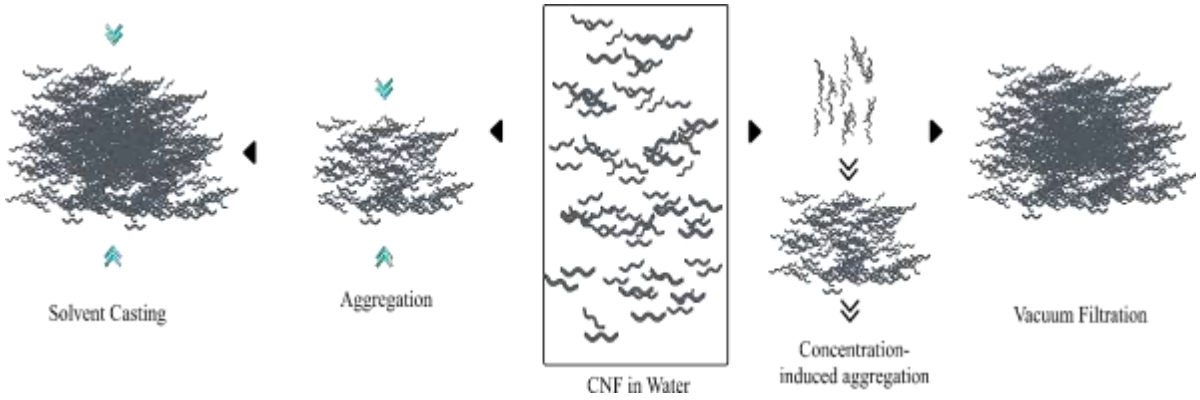


Figure 2.21. Preparation of Nanopaper (left) solvent casting (right) vacuum filtration.

The fibrous network of nanopapers is analogous to conventional paper but instead of microfibers they consist of nanofibers. Besides filtration and casting, an industrial procedure of using the Rapid-Köthen are often used to fabricate CNPs (Sehaqui, 2010).

Physical properties of nanopaper are an attractive property. The diameter of the cellulose nanofibers is generally smaller than optical wavelength of light. This phenomenon leads to achieving high transparency. Although degree of transparency of nanopaper highly depends on aggregation of fibers while drying, surface roughness and porosity and space between fibers.

(Nogi, 2009a) Along with various factors including processing methods, drying conditions, degree of polymerization (DP) highly influence the properties of nanopaper.

Glycerol and its Use as a Plasticizer

Glycerol (*Gly*) (chemical formula: $C_3H_8O_3$) also called glycerine is colourless, viscous sweet tasting and nontoxic liquid. The backbone structure of glycerol is widely seen in lipids also called glycerides. With a melting point of 17.8 ^oC and boiling point close to 290 ^oC it is widely used in different industries. The glycerol structure consists of three hydroxyl groups making the compound hygroscopic with an affinity to absorb moisture. It is highly soluble in water due to the polyol groups to form hydrogen bonds with the water molecules. It has a specific gravity of 1.26, slightly denser than water, but forms an aqueous solution.

CNF films or nanopapers itself with casting methodology results in nanopapers with high agglomeration and non-uniform thickness. They often turn out to be brittle due to lack of moisture in the air while drying. Excessive drying of the NFC nanopapers can lead to shrinkage and deformation of their structure. These drawbacks can be mitigated with the use of a plasticizer like glycerol.

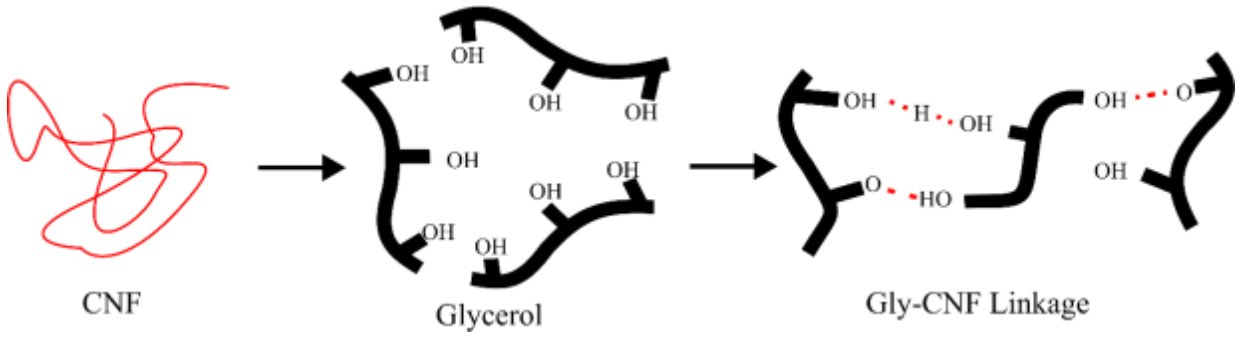


Figure 2.22. Representation of hydrogen bonding between CNF and Glycerol during Heat Treatment

Plasticizers are low volatility liquid are used to make materials softer and more flexible and some of these plasticizers are more competent than the others. They cross-link with polymers when added to increase their flexibility and easily mold them. Similarly, Gly as a plasticizer bond with CNF by making hydrogen bonding between the triol that is, three -OH groups of glycerol with OH

groups of the nanocellulose matrix. As a result of which CNF films become more pliable and less rigid (Dorris and Gray, 2012).

By introducing Gly in CNF due to its fluid nature Gly penetrates through the fiber matrix forming hydrogen bonding by reducing inter fiber hydrogen bonding between fibers. This causes fiber-fiber distance and fiber slippage leading to weak intermolecular forces.

2.7.5. Nanopaper Properties

Nanopaper from CNF has shown some promising aspects due to their modifiable nature. Some of these significant properties are:

2.7.5.1. Mechanical Properties

CNF shows high aspect ratio and subsequently the stacking of these fibers under environmental conditions leads to refined strength and stability. The numerous hydroxyl groups (-OH) lead to good bonding amongst the fibers leading to tightly packed structure. Moreover, during papermaking process the CNFs can be made to align in a directional manner leading to anisotropic films have shown higher modulus and strength values. When CNFs are parallelly packed and distributed in the nanopaper, a maximum number of interfaces are found. This leads to easy sliding of individual CNF. These interfaces allow the transfer of load thereby improving mechanical strength (Kafy, 2017b). The tensile properties of nanopaper can be measured by the elongation and deformation of the dog bone shaped specimens under constant speed as discussed in the results and discussion chapter 4. The uniaxial force, F, required to elongate the sample, ΔL is noted. The tensile stress, σ_t is calculated by dividing the force applied by the cross-sectional area of specimen, A.

$$\sigma_t = \frac{F}{A}$$

The strain, ε_t, of the specimen is the change in length divided by the original length of the specimen,

$$\varepsilon_t = \frac{\Delta L}{L}$$

The recorded stress is in the units of N/m^2, or Pa or Mega Pascal is generally plotted against strain. This stress-strain curve is used to find properties like tensile modulus or young's modulus, E_t. This is calculated by finding the slope of the stress-strain curve in the linear region.

$$E_t = \frac{\sigma}{\varepsilon}$$

Some other tensile property which can be determined from the stress-strain curve is the ultimate tensile strength, σ_U is the ultimate or maximum stress withheld before the rupture.

2.7.5.2. Surface Properties

The hydrophilic nature of nanopaper provides excellent wetting properties. The abundantly dispersed hydroxyl groups (-OH) makes it easier for their surfaces to have lower contact angle with liquids, indicating the spread of liquids over their surface area. The -OH groups readily form hydrogen bonding with water or polar molecules showing enhanced adhesion and uniform deposition. As result, printed inks and deposited electronics will adhere well to the nanopaper surface. Hydrophilic surfaces have reduced surface tension compared to hydrophobic surfaces. An important property which is the surface energy defines the extent of deposition of printable electronics in turn effecting their adhesion properties. It has positive correlation to the strength of bulk interactions and surface exposure. Usually, a surface with low energy has poor wetting qualities than surfaces with higher energy levels. This results from poor bond formation so there is minimal energetic reward for the liquid to split bulk bonding in the benefit of interacting with surface.

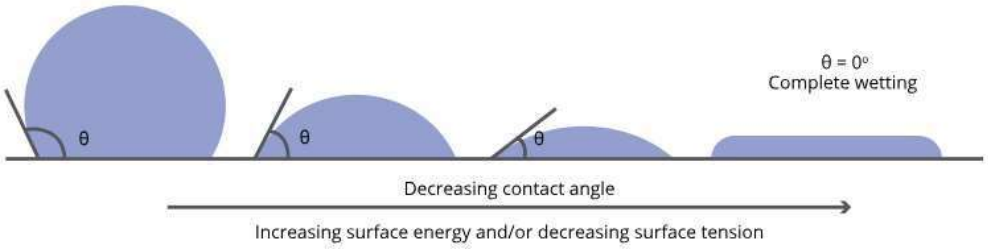


Figure 2.23. Basic Relationship between contact angle and surface energy taken from Ossila Equipments

Since, the CNF films were polar due to their hydrophilic nature, two reference liquids were being used to determine their energies; Fowkes and Extended Fowkes model were used to find their

respective values. Fowkes' theory assesses the interactions between a liquid and solid in terms of 'dispersive' (Van der Waals) and 'polar' interactions. These interactions will sum to form overall energy:

$$\sqrt{\sigma_l^D . \sigma_S^D} + \sqrt{\sigma_l^P . \sigma_S^P} = \frac{\sigma_l(1 + \cos\theta)}{2}$$

Fowke's equation relating solid and liquid phase interactions with surface tension and contact angle.

Where, σ_s^D and σ_s^P are the dispersive and polar components of the surface energy of solid respectively, and σ_l^D and σ_l^P are the dispersive and polar components of the surface tension of liquid respectively.

2.7.5.3. Surface Morphology

CNPs are characterized by high specific surface area, which is the surface area per unit mass.

$$Specific\ Surface\ Area = \frac{Amount\ of\ Surface\ Area}{Unit\ Mass\ of\ Fibers} \left(\frac{cm^2}{g}\right)$$

The surface area of nanopapers differ between 500 m^2/g to several hundreds of m^2/g depending on their fabricating conditions. This results in increased porosity or a mesoporous or even microporous structure, with diameters between 10-70nm. Since cellulose nanopaper is formed of a fibrous network of multiple nanofibers, the surface topography indicates that of a porous nature. The intertwining of fibrils leaves gaps and voids between them. Heat treatment while drying can densify the CNP, as the solvent evaporates the fibers consolidate through pore size reduction.

2.7.5.4. Optical Properties

The occurrence of light transmittance through nanofibers is possible due to their hollow structure, which is formed during chemical hydrolysis and fibrillation steps. The process of transmitting light through nanofibers is called "Light Guiding" which is analogous to that of optical fibers. This occurrence is achieved through Total Internal Reflection when light travels from a medium with a higher refractive index (μ) into a medium with lower refractive index then the path of this light bends at an angle greater than the critical angle. Instead of escaping into the surrounding medium, the same light is reflected back into the higher refractive medium (Keiser, 2021). Removal of lignin, hemicellulose, and other impurities from the surface of the nanofibrils, give rise to certain

pores. These pores are responsible for scattering light causing an optical haze that is detrimental towards incorporating CNP in electronics as a display or transparent substrate (Zhu, 2013).

2.7.6. Mechanism of Film Formation of 3D Nanocellulose Films by Filtration and Casting:

2.7.6.1. Filtration Theory:

Cellulose nanofibers are like a complex network of nanofibrillar structures or fibrils. They remain afloat as a cluster of fibrils which are kinked together in the CNF slurry. These complex networks of fibrils remain afloat in water as a suspension due to the formation of hydrogen bonding with H_2O molecules. With the assistance of vacuum, a "wet" cake of nanocellulose fibrils/fibers start forming with adjacent to the filtering medium. Due to their nanoscale sizes, filter size which acts as the filtering media for nano-paper fabrication plays an important role. The assisted vacuum is used to draw the liquid through the filter and trap the nanofibrils on the membrane. This leads to the formation of a wet mat of nanocellulose which can be pressed, dried, and consolidated to form a nano-paper.

The cake starts forming adjacent to the media. Solution or dispersion of nanofibrils in water is poured onto the filtering funnel and filtration time is noted. Nanofibrils at the bottom of the funnel that is in direct contact with the porous membrane are arranged haphazardly during the fast filtration rate period. Where as, nanofibrils are more orientated in layers with more passage of time; as the deposition of the nanofiber mat on the membrane enables the fibers to rearrange themselves in a specific anisotropic orientation, i.e., they are unidirectional. The interesting focus around filtration is how quick and efficient it is compared to casting. One of the main reasons for, the arrangement of fibers in accordance with difference in their in-planar orientation is due to the pressure difference applied at the membrane. Practically, shown by Obed (2019) when a fluid flows from the downstream side of the filter to its upstream side, there will be a change in the original pressure due to which some of the momentum of the fluid is transferred to fibers as drag force, given by:

$$F^* = F_f \mu U_0$$

Where, F= drag force (F) acting on a unit length of each cylinder/fiber.

The drag force working on the nano-fibrils opposite to the motion of the fluid, will let them align themselves in a certain direction resulting in different properties. A slower filtration rate will give

rise to a more ordered fibril orientation with high packing density. Whereas a faster flow/filtration rate can result in less time for nanofibers to align themselves with a lower packing density and random fibril entanglement.

To add, a faster filtration rate results in a higher shear force on the nanofibers due to higher shear rate is working on the fluid. Shear rate can be calculated by both geometry and speed of the flow of the fluid. The shear rate, γ, is defined as the velocity gradient perpendicular to the direction of flow, and can be calculated as:

$$\gamma = \frac{dv}{dy}$$

where dv is the change in velocity in the y-direction and dy is the distance in the y-direction and the shear rate, reciprocal seconds, denoted $s^{-1,}$ or 1/s.

Viscosity is another important parameter engaged during filtration of nanocellulose fibril suspension. It is the resistance to flow. The viscosity, η, is the relationship between the shear stress and the shear rate.

$$r = \eta\gamma, \; r = shear\ stress\ and\ \gamma = shear\ rate$$

Nanocellulose filtration is a laminar flow in presence of a pressure difference applied but at the same time, the viscosity of the CNF suspension increases with time of filtration. This gives rise to dynamic viscosity and this viscosity of the nanocellulose slurry influences the resistance to flow and contributes to the pressure drop across the filter. The phenomenon of the increase in viscosity with time during the filtration of nanocellulose fiber slurry through a porous membrane to form a wet cake of nano-paper is commonly known as filtration consolidation. This phenomenon occurs because as the nanocellulose fiber slurry is filtered through the porous membrane, the individual fibers in the slurry start to encounter each other and form a network of entangled fibers.

As the filtration process continues, more and more fibers become entangled, resulting in a denser and more compact structure. This, in turn, leads to an increase in the viscosity of the slurry, as the movement of the fibers through the pores of the membrane becomes more restricted. The increase in viscosity (dynamic viscosity) also leads to a slower rate of filtration, which means that more fibers can intercalate with each other and form a denser structure.

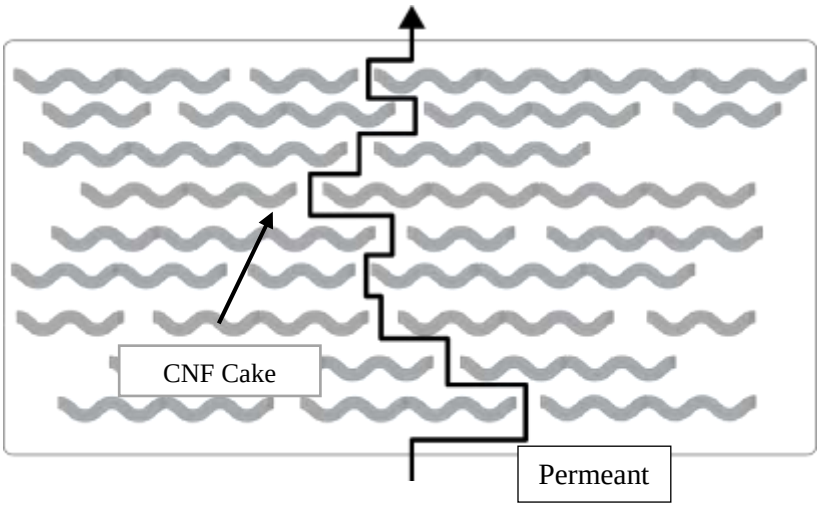


Figure 2.24. The fibrils form a network.

During the 1800s, a renowned French scientist Henry Darcy formulated an equation, famously known as the Darcy's Law. This equation defines the flow of fluid through porous media and through beds of other porous materials. The equation defines that the flow of the fluid (units = volume per time) flowing through a porous membrane on a filtering platform of length L, and area A, is given by equation below. The negative sign is because the fluid flows down (negative) the hydraulic gradient from higher values to lower values:

$$Q = -\frac{kA}{\mu}\frac{\Delta P}{L}$$

Where, Q is the volumetric flow rate (mL^3/s), k is the permeability of the membrane (m^2), A is the area of the membrane (m^2), ΔP is the total pressure drop across the membrane where the vacuum is provided (mm Hg.), and L is the length of the bed (m) and u being the viscosity of water (filtrate) (unit).

Darcy's Law: The rate of flow of fluid through a porous medium is directly proportional to the pressure gradient across the medium and cross-sectional area of the medium and inversely proportional to the viscosity and length of the medium (Perlmutter, 2014).

The discharge rate Q is the volumetric flow (mL/s) but generally the flow of fluid is written in terms of speed or velocity. The discharge head can be re-arranged by dividing throughout by area A to express in Darcy Flux.

$$q = \frac{Q}{A} = -K \frac{dh}{dx} \left[\frac{m}{s}\right]$$

Hence, the differential equation for Darcy's law is:

$$U = \frac{Q}{A} = -\frac{k}{\mu} * \frac{dp}{dx}$$

Here, μ is the superficial velocity of flow (m/s) and the negative sign shows the pressure is decreasing in the direction of the flow.

In accordance with these equations, it can be noticed that for a particular slurry/suspension, the volumetric flow output is directly proportional to the permeability coefficient "k". The pressure difference ΔP being the driving force for the fluid to flow through the membrane. In this context, the flow of the slurry/solution is laminar.

2.7.6.2. Permeability and Pressure Drop

One important factor which has an impact on the Darcy's law is the "permeability" of the membrane. Permeability is the property of the membrane which depends on porosity and raw material used to manufacture it. It is a property by the virtue of which CNF slurry can easily pass through the membrane. According to filtration, the pressure drops result in a form of resistance to flow and influences the fluid in this case, the CNF slurry through a complex fibrillar maze of pores that form during the nano-paper formation. These are due to fibers bonding with each other and distributing like mat of interwoven fibrillar network.

Porosity is the amount of void space present in the total volume fraction of the material defined by the relation:

$$\psi = \frac{Vvoid}{Vtotal}$$

Porosity and tortuosity will increase resistance in flow but also influence the structural properties of the nanopaper.

2.7.7. Solution Casting Methodology:

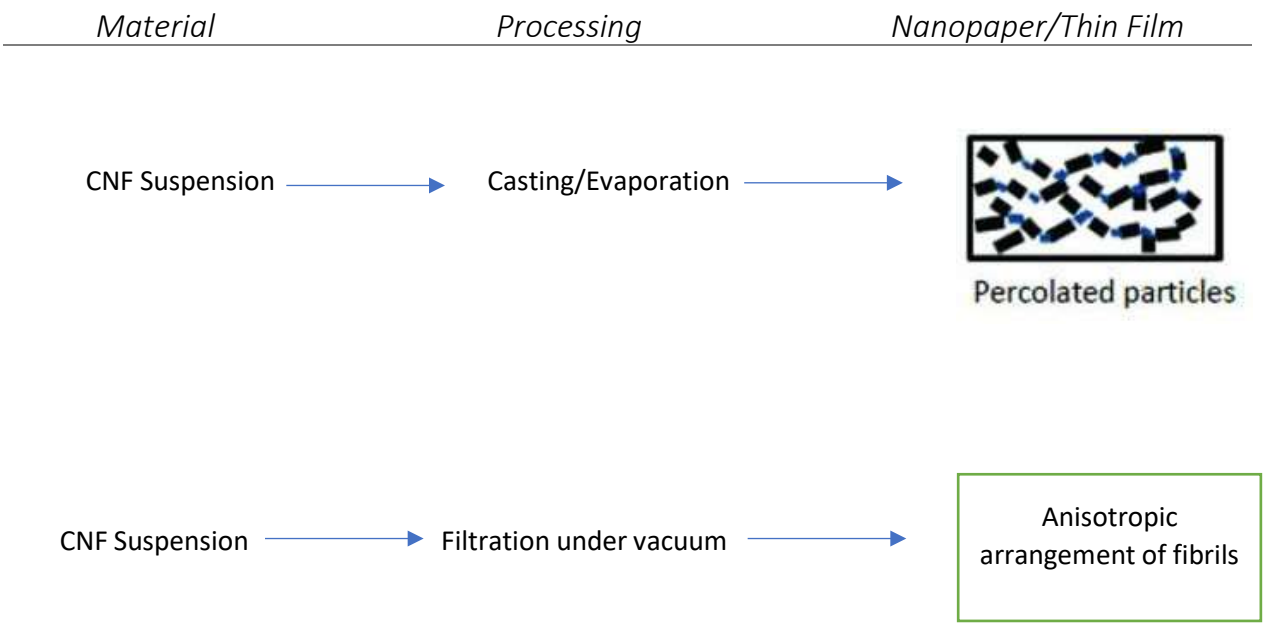
Solution casting has been a widely used coating technique to manufacture nanocellulose thin films. Over the years, solution casting has led to the development of various polymer re-enforced composites. With compared to suction filtration, casting not only retains almost 100% of the fibers but also could be fine tuned to have different properties by controlling the rate of evaporation (CNP Fabrication, 2014). In this method, different composites of phases are dispersed in a suspension by dispersing them and eventually evaporating the solution. After evaporation when the solvent is completely removed, a wet cake or thin film is left behind. Various procedures are considered like constant agitation, stirring or sonication for easy dispersion of the nanofibrils in it (Bhatnagar and Sain, 2005).

Solution casting and vacuum filtration are two main methods of preparing CNF-based thin films. Even though both lead to formation of "wet" cakes, but two methodologies are fundamentally very different. According to Zuo, (2016), solvent casting causes a rather increase in concentration, homogenously when the solvent evaporates. This leads to some degree of aggregation as nanoparticles in this case nanofibrils have high surface charges leading to constant state of instability.

Isobe, (2018) in their research proposed how solution casting gives clear transparent nanopaper but only at lower concentrations around 0.5wt.%. Even though, this diluteness can lead to a few problems such as a greater energy consumption and extended time for drying. CNF fibrils remain individually isolated at lower concentrations. Li (2020), in their experiments have shown multi-stage drying through constant-drying period and falling drying period by regulating the humidity conditions. Even though higher RH prolongs the drying period of the films but maintaining a humidity between 40-70% reduces overall haze of nanopaper.

In Zhu, (2013), haziness in nanopaper is the measure of forward light scattering. This could be calculated by knowing the transmitted and scattered light travelling through the films. Isobe, (2018) also claimed that the haziness of the nanopaper was monotonically increasing with its concentration. CNF slurry consisting of solutions tend to give rise to in-homogenous aggregation in dispersion. The bigger aggregations give rise to cavities which are formed due to an uneven tight packing of the fibers. Unlike drag forces acting on fibrils in filtration imparts enough driving force to arrange the fibrils along the planar direction; evaporation causes nanopaper to take its

shape in casting. The change in weight helps to find the amount of water lost in the process of drying over time. This can be accounted for by measuring the drop in weight with the help of a weighing scale.



2.8. Porosity and Concepts of Porosity through Percolation of Nanofibers duringNanopaper formation

The extent of porosity in nanopapers due to processing parameters have a significant impact on their mechanical properties. This is governed by the temperature and drying conditions while preparing the films. Due to presence of air voids instead of nanofibrils, the ultimate tensile properties such as strength and modulus are deteriorated to greater extent. Besides porosity, density of nanopapers plays an important role in suggesting a positive characteristic trend for modulus and strength. Lower porosity in CNF films results in a denser nanofiber network which ultimately exhibits CNPs with higher packing density. Hsieh, (2016), showed increase in light scattering for nanopapers with low density as fibers were disproportionately distributed over the fiber matrix. The extent of porosity of these films give rise to percolation concept in nanopaper. According to research established, it has been made evident that with decreasing porosity integral properties of the film/nanopaper are pronounced till a great extent.

The percolation concept deals with the connection amongst fibers while the nanopaper is fabricated. Fiber's entanglement and conformation lead to the development of a connected network in a multiphase system. Due to lower concentration of fibers, no network can be detected.

With increasing concentration of the disperse phase in this case nanofibrils, a further connectivity is established. Each site can be randomly occupied with probability *P*, or unoccupied with probability *(1-P)*. The occupation of the site defines its local property. When the chances of site occupation with CNF increases then a percolation threshold is reached, which is the establishment of a continuous network this gives rise to a synergistic effect this is, φ_t. Porosity or void fractions amongst fibers are air cavities that form due to lack of fibrillar connection at those points. Hence, the two concepts percolation and porosity are very closely related. The importance of the percolation networks discusses that some properties such as mechanical, strength will improve sharply when the volume fraction of the dispersed phase exceeds this threshold. Porosity of nanopaper is calculated by one minus the ratio of density of the film found from its mass and volume and cellulose density as outlined in below equation,

$$\rho_{cellulose} = 1.5\ g/cm^3$$

$$Porosity = 1 - \frac{\rho_{nanopaper}}{\rho_{cellulose}}$$

Specific pore volume of the nanopaper can be defined as:

$$V_P = \frac{1}{\rho_b} - \frac{1}{\rho_s}$$

$\rho_{cellulose} = \rho_s$, $\rho_{film} = \rho_b$

2.8.1. Percolation Model

A percolation threshold model defines this phenomenon very clearly. This model was proposed by Redondo, (2022) to describe the mechanical properties of cellulose and polymer nanofibers.

This model considers a homogeneous filler distribution as well as dispersion across the matrix. Here, in case of nanofibrils it explains fibrillar interaction and bonding due to Van Der Waals forces and hydrogen bonding. The beginning of percolation describes a lot about the filler's aspect ratio. Anywhere below the threshold φ_t, the series of mechanical properties follow a simple series model. And above it, they form an assembly of rigid network like structure.

The percolation model states as:

E_c= modulus of the thin film

E_n= rigidity of network

$$E_c = \frac{(1 - 2\psi + \psi\,\varphi_f)E_m E_n + (1 - \varphi_f)\psi E_n}{(1 - \varphi_f)E_n + (\varphi_f - \psi)E_m}$$

There is an upper and lower bound for these volume fraction φ,

$$\psi = \begin{cases} 0 & \text{for } \varphi_f \le \varphi_t \\ \varphi_f\left(\dfrac{\varphi_f - \varphi_t}{1 - \varphi_t}\right)^b & \text{for } \varphi_f > \varphi_t \end{cases}$$

The upper bound is the maximum potential property for a thin film regardless of the phase geometry.

The lower bound is the minimum amount of filler required to create a continuous network showing minimum possible mechanical characteristics of porosity (**ψ**).

Now to simplify, the volume fraction of the percolation threshold φ_t assumes an isotropic filler arrangement and a fixed aspect ratio:

$$\varphi_t = \frac{\frac{2L}{D} + \frac{4}{3}}{\frac{32}{3}\left[1 + \frac{3}{2}\left(\frac{L}{D}\right) + \frac{3}{8}\left(\frac{L}{D}\right)^2\right]}$$

m, f and c, refer to matrix, filler, and thin film composite respectively. φ_f is the volume fraction of the filler, b=0.4 is the critical percolation exponent (pre-established) for a 3D percolating network. E_m, E_n, E_c are young's modulus of matrix, filler, and thin film.

It is important to keep in mind that the filler here is air, as 100% nanopaper was considered while fabricating the films (Shen, 2023).

2.9. Polymer Infusion to Enhance Optical Properties of CNP – Thin film composites.

Attributing to porous nature and fiber type from chemical purification nanopapers scatter light and only show contact transparency. Transmittance characteristic enhancement requires to process and produce the film composites mostly depend on the NC dispersion within the main polymer matrix, which is important for the performance of the final material.

There are several processes for making cellulose-based composites:

- Solution Casting – Used widely in packaging industries and film applications.
- Impregnation – As a filler for improving barrier properties.
- Coating – Coating NC films with conductive materials for renewable electronics as well in pulp and paper industries.

An interesting property yet to discuss, is the ability of nanopaper to transmit light through it. Plastic substrates because of their high flexibility and transparent behaviour host a lot of high performing electronics which have been developing over the years. Although plastic substrates have been in the pinnacle, there are a lot of drawbacks in dealing with them. Some of these factors add to pollution, its high processing parameters, and instability. Paper based products due to their tunable and modifiable fibers as well as nanofiber dimension can transmit light instead of scattering it. When the fibrillar dimensions are smaller than visible light range (400-700) nm then cellulose can help propagate light instead of scattering it. Scattering is the phenomenon where due to the difference in the refractive index (n) of cellulose nanofibers and its surroundings the incident light undergoes scattering instead of getting permeated. Regular paper composed of microfibers (~25 µm diameters) are rough and course with peak-to-valley roughness values up to hundreds of micrometers. On the contrary, nanopapers fabricated either via casting or filtration with slight modifications can be rendered hazy transparent or even transparent. The presence of pores even though increases the resultant surface area of the CNP, also causes haziness due to light scattering.

These are voids on the nanopaper and due to a difference in the refractive indices between CNF and air as well as irregularity in pore shapes, the light tends to deviate from its regular path. The cumulative scattering of light results in only contact transparency that is only when nanopaper is in direct contact with the substrate.

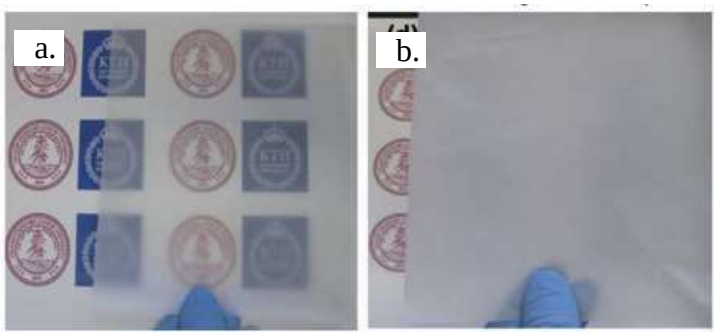


Figure 2.25. Nanopaper in contact with substrate underneath indicate its transparent properties (a) and (b) same nanopaper 2 inches from the substrate showing its large light scattering referenced from Liangbing 2013.

To minimize this scattering and tangibly increase the clearness of these films, they could be treated with the help of some additives or polymers of similar chemical together with refractive properties. The insertion of some acrylic resins or synthetic polymers could provide nanofilms with better mechanical aspect and end up increasing their transmittance more than 80% (Hu, 2013).

This half of the research discusses the use of two synthetic polymers, Polyvinyl Alcohol (PVA) and Polymethyl methacrylate (PMMA). PVA is a water-soluble synthetic polymer derived from vinyl acetate. PVA is a thermoplastic polymer, that becomes mouldable at an elevated temperature and is widely used in film-forming properties, with good strength and transparency. PMMA is a hydrophobic alternative which is also a transparent thermoplastic polymer. Acrylic resins can form continuous film when used as a coating in nanocellulose films.

Even though CNF are hollow fibrils and not spherical by nature, Rayleigh's law could provide us with some insight about the factors governing transmittance:

$$\frac{I}{I_o} = \exp\left[-\frac{3\phi_p x r^3}{4\lambda^4}\left(\frac{n_p}{n_m} - 1\right)\right]$$

Where I and I_o are the intensity of transmitted and incident light respectively, ϕ_p is the volume fraction of the particles, x is the defined optical path length, r is the radius of the spherical particles, λ is the wavelength of light, n_p and n_m are refractive indices of particles. According to this law,

transparency of CNF films depends on (a) refractive indices of the materials (b) size of CNF (c) volume fraction of CNF which can be related to their porosity.

2.9.1. PVA and Cellulose nanofibrils (UW) – A Hydrophilic Alternative

PVA with 89.00-98.00 molecular weight and 99% hydrolysed was used with UW CNF refined slurry. “99% hydrolysed” refers to the degree of hydrolysis of PVA molecules. Here, water molecules hydrolyse acetate groups (-$COOCH_3$) into hydroxyl groups (-OH). PVA with higher molecular weight results in longer polymeric chains giving rise to enough opportunities for entanglement and interpenetration with nanofibers. PVA is one of the most biodegradable with a refractive index of 1.47. The CNF (UW) and PVA films were fabricated through solvent casting method. PVA crosslinked with the hydroxyl groups of water to form homogenous solution. CNF solution was highly ultrasonicated before blending with PVA. The two were mixed under vigorous stirring for one and a half hour to obtain the PVA/CNF hybrid solution. PVA has independent hydroxyl groups that link with other hydroxyl groups of CNF. Besides hydrogen bonding the intertwining of PVA and CNF chains occur during film formation.

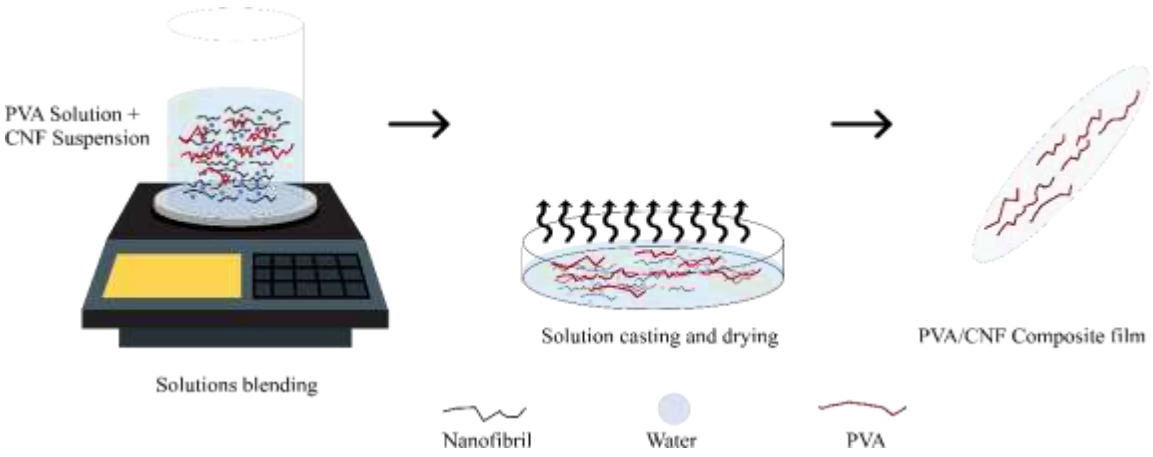


Figure 2.26. Linking of PVA and CNF at an elevated temperature and film formation through Casting.

2.9.2. PMMA and Cellulose nanofibrils (UW, UM) – A Hydrophobic Alternative

PMMA is a thermoplastic transparent polymer composed of methyl methacrylate monomers. These monomers are bonded with ester linkages (-COO-) that polymerize to form PMMA. During film formation, owing to the similar refractive indices(n) between PMMA, n=1.49 and CNF,

n=1.45, (Niskanen, 2022a) the resin films up the gaps between nanofibrils thus increasing the total porosity and 92% of visible light pass through it. Even though the melting point of PMMA is much lower than nanocellulose about 160^{o}C it has excellent UV resistance properties making it suitable for outdoor applications (Jamaluddin, 2021).

Nano paper being hazy makes PMMA a great candidate as a pore-filler to counter the disadvantages of CNF. Moreover, the backbone of PMMA consist of carbon and oxygen atoms, with methyl groups(-CH_3) attached to them .The absence of polar groups such as hydroxyl or carboxyl groups contribute to its hydrophobicity (Turbak,2018). PMMA being a nonpolar liquid dissolve in organic solvents like xylene, toluene, and chloroform. Chloroform was chosen as the designated solvent for the dissolution of methyl methacrylate.

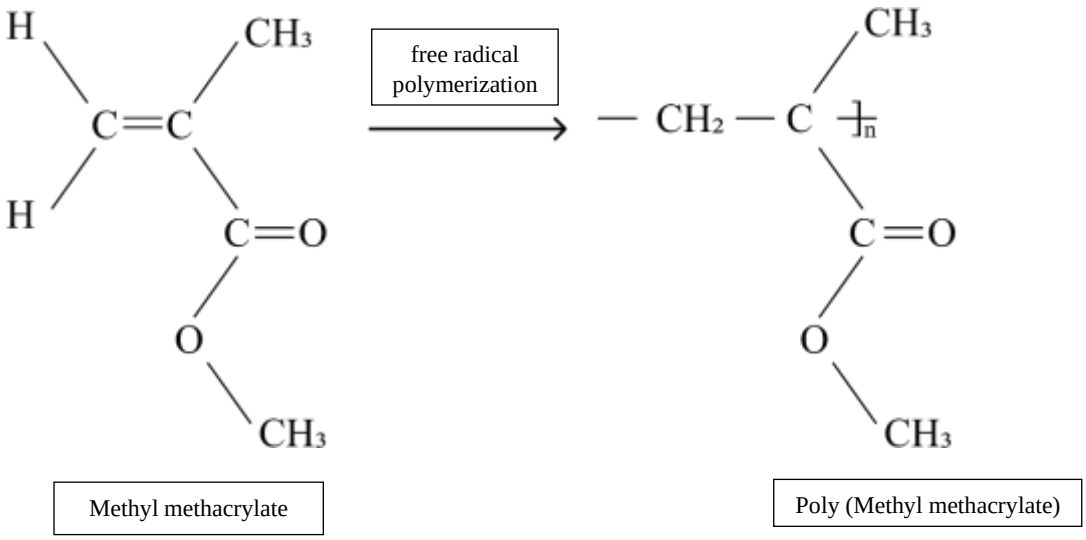


Figure 2.27. Showing polymerization of Methyl Methacrylate to Polymethyl methacrylate.

UV crosslinking is a popular method for curing acrylic based resins. Any acrylic resin will contain photo initiators which absorb UV light and generate free radicals in their excited state. These free radicals react with the monomers present in the coating and by attacking the double bonds of PMMA, initiating a sequence of polymerization (Andrzejewska, 2001).As this phenomenon progresses, the acrylic resin particles form a constant three-dimensional network enhancing their properties.

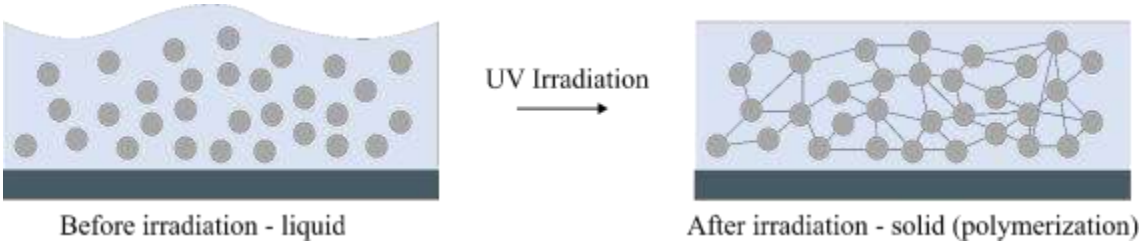


Figure 2.28. UV crosslinking of acrylic resin coated Nanopaper under UV irradiation.

The PMMA can form a continuous film matrix when used as a coating on CNF films. The AR solution fills in the voids and pores of nanopaper through capillary action.

Capillary action or wicking refers to the phenomenon of fluids imbibing into pores due to surface energy through action of capillary pressure. Capillary pressure is the differential pressure between inside and outside of a curved surface (Nogi, 2009b).

This is also known as Laplace pressure and for a pore with a circular cross section (*radius=r*) and the pressure is given by:

$$P_{cap} = 2\Upsilon_{lv} * \cos(\theta)/\mathrm{r}$$

Where, Υ_{lv} are free energies of the liquid vapour interface and θ is the contact angle measured via experimentation.

The resin not only attributes to the smoothness by reducing light distortion but also elevates the paper's mechanical strength (Song, 2018a). This enhanced durability makes nanopaper a perfect suit for optoelectronics (Gao, 2019a).

2.10. Conductive Nano paper and Deposition of Silver Nanowire as a conductive filler on CNP

Next generation green electronics have attracted immense attraction owing to its high load bearing capacity, low surface roughness, excellent optical properties. Silicon based materials and plastic based substrates such as Silicon Dioxide and PET. But due to their low thermal stability, non-biodegradability, and oxidising properties these substrates have impeded the growth of new compelling devices such as electronic skin, solar cells, OLEDS and many more. Nanopapers being highly tractile and lower surface roughness than regular papers, allow deposition techniques such

as ink-jet printing, sputtering and filtration to develop conductive lines (Hsieh, 2013). To mitigate surface roughness, researchers have developed nanopaper with smooth texture by modifying the processing conditions as shown by Barr, (2011). Gao, (2019) designed a flexible perovskite solar cell with a total power conversion energy around 3.2 %.

A significant challenge faced during the development of conductive nanopapers with efficient optical properties is to improve conductivity while maintaining optical transmittance. Non-uniformity amongst conductive materials such as silver nanoparticles and dispersion of conductive materials over the substrate without considerable loss of transparency effect the working performance of devices Van De Groep, (2012); Kim, (2013).

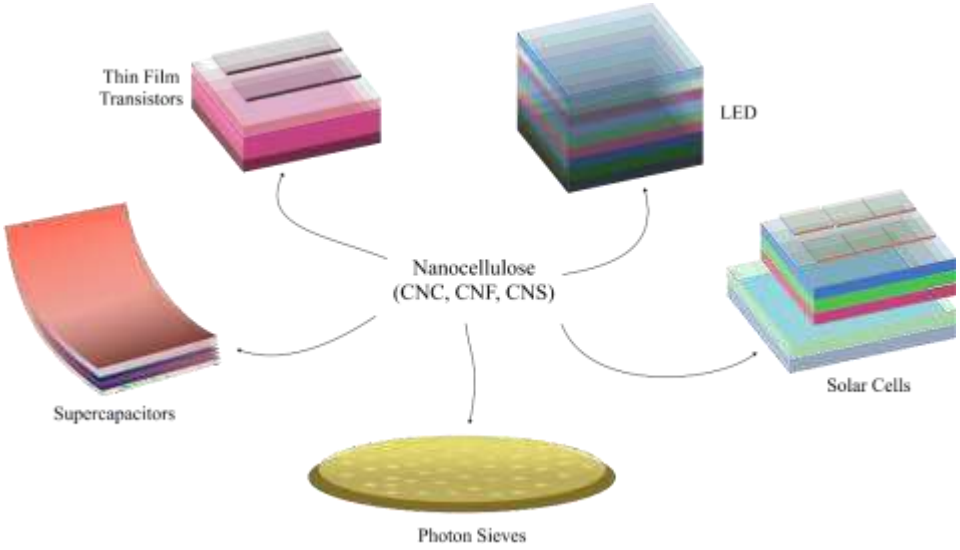


Figure 2.29. Integrating nanopaper and nanocellulose in optoelectronics and device architecture fabrication.

For electronics, electrical properties like di-electric constant and resistance are of major importance. The di-electric constant of neat cellulose is around $k = 6$ *or* 8 whereas, for porous nanopaper it falls to around $k = 1.3$ *to* 4 at 1MHz (Tobjörk and Österbacka, 2011). CNP has been demonstrated as a gate insulator in devices. This has been achieved by adding certain materials eg., oils, electrolytes and resins (Liao, 2016). As shown in figure 2.29., nanopapers can be widely used in OLEDs and LEDs as a transparent screen, for energy storage purposes in supercapacitors and batteries as a flexible electrode, solar cells and photovoltaics such as Perovskites have promising scope to employ CNPs due to their propitious optical haze which elongates the optical path length for more absorbance of light rays directly converting the energy (Liao, 2016). Nanopapers are also widely used as a substrate for photovoltaics (PV) due to their bendable

properties. Regular paper has been applied in PVs, but the gross current density and open voltages were sufficiently low giving rise to poor performance. A solar cell using poly (3- hexylthiophene) (P3HT):1-(3-methoxycarbonyl)-propyl-1-phenyl-(6,6) C61 (PCBM) on a paper substrate was also made; however, the resulting performance was not as expected.

Porous nanopaper makes it more efficient to fabricate these devices and enhance their performance by providing structural advantages to manipulate electrons, ions and even photons. This subdivision of the thesis deals with turning nanopaper conductive by infusing some conductive material while preparing each specimen. Silver nanowire has very high intrinsic conductivity around 6.29×10^{7} $(\Omega.m)^{-1}$. They have high aspect ratio and thermal stability which makes them a good alternative than other expensive nanomaterials. The conductive nanopaper encompasses their resistivity, bending limit and firmness under various conditions. Compared to its other competitors like indium tin oxide, which is highly brittle and breaks easily (Chen, 2001) silver nanowires have gained popularity solely based on their stability and high conductance (De, 2009). Yiming, (2020), were successful in preparing a novel CNF/AgNW conductive paper with unique hierarchical features through "blending and filtering" procedure. The nanopaper showed increased conductivity with higher doses of nanowire solution. A conductivity as high as 154.7 S/cm was noticed in these papers suitable for EMI shielding. They exhibited high values of young's modulus at 2.1 GPa, advancing their strength. (Liu, 2022a), founded a nanopaper with a conductivity around 1615 S/cm with only 0.5wt.% AgNWs on a nano-paper surface.

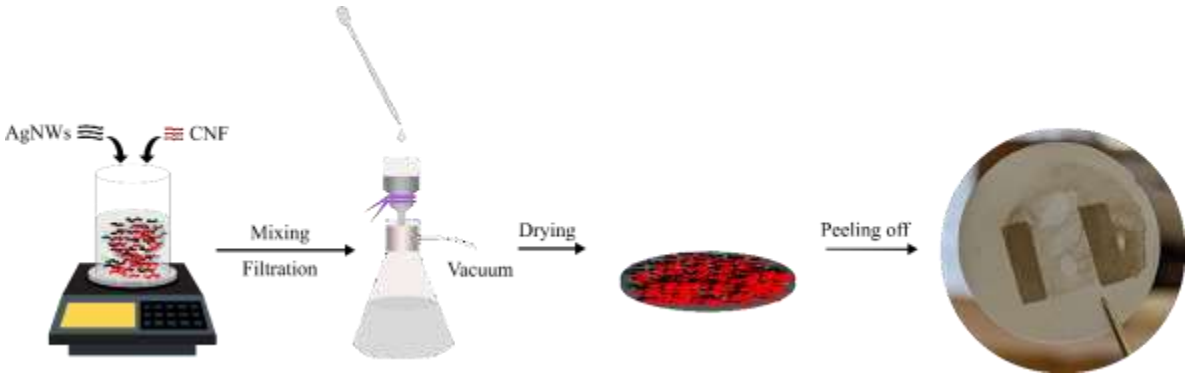


Figure 2.30. Representing a method of filtration to deposit nanowire suspension on CNP.

2.10.1. Electrical Conductivity

Nanocellulose altered its electrical property from insulator to conductor with the addition of conductive fillers. The conductivity majorly depends on the deposition method and on how well the nanowires are connected amongst each other within the nanocellulose matrix.

A continuous network where the nanowires are connected and inter-linked will govern the conductivity of the specimens. According to statistical percolation theory of geometry of conductive fillers, percolation process refers to the formation of a continuous conductive passage through the nanopaper. The nanowires being randomly distributed in the matrix define the percolation network. Percolation was said to occur with the interconnection of nanowires covering the initial defined system. The percolation threshold is the minimum concentration of nanowires required to create a connected pathway; below this point, the nanowires are too dispersedly distributed and above the threshold the linked nanowires provide a pathway for the electrons to travel.

Identifying the percolation threshold would help modify the characteristic traits of conductive nanopapers before incorporating them into different applications.

The percolation theory for conductive nanowires state that, the conductivity of films σ depends on volume fraction of conductive filler Φ and can be expressed as the scaling formula:

$$\sigma = \sigma_0.(\Phi - \Phi_c)\text{^}t$$

Where, σ_0 and Φ_c are conductivity of fillers and percolation threshold respectively. 't' is the critical exponent which depends on the sample's dimensionality and scalability. The value of t changes with each material. By examining for 2D and 3Dimensional networks value of t has been between t=1.6 and 2 (Nguyen, 2014), defines how a component behaves around the percolation threshold. The experimentation has showed an increase in conductivity with increasing the volume fraction of nanowires attributing to the formation of conductive pathways. The conductivity was measured via two different methods: (i) 2 Probe Multimeter Method (ii) 4 Probe Measurement Method.

Advantage of Using 4 Probe over 2 Probe Measurement:

2 Probe Method using Multimeter	4 Probe Method – Linearly distributed probes
• Two Probe method is appropriate for measuring resistivity of high resistivity samples, e.g., polymer films. The resistivity is calculated from the voltage drop (V) and current (I) as: $$\rho = \frac{RA}{L}$$	• As the current I is added through the point contacts located on the having a uniform resistivity ρ; the current distributes radially and the current density around the contact is given by: $$j = \frac{I}{2\pi tr}\, r$$ And resistivity is given by: $$Rs = \frac{\pi}{\ln(2)} \frac{\Delta V}{I}$$
• Contact and spreading resistance are large and true resistivity cannot be separated from measured resistivity.	• Contact and spreading resistance are low with voltage probes and true and measured resistivities can be differentiated.
• 2 probes for measurement.	• 4 equidistant probes for measurement.

Rough nanopaper surface can lead to fault when printing or depositing conductive nanowires, leading to manufacturing defects. Decreasing roughness also decreases porosity of the nano paper (Xuezhu, 2016). Some devices nanopaper has supported are listed below:

- Solar cells: Extent of haziness in nanopapers let's them integrate with solar cells as a conductive electrode or a light absorbing substrate especially in crystal cells like perovskites. Gao, (2019) demonstrated a nanopaper with high scattering through deposition of silver nanowire and nanotubes. Ha, (2014), developed angle-independent transparent paper infused GaAs solar cell.
- Organic Light Emitting Diode: OLEDS displays require high transparency and good flexibility. OLEDS are fabricated mainly on glass and PET. But the rigidity of glass and low coefficient of thermal expansion of polyethylene not only increases cost but is also a lengthy process to fabricate films. CNPs on the other hand stands as a good replacement for these substrates. Zhu et al. 2013, manufactured a highly flexible OLED with 100% nanocellulose (Fang, 2014).

- Supercapacitors: CNPs are widely incorporated as electrodes on supercapacitors. High surface area and porosity may be modified accordingly to increase capacitance of these devices. Capacitance is the ability of a material to hold charge. Kime(2018), prepared BNC nanopaper from a species of glucoacetobacter. It showed significant capacity of 20 mF/cm^2 (Wang, 2017).

Outlook

Recently scientists have widely based their research on finding sustainable and bio-derived substrates to replace non biodegradable materials like PET, glass in electronics to mitigate the production of yearly electronic wastes. Materials such as nanocellulose has attracted a lot of attention due to its programmable biodegradability, tunable surface properties, mechanical strength and low toxicity. Nanopaper provides various features generally not found in regular paper such as high transmittance and lower porosity. Even though some extent of porosity is natural and tuned according to its application. For wearables,

CNPs has excellent flexibility and bendable nature. Whereas, for optoelectronics the haziness and transparency of nanopaper can be implied. At the moment, deposition of conductive materials such as nanowires, tin-doped indium oxides, carbon nanotubes should be deemed to be industrially scalable into making solar cells, LEDs, conductive sieves etc.

Even though scientific exploration on nancoellulose is at a full swing, various drawbacks have limited their scalability. Such as heat dissipation in electronics is an unavoidable issue even with the use of NC, high hygroscopicity of CNPs due to their hydrophilic nature may degrade the electronic, roll-to-roll production of nanopaper is still not possible to their high cost of manufacturing and need of special membranes while film formation.

To summarise, NC has shown promising results when composed of other polymers and expressed flawless characteristics as a film. The surface qualities can be adjusted by introducing hydrophobic materials on their surface during extraction procedures. Overall, good flexibility and high light transmittance makes nanopaper an efficient substrate for electronics.

Chapter 3 Materials and Methods

3.1. Materials

In this chapter a detailed description is done about the raw materials and methodology used for the extraction of nanocellulose fiber, preparation of nanopaper and film composites. All raw materials either prepared in the laboratory or purchased are also mentioned here.

3.1.1. Materials

Listed below are different sources of fibers and chemical reagents used for this research project. The cellulose sources originated from United Sates and Canada. Dried CNF fibrils were purchased from the renowned University of Maine, Forestry Department, USA and two different sources of Bast Fibers were purchased from USA and Canada, respectively. Chemicals and reagents were all provided by either Millipore Sigma, Fisher Scientific and VWR, all located in Canada.

The materials are articulated further in each segment of this chapter.

Raw Fiber (Hemp)

In the production of nanocellulose fibril slurry, hemp from *Cannabis Sativa* bast as well as bast-hurd fibers from three different sources were used. These were broadly supplied by Unretted-Processed (UP) Bast Fibers from IND Hemp Oil Seeds & Fiber, United States. The cellulose content among UP Bast Fibers were as high as 96.59.

Freeze -Dried Nanocellulose Fiber (Softwood)

The freeze-dried nanocellulose fiber was provided by the Process Development Center of University of Maine, United States. The standard CNF slurry was bleached and freeze-dried to produce up to 98.0% fines (CNF content). The cellulose is insoluble but dispersible in water near neutral pH. Nominal width of fibers was around 45-50 nm according to Philips CM10 transmission electron microscope (TEM), with their lengths varying up to certain hundred microns. The fibers were extracted from Softwood- *Pinus*. The self life of the nanofibers were around 2 years. A detailed specification sheet has been attached to the appendix at the end of this thesis.

3.1.2. Chemicals for Treating Hemp Fibers to obtain CNF (UW):

1) Sodium Hydroxide:

Laboratory based Sodium Hydroxide (NaOH) pellets, ACS ≥97.01% and with a density of 2.13 g/cm^3 at 20 °C was purchased from Sigma Aldrich, Canada. They were white round pellets, and it deliquesces when contact with atmospheric conditions. Recommended to keep it sealed when not in use.

2) Hydrochloric Acid (HCL):

37% concentrated Hydrochloric Acid, ACS ≥95% and a density of 1.2g/mL at 20 °C was purchased from Fisher Scientific, Canada. HCL is a transparent liquid and highly corrosive and recommended to be used under the fume hood.

3) Hydrogen Peroxide (H_2O_2):

30% concentrated Hydrogen Peroxide was bought from Sigma Aldrich, Canada. It has a vapour density of 1.11 at 30°C. This acts as the oxidising agent during bleaching of cellulose.

4) Sodium Silicate ($Na_2SiO_3.5H_2O$)

Lab grade Sodium silicate was ordered from Ward's Science, United States. The chemical is in anhydrous state and appears white in colour with a density of 1.18 g/mL at 30°C.

3.1.3. Chemicals to Form Film-Composite with CNF:

1) Polyvinyl Alcohol (PVA)

Polyvinyl alcohol granules were provided by Millipore, Canada with molecular weight around 89,000-98,000 and 99% hydrolysed. The viscosity of the material is about 11.6-15.4 cps at 20°C. PVA has a white or off-white appearance possibly due to their semi-crystalline structure.

2) Polymethyl methacrylate (PMMA)

PMMA with linear formula $[CH_2C(CH_3)(CO_2CH_3)]n$, was used as an acrylic resin in coating of the nanopapers to increase its visual transmittance. PMMA is a thermoplastic polymer composed of methyl methacrylate monomers. It was purchased from Millipore Sigma, Canada. Their average density is around 1.2 g/cm^3 and are highly insoluble in water.

3) Silver Nanowire Solution – AgNWs

Silver nanowires dispersed in 0.5 wt% isopropyl alcohol suspension with dimensions as (l×d) = 120 nm ×50 µm. A vial of 25 mL was purchased from Sigma Aldrich, Canada. The dimensions were chosen according to the pore diameters noticed in nanopapers formed under several temperature ranges. The visual appearance of silver solution was greyish to yellowish grey and rendered the CNPs grey when filtered onto them.

3.1.4. Apparatus used to extract CNF from Hemp-Bast Fibers:

1) Milling Sieve

UP Bast pulp was washed after every step of chemical pre-treatment with a US standardised testing sieve no. 325 according to the ASTM E-11. The sieve is about 19cm in diameter with a mesh opening of 45 microns. A curved flat based sieve is attached to the collection container that helps to classify and separate the milled material according to different size fractions. A sieve of mesh opening of 1/8" 3.1 mm was considered for this purpose, which determines the size range of the material that can pass through it.

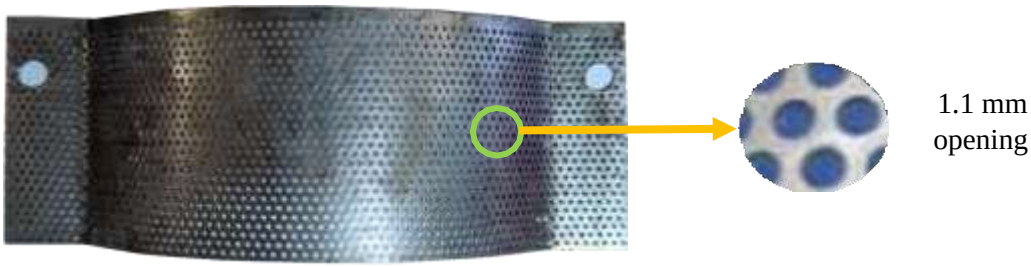


Figure 3.1. Typical sieve with 3.1mm opening for the Thomas Wiley Mill, Model 4

2) Condensation Reflux Column

The condensation column is used to assist the chemical reaction for extracting CNF by accelerating the reactions thermally. The fiber mixed with chemicals is agitated and immersed in a silicon oil bath, and the condenser helps to cool down the vapours formed in the column and return them to the round bottomed flask.

3) Ultrasonicator

An ultrasonicator from Sonics Vibra Cell Model VCX 130. The ultrasonic device generator creates sound waves to agitate particles in a solution. The net power supply of this device is 130 Watts working at a constant frequency of 20KHz. The sonicator is provided with a 6mm probe which can process liquids up to 50mL.

3.1.5. Nanopaper Fabrication Apparatus

1. Solution Casting Set-up Apparatus:

1.1. Polystyrene Petri Plates

Polystyrene petri plates about 86mm in diameter from Thermo Fisher, Canada which were lined with Glass-Fiber Reinforced Teflon sheets from Fluoro Plastics, USA were used as the medium to cast the CNF suspensions.

1.2. Glycerol

Ultrapure glycerol, 99.5+% was purchased from Fisher Scientific, Canada. Glycerol has a steady melting point around 290 °C and a specific gravity around ≥1.249. The main motif to use glycerol was to plasticize the films for ease in separating them from the petri plates.

2. Filtration System Set-up Equipment:

2.1. Filtering Funnel

A Buchner funnel with fine porosity disc with fritted glass is used. The holding capacity of this funnel is about 150mL with pore size about 10-15 um (Porosity = medium) was purchased from PYREX$_{tm}$ from Thermo Fisher, Canada. The diameter of this stage is around 5.9cm which highly governs the size of the nanopaper thus formed.

2.2. Vacuum Filtration Kit for Films

A standard filtration kit from VWR Filter holder with a fritted glass support base. The stage is 4.7cm even though the working exposed surface area is around 4cm as discussed in the results and discussion section. The unit is supplied with a 300mL graduated cylindrical funnel.

2.3. Poly-Vinyl Di-Fluoride Membrane

Durapore membrane filters made of poly-vinyl di fluoride and hydrophilic in nature was provided by Sigma Aldrich, Canada. The filters came in two different diameters (size) of 4.7cm and 6.0cm respectively. The water permeation rate/flow rate is about >0.33 mL/min-cm^2. They have a porosity of about 70% and maximum withstanding temperature of 85 °C.

2.4. Vacuum Pump

A Welch (8917) Vacuum Pump was used to provide the necessary vacuum required for the filtration system. The pump could produce a maximum vacuum of 29 in. Hg observed in a Swagelok Vacuum Gauge. The flow of vacuum from the pump into the filtration column was regulated with the help of a "T" shaped bleed valve which maintains a uniform flow. Needle valves are vastly incorporated to regulate the pressure inside the vacuum filtration column. To decrease the overloading vacuum created in the system, the valve is opened slightly to release a small amount of gas and this process is known as "bleeding off".

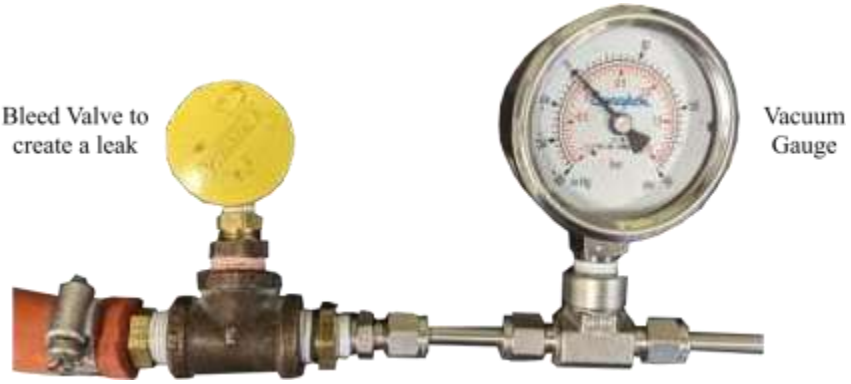


Figure 3.2. A bleed valve to create a leak to apply low vacuum and a vacuum gauge from Swagelok to observe the pressure difference.

2.5. Semi-Automatic Sheet Former Machine for Pressing Bound Water

The Semi-Automatic Sheet Former Machine Model UEC 2005D was provided by Universal Engineering Corporation, India. The paper forming machine is equipped with a pneumatic sheet press fastened by four support rods and the bottom of the press was made movable with the help of a pneumatic cylinder fixed with the table. The equipment has two pressing options – Pressing I and Pressing II. The wet cake of nanocellulose web like structure is carefully peeled off and placed between two Whatman Filter papers and stacked centrally in the press with a drying plate made of stainless steel on the top. The effective pressure is raised to 400±10 kPa for 20 seconds continually.

This helps in getting rid of the bound water in CNF cake and smoothen out the wet network surface for drying in the later stages.

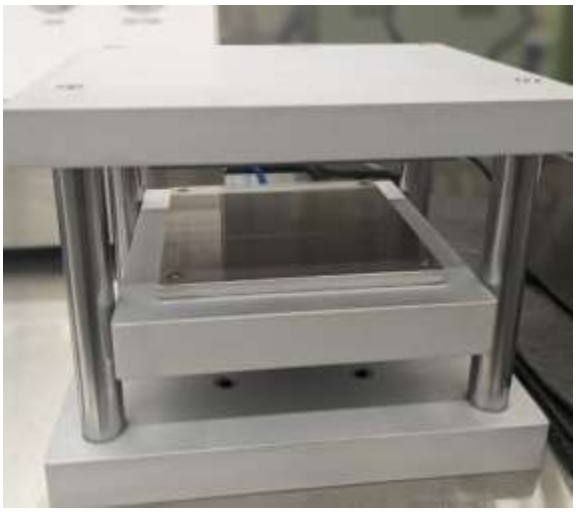


Figure 3.3. Press provided with the Sheet Former machine.

2.7. Drying of Nanopaper through Hot Pressing

Hot pressing of nanopapers formed from filtration works by applying heat and pressure to the nanocellulose film composite. This process is carried out by two large parallel plates of hot press to dry the nanopaper and consolidate it through rapid evaporation of the water. The plates are heated to different ranges of temperature starting from – room temperature (when no heat is applied) to 110°C for variable timings. This technique is widely used by authors, to dry nanopapers and films for faster production of samples. Figure 3.4. depicts a typical bench top parallel hot press that was used in this research project.



Figure 3.4. Parallel Hot Press

3.2. Methodology:

3.2.1. Methodology to Extract Nanocellulose Fibers (CNF) to produce Nanopaper:

Mechanical Disintegration

Materials:
Hemp: Un-retted/Processed Bast hemp fiber
Procedure: Hemp bast fibers were mechanically chopped and disintegrated into smaller particles in a mill known as the Wiley mill, suitable for chemical treatment further.
Sieves used: 3.1 mm in opening.
Rate of disintegration: 100g/hour, depending on method and rate of feeding.

This mill was manufactured by Thomas Scientific, USA Model 4, is particularly used for grinding fibers with minimum moisture loss. In the mill, the material is loaded into the hopper, from the hopper the materials are guided by gravity into the path of a revolving steel blades mounted on a stationary box as noticed in figure3.5. Revolving knives work against the stationary knives and the disintegrated fibers are forced through a sieve with an opening of 3 mm and collected in a collection vessel underneath. It rotates at 800 rotations per minute and at a frequency of 60 Hz. A safety switch is provided on the right side of the adjustable knob.

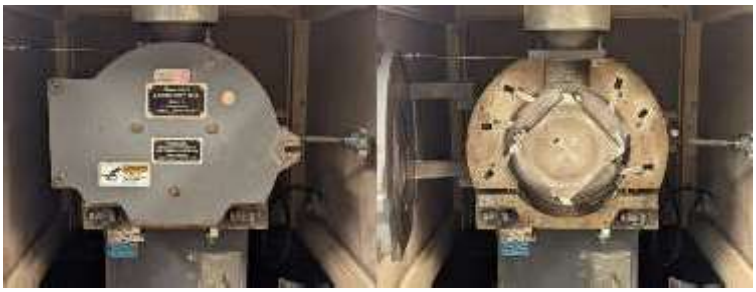


Figure 3.5. Standard Thomas Scientific Wiley Mill Model 4.

In a sequence, a series of chemical treatments are done to remove impurities such as pectic polysaccharides, hemicellulose, and lignin from the fibers. These impart colour to the nanocellulose are hence undesirable for the end product.

These sequential steps are especially performed to extract good grade cellulose and to decrease energy consumption during the fibrillation process.

1st Step: First Alkaline Treatment (10 wt.% NaOH)

Materials – Disintegrated fibers –3mm, sodium hydroxide pellets, tap water, flat bottomed beaker, magnetic pellets.

Concentration – 100g fiber + 400 g NaOH pellets + 4000 mL tap water.

Procedure – About 100g fibers are weighed and kept aside.

400 g NaOH pellets were weighed and added to a flat beaker and about 4000mL water is added to it.

This solution was agitated at around 200-300 rpm on hot plates without any temperature.

After good homogenization of the solution, fibers were added and left to react.

Reaction occurred in room temperature for 4 hrs with mild agitation.

NOTE: All the above steps were carried out carefully with PPE and under the fume hood.

The fibers were washed with water thoroughly at the end of the reaction until neutral pH.

2nd Step: Second Acidic Treatment (1M HCl)

Materials – First treated fibers (kept in cool condition), hydrochloric acid (HCl, 37% concentrated, Fisher Scientific), beakers, tap water, magnetic pellets, reflux condenser column.

Concentration- 100g fiber+ 262.4mL hydrochloric acid + 3200 mL of tap water.

Procedure- 1) The alkaline treated fibers submerged in water was filtered using a U.S Standardized sieve (25um opening).

2) 2 flat beakers (2L) were filled with 400 mL of water first and 131 mL of HCL was added to the beakers and made up to 1600 mL each. This was to avoid boiling and splashing.

3) Each balloon is added with 25 g of fibers and 800mL of chemical solution is added to each

4) The balloons are attached to the reflux column and treated for 2 hrs at 80°C with mild agitation (about 200-300 rpm). A schematic of the reaction is shown in figure 3.6.

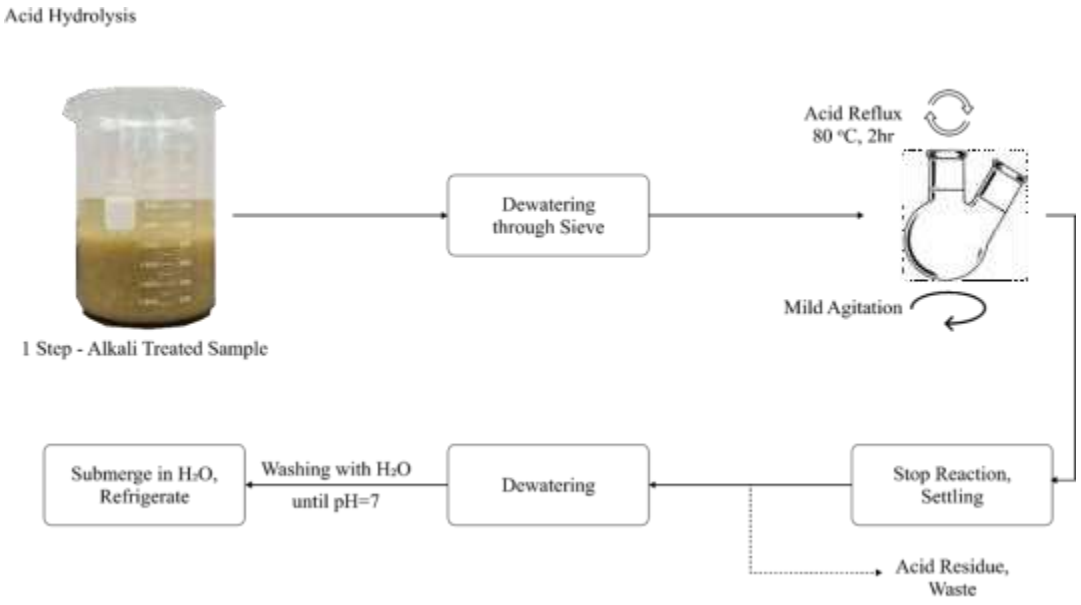


Figure 3.6. Schematic flow diagram of Acid hydrolysis of cellulose (Hemp Bast Fibers).

3rd Step: Alkaline Treatment (5 wt.%)

Materials: Acid and alkali treated fibers kept in water (cool condition), NaOH pellets, round bottomed flasks, reflux condenser column, magnetic pellets, tap water, spatula and weighing scale.

Concentration: 100g fiber+ 160 g NaOH+ 3200 mL tap water.

Procedure: 1) Two flat bottomed 2000mL beakers were filled with 200mL first and each beaker was added with 80g of NaOH pellets, this solution on each were stirred continuously.

2) The solution while in continuous agitation was made up to 1600mL in each beaker with NaOH pellets getting dissolved.

3) Around 25 g of fibers were introduced in each of the four round bottomed flasks and 800mL of stock solution was added to the round flasks.

4) Balloons were attached to condenser column and reacted at 80°C for 2 hrs with mild agitation.

The fibers were washed with water thoroughly at the end of the reaction until neutral pH.

Washing was done with a US standardized sieve with a mesh opening of (25-45) microns and 18cm in diameter, mesh number 500.

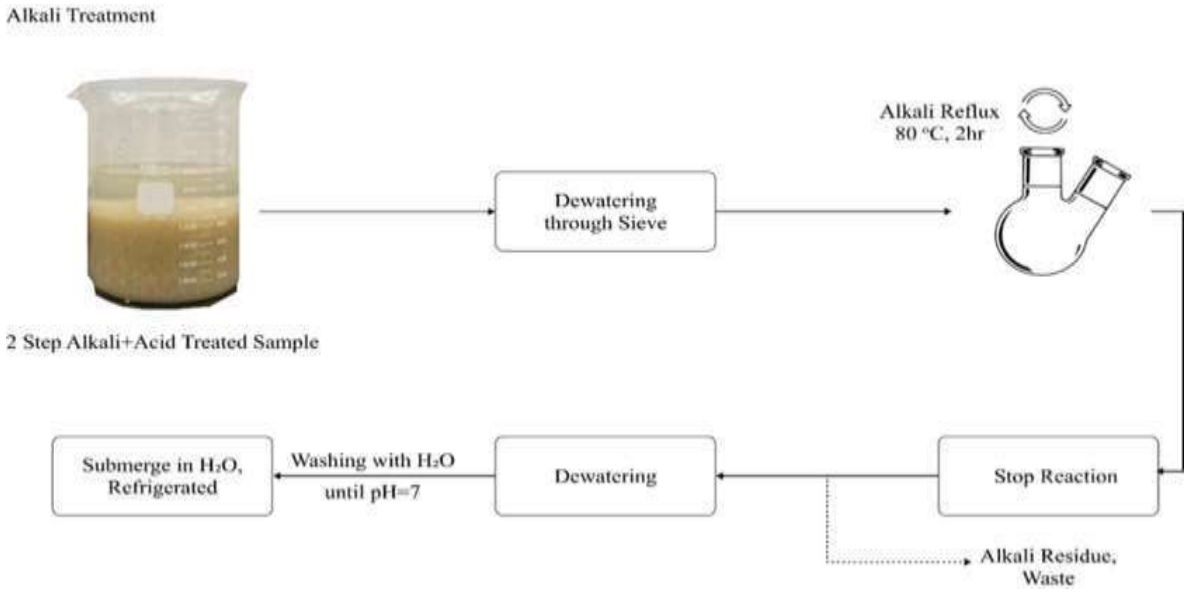


Figure 3.7. Schematic Flow Diagram of Alkali Treated Fibers after NaOH treatment.

Final Step of Chemical Treatment

Bleaching with 2 wt.% Hydrogen Peroxide (H_2O_2)

Materials: 30% concentrated Hydrogen Peroxide (Fisher Scientific), Sodium Hydroxide (NaOH) pellets, Sodium Silicate (Na2SiO3), tap water, magnetic pellets, reflux condenser column.

Concentration: 100 g pre-treated fibers+24g NaOH pellets+ 213.12 g H_2O_2+ 96 g Na_2SiO_3

Procedure: 1) Pour 200 mL of tap water in a flat-bottomed flask and consecutively add 12g NaOH pellets, 196 mL $H_2O_2$was weighed via measuring cylinder and 48g of Na_2SiO_3 (anhydrous) to this solution. Makeup to 1600 mL of tap water in this 2000 mL beaker. Repeat this for the second beaker.

2) Keep the solutions stirring with mild agitation for 10-15 minutes. Until a homogenous solution is obtained.

2) Weigh and add 25g of fibers in each round bottomed flask and add each of the 800 mL solution into the round bottomed flasks.

4) Attach these flasks to the reflux condenser and reacted at 80 for 3 hours.

The chemically bleached fibers were washed with tap water until neutral pH was received.

3.2.2. Masuko Sangyo – Supermass Colloider/ Refining of Cellulose to Nanoscale Slurry

The extraction and production of nanofibrils is implemented by fibrillating chemically treated cellulose fibers into nano-scale fibrils with strong mechanical treatment. For this purpose, a grinder commonly termed as Masuko Sangyo Super Mass Colloider MKCA6-5J ®, Tokyo, Japan was used. This consists of feeding the pulp constantly at a uniform rate through the stainless-steel hopper and engages breakdown of cell wall structure by imparting shear forces created by two grinding stones moving in countersense direction. The production of CNF by passing a 5 wt.% concentrated pulp for around 15 cycles gave rise to nanofibrils with diameter ranging between 25-50 nanometers. The pulp fed to the refiner, is less coarse than raw hemp fibers is forced through a gap between the rotary and stationery stones. The stones are made of nonporous resins and aluminium oxides or metallic oxides. Once, the pulp meets the grooves on the stones they are

grounded by compression, shearing, and rolling friction forces that fragment the fibers into sub-structural fibrils through fibrillation. The distance between the stones can be adjusted and with passage of more cycles, cellulose is fibrillated farther closing the gap from 1.5mm distance to 1.15mm clearance between the two stones. The grinding of pulp required as many numbers of passes as 12-15 cycles with respective gaps to observe nano-size fibers. Whereas subsequent passes did not alter the morphology any further. To mitigate clogging of fibers, the disks were adjusted to a higher gap which enables the flow of material from within.

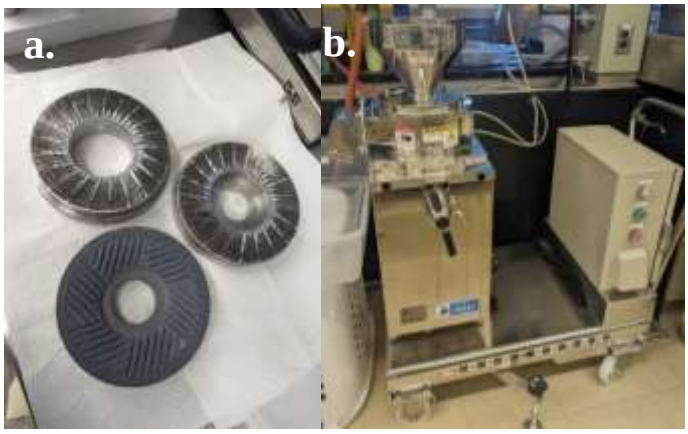


Figure 3.8. Masuko Sangyo Super Mass colloider MKCA6-5J ® used in lab to produce CNF.

3.3. Methodology to Fabricate Nanopaper through – Solution Casting and Vacuum Filtration

Nanopaper Processing and Fabricating Methodology

3.3.1. Solution casting

The CNF sources were first dispersed in tap water by ultra-sonication for 1 hour to form a homogenized suspension. A consistent concentration of 1.5wt% of suspension was prepared each time of the two sources. The freeze-dried suspension was first thoroughly mixed in a Ninja NJ600WMC professional blender to get rid of bigger aggregates before degassing in a sonicator. 15 g of CNF slurry was weighed and dropped on teflon lined polystyrene petri dishes 86mm wide. The petri plates were kept undisturbed for 72 hours in room conditions around 25°C±3 and 50% relative humidity. CNF slurry which was added with plasticizer- Glycerol, were crosslinked first on a hot plate (MS304S, Mettler Toledo, Switzerland) with mild agitation for an hour at a constant temperature of 70°C.

3.3.2.Vacuum Filtration

A suspension as low as 0.05wt%- 0.3wt% was prepared to sonicate. The suspensions were sonicated completely, followed by vacuum filtration for 10minutes for the bigger membrane (6cm in diameter, 0.1 μm PVDF, VVLP09050, Millipore Sigma, Canada) and 30 minutes for the smaller filtering membrane (4.7cm in diameter). Filtration time may differ if the same membrane has been re-used more than 3 times. This arises from clogging of the infinitesimal pores of the membranes. The filtration process was carried out until there was a 30 second difference in the last few drops of filtrate and a wet mesh like cake was formed with 90% bound water content.

The cake was peeled off from the membrane and sandwiched between two thin Whatman filter papers (Whatman Filters, No. 45, England) and pressed in sheet former to do away with the excess free water of nanocellulose cake. Samples were dried under room temperature as well higher temperatures in a parallel hot plate at pressures around 2.4 MPa and between 50 ˚C-110˚C.

3.4. Addition of Polymer to fabricate thin film composites.

3.4.1. Casting PVA/CNF Films

Standard solutions of 200mL with varying CNF and PVA quantities by weight were obtained. The PVA solutions were homogenised on a hot plate (Mettler Toledo, Switzerland) at a constant temperature of 70˚C for 1 hour; following which the CNF and PVA suspensions were mixed under constant stirring and subjected to mild sonication thereafter. About 20g of each solution were casted on polystyrene petri plates of 86mm diameter. The petri plates were left for drying outside at room temperature (20-25) ^{o}C and normal relative humidity for 24 hours. Then they were inserted in a convection drying oven at 40^{o}C and monitored till completely dry. Their thickness was measured by a digital micrometer was around 50 microns for these thin film composites.

3.4.3. Depositing PMMA on CNF nanopapers

PMMA was weighed in a scale and slowly mixed with chloroform in smaller proportions over a period of half an hour while agitating in a hot plate at 50 ^{o}C.

The solution was kept for an hour at 50 ^{o}C. until it was homogenised, and a clear liquid of some viscosity was obtained. For better dispersion of the polymer, it was subjected to sonication for 30 minutes. The samples were pre-conditioned at 50 ^{o}C, before coating. Acrylic resin (AR) is coated over nanopaper from UM, UW through three modes of coating and their efficiencies are also noted.

The coated sample was then cured in a UV crosslinker at a constant wavelength of 365 nm and energy dosage of (12×10^4) μm/cm^2 for 6 minutes and dried in a vacuum chamber at 90 ^oC following the next 24 hours.

3.4.4. Deposition of Silver Nanowire (AgNWs) on CNP Produced from UW CNF

All substrates fabricated were from UW CNF slurry of a diameter 4cm each. Nanowires were provided by Milipore Sigma, Canada of high aspect ratio (*diameter*×*length=120 nm* ×*50 μm*). The nanowire solution was filtered through the same column as nanocellulose in a chronological sequence right after filtering the CNF suspension to form the wet mesh of nanopaper. The aqueous solution of silver nanowire in Iso-propyl Alcohol (IPA) at a specific concentration (10mL) was added and filtered in the same manner. The sheet obtained was pressed in the paper machine and dried in the hot press at room temperature with a pressure around 2.4MPa. The film composite was then fitted between two metal plates and left in room for drying for the next 48 hours.

3.5. Cellulose Nanofiber (CNF) Characterization Methodology

Optical Microscopy

Optical microscopy images of milled fibers were observed by Leica MDG36 connected to a digital camera. The magnification used was 12.6 times. Each fragmented fiber was separated from one another with a help of a sharp pointy needle under the microscope.

Transmission Electron Microscopy

The Transmission Electron Microscopy was performed to observe the dimensions of the refined slurry as well as freeze dried nanofibrils, especially their diameters. TEM uses a stationery electron beam transmitted through a thin sample and transformed into non-uniform electron ray. The scattered electrons are focused by an electromagnetic objective lens into the image plane.

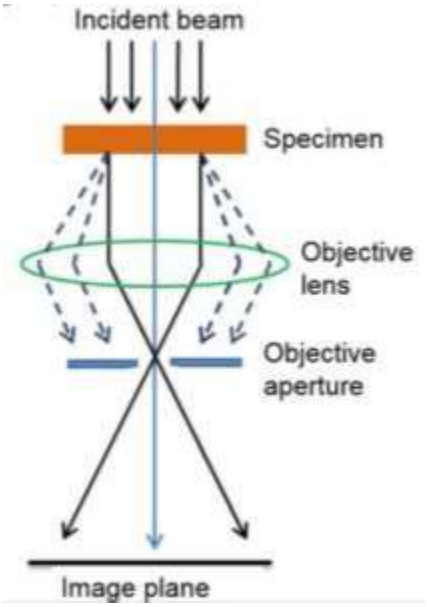


Figure 3.9. Schematic diagram showing the method of image configuration in bright-field imaging mode in TEM. Dashed lines show the scattered electrons revised from Reza 2015.

A Philips CM10 TEM was used in this procedure. A CNF suspension of 0.1wt.% was prepared by diluting the existing nanocellulose for both UW and UM samples. The suspension was highly sonicated for 3 hours to disperse the fibrils in order to obtain a very homogenize sample. Agglomerates would cause the fibrils to bind together when observed underneath the microscope.

A 2uL drop of this suspension is added with the help of a digital pipette onto an ultra-thin Copper mesh also known as, TEM grids coated with Formvar to hold the fibrils in place of 200 mesh size (01700-F, Ted Pella, USA). The grids were dried overnight in under the fume hood and analysed under TEM. It is important to correct the background before imaging in TEM, to obtain a good contrast between the fibrils and substrate medium. A magnification as high as 64 000x was worked on to attain desirable micrographs.

Chemical Composition Characterization – Fourier Transfrom Infra-Red Transmission

The chemical composition or available functional groups of fibers were attenuated by Fourier Transform Infra-Red Transmission (FTIR). The FTIR used here was a Bruker Tensor 27 / Hyperion 2000 FTIR System. A flat round pellet consisting of mixture of 1% cellulose nanofibers sample in potassium bromide (KBr) was pressed with each step of chemically treated dried powdery fibers to analyse on FTIR. The tests were carried out under the transmittance range of 4500cm^{-1} and 500cm^{-1}. FTIR analysis follows a standardization according to ASTM E168, 1252.

3.6. Cellulose Nanopaper Characterization

3.6.1. Mechanical Properties

Tensile testing to examine the young's modulus and strength of the nanofilms were carried out using the universal tensile testing machine provided by TestResources Inc. MiniTec apparatus. The specimens formed were cutout in a dog-bone shape as specified by ASTM D882-12 for micro tensile testing of thin films.

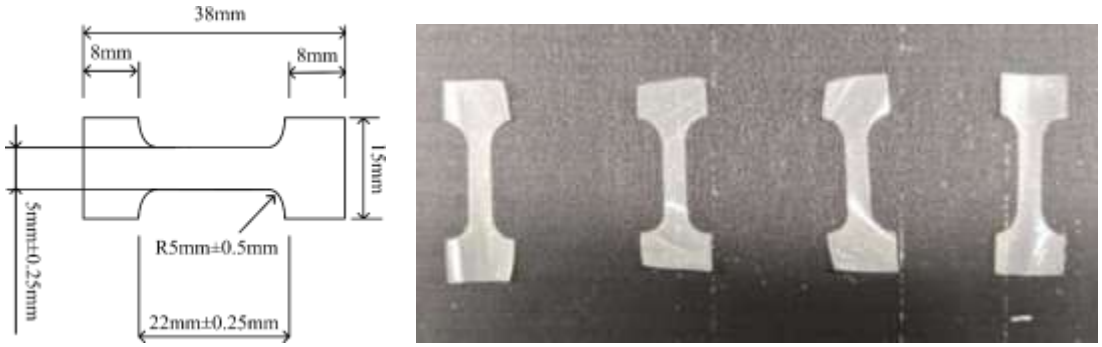


Figure 3.10. Dog-bone shaped films were moulded in compliance to ASTM D882-12 for tensile testing of PVA/CNF thin-films.

Micro-tensile testing was chosen to avoid any excess material processing and use. As noticed in figure 3.10., there is a thin rectangular section which is subjected to the test, by gripping the specimen with the long side of it parallel to the loading density. As seen in figure 4, the rectangular dog bone structure is 22mm in gauge length, and a width of 4.40±0.3 mm with a thickness varying between 30-90 μm or 0.03mm to 0.09mm.

Around 10 specimens of each kind were tested for significance in tensile values. The specimens were tested at a crosshead speed of 5mm/min equipped with a pre-load of 0.2N. All samples were preconditioned in a humidity chamber at 23°C ± 3°C and 50%±5% relative humidity.

3.6.2. Water Contact Angle Measurement

The contact angle measurement was done in accordance with ASTM-D5946 a standardization test for contact angle measurement of polymer films. The set-up consists of a source of illumination, the stage to place the drops equipped with a minute syringe, and a microscope coupled to a CCD camera. An LED light bulb is used to provide light of equal intensity. A small specimen of

dimension 2×2 cm was cut and pasted to a frosted microscopic slide with the help of double-sided tape.

Two different liquids – (a) Water (b) Diiodomethane were used as reference liquids which attributed the surface energy of films fabricated under different conditions. To measure the contact angle, a drop consisting of 2 μL was formed at the tip of the hypodermic needle attached to a screw syringe. The substrate is then raised till it touches the sessile drop by controlling the Y axis of the stage (the stage is a flexible X-Y translation stage). The syringe is supplied with a New Era NE-1000 Syringe Pump which is responsible for forming the spherical drop. After the immersion of a drop on the substrate, the gradual change in the contact angle is measured and calculated with a circle fitting approach as this approach fits best on the drop. This is captured by an inbuilt MATLAB software for the following 30 seconds, with 3 seconds of interval for all the samples.

3.6.3. Optical Properties

Thin films of samples with $4\times1_{(l\times b)}$ cm in dimensions were attached to a Peltier cuvette holder. The UV Vis used for this study is a Jasco J-815 with 150 W Xe arc lamp. The samples were measured between a wavelength of 200-800 nm with a 163-900 nm (Nitrogen gas purge).

The transmittance and absorbance values were determined with air as the standard. To calculate transmittance formula has been used:

$$T\ (\%) = 10^{(2-Absorbance)}$$

3.6.4. Surface Morphology

3.6.4.1. Scanning Electron Microscopy

The scanning electron microscope was used to determine the surface topography of the nanopapers. A Carl Zeiss Leo 1530 Gemini Field Emission SEM was used to analyse the samples. The specimens were gold sputtered before inserting into the equipment. Magnification such as 10 000x was used in the secondary electron mode. Cross-sectional images were obtained by breaking the samples or cutting them with a fresh razor blade under cryogenic conditions using liquid nitrogen (N_2).

3.6.4.2. Porosity

The density of nanopapers were calculated from their real weight and dividing it by the area and thickness of each sample dried under different temperature. The two parameters, thickness and drying temperature were inversely correlated. Thickness was measured with a digital micrometer. Porosity was mathematically calculated according to the equation below considering the nanopaper density and cellulose density as 1500 $kg.m^{-3}$ as mentioned in PubChem properties of Cellulose, respectively.

$$Porosity\ (\%) = (1 - \frac{\rho_{nanopaper}}{\rho_{cellulose}}) \times 100$$

3.7. Polymer Combination to Produce Thin-Films

Deposition of PMMA (Acrylic Resin)

Polymethyl methacrylate granules (PPMA) were purchased from Millipore Sigma, Canada has a chemical formula (C5H8O2)n. The granules were weighed in a scale and dissolved in Chloroform (CH_3Cl) under constant agitation. Nanopapers were mounted on a glass petri dish taped on either side with translucent tape. About 150-200 µL of the solution was pipetted out and dropped on the CNP. A microscopic slide was pulled at an angle. The sample was cross linked in a UV crosslinker.

3.8. Electrical Characterization of Conductive Nanopaper

3.8.1. 2 Probe Measurement

The electrical conductivity was measured with the help of two probe multimeter EX410A, Extech Instruments, USA. The resistance (R) was measured along the length (l) of the specimen and their total area exposed (A). Samples were pre-conditioned by keeping in a desiccator containing absorbent, and humidity as low as 12%±5%. Silver nanowire was filtered on the nanopaper to turn it conductive.

Resistivity can be calculated by,

$$\rho = \frac{RA}{L}$$

Where A is area,

$$A = L \times t$$

Substituting value of A in previous resistivity formula,

$$\rho = \frac{R \times L \times t}{L} = R \times t$$

Conductivity (S/cm) is the reciprocal of the obtained resistivity:

$$\sigma = \frac{1}{\rho}$$

Resistances measured via 2 probes included a parameter, also known as "contact resistance," as the current is passed through the same two probes measuring the voltage difference between two points. Probes were maintained at a constant distance of 0.5cm (L) from each other while measuring. A repetition of 5 measurements were averaged to find the value.

3.8.2. 4 Probe Measurement

The four-probe measurement or the Kelvin technique, named after the scientist, is a resistance meter working on DC current (I) between the two outer probes while the ones in the middle calculate the voltage drop across the specimen (V).

It is a rather popular method to calculate the conductivity (σ) of thin conductive films. Here, 4 probes are co-linearly arranged and the sheet resistance (R_s) can be calculated as follows:

$$R_s = \frac{\pi}{ln2}\frac{\Delta V}{I} = 4.53236\ \frac{\Delta V}{I}$$

Where, ΔV and I value could be gathered directly from the multimeter used by Keithley TestSources, USA. If the thickness of the material is known, then the resistivity (ρ) can be found by:

$$\rho = Rs.t$$

And t is the thickness of each sample depending on the loading density (g/cm^3) of the samples. The conductivity was again measured as the reciprocal of the resistivity thus found. The inter-connection of nanowires was compared to the percolation concept which stated that nanowires require to reach the percolation threshold otherwise under this threshold the film composites are highly resistant to the flow of electrons. If the thickness of the film is considerably larger than the distance between probes, then or if the sample is around 40% smaller than the probe spacing the aforementioned formula holds true. Each substrate was analysed 5 times on either side of the specimen, but resistance was only noticed on the filtered side.

Chapter 4 Results and Discussion

4.1. Bast Fibers and Fiber Characterization Mechanical Fragmentation

The source of fibers- unretted processed (UP) Bast Fibers from IND Hemp Oil Seeds & Fiber, United States. Figure 4.1 shows a schematic of the process of grounding fibers in the mill at a rate of 100g/hr which has been standardised. IND Hemp from USA was most widely used to produce CNF slurry for this research.

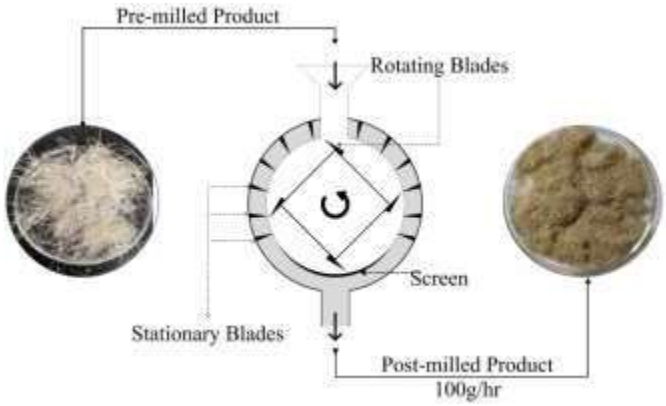


Figure 4.1: Working Mechanism of Thomas Wiley Mill

Morphology

They were apparently powdery and placed on a laboratory glass slide sized (1" x 3" (25.4x76.2mm) drenched in a drop of water. This let the fiber individualise and separate making it easier to analyse. A tabular column gives a direct relation of the fiber length to its aspect ratio. The lengths of the fibers from three different sources did not vary as such (shown in Table 5).

Table 5 Lengths of fibers after Milling and their respective aspect ratio.

Length of Fiber (µm)	Aspect Ratio of 3mm Fiber	Length of Fiber (µm)	Aspect Ratio of 3mm Fiber	Length of Fiber (µm)	Aspect Ratio of 3mm Fiber
1059.2	5	3510.6	24	3087.4	41
1946.3	9	3324.5	25	4144.5	41
2141.7	12	3730.6	25	4123.4	46
4792.0	13	3551.2	26	2890.4	46
5105.3	14	3990.5	26	4170.2	50
2785.1	15	3279.9	27	8208.8	54

2584.9	15	5276.3	28	3274.1	56
2979.0	15	3214.1	28	6985.7	59
1971.5	16	3137.8	29	6868.8	72
3012.1	16	5391.8	30	5328.2	73
2605.0	20	3731.7	31	5172.1	75
4253.8	23	4158.4	32	5950.8	85
4887.0	24	4512.2	39	3439.2	104
2686.9	24			6307.6	105

The aspect ratio obtained through analysing is classified as poor or good in nature. According to the aspect ratio obtained from the analysis, the fibers after first step of disintegration showed a range of size from 1000 microns to around 6000 microns. The variation in their length depends on the pattern of feeding through the hopper, the number of times the fibers are rotated inside the grinding chamber in the rotating blade/shaft also the starting fiber bundles provided by the manufacturer. CNFs are considered for their high aspect ratio and fiber length and an initial fiber length of a few thousand microns make it a good source for subsequent treatments to extract the desired nanocellulose.

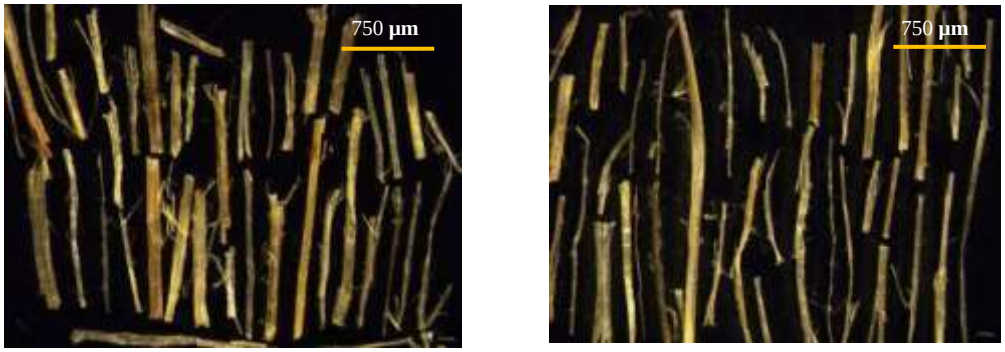


Figure 4.2. Bast fibers after dis-integration under optical microscope separated from each other.

Depending on the aspect ratio, a histogram distribution of their sizes has been displayed. Maximum particles have an aspect ratio between 15-35, which typically means that the lengths of the fibers are 15 to 35 times longer than its width.

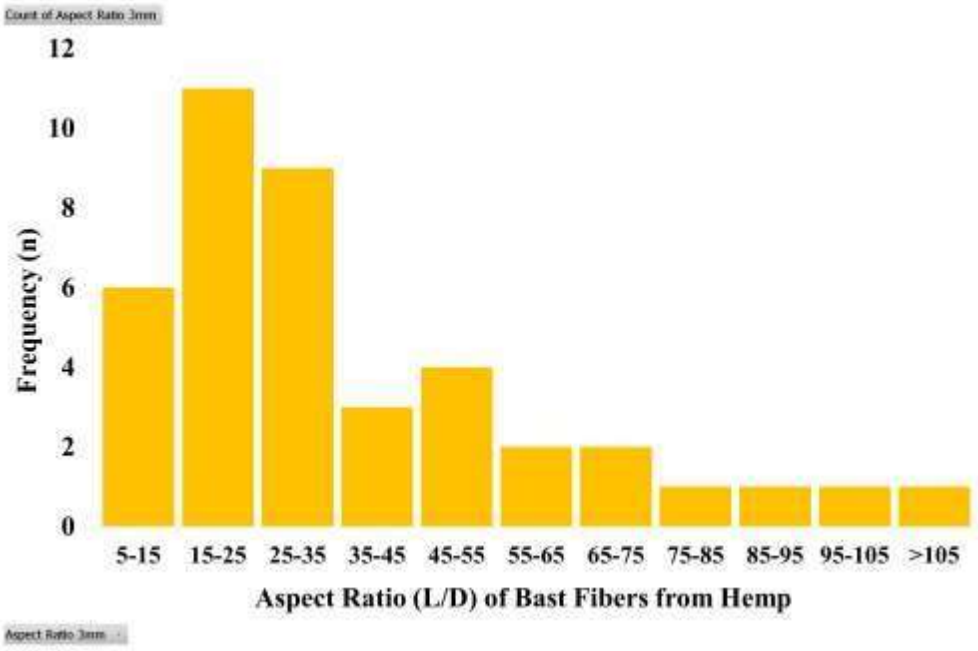


Figure 4.3. Histogram of Aspect ratio (L/D) after mechanical breakdown in the Mill

4.2. Chemical Pre-Treatment

The fibers after first step of mechanical grinding were subjected to a series of chemical treatment or chemical degumming. These cumulative steps help in dissolving all non-cellulosic compounds, exclusively lignin, pectin, and hemicellulose in naturally occurring fibers.

Hemicellulose being composed mainly pentoses such as zylose and arabinose and hexoses like mannose and glucose has a lower molecular weight. Lignin is amorphous in nature which gives rigidity to the plant structure and external hindrances.

The main aim to pre-treat the lignocellulosic biomass is generally focused on (i) Increase the exposed area of cellulose (ii) dissolve hemicellulose and lignin (iii) minimize capital and operating cost to generate CNF solely through mechanical methods.

4.2.1. Sodium hydroxide (NaOH) used at 10 wt.% plays an imminent role in de-structuring lignin by cleavage of ether bonds. The fibers are observed to lose their dark colour transitioning to a lighter brown shade, due to breakdown of lignin and hemicellulose. Besides dissolving lignin and hemicellulose, hydroxide partially reduces the amorphous hydroxyl groups as shown in reaction figure 4.4. below. The alkali causes ionization of carboxylic groups (-COOH) and introduces an Na^+ ion that leads to the formation of (-COONa), as seen by (Masłowski, 2018).



Figure 4.4. (top) Reaction of NaOH on cellulose compounds (below) Before and After NaOH treated bast fibers.

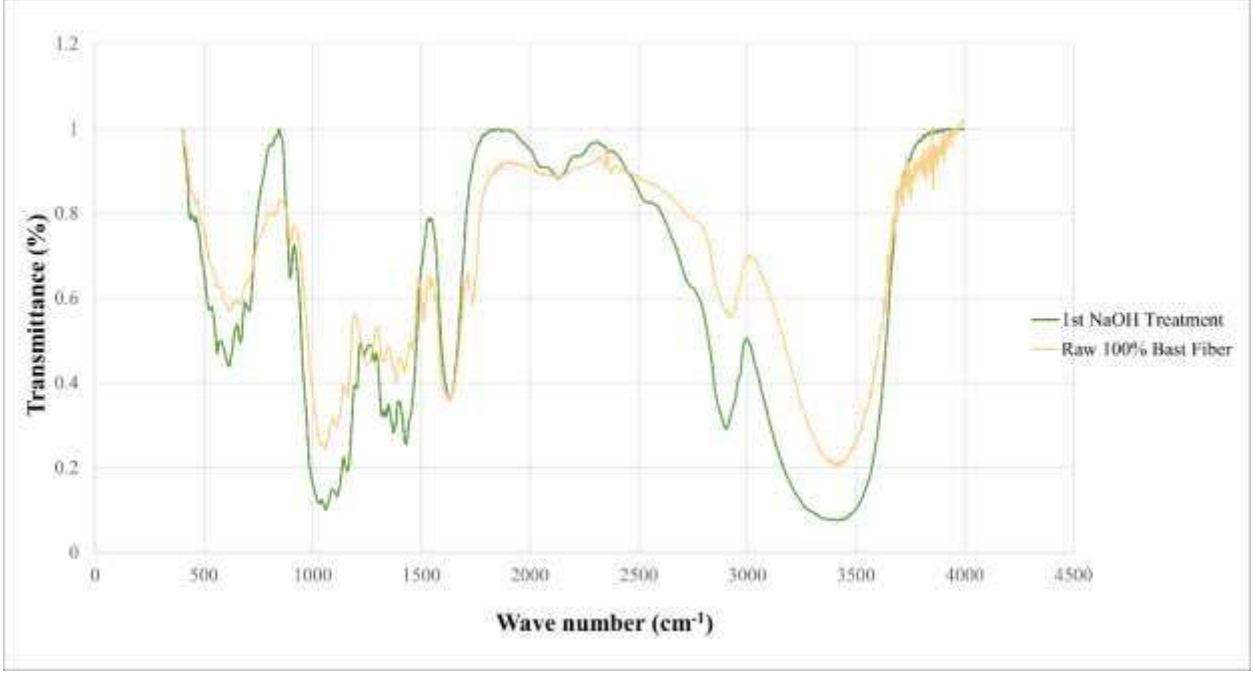


Figure 4.5. FTIR plots (a) Raw 100% Bast fiber, (b) 1st Step NaOH Treated

This FTIR (Fourier transform Infra-Red) plot indicates the disappearance of two major peaks around 1737 cm^{-1} which represents C=O of hemicellulose carboxyl and acetyl groups and 1508 cm^{-1} is C=C are vibrations of benzene and guaiacyl/syringyl groups of lignin, as seen in figure 4.5.

This alkali treatment also reacts with susceptible groups in lignin, where the hydroxide ions attack the complex ester groups linking the hemicellulose and lignin splitting it down to simpler phenolic

groups. This degradation is more substantial at lower reaction time and higher concentrations. (Wang and Yin, 2017).

4.2.2. Acid Hydrolysis of One-Step Treated Fibers

The alkali treatment is further enhanced by an acid hydrolysis step. Acid hydrolysis is the most common procedure to extract cellulose from any cellulose based materials.

The treated fiber which is now submerged in tap water kept in refrigeration condition is dewatered through a sieve of mesh opening of 45 microns. The main motif to use hydrochloric acid instead of sulfuric acid was to subject the fibers to a milder acidic reaction which will prevent the cellulose from degrading. A molecular representation of hydronium ion attacking the cellulose chain in noticed in figure 4.6, as discussed in the literature review section. The fiber was observed to lose most of its darker pigment containing more quantities of lignin and xylose. The appearance of the alkali (first step) treated pulp is a lighter shade of lighter yellow, indicating loss of hemicellulose material. Similar results were noticed by Wulandari, (2016) and Masłowski, (2018).

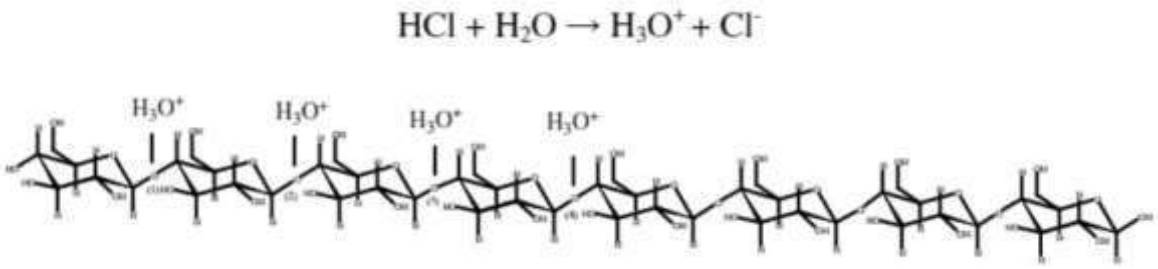


Figure 4.6. (top) Molecular representation of hydronium attack on cellulose

Since, the acid reaction was much short lived i.e., for an hour, cellulose degradation did not progress far enough, and produced large fragments of cellulose fibers which caused settling in water if left undisturbed for a while. Between each of these steps, the fibers were washed and rinsed under tap water to quench the reactions. However, there is subsequent amounts of lignin present even after the initial two step treatments till before the pulp is bleached.

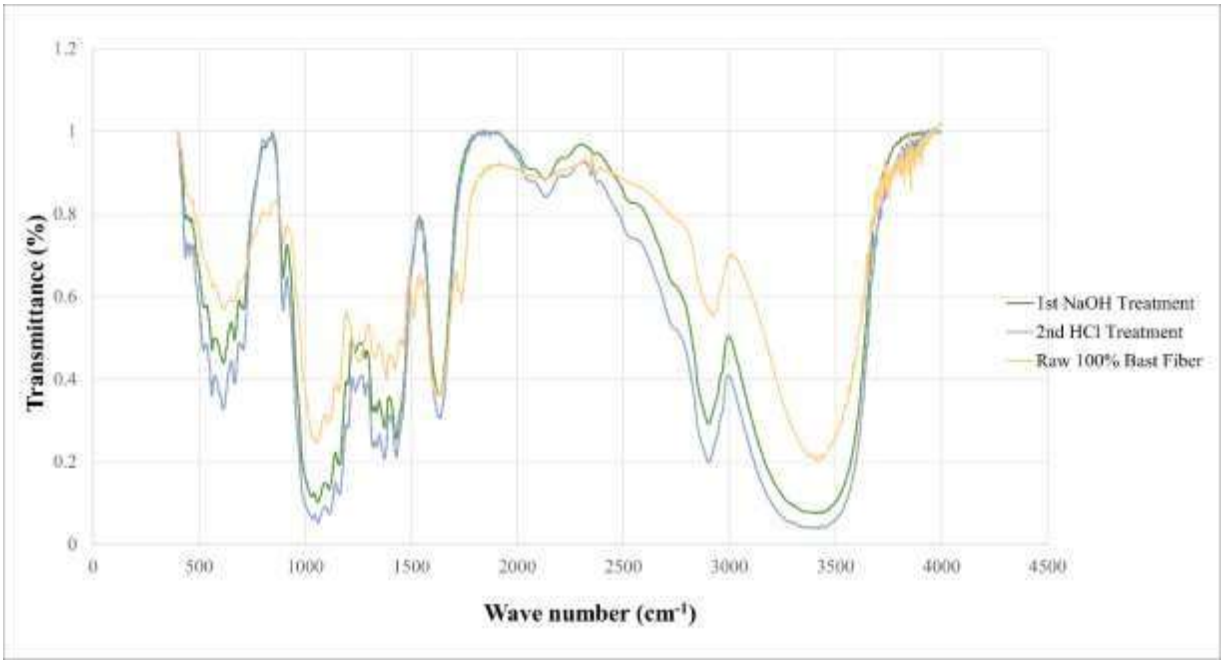


Figure 4.7. FTIR plots (a) Raw 100% Bast fiber, (b) 1st Step NaOH Treated (c)2nd HCl treatment.

The FTIR analysis was shown once again to show the disappearance of lignin and hemicellulose along with increase in intensity of the functional groups such as -OH and C=O groups.

Table 6 Steps of Chemical Treatment and Oxidation with their Respective Appearance

Steps	Reaction Temperature	Treatment Type	Reaction Time	Appearance of Product
1	room temperature	1st NaOH	4 hours	Brown
2	80 °C	2nd HCl	1 hour	Yellow
3	80 °C	3rd NaOH	1 hour	Light Yellow
4	80 °C	4th H2O2	3 hours	White

4.2.3. 2nd Alkali Treatment

The fibers were exposed to a second and last step of chemical pre-treatment. The fibers which have disintegrated by now and transitioned into pulpy consistency is refluxed once again with 2% by weight sodium hydroxide pellet solution. This step ensures that the remaining of the lignin is solubilised and further delignification of the pulp takes place at moderate conditions. The physical stiffness of lignin is from the strong polyring bonds of C-O-C, C-C and other hydrophobic bonds.

The appearance of the pulp at this stage, is a lighter shade of yellow and due to high delignification, the fibers appear to swell. The swelling increases good accessibility of the internal cellulosic material, increasing the overall surface area.

4.2.4. Oxidation and Bleaching H_2O_2

Bleaching of the chemically treated fibers were particularly performed for the purpose of solubilizing and removing chromatophores which imparts colour to the fibers.

The pulp which was mostly free of non-cellulosic material was divided in equal proportions and reacted with 2 % by weight of a 37% concentrated hydrogen peroxide under reflux as mentioned in the methodologies. The pH was maintained at 11 for optimum reactivity and reaction time and temperature were kept constant for 3 hours at 80^{o}C.

There has been growing concern over the usage of Chlorine and chlorine-based chemicals for bleaching in industries. These materials combine some oxygen-based chemicals such as hydrogen peroxide in terms of bleaching efficiency, environmentally friendly and milder in nature.

Hydrogen peroxide causes oxidation of the conjugated chromophores causing further delamination of fiber bundles. Controlling the pH and temperature of the reaction along with time, regulates the concentration of the per hydroxyl ion production.

$$H_2O_2 = H^+ + HO_2^-$$

Peroxide generally works in alkaline conditions when the per-hydroxyl ion, OOH^- is formed:

$$H_2O_2 + OH^- = OOH^- + H_2O$$

NaOH and Na_2SiO_3 were used to stabilise the pH during reaction and preventing the excessive decomposition of the peroxide by forming complexes with heavy metal ions if present in the solvent.

The per hydroxyl acts as a nucleophile; a nucleophile is a chemical species that tends to donate or share a pair of electrons with an electron-deficient atom known as an electrophile. The nucleophilic attack occurs on the conjugated double bonds on the chromophores (groups absorbing light imparting color). Conjugated double bonds exhibit delocalized pi-electron systems, which give rise to unique chemical properties.

The bleaching was monitored for 180 minutes; with time the fibers were observed to lose colour. Brightness was heightened with increasing time and temperature of the fiber, observed in figure 4.8. The difference in colour had started getting visible in after 30 minutes from the start of reaction. The pulp was washed and rinsed until it reached a neutral pH.

Varied time and temperature show different grades of bleaching. The maximum brightness was noticed when the reaction time was kept constant at 80 degrees Celsius for 120 minutes, as discussed in the table below.

Table 7 Reaction time, temperature, and their corresponding appearance for Bleaching

Temperature	Time (min)	Appearance
80 °C	180	White, Pulpy
80°C	120	Yellowish white
70°C	120	Pale yellow

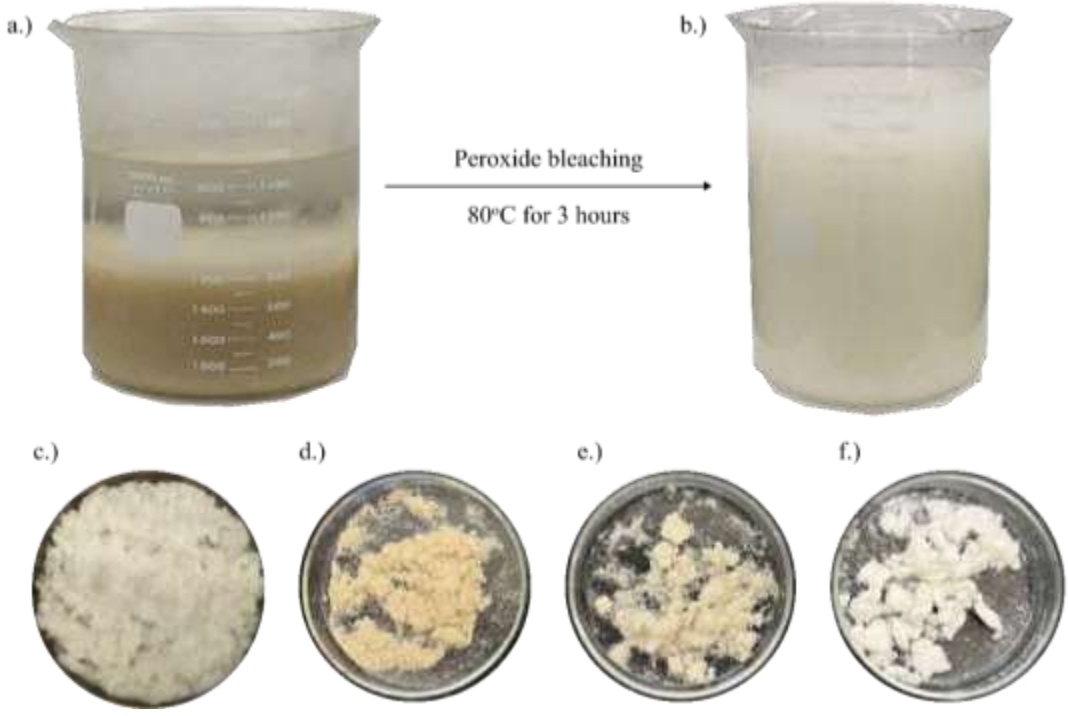


Figure 4.8. a.) Alkali-acid-alkali treated, b.) 3 Step Treated and Bleached, c.) Bleached Pulp rinsed through sieve, d.) UP-100% Bast, e.) 3-Step treated, f.) Bleached

Additionally, the alkaline environment during bleaching helps in swelling of the cellulosic fibers increasing their surface area. Images above show the difference in colour of un-bleached compared to bleached fibers (figure 4.8- a-d).



Figure 4.9. All chemically treated pulp showcasing the loss of colour and fiber size

4.3. Process Flow Diagram of Extraction of CNF and Preparation of CNP

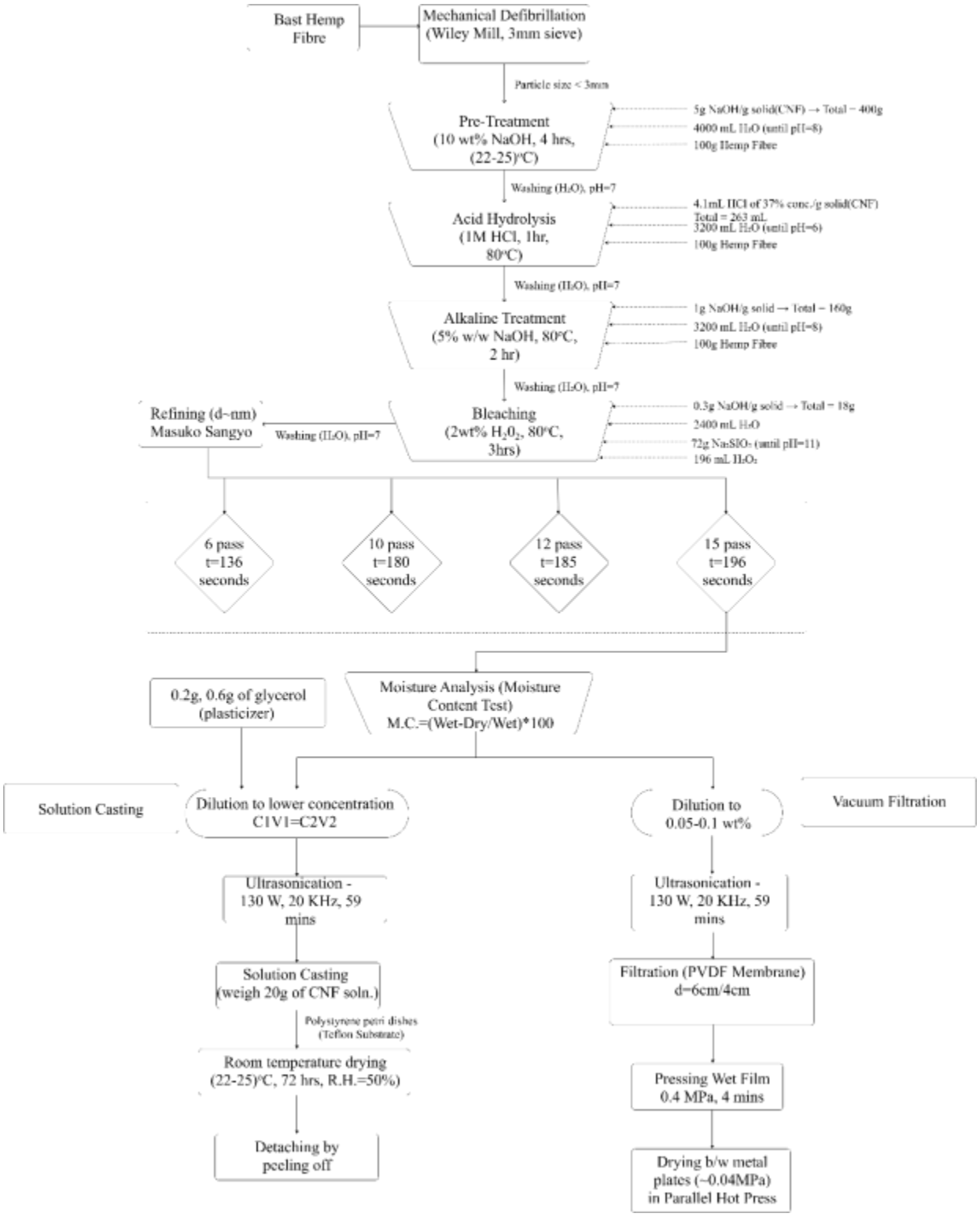


Figure 4.10. PFD for Extracting, refining nanocellulose and fabricating UW (Bast) nano paper through 2 broad methodologies.

4.4. De-Fibrillation through Masuko Sangyo or "Super Mass Colloider" – Grinding

The chemically pre-treated fibers are void of non-cellulosic constituents along with delignification from alkaline conditions. The micron sized fibers are now exposed to high shear fibrillation to produce nanoscale fibers, also known as nanocellulose fibers. The inter-fibrillar hydrogen bonding is increased by delamination of the walls and to benefit the most out of these delaminated fibers, reverse coalescence must be averted.

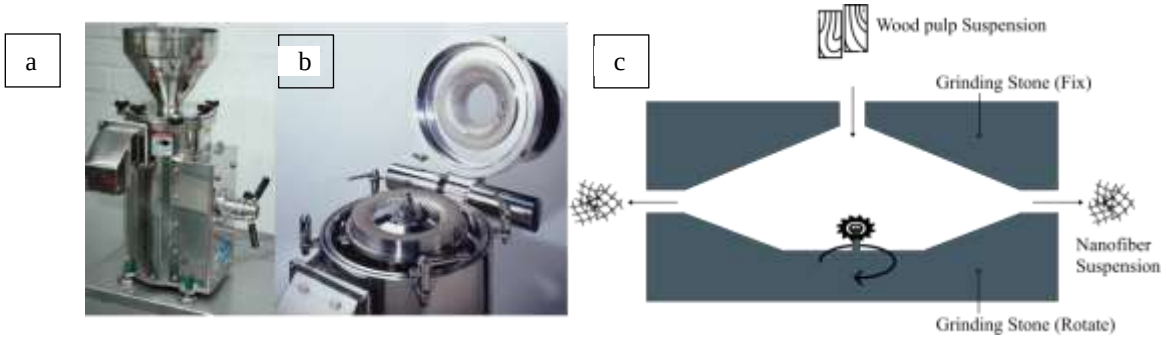


Figure 4.11. A Typical Masuko Grinder - a) Exterior structure b) Countersense Stones c) Cross-sectional frontal schematic of Masuko Sangyo

A pulp slurry was adjusted to 5% by weight by adding exactly 2000mL tap water, to the sieved pulp fiber. It is then passed through the Masuko Refiner at a high frequency. The cell wall of the fibers is broken down due to high shear from the grinding stones with countersense rotation. Fifteen different passes were evaluated with around 10mL sample collected from the sixth, eighth, twelve and finally fifteenth pass to compare the extent of fibrillation at each stage. The degree of fibrillation and quality of cellulose was controlled by altering the gap between the two plates. Refining pulp fibers at a higher consistency led to better fibrillation as more interparticle shearing occurred leading to the exposure of the inner surfaces of the fibers. Moreover, with high starting concentration perse 5 wt.% instead of 3wt.% of fibers, the particles formed smaller fibers which resulted in its gel-like homogenous aspect. It can be attributed to the complex interplay of fiber-fiber interactions, mechanical shearing, and the viscoelastic properties of the nanocellulose suspension during the refining process. The increased friction and shear forces at higher concentrations contributed to the development of a more uniform and gel-like appearance.



Figure 4.12.: (left) After masuko 2 % (w/w) (right) after masuko 3.1%(w/w)

Table 8 Different Processing Conditions used to obtain CNF – Gap (mm) according to no. of passes through the masuko of 5 wt.% treated pulp.

Cycle	Time (Seconds)	Ampere	Gap (mm)
1	10	8.5	1.4
2	11	8.5	1.4
3	11	8.5	1.3
4	19	8.5	1.3
5	24	8.5	1.2
6	58	8.5	1.2
7	65	8.5	1.2
8	94	9	1.2
9	98	9	1.15
10	121	9	1.15
11	105	9	1.15
12	97	9	1.15
13	86	9.5	1.15
14	90	9.5	1.15
15	135	9.5	1.15

After few passes through masuko refiner, and by decreasing the gap between the two stones, the time for fibrillation was longer and so was the energy consumption as detailed in table 8.

This suspension in the end of the grinding mechanism, was converted into a stable suspension gaining a gel-like property. This gel was rubbed between two fingers to check their aspect and physically felt like a smooth paste. The zero point of the grinder clearance alters according to thermal expansion and wear and tear of the stones. Image below shows the visible difference between 6th Pass (on left) and 15th (on right) Pass CNF Slurry through Masuko grinder.

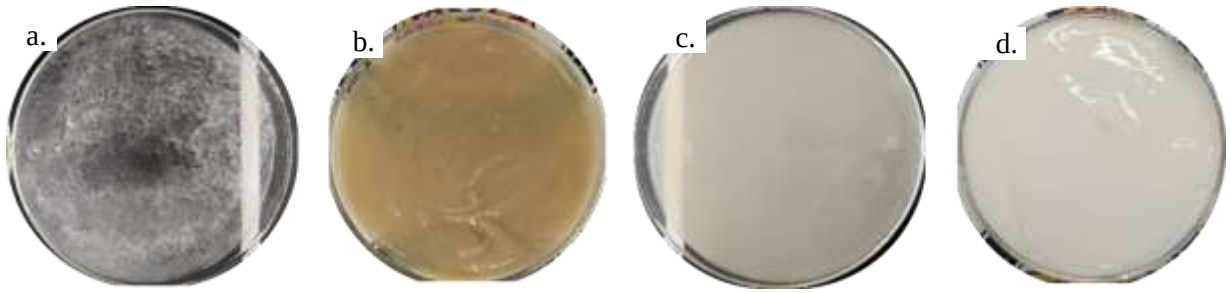


Figure 4.13. Images of fibrillated cellulose fibers – NFC, a. 6th pass T+B, b. 15th Pass UT/UP Bast, c. 15th Pass 3 Step Treated, d. 15th Pass T+B.

4.5. Characterization of Fiber

Transmission Electron Microscopy (TEM)

4.5.1. Transmission Electron Microscopy (TEM) of UWaterloo CNF Slurry:

Two micrographs of two different passes and degree of fibrillation have been included. The images acquired after performing TEM on 12th pass and 15th pass through Masuko are represented on Figure 4.14 respectively.

Figures show the two micrographs of Nanocellulose fibers from unretted and Bast bundles. It can be clearly detected in the left image, that the fibers have a 50:50 ratio of Fibrillated: Un-fibrillated. Comparing the two micrographs the one on the right has a higher magnitude of fibrillated fibers in their nanoscale (nm). After 12 passes through the masuko refiner, at a magnification of the nanocellulose fibers range between 50 to 100 nanometers in diameter, possibly nearing some several micrometers in length. This shows that grinding through 12 passes has resulted in fiber's cell wall fibrillation and its decrease to nanofibers. De-fibrillation exposes interlaying walls of the fibers, the nanofibrils through action of shear force being imparted on their surfaces.

On the other hand, 15th pass micrograph shows a greater number of fibrillated and exposed fibrils in nanometer dimensions, stating that increasing the number of cycles results into smaller fibers.

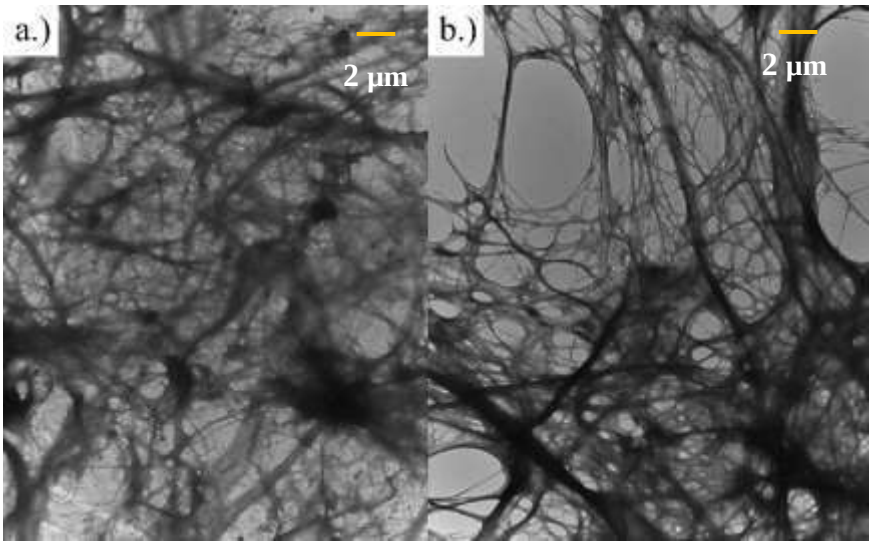


Figure 4.14. TEM graph (a) 12th Pass in Masuko (b)15th Pass in Masuko

To measure the visible number of fibrils, particle size distribution was carried out with the help of ImageJ software (ImageJ, USA). It is clearly seen that the frequency of fibrillated nanofibers intensified with more passes, as observed in figure 4.17 (b). Each nanofiber is a hollow cylinder arranged in an overlapping manner which flatten upon drying and desorption of solvent, as seen while pressing nanopaper (figure 4.15.) This describes how pressing may get rid of internal pores and spaces by flattening the fibers unlike in casting.

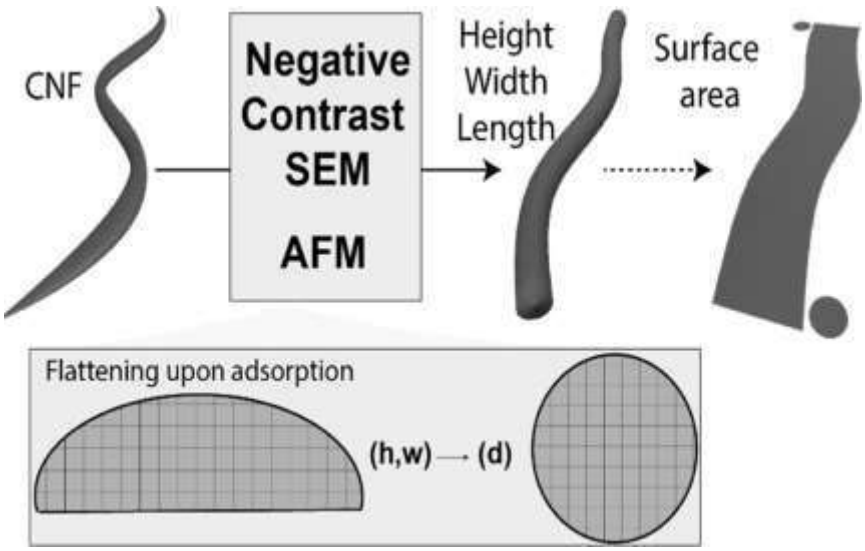


Figure 4.15. Defining higher surface area of nanofibers due to flattening adapted from (Mattos et al., 2019)

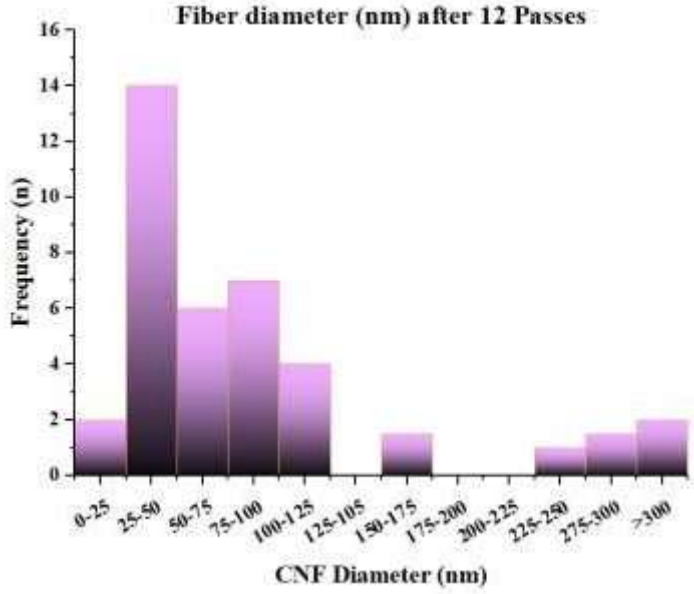


Figure 4.16. Histograms depict the Frequency of Repeating Fibers in 12th Pass.

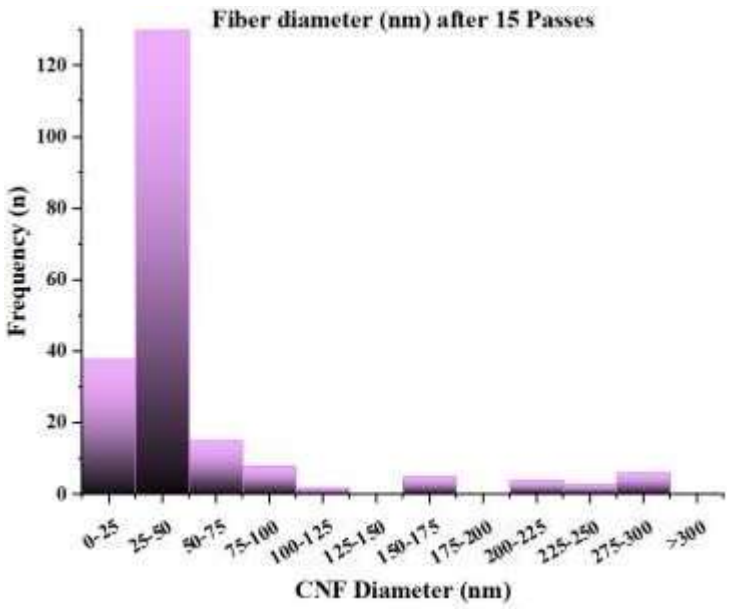


Figure 4.17. Histograms depict the Frequency of Repeating Fibers in 15th Pass.

By the time, the fibrils passed through the 15th Pass, with a working gap of 1.15 mm between the grind stones, the maximum nanofibrils lied between 25-50 nanometers range.

It is well understood that the time of fibrillation and the gap maintained between the plates have high influence on the scale of fibrillation introducing new nanofibers.

4.5.2. Transmission Electron Microscopy of UMaine Freeze Dried CNF:

Similarly, UM nanofibrils were observed under transmission electron microscopy to analyse the size distribution of nanofibers.

Image 4.18. depicts the uniformity in fiber diameter. Most fibers had a nominal width around 50-80 nanometers comparable to data specification sheet in Appendix B. The fibers are observed to be well refined with smaller range of diameters. A few bigger fiber bundles were noticed mainly due to inefficient dispersion during sonication of the fibers prior to sample deposition.

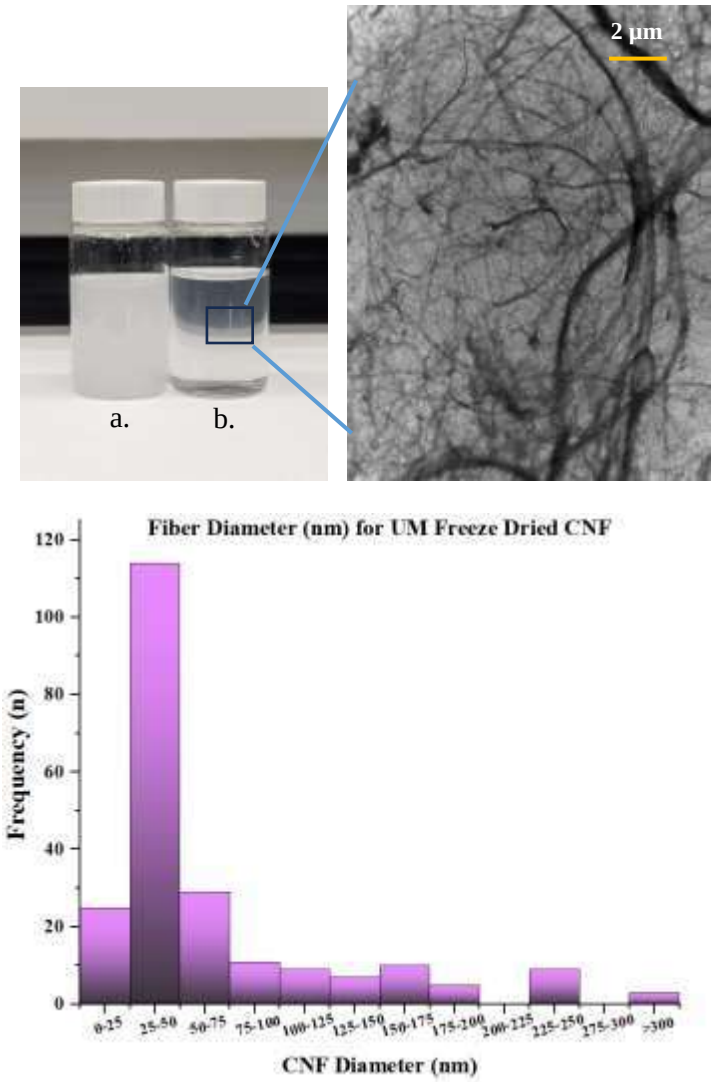


Figure 4.18. (top left) a.) 0.2 wt.% CNF solution, b.) Centrifuged, supernatant used for TEM, (top right) TEM micrograph of dispersed UM fibers, (below) Histogram distribution of freeze-dried fibers.

4.5.3. FTIR (Fourier Transform Infra-Red Characterization)

The chemical composition of cellulose and nanocellulose was measured with FTIR analysis. The dried cellulose samples were mixed with KBr powder and pressed into a circular disc pellet. KBr was used as the reference as it is transparent in the IR region and the resulting spectrum gives characteristics of the nanocellulose sample given in table 9. All FTIR data was analysed according to ASTM E168 for composite materials such as fibers.

Table 9 Some expected FTIR Peaks associated with Nanocellulose Extraction and Freeze-dried CNF

Peak Wavenumber(cm^{-1})	**Corresponding Chemical Bond**
3,280-3,494	OH (Stretching)
2,940	C-H
897	C-H
1,072	C-O-C
1,638	O-H (Bending) (Absorbed water)

The large band around 3280-3500 cm^{-1} corresponds to O-H stretching on the surface of nanocellulose (Omorogbe, 2017.). The significant peak at 2940cm^{-1} lies with C-H stretching defining the characteristics of methyl and methylene groups of nanocellulose. C-O-C stretching was noticed in all the spectra around 1072 cm^{-1} as noted by Stanley et. al., (2018).

1640 cm^{-1} is the stretch for absorbed water O-H bending. The vanishing of peaks refers to the dissolution of hemicellulose and lignin with progressing chemical treatments. Figure 4.19. shows stacked plot of the peaks, where increase in peak intensity with each acid and alkaline treatment was noticeable.

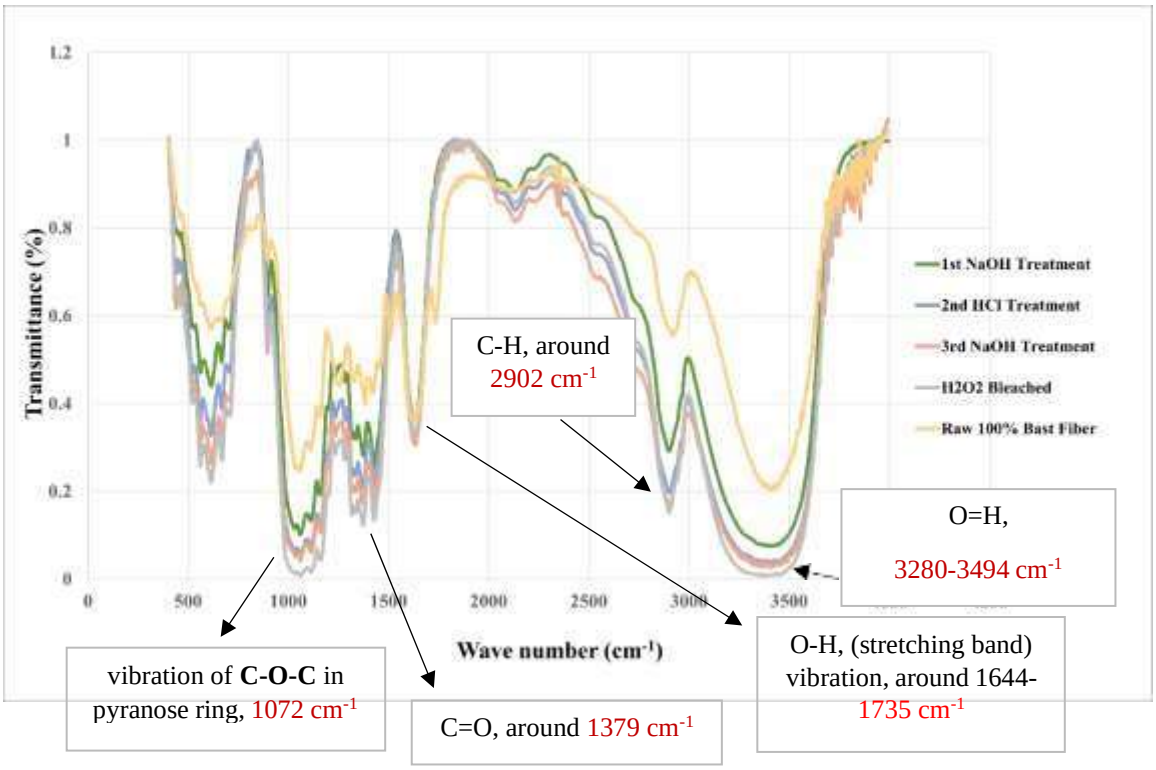


Figure 4.19. Overlay stacked plot of each step of chemical treatment of UW CNF through FTIR Analysis.

The chemical composition of UM freeze-dried nanofibers was also examined similarly, the already dried nanofibers were disintegrated farther in a mortar and pestle. A small quantity of fibers was then mixed with KBr similarly and pressed under in a parallel plate to form pellets.

Referring to table 9, UM fibers have similar functional groups as UW nanocellulose. The peaks are also known as absorbance bands and corresponds to the various vibrations of the fiber's atoms when exposed to IR radiation. Even though the similarity of peaks is visible, the UM nanofibers show sharper peaks indicating purer functional groups.

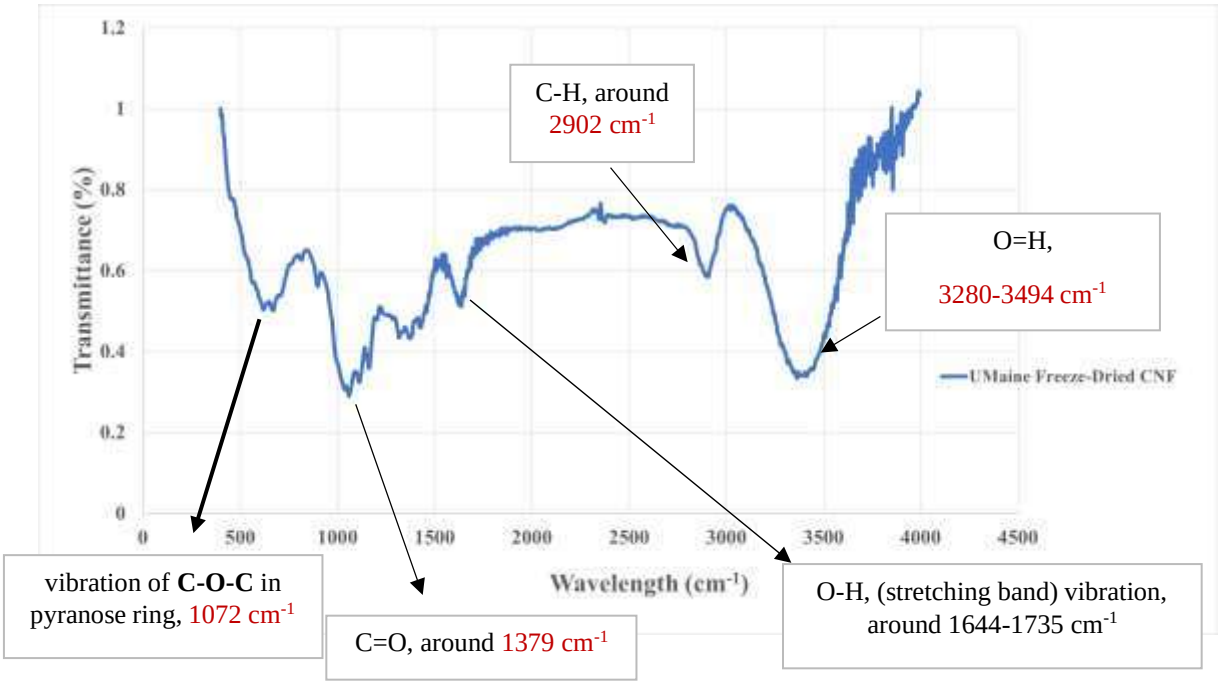


Figure 4.20. Plot of functional groups of UM CNF through FTIR Analysis.

Preparations of Nanopaper

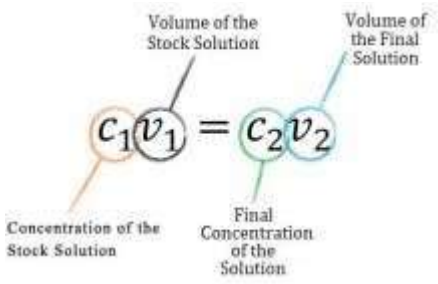
4.6. Fabrication of Cellulose-nano paper (CNP) through Solution Casting:

NFC nano-paper was prepared by using solution casting.

The moisture content formula below is considered to calculate the solid content:

$$\mu = \frac{(weight\ before - weight\ after)}{weight\ after} \times 100 = moisture\ content\ in\ \%$$

The solid content of nanocellulose fibers vary between 3% to 3.5% depending on the amount of sample lost during chemical treatments and refining. Due to reduction in fiber size with each level of chemical exposure, fiber lengths smaller than 45 microns (mesh size), tend to permeate and wash through. All solution casted films in this chapter were fabricated from a parent slurry of 3.2 by wt.% to maintain consistency in the results shown here forth. The 3.2% by weight concentrated CNF slurry after refining is mixed with tap water to bring down its concentration to about 2%. The dilution formula with respect to concentration has been considered to evaluate the amount of water to be added to the slurry:



The mixture containing a diluted parent slurry of 2 wt.% is subjected to high frequency (20KHz) sonication in a cold ice bath for 60 minutes.

The sonicated sample is weighed in a weighing scale in grams and drop casted in polystyrene petri dishes, lined with glass-fiber reinforced sheets.



Figure 4.21. (left) Solution casted CNF slurry. (right) Glass Fiber reinforced Teflon sheets

4.6.1. Drying Solution Casted Nanopapers of Hemp CNF Slurry:

The solution casted films were weighed about 15g each and dropped in petri plates. Different modes of drying were considered while evaporation of the residual water in the petri dishes. Some modes of drying considered were using a hot plate (Mettler Toledo, Switzerland), the hydraulic hot press (Carver Inc., USA), and a Rapid sheet dryer provided by the Semi Automatic Paper Machine (Universal Engineering Corporation, India).

. Table 10 Different Modes of Drying undertaken to find the optimum condition for Drying.

Methods Used for Drying	**Composition of Nano-paper (Thin film)**	**Time and Procedure undertaken while drying**	**Nano-paper**
Hot Plate	Bleached and mechanically de-fibrillated nanocellulose sample with 2 wt.% concentration was used. 200gm of slurry was agitated and sonicated for 60 minutes. 15g of slurry solution were dropped on petri dishes.	• The petri dish was left for drying in room conditions for 24 hours. • The semi-dried sample was peeled off with the Teflon sheet. • Dried on hot plate by heating at 40^{o}C for 15 minutes.	
Parallel plate Hot Press		• The petri dish was left for drying in room conditions for 24 hours. • The semi-dried film was peeled off and sandwiched with another Teflon sheet. • Compressed at 40 ^{o}C and 2.4 MPa for	
Hot Pressed at Higher Temperature (Rapid Sheet Dryer, Semi-Automatic Paper Machine)		• Weighed solution was left for drying for 24 hours and then dried within a rapid sheet dryer at 70 ^{o}C.	
Hot Pressed at Higher Temperature (Rapid Sheet Dryer, Semi-Automatic Paper Machine)		• Weighed solution was left for drying for 24 hours and then compressed in rapid sheet dryer between (50-54) ^{o}C.	

Cellulose nano-papers (CNP) showed high shrinkage when dried at higher temperature than room environment. Whereas CNP dried at a lower temperature like drying in the Rapid sheet Dryer comparatively resulted in a lower degree of shrinkage. This is due to the faster evaporation rate and shorter time during drying which contributes to the opaqueness of the films, as shown in case of hot plate drying or parallel plate pressing.

Nanofibers are nanoparticles with high surface charge, that is, they tend to agglomerate to stabilise themselves in a matrix. A decrease in fiber size will lead to an increase in the surface charge. The nanofibers in this case are in constant state of agitation and thermal motion known as Brownian motion. To minimise this state of restlessness, nanofibers form irreversible agglomeration while drying. The tendency to form agglomerates is also directly proportional to the concentration of the slurry casted. These nano sized particles either stay put by forming inter hydrogen bonding or even Van der Waals force. The magnitude and strength of Van der Waals forces and hydrogen bonding are dependent on the distance between the fibers, the surface area of contact, and the polarizability of the materials.

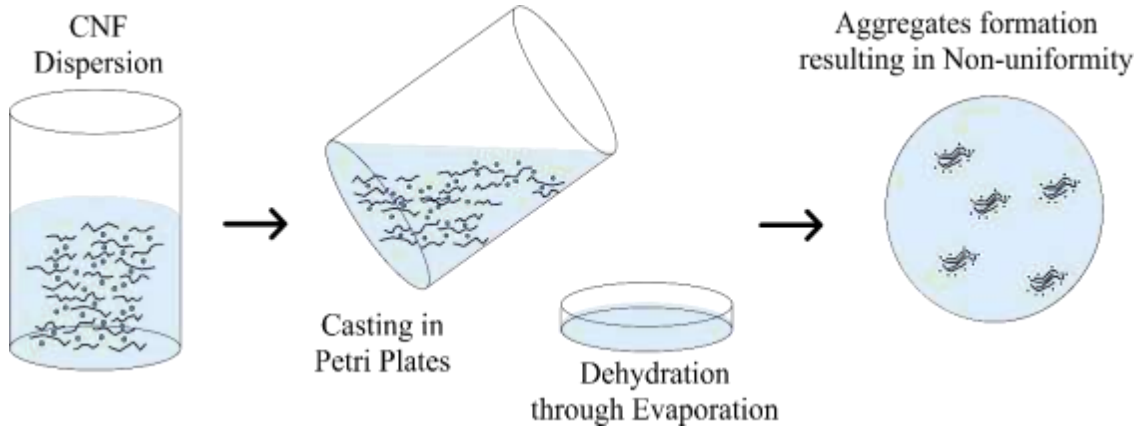


Figure 4.22. Visual representation of agglomerates that form during un-even humidity drying of nanopaper via Solution Casting.

When the concentration of CNF/NFC dispersion is increased at a faster rate during casting, CNF tend to form an inhomogeneous aggregation. This isotropic or disorganized arrangement of entanglement of fibers hinder the tight packing of nanofibrils causing cavities within their matrix. This makes the thin film more white and less transparent.

To produce low-haze, smooth and less wrinkly paper through casting, drying temperature, moisture content in the air and concentration of CNF slurry needs to be optimised. Due to the water content (%) being high in diluted slurries, the evaporation time is stretched. The nanofibers remain individually isolated in the diluted slurry giving them enough time to conform and align themselves. Nanocellulose fibers tend to have self-assembly properties due to their branched fiber networks and exposed larger surface area with which they manage to orient themselves in the direction with maximum intertwinement. As the solvent evaporates, capillary forces come into action through inter-fibrillar movement of water molecules causing collapse of fibers. But hydroxyl groups on the surface of these fibers promote intermolecular hydrogen bonding. This explains that increasing the water content of the slurry can lead to disintegration of aggregates leading to the formation of low-haze and efficient nano-papers through casting as mentioned by Isobe et al., (2018) and C. Li et al., (2020) in their works, respectively.

Another set of three solution casted films were drop casted from a CNF slurry of 1.5 wt%. One of which was a neat 100% CNF film and the other two had small amounts of glycerol added to them. The Gly here acts as a plasticizer for better flexibility as outlined before in figure 2.22 in literature review. In case of freeze-dried UM-CNF, up to 1.5g of the dry sample was weighed in a weighing scale and about 100 mL of tap water was added.

$$C_1V_1=C_2V_2$$

$$3.1(\%) \times 100\ mL = 1.5(\%) \times v2$$

$$V_2= 206.6\ mL$$

Therefore, V to be added was 206.6-100= 106.6 mL

The plates were kept unbothered for 72 hours in room temperature and humidity. They were monitored over three days till dry. These films took longer to dry off since the water content in the casted slurries were high.

The thickness of these films was measured by a digital micrometer and an average of 5 measurements were taken along with their standard deviation.

The high deviation was presumably due to aggregate formation on the nanopaper while drying, owing to the absence of constant relative humidity. Fibers may have collapsed together on different spots over the specimens causing an uneven thickness.

Conc. sonicated slurry = 1.5 wt.%

Density of glycerol: 1.26 g/mL

Per petri dish: 15g slurry

Table 11 below shows the aspect, visuals, and thickness of nano-paper fabricated from a dilute slurry of UW CNF:

Final Composite	**UW CNF Content**	**Gly Content**	**Thickness micron (um)**	**Nano-paper**
100 % CNF slurry	15g CNF (UW)	0	55±3.2	
83.33% CNF + 16% glycerol	0.225 g CNF	0.045 g	60±2.1	
62.5% CNF+37.5% glycerol	0.225 g CNF	0.135 g	60±2.2	

Nano-papers observed in table 11 draw a comparison between the visual appearances of different films. All the nanopapers took about similar time while drying. CNP drying through solvent evaporation, takes places at the center and then proceeds around the edges. Neat (100%) CNF film apparently shrunk and corrugated more than the ones with glycerol. The glycerol promoted plasticization of the films corrugating them less (Roy et al., 2022).

4.6.2. Solution Casted Cellulose Nano-paper (CNP) Characterization

Mechanical Properties of Solution Casted Nanopaper from Hemp (Bast) UW-CNF and Softwood UM-CNF

The mechanical properties of cellulose nanopapers (CNP) can be tailored depending on their preparation methods. All CNPs in this chapter were fabricated via solution casting technique and with two different CNF sources, as described in methods and methodologies of this thesis. CNPs produced through casting from solutions of similar concentrations are evaluated and compared. The tensile properties of the casted nanopapers were determined from stress-strain curves following ASTM method: D882-12 for tensile modulus as well as tensile strength. The average of modulus, that is how stiff the sample is and the average of strength that is maximum stress withstanding capability of the sample was calculated and studied. The standard deviation was calculated using the testing of 10 specimens each. Here, the mechanical properties of CNPs were scrutinized according to their source and addition of plasticizer (Gly). The tensile modulii were as following:

Table 12 Mechanical Properties for Solution Casted Nano-papers from UM CNF and UW CNF

Fiber		Property	100% CNF	83% CNF + 16% glycerol	62% CNF+37.5% glycerol	Units
UW	Tensile (MPa)	Modulus	386±24.63	198±15.71	95±15.37	[MPa]
		Strength	39.6±3.90	35.8±6.20	22.3±5.7	[MPa]
UM		Modulus	495±20.21	198±14.86	95±13.66	[MPa]
		Strength	48.2±2.70	45.3±5.6	22.3±5.2	[MPa]

By observing the decreasing trend in mechanical properties with addition of Gly in the films it can be understood that even though plasticizers increase matrix softness due to Gly's low viscosity compared to CNF, it makes it easier to peel the films from their molds reinforced with Teflon sheets, but also reduces its effective tensile strength compared to pure nanocellulose films. As a plasticizing agent, glycerol being an oligomer can penetrate through interfibrillar spaces increasing the volume available between nanofibers and in turn reduces their probability for physical entanglement and decreasing tensile properties. Hence, it may be noted that the occupation of glycerol in nanofibrillar sites disrupts hydrogen bonding sites.

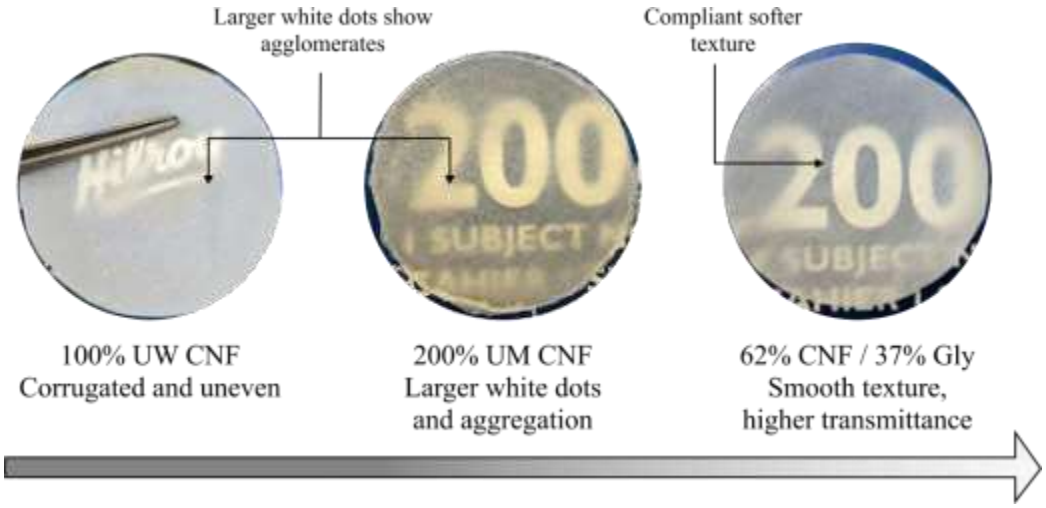


Figure 4.23. Casted CNPs under different conditions.

The graphical representation show comparison between UW-CNF and UM-CNF Nanopapers fabricated from Solution Casting:

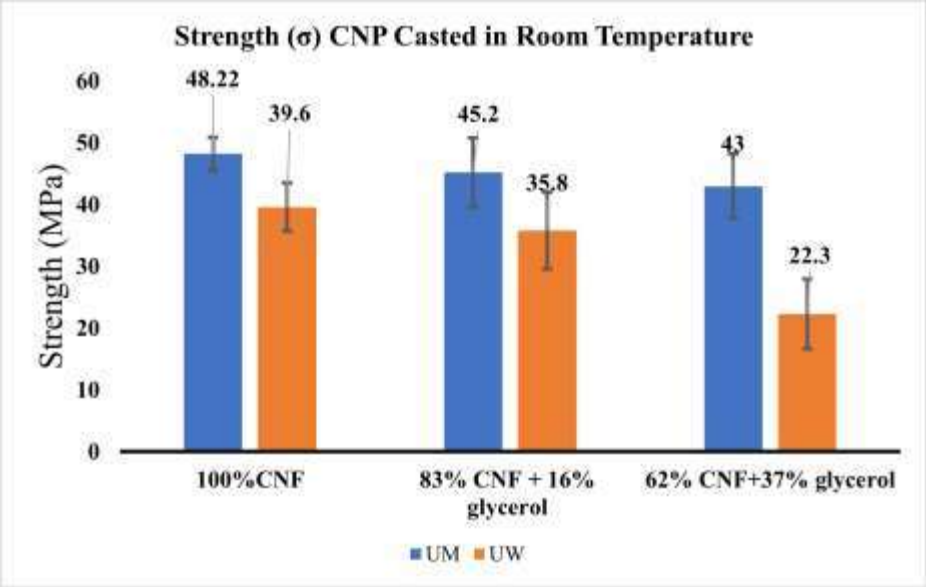


Figure 4.24. Tensile Modulus (MPa) of Solution Casted UW and UM CNF respectively in room temperature.

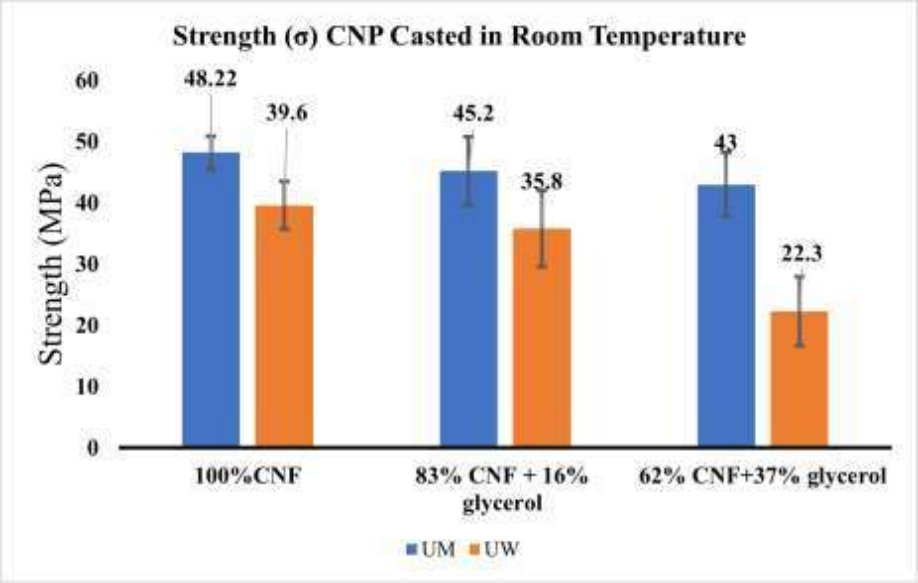


Figure 4.25. Tensile Strength (MPa) of Solution Casted UW and UM CNF respectively

Since casting requires a regulated and constant relative humidity while drying as well as air flow, to prevent it from forming agglomerates. Due to lack of this phenomenon, while drying the nano-paper specimens in room conditions they formed aggregates on certain sections of the films causing more opacity leading to uneven distribution of nanofibers while drying and non uniform thickness. This resulted in higher standard deviations amongst nanopapers from the same stock solution and prepared under similar conditions.

4.7. Fabrication of Cellulose-nano paper (CNP) through Vacuum Filtration:

The second methodology adapted to fabricate nanopaper was through the suction filtration method. The refined slurry of UW CNF or the freeze-dried nanofibers from UM were firstly diluted to a concentration much lower than what was performed in solution casting. Since high concentration CNF solutions only allow casting otherwise the gel like slurries would take up high operational time.

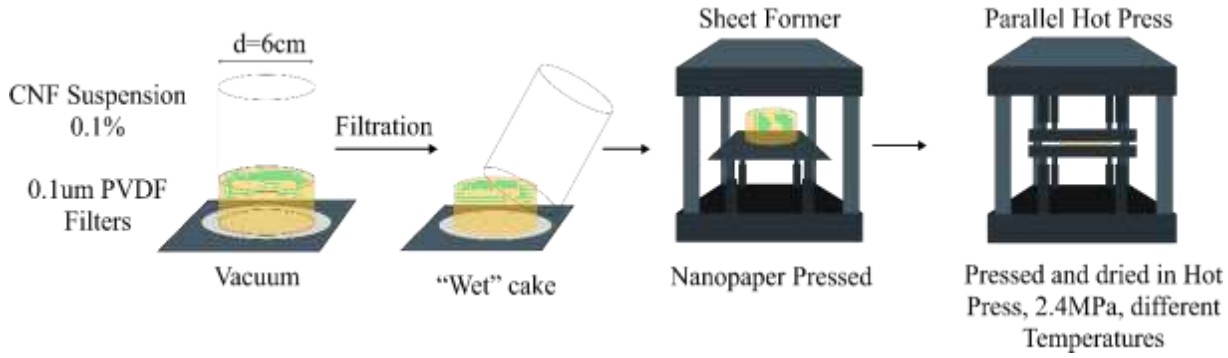


Figure 4.26. Exhibits the filtration and pressing of nanopapers.

The CNF slurry and freeze-dried CNF were diluted to a concentration of preferrable solid content. A mathematical estimation was performed here to understand the minimum required grammage to form a nano-paper of considerable thickness whilst maintaining its transparency.

The nano-paper demonstrated here is fabricated from two different sources of nanocellulose fibers (CNF).

Table 13 Sources and Physical Phase of CNF from UM, UW, respectively.

CNF Type	Source	Phase	Fiber Diameter (nm)
UM	Pinus (Softwood)	Freeze-Dried	50nm
UW	Hemp (Bast fibers)	Slurry	25-50nm

Two hydrophilic porous filtering membranes of 2 diameters made of polyvinyl di-fluoride (PVDF) are used to form the respective nano-papers.

1) 4.7cm in diameter

2) 5.9cm in diameter

To find minimum CNF content for a diameter of 5.9cm membrane a few anticipated values were considered from intensive literature review.

Parameters considered:

Density of desired nanopaper = 1.48 g/cm^3

Desired thickness of nanopaper = 50 µm

} Review through Literature

The volume occupied by the nanofibrils in an area of 27.32 sq.cm was approximated to 0.13 cubic centimeter.

Considering the density of the desired thickness of nanopaper, the mass of cellulose calculated was:

Density = Mass/Volume

Mass = Density × Volume

Mass = 0.2 g

Therefore, according to the estimation considered, 0.2 g was measured to be the CNF mass by weight to fabricate a nanopaper. **Even though 0.2 g of nanocellulose was calculated to be the minimum amount of nanocellulose required for a diameter of (5.9 ≅ 6) cm membrane an** additional experiment was performed with **0.1 g of nanocellulose** fibers for the same diameter. This was to investigate if there was a possibility to fabricate a CNP with a lower grammage to control it's contact transparency or visibility.

Similarly, the filter membrane of smaller diameter 4.7cm had a particular mass estimated to form nanopaper of substantial transparency.

- All concentrations were in weight percentage and a volume of **100mL of CNF dispersion** was filtered each time to make the thin film.

Table 14 Shows Nanopapers from CNF UW and UM of different Grammage (mg/cm^2).

Concentration of CNF soln.(wt.%)	Mass of CNF per CNP (mg)	Type of CNF	Filter diameter (cm)	Grammage (mg/cm^2)	Thickness (µm)
0.05	50	UM	4.7	2.9	40
0.05	50	UW	4.7	2.9	40
0.05	75	UM	4.7	4.3	80
0.05	75	UW	4.7	4.3	80
0.05	50	UM	6.0	1.8	**Not Formed**
0.05	50	UW	6.0	1.8	**Not Formed**
0.10	100	UM	4.7	5.8	90
0.10	100	UW	4.7	5.8*	90
0.10	100	UM	6.0	3.7*	60
0.10	100	UW	6.0	3.7	**Not Formed**
0.20	200	UW	6.0	7.3	**Not Formed**
0.30	300	UW	6.0	11.0	150
0.50	500	UW	6.0	18.3	200

"*Specimens particularly formed for carrying out characterization and establishing results for this research project."

It was observed that nano-paper of similar grammage could not be formed from UM+UW on the same filter membranes. It was speculated that the fiber length of UW CNF fibrils was non-uniform and consists of a longer range of dimension resulting in a lower aspect ratio compared to UM CNF.

- UM = least grammage 3.7 mg/cm^2 on 6cm membrane → FORMED

- UW = least grammage 3.7 mg/cm^2 on 6cm membrane → NOT FORMED.
- The least grammage required for UW CNF on 6cm membrane → 11 mg/cm^2**.**

4.7.1. Comparing Results of Different Flow of Filtration(mL/s) of Nanopaper Formation:

The randomly distributed fibrils may be the reason for porous, hollow, and unstable nanopaper owing to structural discrepancy. To manipulate their full capability, a unidirectional arrangement would result in better assets. One major difference in the arrangement of fibers between casting and filtration is the driving force which leads or forces the fibers to be arranged in a certain manner while the solvent is getting filtered whereas, casting only results in randomly arranged nanofibrils to minimise their surface energy. Vacuum Filtration shows better films by increasing orientation of the fibers in the plane of filter. Moreover, vacuum filtration results in a wet cake of CNF (outlined in literature review in this thesis) which has a stable wet strength that can be subjected to high pressure and temperature compression. Meanwhile, casting only allows evaporation leaving behind no room for pressing like conventional paper making.

This portion of the thesis stresses upon the volumetric filtration rates and how it effects the wet cake permeability with continuous deposition of nanofibrils.

1st Experiment:

- 100 mL of each concentration was filtered through two diametric membranes (PVDF), 5.9cm and 4.7 cm respectively.
- The working diameter of the smaller membrane was around 4 cm whereas for the larger membrane was as it is.
- Vacuum pressure applied across the filtering column was 0.98 bar.

Table 15. 6cm Diameter PVDF membrane filtering 0.1wt% UM CNF soln., 100mL.

Volume (mL)	Time (s)	Volumetric Flow Rate (mL/s)	Permeability, k ($\times 10^{-8} cm^2$)
20	16	1.25	43.99
40	68	0.30 < **75% decrease**	8.690
60	127	0.16	3.338
80	216	0.09	1.415
100	482	0.04	0.635

Table 16. 4cm Diametric PVDF Membrane filtering 0.1wt% UW CNF soln., 100mL.

Volume (mL)	Time (s)	Volumetric Flow Rate (mL/s)	Permeability, k ($\times 10^{-7}$ cm^2)
20	46	0.44	4.487
40	189	0.11 < **75% decrease**	0.945
60	383	0.05	0.400
80	818	0.02	0.144
100	1446	0.01	0.031

Referring to tables 15 & 16, a set of formulae have been used to determine the values of volumetric flowrate (mL^3/s) and Permeability (cm^2) of the suspension and cake, respectively.

$$Volumetric\ Flow\ Rate\ (ml/s) = Volume\ of\ Solution\ (ml)/Time(s)$$

It was noticed that the permeability of the cake decreased with time, this is because layers of CNF sheets formed one on top of another as they were dragged along the plane of filtration. Eventually

with layers of deposition, the solvent, which is water, follows a tortuous path or snakes its way through the “wet” cake bringing down the overall permeability drastically. The permeability of the cake can be measured according to the Darcy’s Law as mentioned in chapter 2, 2.7.

Initially, when the filtration starts the CNF fibrils remain dispersed in the liquid and filtration is relatively high as seen in tables 15 and 16, the starting flow rates (mL/s) were much higher. With time, the CNFs begin to deposit onto the filter media forming a porous dense matrix. Permeability is observed to be decreasing over time as this dense matrix resists the flow of fluid through the wet cake, where the liquid now must follow a tortuous and elongated path to escape the filter medium. For both 5.9 cm and 4 cm diametric membranes, the permeability of the cakes is lowest when the entire “100mL” volume is filtered. Permeability has been noticed to decrease by around 75% after the filtration of the first 20mL, for both the filtration setup. NC fibrils proceed forming a web intermesh restricting free filtration of the solution as mentioned above.

4.7.2. Nanopaper through Filtration and Hot-pressing (UM, UW)

4.7.2.1. UM Filtered and Pressed Nanopaper

The freeze-dried CNF was gradually dispersed in water through a series of mechanical agitation and sonication. Dried CNFs are aggregated and the redispersion of these clusters often get difficult without any surface modification or addition of surfactant.

But using water as a solvent medium for dissolving did not require any such redispersing agent. The nanofibrils readily form hydrogen bonds with the water molecules making it easier to dissolve.



Figure 4.28. Representation of Nanopaper manufacturing from Freeze-dried UM CNF

High speed agitation and mechanical energy attribute to the dissolution of nanofibrils in water. Shear force imparted during mechanical agitation while mixing about 0.5g of freeze-dried CNF in 500 mL tap tore apart the Vander Waal forces and hydrogen bonding amongst the agglomerates and formed inter molecular hydrogen bonding between these nanofibrils and water molecules due to the difference in electronegativity between the solute and solvent. Nanocellulose films or nanopaper were fabricated at different grammages (mg/cm^2) as mentioned earlier. The nanopaper discussed here was a 0.1g CNF by mass, 6cm in diameter and dried at different temperatures and pressed under the influence of an automatic sheet former machine as well as parallel plate hot press.

During filtration and drying phase of CNF, the water content present in the "wet" cake and nanopaper thus formed contains two segregations of water. The water held by nanocellulose slurry after filtration can be classified into two states:

(i) Free Water (ii) Bound Water (Sinquefield et al., 2020b)

Free water is defined as the bulk water that makes up for the (>95%) of the solution. This comprises of the free amount of unbound water that gets drained during majority of filtration and bound water is the amount that interacts with nanofibrils at a molecular level binding with them at particular sorption sites. (Solhi, 2023).

The wet cake like mat is pressed twice in the semi-automatic sheet former machine in the sheet presser. These are two stainless steel parallel plates which are hinged and work like a hydraulic press. The cake is sandwiched between two blotters made of filter membrane (Whatman Filters, No. 45, England) and placing a stainless-steel disc on top as a uniform pressure distributor. A pressure of 400kPa ± 10 kPa was applied to the sandwich twice. Before the second pressing, the blotters were replaced with a fresh set of filter papers. This procedure was carried out for 20 seconds each time.

Table 17 Showing Nanopapers (CNP) Properties from UMaine CNF Pressed at Different Temperatures.

Sample Name	Grammage (mg/cm^2)	Pressure (MPa) Hot-Press	Temperature and Time	Thickness (µm)
UM 01	3.7	2.4	• 25 °C • 30 minutes • room drying 72 hours between plates	60±0.05
UM 02	3.7	2.4	• 50 °C • 2 hours	40±0.06
UM 03	3.7	2.4	• 110 °C • 10 minutes	30±0.06

Pressure was applied to nanopaper to increase its packing density and compactness of the fibers. It also widely reduces pores by decreasing fiber-fiber distance and other defective voids. During drying under pressure, nanofibrils lose their swelling capacity and conformability of the fibers, this action is also known as hornification, (Fernandes Diniz et al., 2004). A similar value of pressure has been kept constant while drying all the nanopapers as mentioned above to maintain

uniformity. The room dried nanopapers were pressed in the Parallel Plate Hot Press with no working temperature for half an hour and then left for drying for 72 hours between stainless steel metal plates mentioned in the materials and methods section of the thesis. Drying temperatures on the other hand, has been increased to reflect on their morphological properties and thickness. During drying, the water evaporates depending on the temperature and time provided forming a denser network. It is to be noted that, CNF degrades around 279-280 ^{o} C, (Yildirim and Shaler, 2017) hence using 110 ^{o} C to dry nanopapers which was 10 degrees above the threshold of water evaporation. Varying drying temperature highly effects structural arrangement of nanofibrils that directly varies its effective thickness.

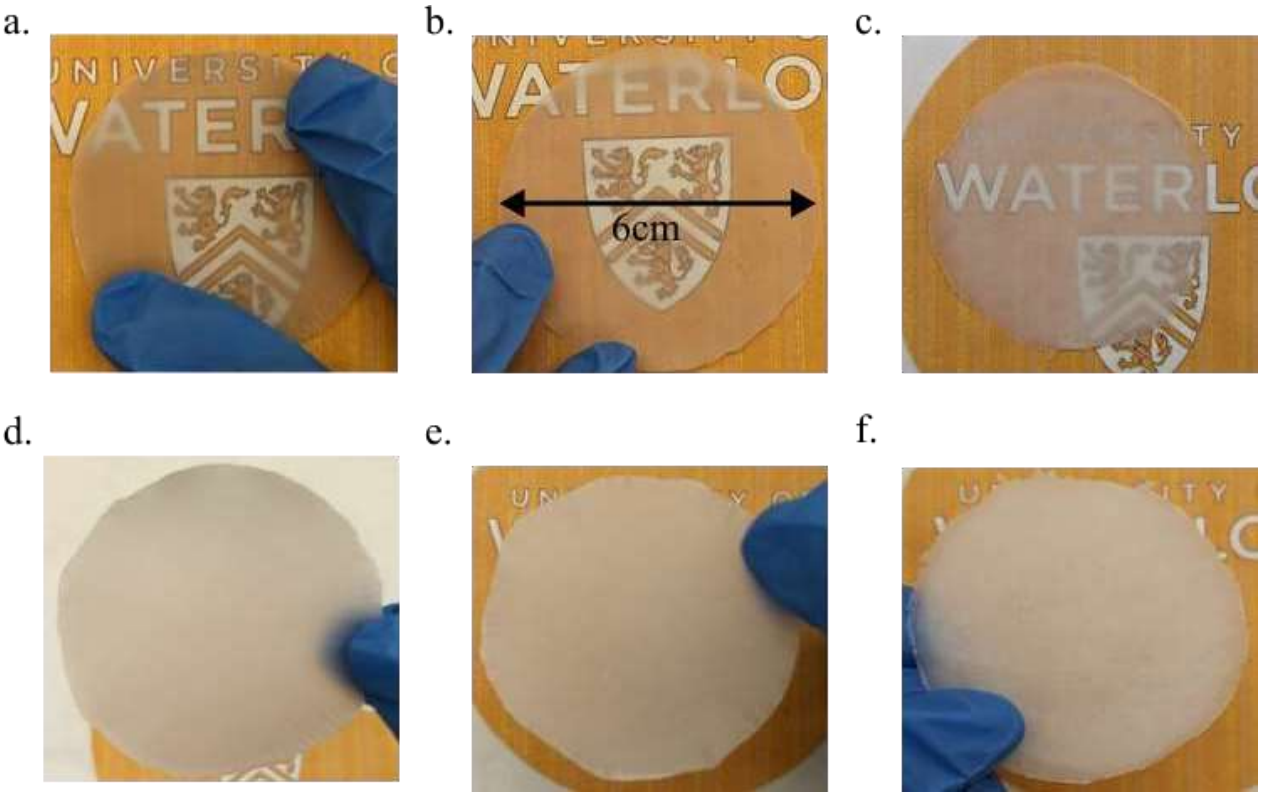


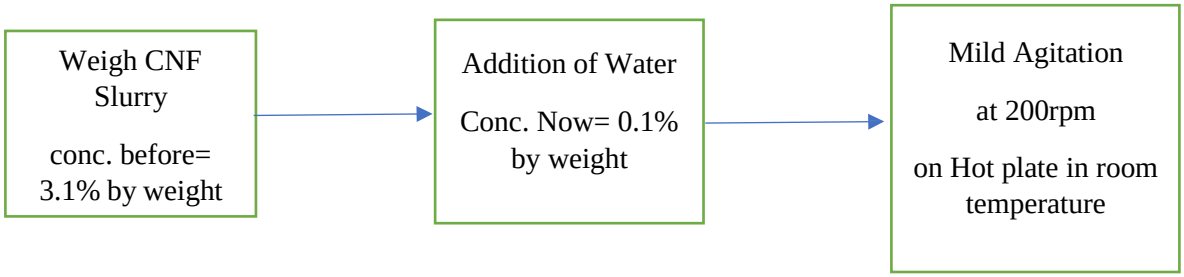
Figure 4.29. Shows UM Nanopapers of 3.7 mg/cm^2 grammage and varied drying temperature, (b) 25 ^{o}C (room temperature) (c) 50 ^{o} C (d) 110 ^{o} C (e,f,d) are similar samples (b,s,d) from 2cm above the yellow substrate. CNPs showed increasing rate of opacity with increase in drying temperature.

Nanopapers mentioned in figures 4.29, illustrate the change in opacity and aspect with increasing drying temperature. This is to display that nanopapers fabricated at higher temperatures, increased the hazy nature by two folds due to increased degree of cross-linking associated with high heat curing. Thermal discolouration has been noticed due to the ability of carbonyl groups on the CNF which allow chromophore formation in oxidised CNF. On a positive note, high temperature

healing results in a more compact stacking of fibers leaving no or too little inter-laying gaps, explained later while morphological characterization. 110^{o}C CNP had a lower thickness around 0.30±0.06 mm than room dried nanopaper with a thickness around 0.60±0.09 mm and giving it good apparent bendability (Niskanen et al., 2022b).

4.7.2.2. UW Filtered and Pressed Nanopaper

The CNF slurry thus produced in the lab, was diluted via the dilution expression to a similar concentration of 0.1 % by weight. A 500mL, 0.1 wt.% solution was subjected to homogenization. The solution was firstly agitated in hot plate in room temperature (25±2 ^{o}C) for about 15 minutes and solution was ultra-sonicated for an hour for enhanced dispersion of nanofibrils and homogeneity with 0.1 g CNF per 100 mL of the solution.



The filter membrane showed here is 4 cm in diameter attached to a sintered glass filtering funnel and Erlenmeyer beaker. After most of the water was removed and filtration time noted, the web like wet cake was removed from the membrane and pressed similarly like UM nanopapers in the semi-automatic sheet former. After repeating this step twice, the nanopaper was sandwiched between a fresh pair of Whatman Filter papers and pressed in the Carver Parallel Hot Press with varying temperatures.

Pressing Pressure in Sheet Former = 400kPa ± 10 kPa

Parallel Press Pressure = 2.4 MPa

It is to be noted that similar mass of CNF per nanopaper fabrication was used to construct both UM and UW nanopapers on two different sizes of membranes, 5.9cm and 4 cm respectively. Accordingly, the nanopapers for UW were thicker in width as the grammage was automatically higher due to smaller filtering area for the same mass of fibrils.

Table 18 Demonstrates Properties of Nanopapers from UW Pressed at Different Temperatures.

CNF	Grammage (mg/cm^2)	Pressure (MPa) Hot-Press	Temperature (T) and Time(t)	Thickness (µm)
UW	5.8	2.4	• 23-25 °C • 30 minutes • 72 hours in room b/w plates	90±0.08
UW	5.8	2.4	• 50 °C • 2 hours	60±0.07
UW	5.8	2.4	• 110 °C • 10 minutes	40±0.06

The table relates higher drying temperature to the decreasing thickness of nanopaper. There are a few factors that govern the structure of nanopapers along with their organization depending on drying temperature.

These factors can be classified as:

- Drying Rate: Increasing the temperature will give rise to a higher rate of evaporation leading to a faster rate of moisture removal from the wet web like structure. This causes densification of CNF network and the layers of fibrils formed during filtration come closer.
- Morphology: At higher temperatures the rapid evaporation causes faster consolidation and rearrangement of the fibers. This results in more fiber-fiber bonding leading to pore size reduction.
- Structure: Higher temperature also promotes the formation of stronger hydrogen bond by removing moisture completely, facilitating more extensive fibrillar arrangement. Lower drying temperatures may lead to weaker hydrogen bonding, resulting in bigger pores and lower tensile values.



Figures 4.30. UW CNPs of 5.8mg/cm^2 grammage show increase in opacity and light scattering from (left) Pressed at 25 °C, 50 °C (middle) and 110 °C (right)

- ***All test results of 100% CNF films hitherto shown are from Vacuum Filtration as solution casted films were a preliminary experimental set-up to understand nanocellulose fibrillar interaction***.

4.7.3. Comparison with established research

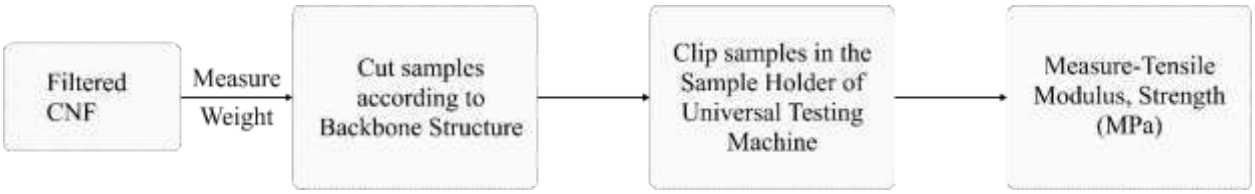
This study focused on obtaining CNF from industrial hemp via a series of mechanical and chemical treatments. Along with procuring nanocellulose, the research deals with comparing two different kind of CNFs and their properties effecting nanopaper formation. The importance of chemically treated fibers helps with a couple of reasons. Firstly, it reduces the humongous amounts of energy consumed while producing CNF only through mechanical procedures. Secondly, to manufacture nanopapers with higher transparency it is important to dissolve any chromophores or impurities that might cause yellowing of the paper. Regulated amounts of reaction time and temperature prevent the cellulose from degradation and altering their properties. Two different processes to fabricate nanopaper have been explored and a contrast between their end results was done. Most papers discuss obtaining nanopaper via filtration method as drying CNF in room temperature without constant humidity can cause lumps of irreversible agglomeration.

Results from characterization of mechanical, surface properties, surface morphology and structural organization are compared to various previously established research papers and their following references are provided with each section of their discussion.

4.8. Nanopaper Characterization

4.8.1. Mechanical Properties

The mechanical properties of CNPs formed from UM and UW nanocellulose fibers were determined from tensile modulus and tensile strength bar charts. The standard deviation was similarly calculated for 10 specimens of each kind.



Mechanical properties were based on their respective drying temperature. It was noticed in the graphical representation mentioned how the tensile modulus *(E)* showed higher values for nanopapers dried at 110^{o}C. Faster rate of evaporation of the bound water resulted in formation of stronger intermolecular bonds which enhances overall strength. The nanofibrils have a denser packing with smaller pores avoiding any air voids in the nanocellulose network.

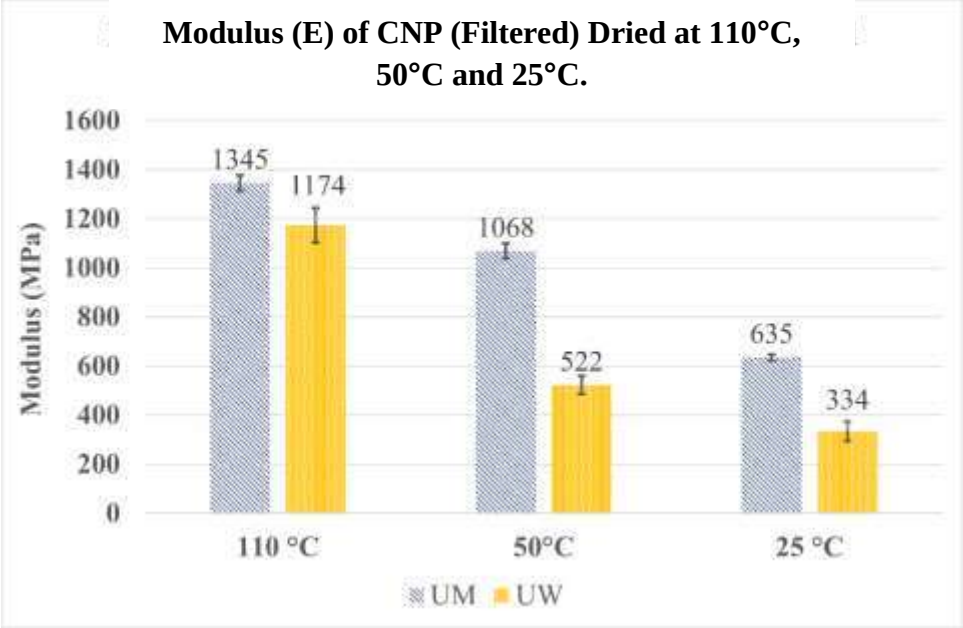


Figure 4.31. Bar charts, show the Effect of Drying Nanopaper with Varying Temperature on Young's modulus (MPa)

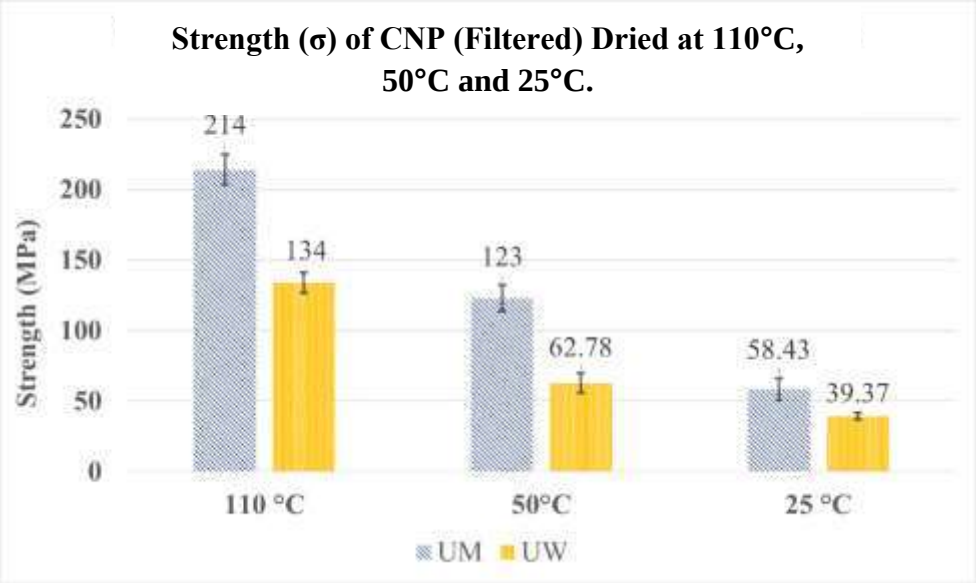


Figure 4.32. Bar charts, show the Effect of Drying Nanopaper with Varying Temperature on Tensile Strength (MPa)

The highest measured modulus for CNP of a grammage 3.7mg/cm^2 was around 1345 MPa from UM formed at 110^{o}C and lowest documented value was about 334 MPa of CNP from UW nanocellulose fibers.

A major difference in modulus and strength were noticed when nanopapers were dried at 50^{o}C than room temperature (25 ± 5)^{o}C . The values significantly doubled producing stronger CNPs and explaining the phenomenon of low packing of fibrils dried at lower temperatures. A difference between fibrillar orientation that can be noticed between casted and filtered films is the directional arrangement of fibers in a multilayered organization. Along with aspect ratio, greater inter-fiber bonding and high degree of fiber alignment (Kafy et al., 2017a) form stronger nanopaper. These results demonstrate that the effective strength increases with high temperature drying as previously shown by Wu et al., (2013) and Niskanen et al., (2022).

A Tukey-Kramer Analysis statistical analysis was done using ANOVA comparing sample averages and determining if the comparison is statistically different. The test significance was 95% of confidence. It is a well-known method of comparing value averages and uses variability of all results simultaneously to compare sample means pairwise at a fixed significance level (α).

The results show significant differences in their modulus among the nanopapers dried at altered temperatures, table 20. The increment in their tensile modulus defines that under higher

temperature the material becomes stiffer and are less prone to deformation. The highest value calculated for modulus is 1345 MPa of UM, 110ºC dried nano-paper.

Table 19 Tensile Modulus and Strength of Filtered UM, UW CNPs Dried at Different Temperatures

Fiber	Tensile	Property	110ºC	50ºC	25ºC	Units
UW	Tensile	Modulus	1174 ± 71	522 ± 38	334 ± 43	[MPa]
		Strength	134 ± 7.3	62.78 ± 7.0	39.37 ± 2.4	[MPa]
UM		Modulus	1345 ± 32	1068 ± 30	635 ± 12	[MPa]
		Strength	214 ± 10	123 ± 9.5	58.43 ± 7.5	[MPa]

Likewise, tensile strength followed a similar pattern, even though some similarity was noticed in the strength of UM and UW nanopapers dried at 25ºC.

Table 20 Tensile Properties and their Statistical Analysis to compare Significant Changes in their Mean.

Sample	Drying Temperature (ºC)	Tensile Modulus (MPa)	Tensile Strength (MPa)
UM	25 ºC	635±12.36 ^{c}	214±10.80 ^{f}
	50 ºC	1068±30.33 ^{d}	123±9.52 ^{c}
	110 ºC	1345±32.57 ^{f}	58.43±7.56 ^{b}
UW	25 ºC	334±43.44 ^{a}	134±7.27 ^{d}
	50 ºC	522 ±37.92 ^{b}	62.78±7.04 ^{b}
	110 ºC	1174±71.37 ^{e}	39.37±2.36 ^{a}

"Different letters in same column represent significant difference (p<0.05) using Tukey HSD Test, with 'a' being the lowest and 'f' being the highest."

"All test results are in significance of 95%"

4.8.2. Normalized Modulus and Strength of UM Nanopaper via Filtration vs. Drying Temperature

The following graph in figure 4.33. shows the modulus normalized to the value of 25^{o}C ±5 ^{o}C and 110^{o}C ± 5^{o}C respectively. The coefficient of determination is R^2= 0.98 was to show the increment in mechanical properties were logarithmically related to their drying temperature. This states that with little amount of heat, the properties jump several folds higher.

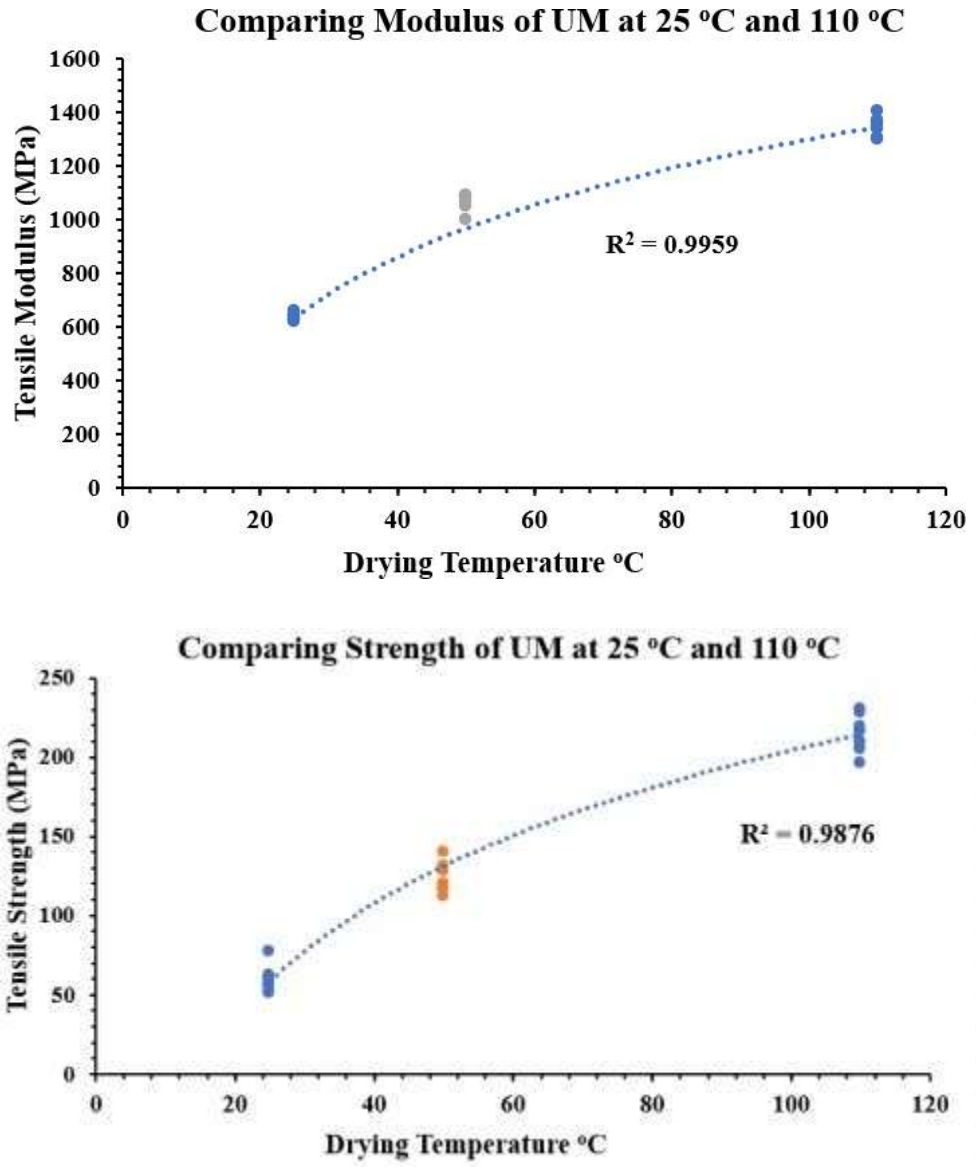


Figure 4.33. Logarithmic relationship of Tensile Modulus and Strength as a function of Temperature

4.8.3. Surface Characterization Analyses

4.8.3.1. Surface Energy of UM, UW 100% CNF Films

The surface energy was calculated by measuring contact angle (θ) using a Dynamic Surface Analysis system (NE-1000X, Syringe Pump) equipped with a video camera and a MATLAB software for analysis.

Surface energies were calculated for room dried nanopapers only, for both UM and UW films, with two different thicknesses due to difference in their grammage (4cm and 5.9cm). It was noticed that neat nanocellulose films were highly hydrophilic due to their polar -OH groups and showed higher values of surface energies due to a collective effect of hydrophilic groups, aspect ratio, crystallinity of CNF and porosity of the films (Du, 2021).

Wettability

The contact angle (θ) of room dried nanopapers from UM, UW were measured over 30 seconds each with two separate liquids, such as, water and diiodomethane. The values of the contact angle can be found in figure 4.34. It was observed that the contact angle between the liquids and surface was dynamic in nature that is there was a decrease in the angle measured. The hydrophilic nature of nanocellulose films caused reduction in the contact angle over time, as water diffused through the nanopores due to water absorption and swelling thus decreasing the tension between cellulose and water interface. The difference in their thickness did not majorly interfere with the penetration of liquids as observed in the similarity of their contact angle data. **Swelling property** of nanocellulose causes reduction in stiffness and formation of **shear stresses** at interface that causes degradation of fiber-matrix.

Table 21 Surface Tension of dispersed and polar components of Two Liquids Used

Sample Properties	**UM**	**UW**
Surface Energy (mJ/m^2)	63.74	64.95
Thickness (nm)	60	90

Table 22 Surface Tension and Thickness Data for Uncoated Room Dried Nanopapers from UM, UW

Reference Liquids	σ_l^D	σ_l^P	σ_l
Diiodomethane (CH_2I_2)	50.8	0	50.8
Water (H_2O)	19.9	52.2	72.1

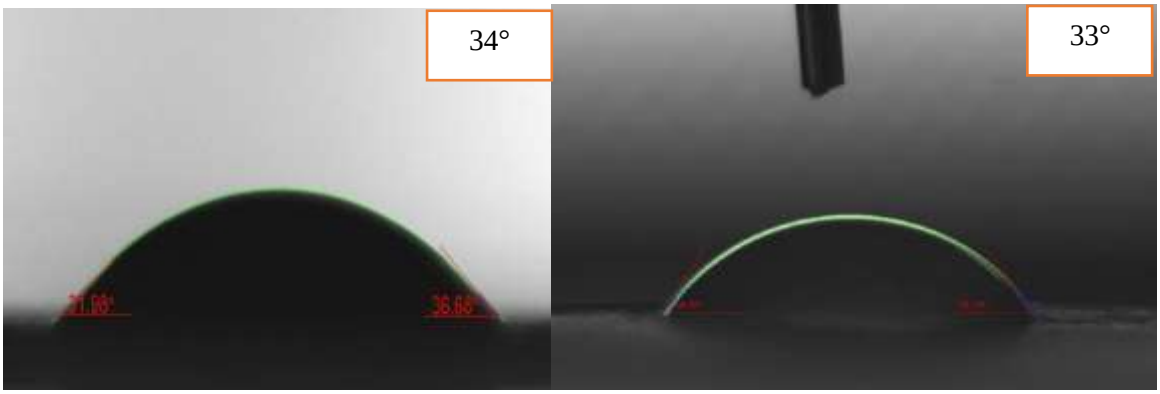


Figure 4.34. Characteristic Water drop after 12 seconds of immersion on UM (left) and UW (right), respectively.

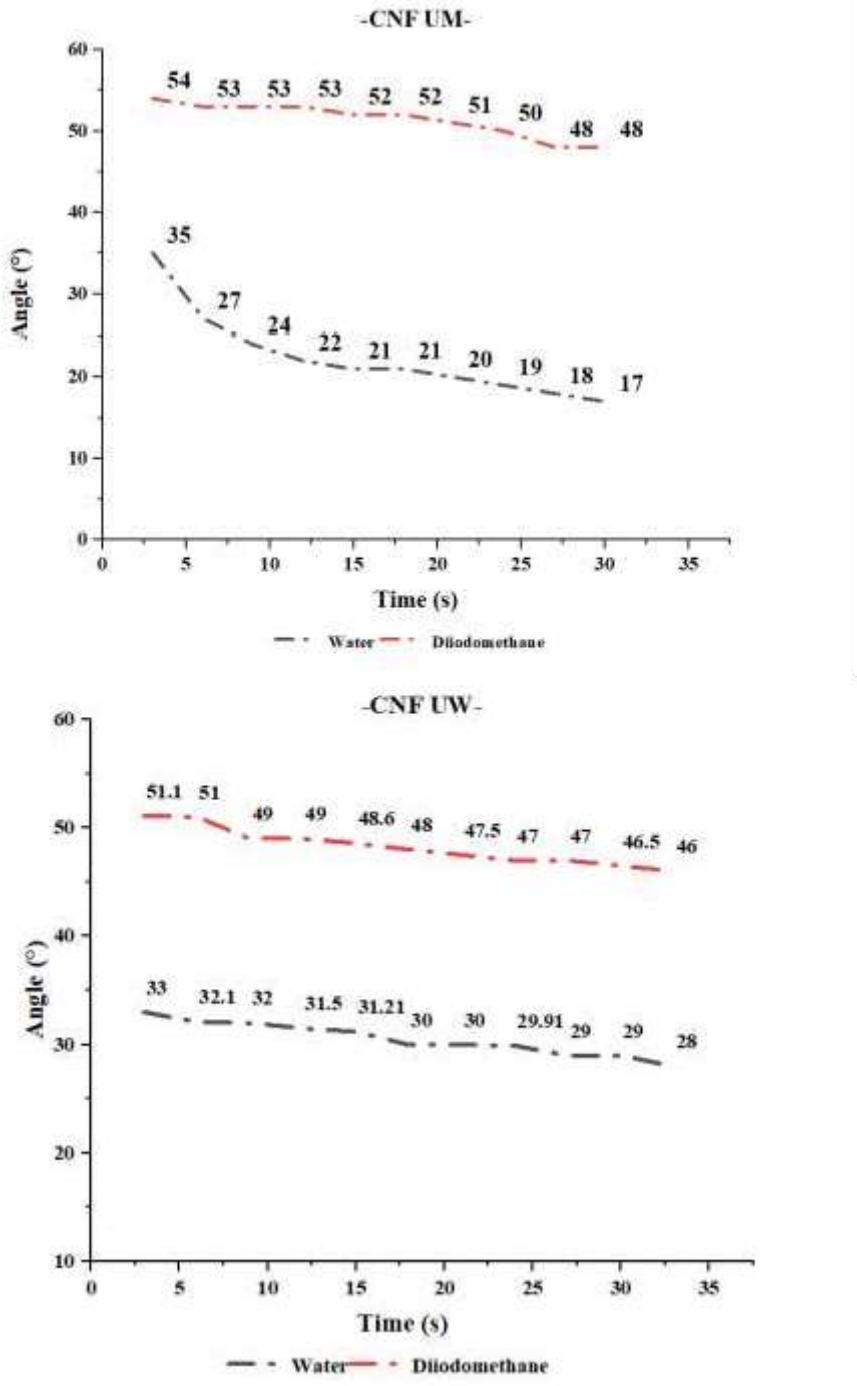


Figure 4.35. Dynamic contact angle of 25ºC dried nanopapers

All WCA measurements were carried out in compliance to ASTM D5946. According to figure 4.35., between UM and UW nanopapers, the stability of a sessile water drop on UW nanopaper was more constant than on UM nanopapers.

The two CNPs, showed similar properties of wetting with liquids even though they have significant difference in their grammage. This is an attribute of the high affinity of surface hydroxyl groups of nanopapers. UM nanopapers have a higher dynamicity with polar solvents could be due to the larger pores on their surface, as visible in figure 4.36.

Table 23 Dynamic Contact Angle, UM and UW Room Dried Nanopapers.

Room dried (25ºC) films were considered for the test	**UM**	**UW**
Water Contact Angle (º)	34 ± 4.9	33±5.2
Diiodomethane Contact Angle(º)	53.4 ± 1.2	51±2.3

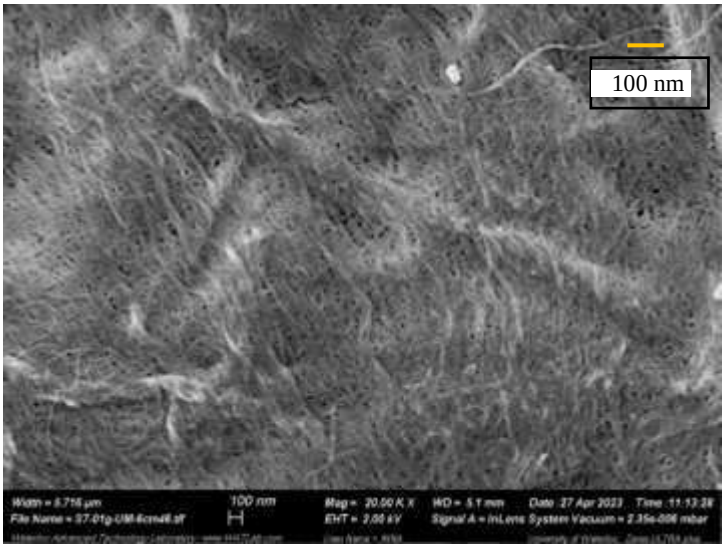


Figure 4.36. UM Nanopaper dried at 25°C prepared through Filtration.

4.8.3.2. Surface Morphology

Scanning Electron Microscopy was used as for the investigation of the surface topography and cross-sectional morphology of the nanocellulose papers.

This thin film of gold is approximately 20-25 mm thick depending on the 139 s exposure time in the gold plasma. Micrographs of each sample pressed and dried at three different temperatures 25°C, 50°C and 110°C are expressed. Images are expressed for three samples (top view) of UM nanopapers, and similar magnification has been maintained to compare their results.

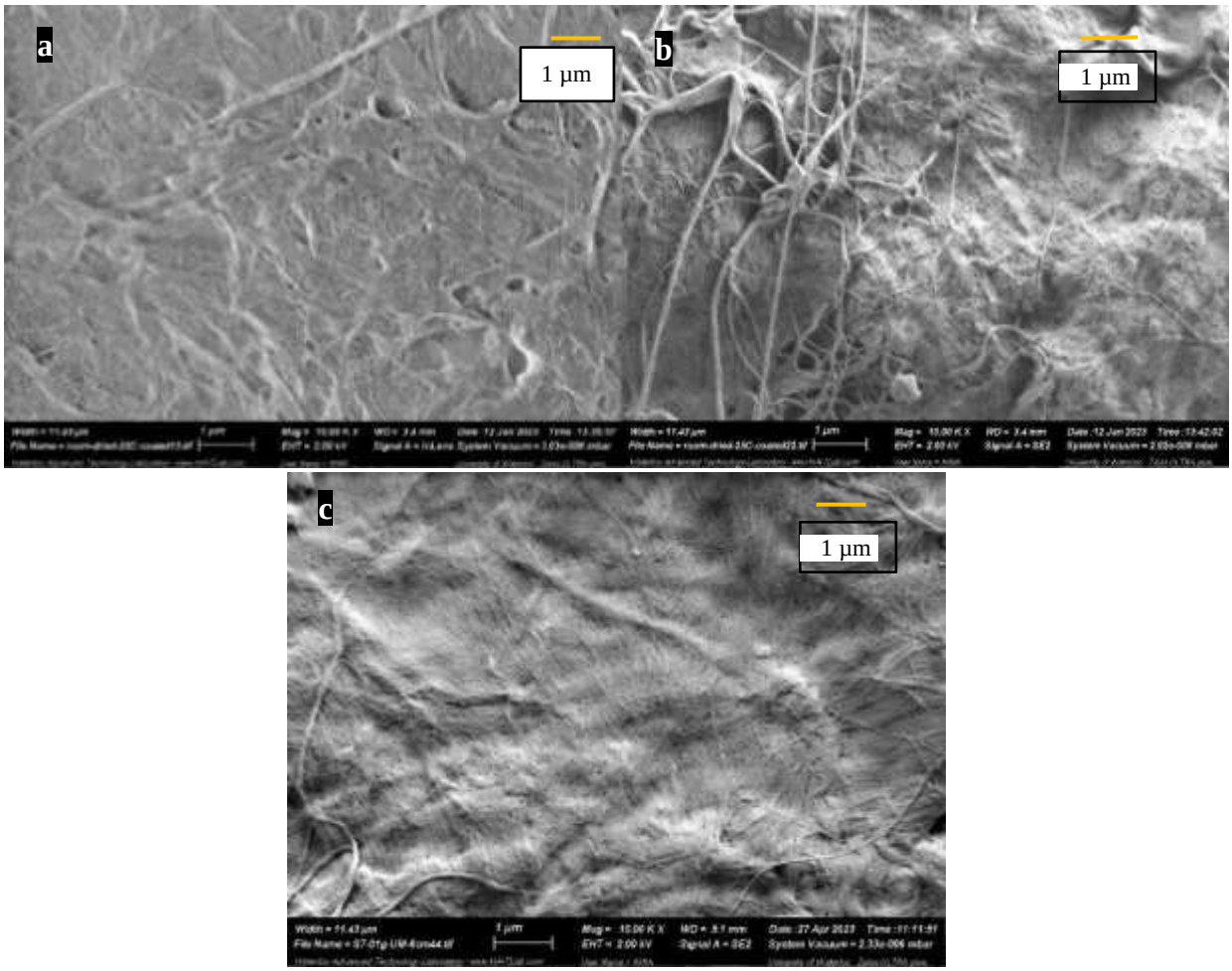


Figure 4.37. SEM micrographs of UM CNP fabricated at (a)25 °C, (b) 50 °C and (c) 110 °C.

Figure 4.37. shows three micrographs of nanopaper fabricated from the similar grammage and same amount of nanofibrils, 0.1g of CNF by mass, per each nanopaper. The films show interconnected NC network like structure which are linked by extensive hydrogen bonding. CNF get deposited during filtration in layers in the form of fiber bundles (Moon, 2011).

The surfaces of the nanopaper qualitatively suggest that with increasing drying temperature of nanopapers, the porosity of CNP decreases. This validates the effect of temperature in the orientation of fibers during drying. Higher temperatures may promote better alignment, leading to a more compact structure and potentially reducing the porous nature of the nanopaper. Due to the nano-meter size which gives them high surface area and abundance of hydroxyl groups all images show good interconnection of nanofibers through hydrogen bonding preventing fiber slippage.

The pore size was calculated via imaging software, ImageJ, USA. An average of multiple pores (30 pores average) was considered to define the difference in their sizes as outlined in table 24.

Table 24 Pore Diameters with respect to Drying Temperature of UM CNPs

Morphology of UM CNPs	Dried at 25°C	Dried at 50°C	Dried at 110°C
Pore Diameter (nm)	70 ± 5.2	55 ± 10.1	38.2 ± 4.6
Thickness of CNP (µm)	60	40	30

The figures 4.38. below compare the differences between fiber network in solution casted and vacuum filtered nanopapers, both dried at room temperature. The casted film showed agglomerates of bunch of fibers and bigger voids leading to the formation of bigger pores. This also contributes to the non-uniform thickness with larger standard deviation in case of solution casted films. On the contrary, fiber-fiber connections are more homogeneous resulting into smaller pore sizes.

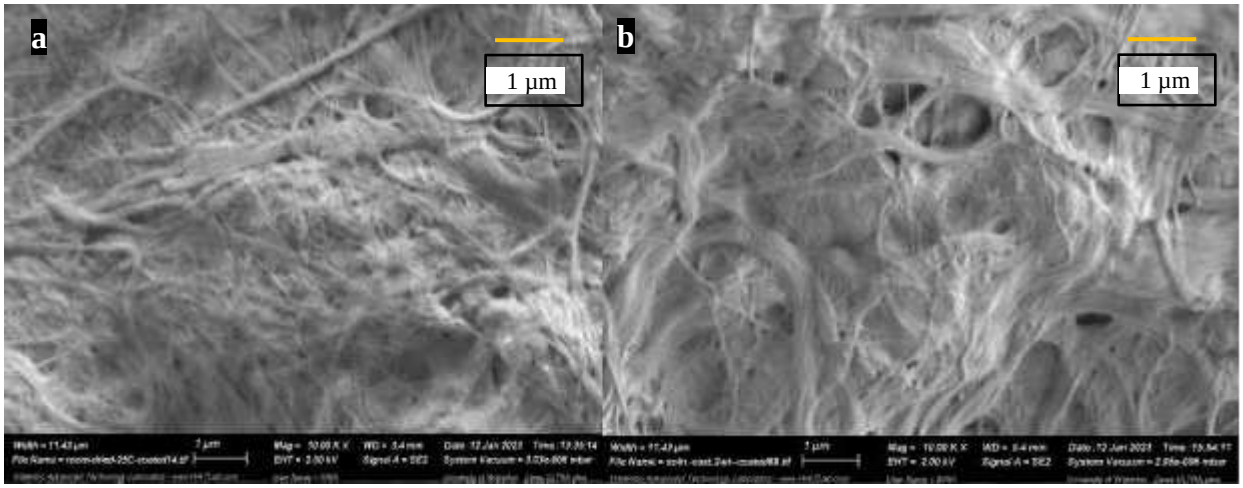


Figure 4.38. Shows CNPs dried at 25° C (a) Filtered Nanopaper 0.1g CNF (by weight) both from UM CNF (b) Solution Casted 0.3g CNF (by weight)

The average pore diameters of casted films containing 0.3 g of CNF by mass, per specimen was around (450±34) nm. The higher deviation was presumably because of fibrillar aggregation during evaporation of solvent. Casted films have pore diameters almost '300x' times larger than films formed from filtration through analysis. Similarly, to understand the layered structure of nanocellulose deposition, figure 4.39, shows FE-SEM of fractured images of nanopapers cleaved in cryogenic atmosphere. The interlayer distances were mapped using software for same three

nanopapers. The cross-sectional width of high temperature dried nanopaper was around 35 µm and the room dried nanopaper had a width of around 62 µm. A layered structure can be seen in the image of nanopaper cross section. This confirms an interesting phenomenon- the nanopaper was created by multilayered nanofibrous flakes which may arise from filtration process. This defined the property of nanocellulose fibrils to self assemble into layers. Increasing drying temperature compacted these layers even closely due to rapid evaporation of water amongst the wet web like network (Wang et al., 2013). With lowering interlayer distance and inherent property of higher surface area of nanofibrils, it is easier for the fibers to bond with existing -OH groups and lower any air cavities resulting in higher tensile characteristics.

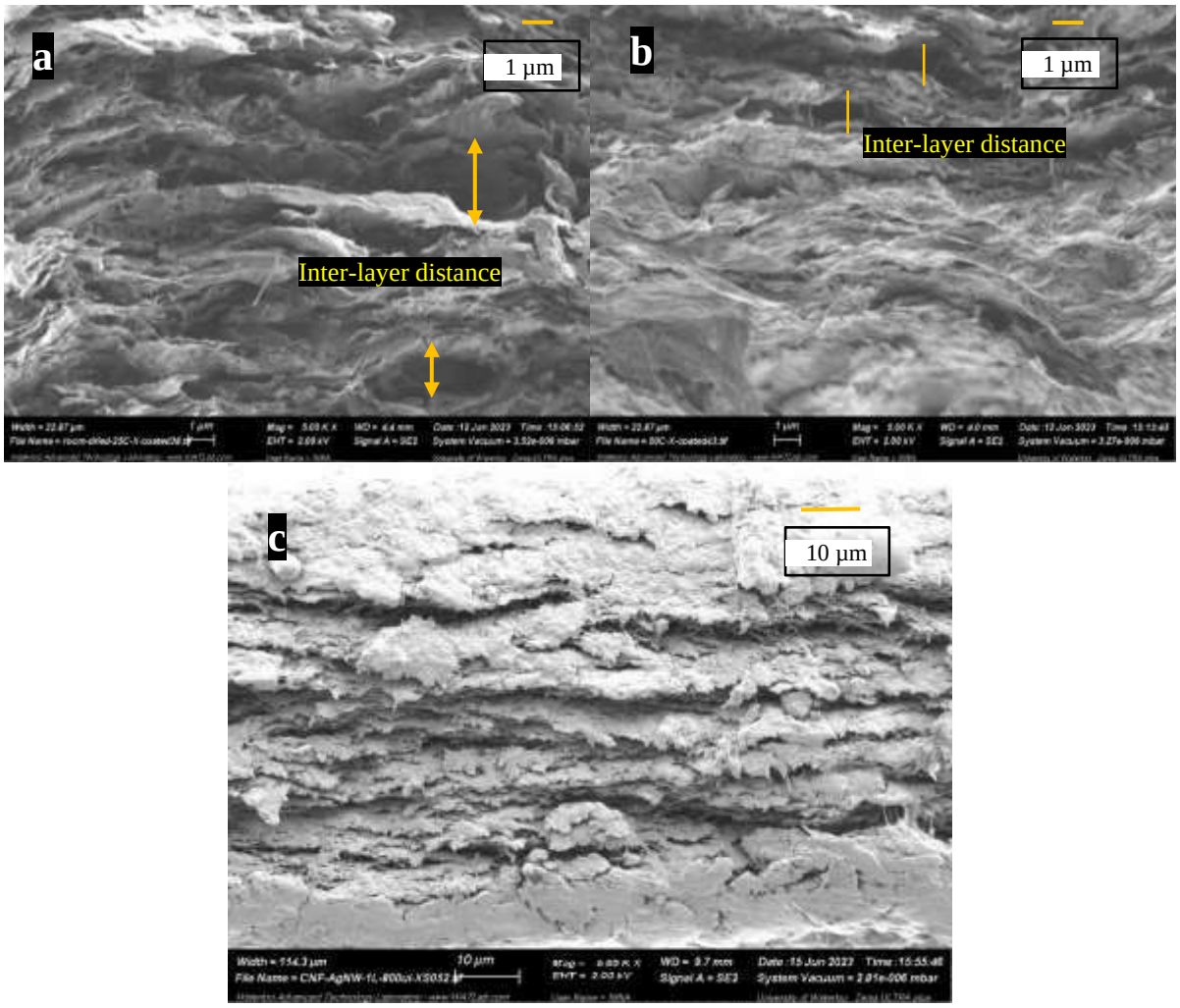


Figure 4.39. SEM micrographs of the fracture surface of the cellulose nanopapers dried at 25°C (top left), 50°C (top right) and 110°C (below)

Table 25 below outlines average distance between adjacent layers of CNPs produced at different temperature ranges and their packing density (g/cm^3).

Properties	**25ºC**	**50ºC**	**110ºC**
Inter-layer distance (nm)	420.5±22.14	188.6±16.9	34
Density of CNP (g/cm^3)	0.645	0.967	1.106

The density is inversely proportional to the thickness of each nanopaper, which also directly comments on the consolidation of fibers during drying these CNPs.

Similarly, UW nanopapers manufactured at 25˚C and 110˚C were tested for their morphological dimensions. Nanopapers of 4cm diameter and 0.1g by mass per specimen were subjected to FE-SEM to delve deeper into its porous structure. Due to the same mass of CNF over a smaller area, the intertwining of fibrils were more dense and wider bundles of fibers formed due to fiber-fiber conformation decreasing overall porosity. Few bigger fibers were noticed in the ariel view of these micrographs which presumably originated from inefficient mechanical refining or even non-uniform deposition of fibrils during filtration procedure. This effects the aspect ratio and lower mechanical stability. The average pore sizes decreased in comparison to UM nanopapers as for a same mass of CNF that is 0.1g, a smaller filtering area was used to get this nanopaper.

Table 26 Pore Diameters with respect to Drying Temperature of UM CNPs

Morphology of UW CNPs	**Dried at 25 ºC**	**Dried at 110 ºC**
Pore Sizes (nm)	42.1±9.8	33±7.3
Thickness of CNP (µm)	40	90

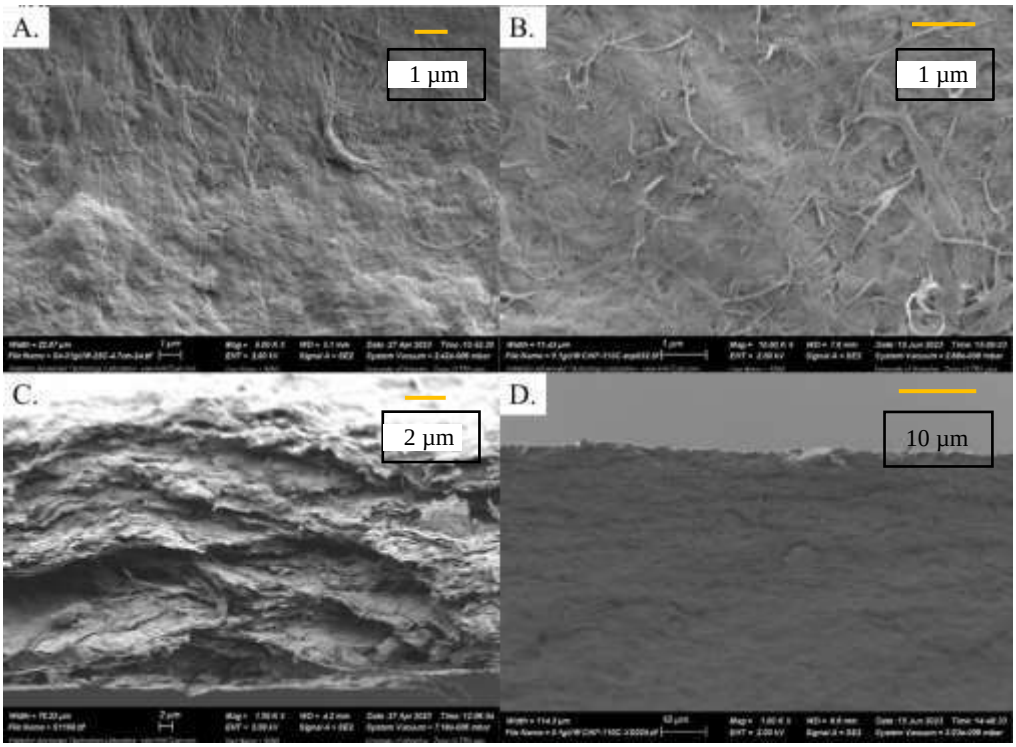


Figure 4.40. UW filtered nanopaper dried at 25°C (A), and UW filtered nanopaper dried at 110°C (B), Cross-Sectional view of Casted UW nanopaper (C), 110°C dried Filtered UW nanopaper (D).

The width of cross section was much more uniform in case of 110 °C dried nanopaper. The room dried paper showed inhomogeneity in the layers caused by absence of any heat treatment and compression (figure 4.40. C, D).

In the formation of conventional micro paper or fabrication of fibrils through casting, fiber defects and non uniform shear transfer along the fibrils, which may develop during extraction and processing are avoided and unaccounted for. During drying, paper shrink which significantly affects various properties and paper made under restraints showed greater modulus than freely evaporated papers. Much analogous to the concept of ***network activation*** where freely individualised fibers are stretched and straightened upon drying under pressure or some weight. This in turn increases their mechanical properties as seen by Kulachenko, (2012) and Niskanen, (2022c).

4.9. Percolation of Fibrils and Porosity Effecting the Strength, and Characteristics of Nanopaper.

Cellulose nanopaper has an integral porous structure ranging between sizes of 20 to a few hundreds of nanometers. The porous structure forms due to the variation of arrangement of these nanofibrils during the formation of nanopaper.

4.9.1. Calculating Porosity of Filtered UM Nanopapers Dried at Variable Temperature

Porosity of these films thus can be controlled by various factors, in this research the temperature provided while drying the nanopapers have given rise to films with different porosities.

In general, the increase in porosity decreases the tensile modulus and tensile strength due to the presence of air instead of nanofibers. The porosity measurement was carried out on UM nanopapers only to showcase how increasing the temperature while drying results in lower porous nanopapers. To find the porosity from equation (I), it is important to find the density of these films. Five films were fabricated at different temperatures to see the general trend of porosity.

Table 27 Thickness Effecting Packing Density of Nanopapers dried at Different Temperatures

Drying Temperature	25 °C	50 °C	70 °C	90 °C	110 °C
Density (g/cm^3)	0.645	0.968	0.978	0.986	1.106
Thickness (µm)	60±0.05	40±0.06	38±0.20	35±0.09	30±0.06

Using the porosity equation

$$\text{Porosity } (\%) = (1- \rho_{film/}\ \rho_{cellulose}) \times 100\% \qquad (I)$$

($\rho_{cellulose}$= 1500 kg/m^3 *or* 1.5 g/cm^3)

The table 28 outlines the different porosities of nanopapers and their respective tensile modulus as well as strength. There was a dramatic increase in mechanical features when porosity was between (35-30) % intending that there was good percolation among nanofibrils, dried between 50 degrees to 100 degrees Celsius.

Table 28 Porosity and Mechanical Properties According to their Respective Drying Temperatures

Drying Temperature (°C)	**25 °C**	**50 °C**	**70 °C**	**90 °C**	**110 °C**
Porosity (%)	55 ± 5.9	34 ± 3.1	31±3	30±2.5	29±2.9
Young's Modulus (MPa)	635±12	1068±30	1156±29	1190±36	1345±33
Tensile Strength (MPa)	58.4±7.6	123±9.5	145±6.7	158±5.3	214±10.8

CNPs dried at room temperature had higher extent of interfibrillar space resulting in higher porosity. Figure 4.41., exhibit the increase of mechanical attributes following a power law curve (Ghanbarian and Male, 2021), between 45% to 65% of fiber volume fraction, beyond 65% of fibrillar fraction, the nanopapers exhibit high values of tensile modulus and strength increasing exponentially.

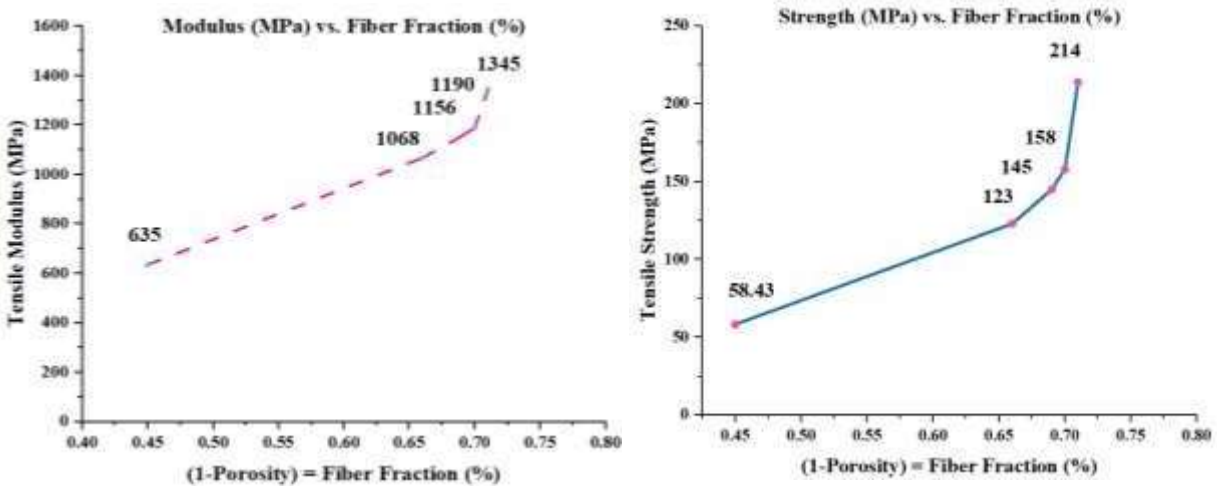


Figure 4.41. Fiber fraction as a function of Modulus of Nanopapers dried at different temperatures, Increasing strength at lower porosities with variation in drying temperature.

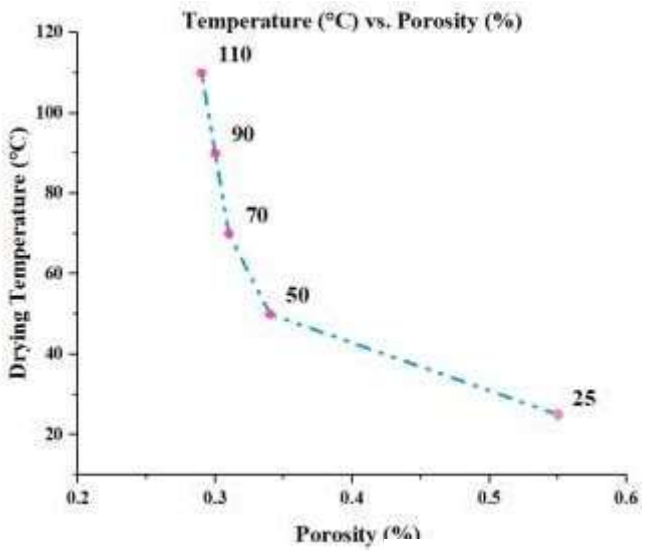


Figure 4.42. Graphical Representation of Decreasing Porosities with Increasing Temperature.

The porosity of nanopapers decrease by 20% by applying temperature from 25ºC and 50˚C during drying which consolidates the fibrillar network and minimizes the pores, figure 4.42. High porosity of nanopapers promotes high specific surface area of the films. Similar results were noticed Meng and Wang, 2019b.

4.10. Addition of Synthetic Polymers to Cellulose Nanofiber Films to Increase their Optical Properties

4.10.1. Poly vinyl Alcohol (PVA) with UW, UM CNF Films – A Hydrophilic Alternative

The gist of this segment is to investigate the properties of different blends of PVA and CNF. As mentioned in section 2.9., Poly vinyl alcohol is a biodegradable hydrophilic filler, and the main objective was to build a film composite with unique properties such as heightened transmittance and physical stability.

The table 29 outlines the thin film composites with different proportions of PVA and CNF that were casted and their properties were examined.

PVA Proportion (%)	CNF UW Proportion (%)	Mass of PVA(g)/ 100mL Water	Mass of CNF (g)/ 100 mL Water
100	**0**	4	0
50	**50**	2	2
10	**90**	0.4	3.6
5	**95**	0.2	3.8

All compositions were considered for a total of 200 mL of solutions and 4g of Polymer (CNF+PVA); variable concentrations were used to observe significant changes in the film characteristics.

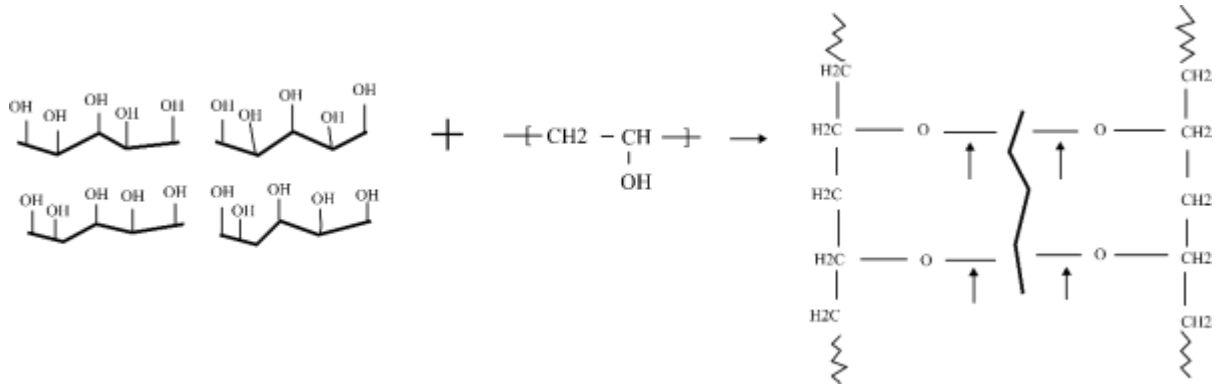


Figure 4.43. Illustration showing Hydrogen bonding between PVA + CNF, arrows show 'H' bonding.

Figure 4.43. elucidates crosslinking via hydrogen bonding between PVA and CNF as both contain hydroxyl groups (-OH) on their surface. Stronger intermolecular forces, enhances bond densities and improve overall transparency.

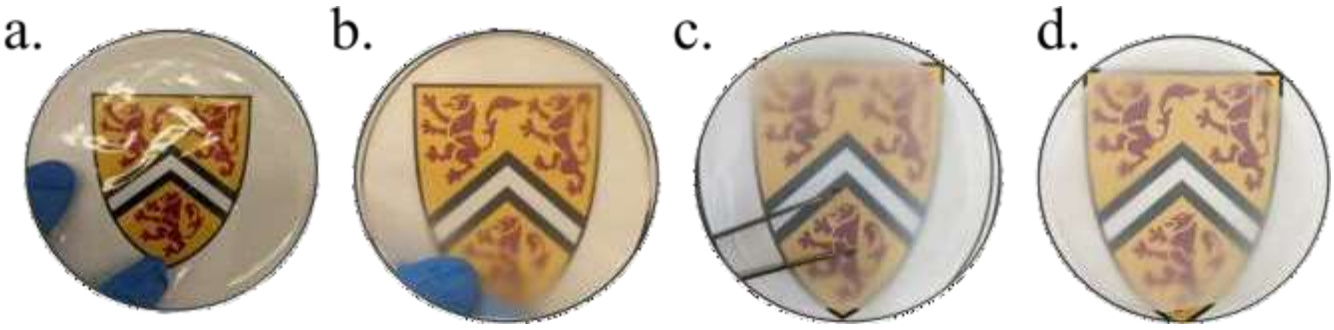


Figure 4.44. Different Proportions of PVA and CNF were casted (A) 100% PVA, (B) 50%PVA/50%CNF (C),10%PVA/90%CNF (D) 5% PVA/ 95% CNF all samples were made from UW CNF.

Characteristic Analysis

4.10.1.1. Mechanical Properties

Tensile Test

Tensile tests were performed according to the standardised ASTM: D882-12. Figures 4.45-4.46 illustrate the mechanical properties of PVA/CNF films.

Table 30 Tensile Modulus (E) and Strength (σ)

Composition of PVA & CNF	**50%(PVA+CNF)**	**10%PVA+90%CNF**	**5%PVA+95%CNF**	**100%CNF**
Tensile Modulus (MPa)	1241±38	900±60	814±44	386±73
Tensile Strength (MPa)	92±5.7	70±7.0	61±9.0	40±15.3

It was observed that the tensile properties of the films improved rapidly with insertion of PVA. Significant increase in modulus was noticed at 50% as well as 10% PVA. The PVA and CNF remain dispersed in each other, where PVA holds the CNF network whereas, CNF gives mechanical agility and stability to the composite as noticed in the works of (Wu et al., 2019) and (Wang et al., 2021). Additionally, increase in the fiber-fiber bond densities most likely favours high strength and ductility.

Figures 4.45. and 4.46. shows the mean comparisons of the mechanical properties of young's modulus and strength of PVA/CNF thin films. Pure PVA has a strength of 48.4 MPa whereas, young's modulus around 707.9 MPa as per Jain et al., (2017).

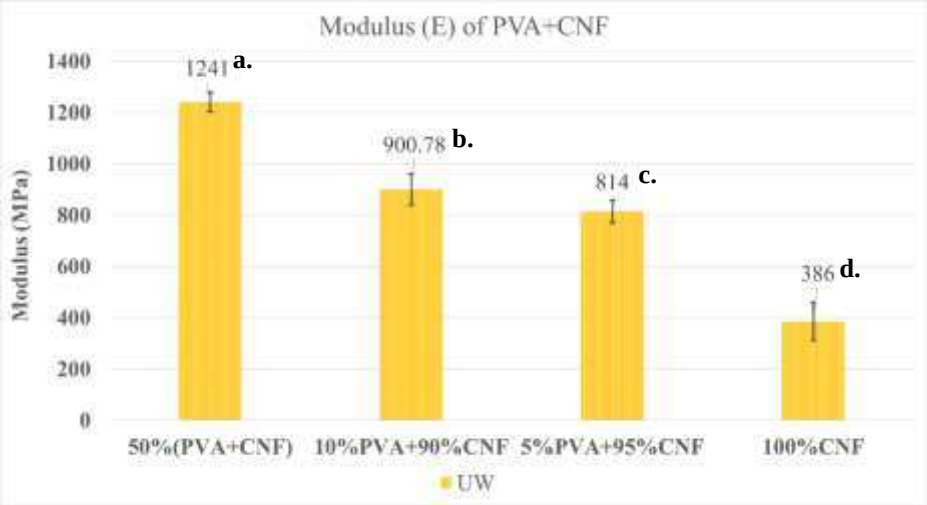


Figure 4.45. Tensile Modulus of Solution Casted Films with decreasing concentration of UW CNF

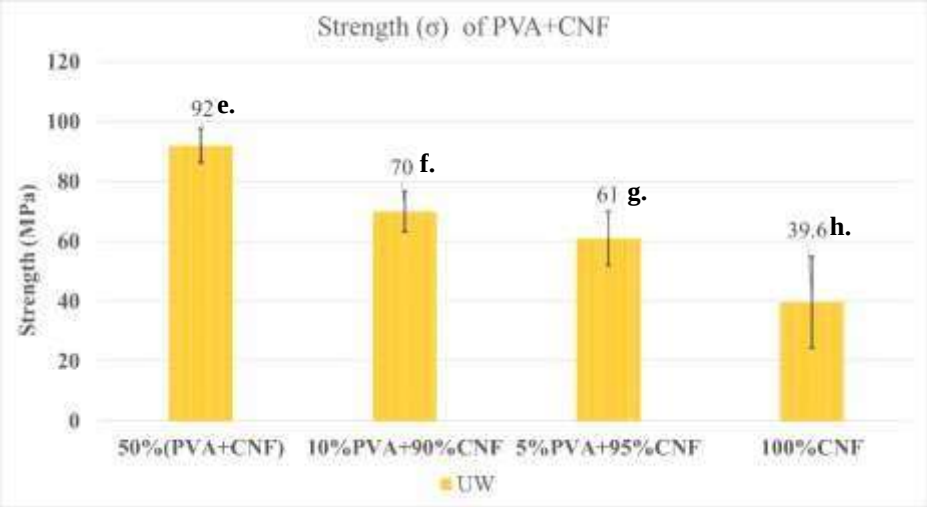


Figure 4.46. Strength of Solution Casted Films with decreasing concentration of UW CNF

Note: Different letters in same column represent significant difference ($p<0.05$) using Tukey HSD Test, with 'a' being the lowest and 'f' being the highest.

4.10.1.2. Optical Properties

UV-Vis-Spectroscopy

Due to the proximity of refractive indices between PVA and CNF, n = 1.47 and n = 1.45 respectively, composite thin films showed higher transmittance than 100% neat CNPs. Owing to the excellent optical transparency of PVA, neat PVA films showed a transmittance as high as 100% in average in a wavelength between 200-800 nanometers.

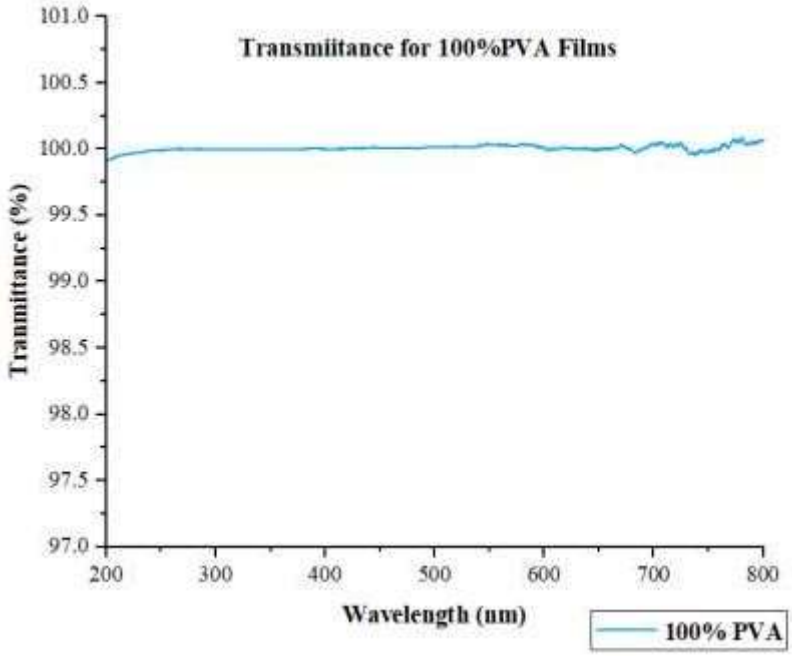


Figure 4.47. 100% PVA Film Transmittance within (200-800) nm

The transmittance (Tr. %) of 50PVA/50CNF and was as high and almost comparable to the 100%PVA film which was around **99.6 %** but with decreasing amount of PVA, the films displayed lower transmittance especially on 700-800 spectrum of light. The Tr. Values of 10PVA/90CNF and 5PVA/95CNF reported values of **98.6% and 98.32%** respectively.

Even though, the spectral analysis reported higher values of transmittance, visually the films formed under lower mass of PVA were corrugated and white, cloudy in appearance. This is due to the uneven aggregation of CNF while drying in the environment as seen in figure 4.48. This highly impedes the passage of light. A range of weight percentages were used to determine the maximum transparency achieved by these composites.

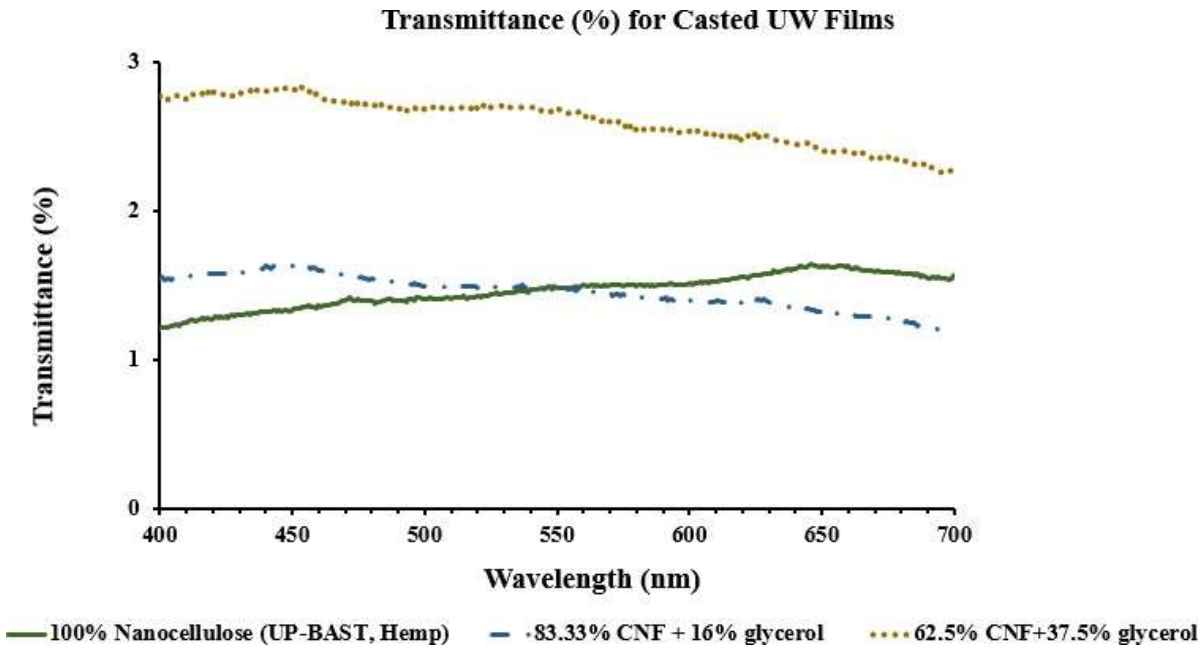


Figure 4.48. Casted films from UW CNF with tr. (%) 1.5%, and 2% and 3.2% for 100% CNF, 83CNF/16Gly and 62.5CNF/37 Gly respectively.

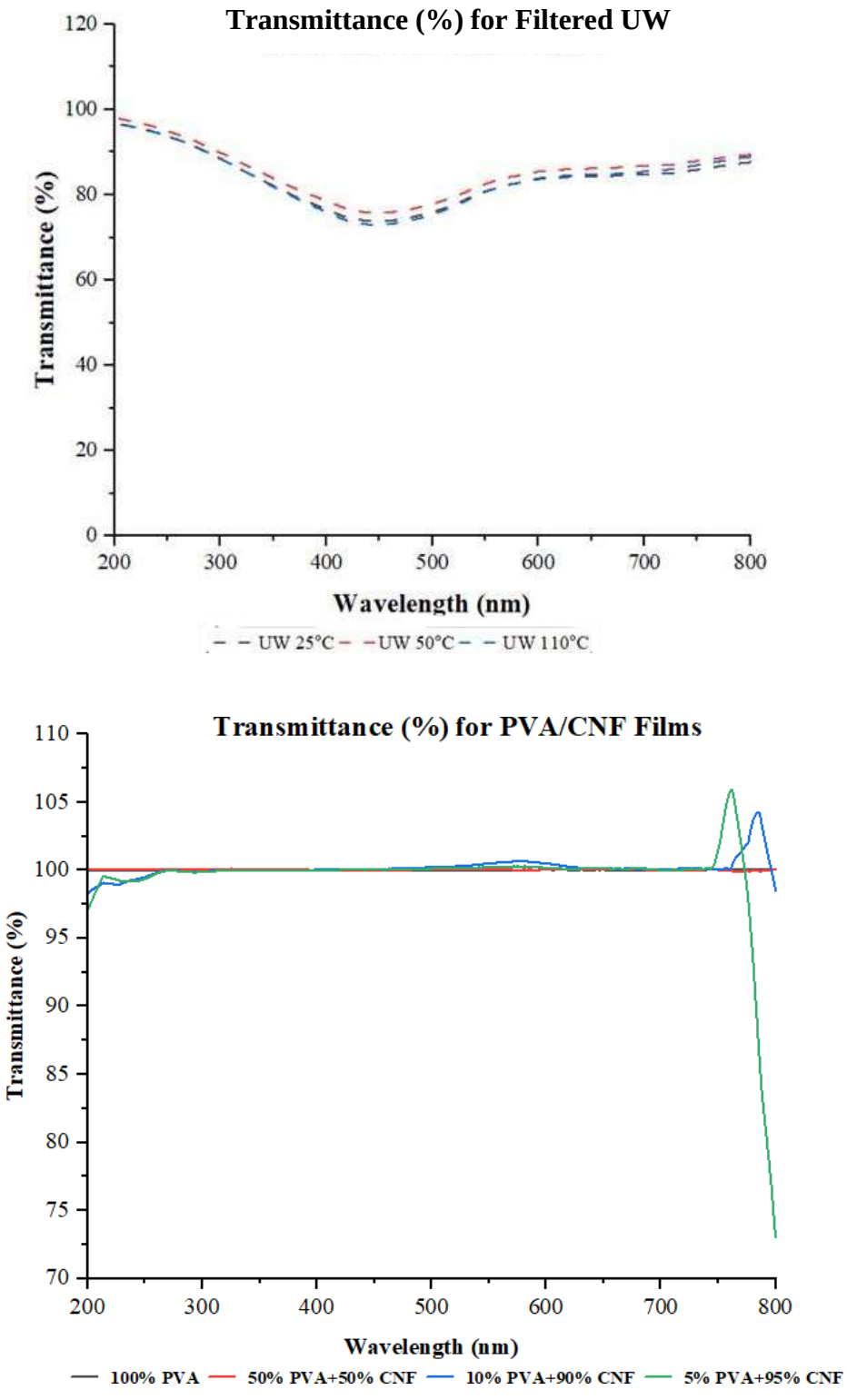


Figure 4.49. display of Tr. Values of filtered nanocellulose films from UW slurry(top) dried at 25°C, 50°C & 110°C for 100% CNF and (below) Casted films with PVA and UW CNF for different compositions.

Filtered UW films had a more even thickness and distribution of nanofibers resulting in an increase as much as 74% transparency comparing figures 4.48. and 4.49 (top). The increased transparency makes this film suitable for hosting several opto-electronics for further inking or printing devices such as OLEDS.

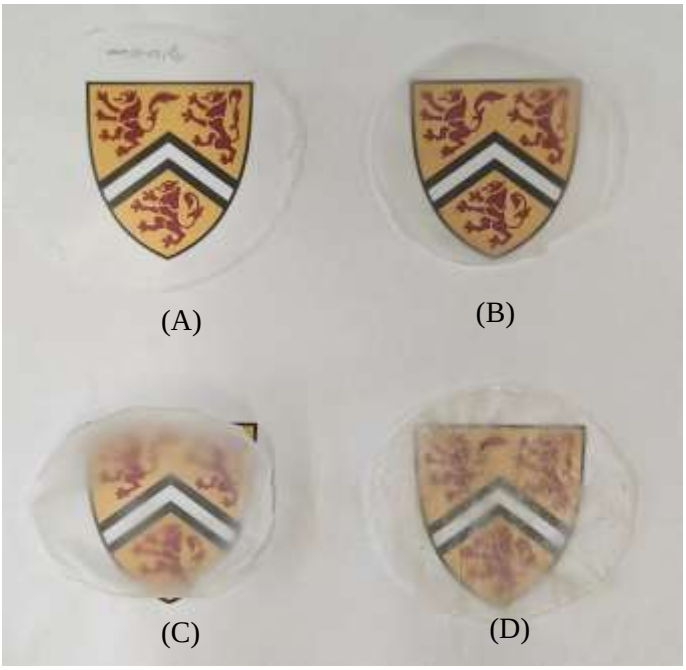


Figure 4.50. Shows graphical representation of PVA and UW CNF thin films (A) 50PVA/50CNF (B) 10PVA/90CNF (C) 5PVA/95CNF (D) 100 CNF.

Table 31 Light Transmittance (%) of different films with combination of PVA and UW CNF

Sample	Light Transmittance (%) at Various Wavelengths (nm)			
Wavelengths(nm) →	**200**	**400**	**600**	**800**
100% PVA	99.60	99.40	99.60	99.70
50%PVA+50%CNF	99.30	98.60	98.30	98.10
10%PVA+90%CNF	98.60	98.30	97.60	96.30
5%PVA+95%CNF	98.30	98.50	97.30	76.90

Table 32 Light Transmittance (%) of filtered UW CNPs dried at increasing temperature (°C)

Sample	Light Transmittance (%) Various Wavelengths (nm)			
Wavelength(nm) ⟶	200	400	600	800
Dried at 25°C	98.60	73.90	83.60	90.30
Dried at 50°C	98.41	72.32	86.91	91.20
Dried at 110°C	98.33	74.1	85.29	91.80

4.10.1.3. Surface Morphology

Scanning Electron Microscopy

The PVA/CNF thin films were observed under FE-SEM at about 2kV working frequency to analyze the nano dimensional structure and surface morphology of the substrate.

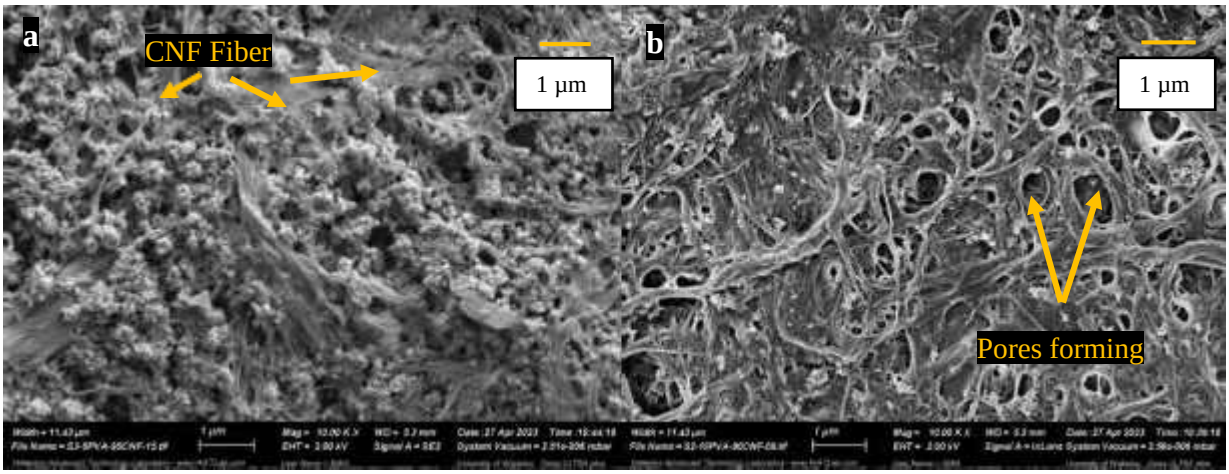


Figure 4.51. SEM graph for (left) 5PVA/95CNF, (right) 10PVA/90CNF.

Images 4.51. and 4.52. show three micrographs of 5%PVA/95%CNF, 10%PVA/90%CNF and 50%PVA/50%CNF, the emergence of pores at lower concentrations of polyvinyl. The PVA formed agglomerates when the CNF concentration was too high as there may be insufficient polymer chains to form a dense entangled network with the nanofibrils. Conversely, when PVA content is high enough in case of 50PVA/50CNF film, the PVA forms a smoother surface had conglutinations, which resulted in better dispersion of PVA and CNF matrix amongst each other (Jain, 2017).

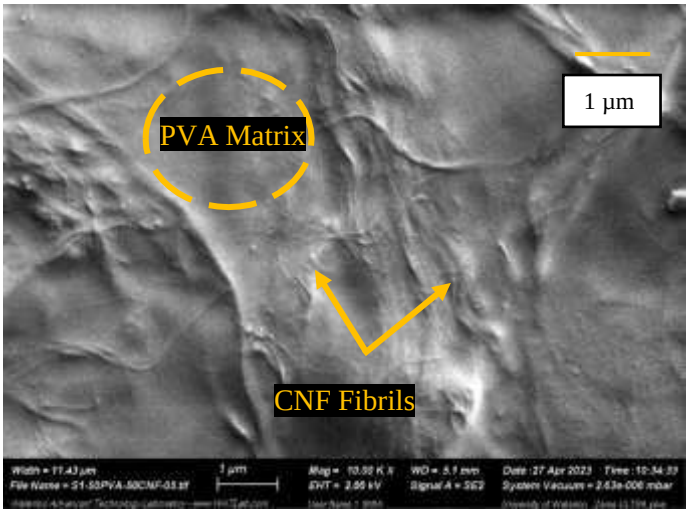


Figure 4.52. SEM graph for 50PVA/50CNF.

4.10.2. Polymethyl methacrylate and CNF Films (UM, UW) – Hydrophobic Alternative

The extreme porous nature of nanopaper and fiber aggregation often leads to a white appearance of the films. The pores or voids cause immense light scattering resulting from a vivid difference in their inherent refractive indices. As discussed earlier, PMMA is a suitable alternative to fill up the porous structure and improving the overall gloss and transparency of these films.

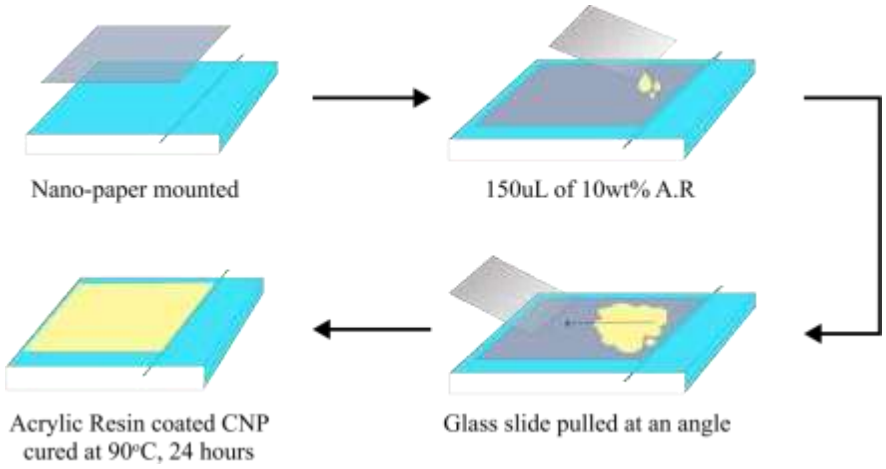


Figure 4.53. Exhibiting the coating of nanopaper with AR using a frosted microscopic glass slide.

It was noticed that using a higher volume of AR solution to coat the nanopapers resulted in tiny cracks on the surface of the nanopaper. This was due to the excess amount of resin hardening over time.

Dr. Blade which is a manual film coater as well as coating with paint brush gave rise un-even thickness whereas, microscopic glass slide showed the best results. Figure 4.54. show the different films formed with AR on CNPs. The haziness was much lowered due to less scattering as the pores were now filled with a transparent material (Meng and Wang, 2019b).

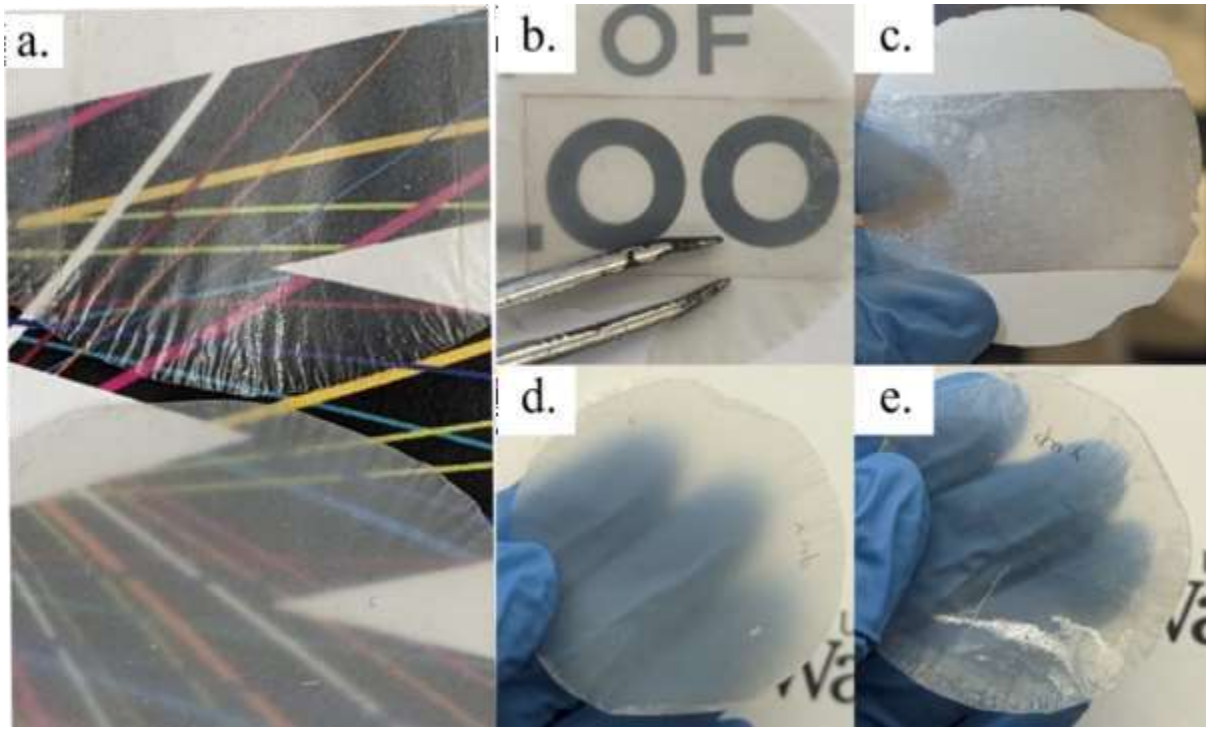


Figure 4.54. (a) Comparing UM 25°C dried CNP, coated and un-coated (b) UW 25°C dried AR coated CNP (c) UM 25°C coated AR with optimum grammage (d) & (e) depict difference in visibility of the coated and uncoated CNPs.

Table 33 Different Modes of Coating and Thickness of AR coated CNPs (UW, UM)

Concentration of AR Solution	Grammage (mg/cm^2)	Area of CNP (cm^2)	Volume(µL) of AR soln. used	Area of CNP (cm^2)	Application Technique	Thickness (µm)
20%	14.05	27.32(UM)	384	27.32	Dr. Blade	150±7.2
10%	3.66	27.32(UM)	100	27.32	Dr. Blade	70±6.9
10%	3.66	27.32(UM)	100	27.32	Brush	75±11.3
10%	5.50(Optimum)	27.32(UM)	150	27.32	Microscopic Glass Slide	80±1.1
10%	12(Optimum)	12.56(UW)	150	12.56	Microscopic Glass Slide	110±0.5

Different analyses were carried out to investigate the characteristics of AR coated nanopaper. Their optical properties, surface morphology and contact angle measurements were compared to 100% nanocellulose films. All samples from UW, UM were room dried (23˚C-25˚C) nanopapers as they appeared to have the maximum visibility or contact transparency.

4.10.2.1. Optical Properties

UV-Vis Spectroscopy

The UV-Vis was carried out between 100% nanocellulose films and AR coated films from both UM and UW CNF. The similar refractive index (n) for AR and nanocellulose causes minimal light bending at the interface when light is made to pass through them.

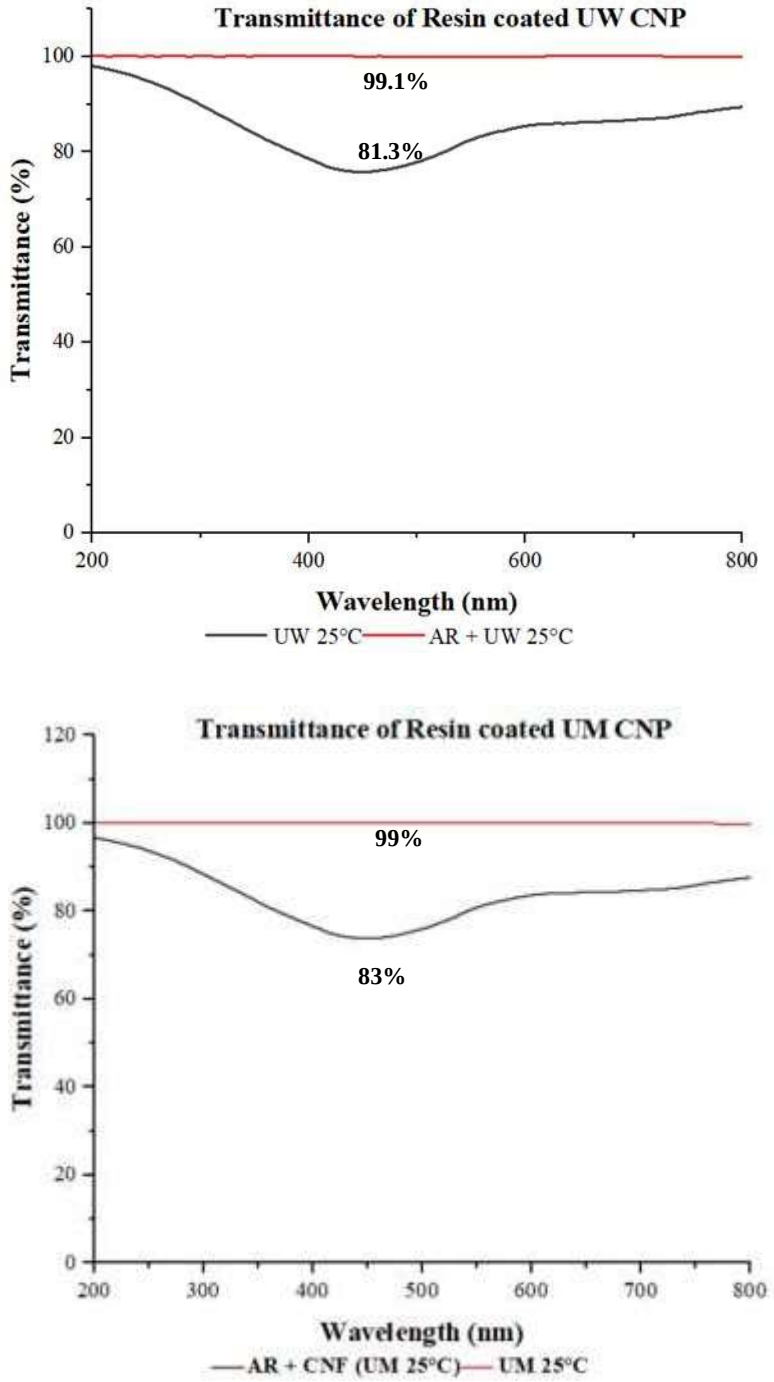


Figure 4.55. Depicts the comparison between AR coated and 100% CNF Films from UW and UM respectively.

As compared to neat CNF films the transparency was the lowest as seen around **83%** in average between 200-800 nm, indicating that nanocellulose films cause light to scatter due to the pores on their surface; light quenching was visible around 450 nm for uncoated films of UM,UW films

presumably Compared to resin coated nanopapers, the transmittance between the same wavelength is much better from **83%** to almost **99%** in average, also as noticed in the figure 4.55. There seemed to be some absorption in the UV region (<200nm) for UW 100% CNF sample, but overall transmittance was enhanced. Even though there was a slight increase in overall thickness from 90 µm to 110 µm with the optimum amount of AR in the nanopaper after coating, the transparency drastically improved. This means PMMA filled the gaps reducing surface roughness which is another crucial aspect to be explored in the future.

4.10.2.2. Surface Morphology – Scanning Electron Microscopy

Some surface topography including cracks and pinholes and cleanliness are important factors to consider for guaranteeing the incorporation of CNPs in electronics. For a stable performance, the optimum amount of AR should be applicated. Both apparent morphology and cross-sectional view was observed.

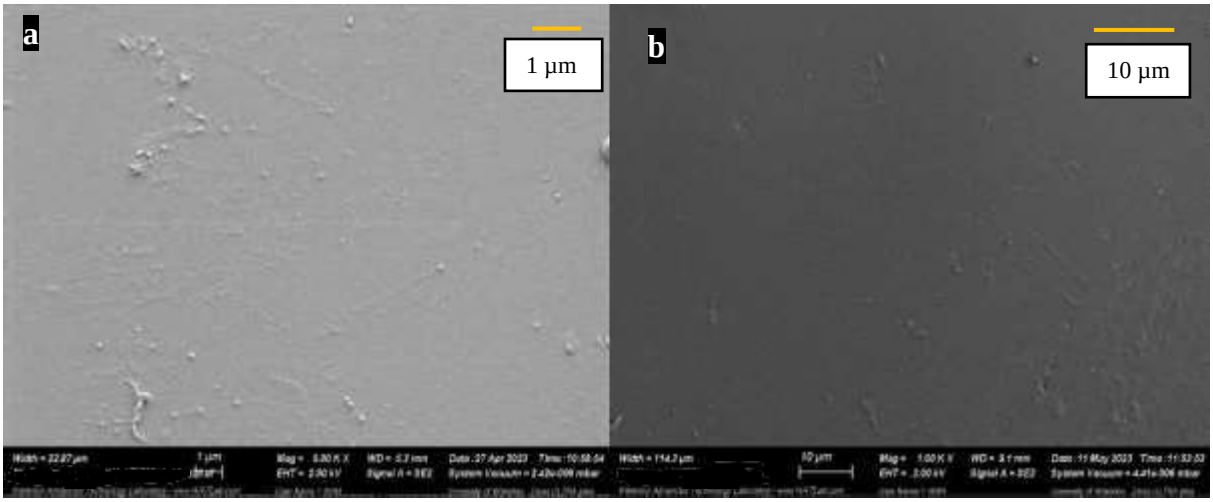


Figure 4.56.UM CNP coated with AR at 5000x and (right) 1000x (left)

Nanopapers in figure 4.56. are in two different magnifications show no cracks as such, but at 5000x magnification smaller nanofibers can be seen to emerge. This could be due to uneven filling of pores. This is an example of a UW coated nanopaper with an AR grammage of 5mg/cm^2 on a surface area of 12.56 cm^2. The surface is smooth and flat shows good compatibility between PMMA and CNF. These results confirm that pores of nanopaper can be removed widely increasing their texture and visibility, as previously seen by Jamaluddin, (2021) and Song, (2018b).

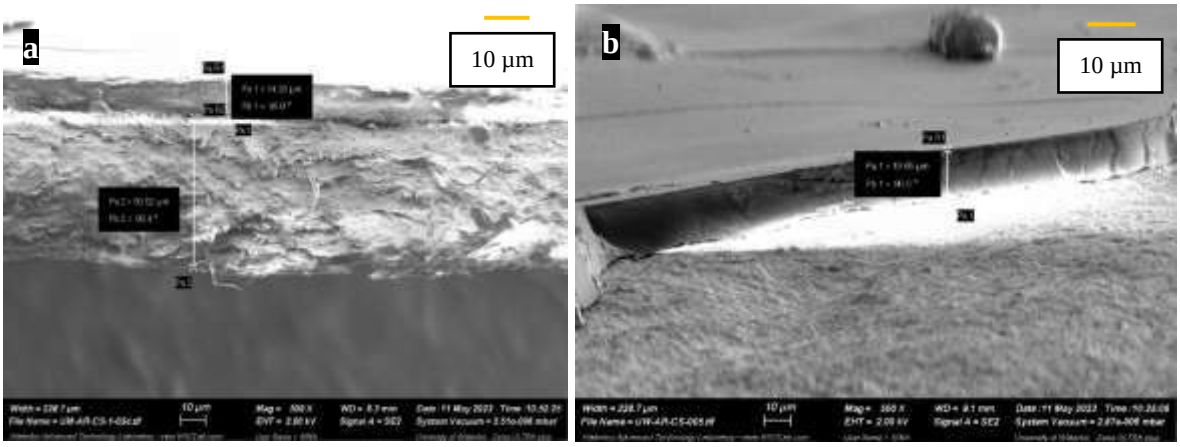


Figure 4.57. SEM image of fractured cross-sectional area of AR coated CNP, coated with (left) Dr. Blade (right) Microscopic glass slide.

In Figure 4.57., we notice a prominent layer formed on the CNF/PMMA interface boundary. A comparison was done between two coating techniques, microscopic glass slide and Dr. Blade, to show the improved finishing of the glass slide application and distinctive layers keeping away the nanopaper from disintegrating by turning it hydrophobic.

4.10.2.3. Surface Wettability and Contact Angle Measurements

Neat CNF films showed dynamic water contact angle (WCA) of an average of 34° for both UM and UW films, irrespective of their thickness. It was demonstrated that CNF films had higher hydrophilicities and tendency to interact with polar liquids.

On the other hand, PMMA coated nanopapers have shown hydrophobic nature and high values of WCA. For UM coated nanopapers the WCA was around 92.6°, and for UW coated nanopapers were 90.5° respectively. The change from hydrophilic to hydrophobic has attributed to the results. Lower the contact angle, the more hydrophilic the pore higher is the capillary pressure and stronger the capillary action. Micro-images in figure 4.58. displays that with deposition of AR on the film surface has turned them hydrophobic and less susceptible to degradation under humidity.

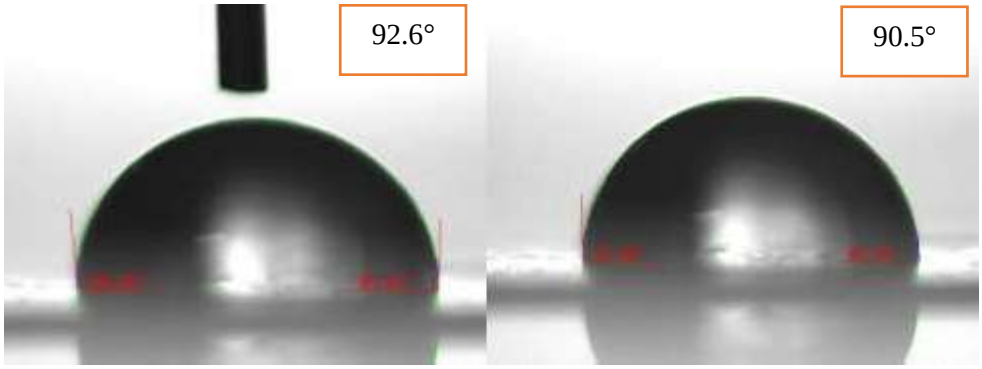


Figure 4.58. WCA imagery of PMMA coated UM CNP (left) and PMMA coated UW CNP (right)

The contact angle stabilised after 30 seconds on the substrates instead of getting absorbed into the structure like neat CNF films as seen in graphical figure 4.59.

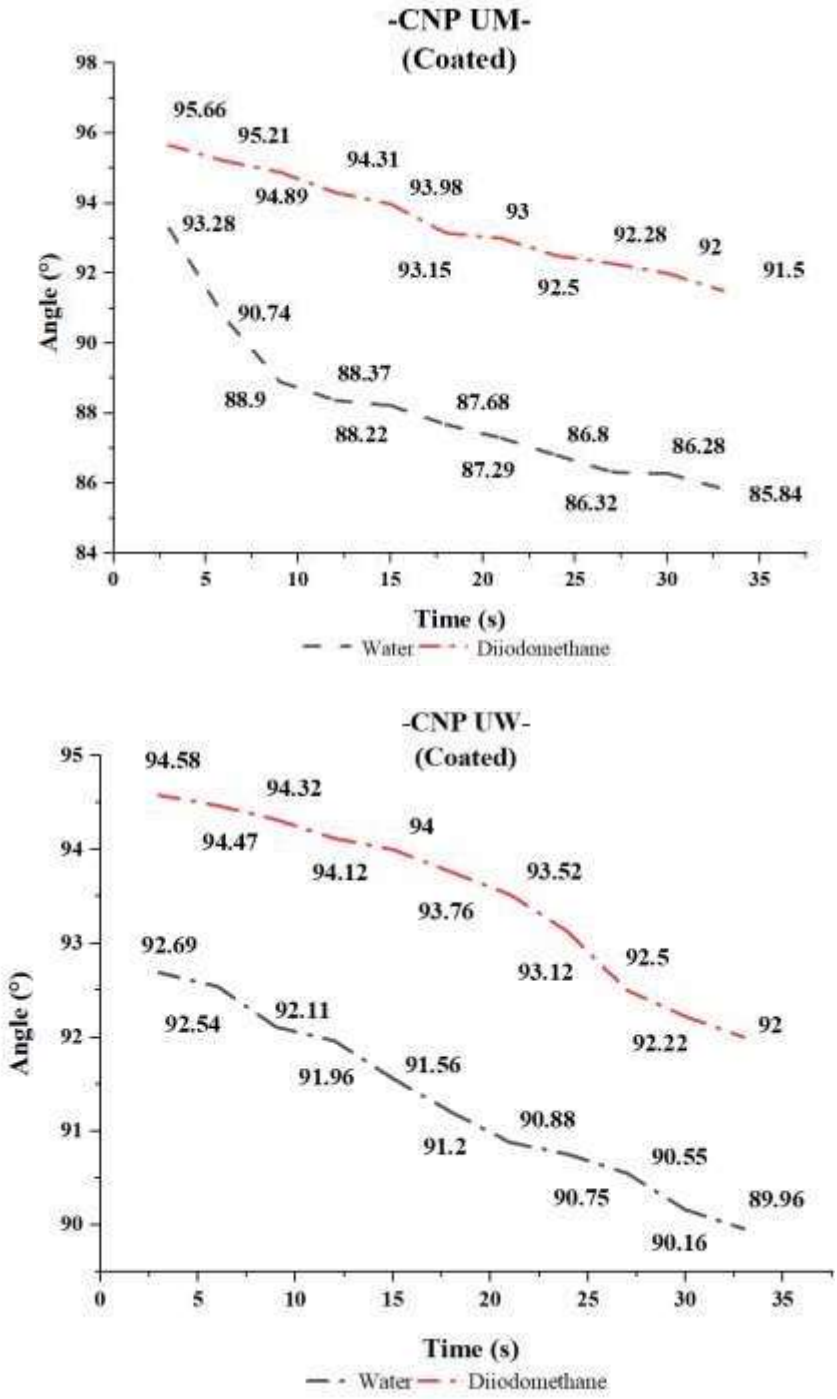


Figure 4.59. Show contact angle physical characteristics after 30 secs on substrates UW (top) and UM (bottom).

4.11. Conductive Nanopaper for Flexible & Wearable Electronics Application

4.11.1 Integrating Silver Nanowire as Conductive filler and layer on Cellulose Nanopaper

As discussed in section 2.10. in chapter 2, the nanowire deposition was done through filtration in a sequence with the formation of nanopaper. The 'filtration coating' methodology was an effective process to produce well percolated nanowire networks rooted in nanopaper surface.

The reason behind selecting the dimension of nanowire was based on the nanopores formed on the surface of nanopaper. Nanowire particles should be big enough to be retained in the wet mesh of paper thus formed. Although a continuous uniform coating is necessary for high conductive performance, but the method of deposition as well as drying method has caused several setbacks in achieving nanopaper's full potential.

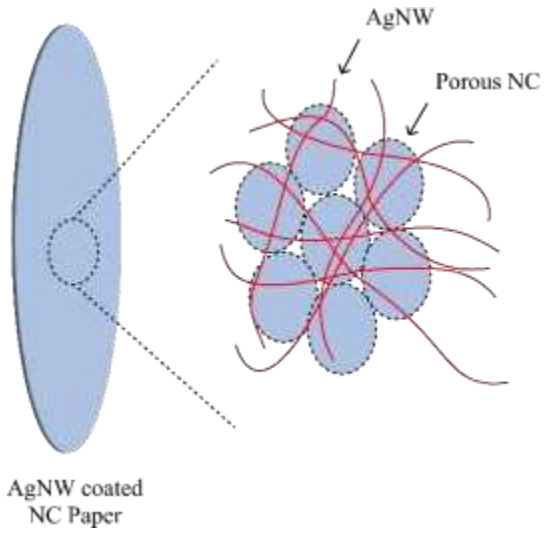


Figure 4.60. Distribution of Nanowire embedded on CNF Matrix.

Higher temperatures were avoided as they could change the intrinsic resistivity of silver nanowires.

While filtering, the nanowire was deposited in two patterns – (a) All over the nanopaper surface (b) In shape of rectangular electrodes, as demonstrated in figure 4.61.

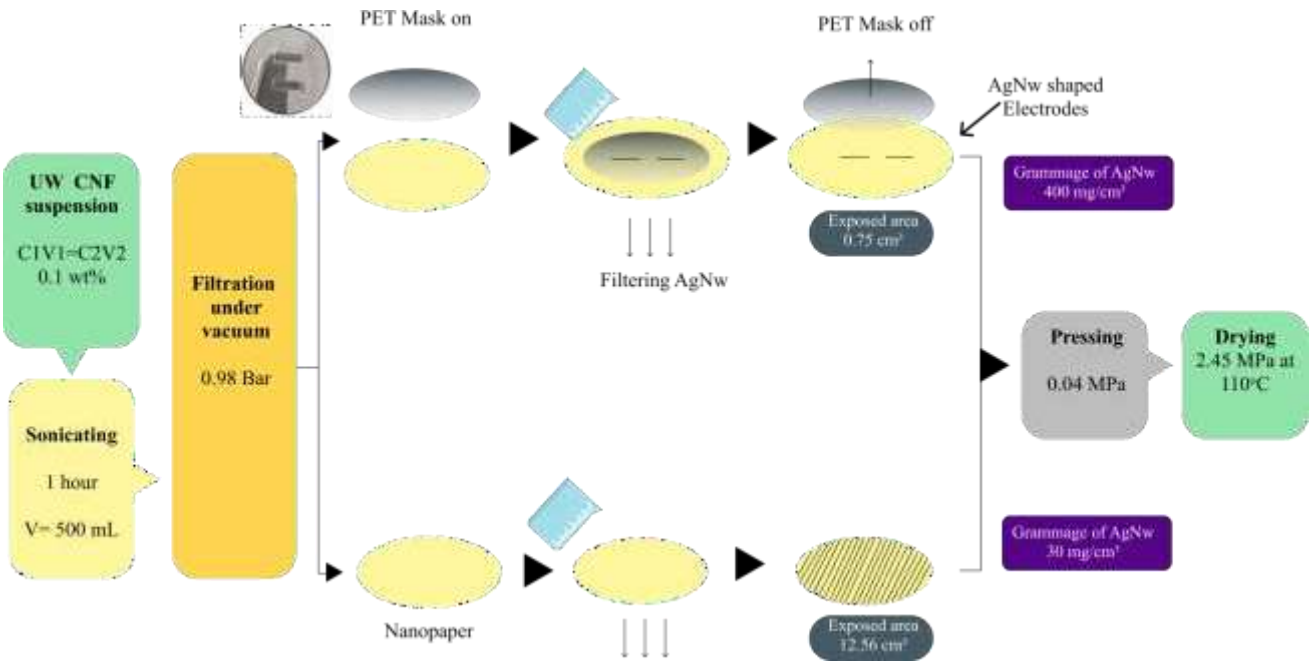


Figure 4.61. Demonstrating the deposition of Silver through Filtration (top) with PET Mask (bottom) without PET Mask.

Besides filtering in patterns or shapes, the nanowire was deposited in two different modes. The nanowire solution was either filtered on top of the wet web of CNF in a 2 layered fashion or it was mixed thoroughly and sonicated together with the nanocellulose and filtered to form a 1 layered structure.

Various analyses were conducted on the film composite thus formed to experimentally observe their morphology and conductivity.

Conductivity $(\sigma.cm)^{-1}$ Measurement Via 2 Probe and 4 Probe Methods:

To exploit the full potential of conductive nanopapers, the ability of the material to conduct electric current is an important aspect. Conductivity is measured as the reciprocal of resistivity (ρ). The resistivity for both the methods were calculated:

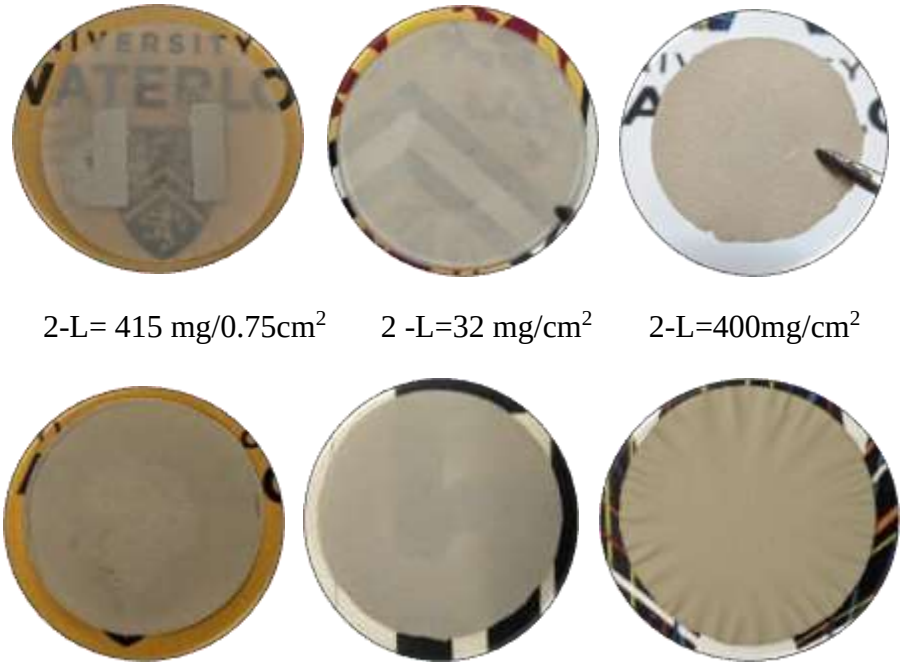
$$Resistivity, \rho = R \times t$$

R =sheet resistance, t=thickness of film.

As discussed in chapter 3, 3.8.

4.11.2. Conductive Nano paper Specimens

Pictures of nanowire infused nanopaper prepared from UW CNF films are shown in figure 4.62. The thickness (Th) of the nanopaper varied with increasing loading density of the silver. The transparency of nanopaper was reduced due to the deposited silver all over the surface area of nanopaper promoting a rather. However, they were still flexible. The nanowires were either formed in a 2 layered (2-L) structure or together mixed with the CNF and deposited as a single 1 layered (1-L) specimen.



2-L= 415 mg/0.75cm^2 2 -L=32 mg/cm^2 2-L=400mg/cm^2

2-L=64mg/cm^2 1-L=64mg/cm^2 1-L=400 mgcm^2

Figure 4.62. Conductive nanopapers with differing nanowire grammage (mg/cm^2).

The silver embedded nanopapers were analyzed for both 2 Probe and 4 Probe Measurements and their results were compared amongst each other in the later half of the discussion.

- The "→" symbol defines that the nanowire solution was added in a series after the CNF suspension as filtered.
- The "+" symbol defines that the nanowire solution and CNF suspension were agitated together and filtered at once.
- Grammage is measured across a surface area of 12.56 cm^2 in correspondence to the silver added in milligrams (mg).

Table 34 Layers, Thickness and Grammage of Nanowire and CNF (UW) film composites fabricated.

Method and Structure	**Layer 1**	**Layer 2**	**Thickness (µm)**	**Grammage of CNF & AgNW (mg/cm^2)**
CNF→AgNW PET Masked	0.1 wt.%, 100mL CNF	**3.8 vol.%,** 10 mL AgNW	110 (only on deposited area)	CNF → **5.8** AgNW→ **415**
CNF→ AgNW 2Layered	0.1 wt.%, 100mL CNF	**3.8 vol.%,** 10mL AgNW	95	CNF→**5.8** AgNW→**32**
CNF→AgNW 2 Layered	0.1 wt.%, 100mL CNF	**33 vol.%** 10mL AgNW	105	CNF→**5.8** AgNW→**400**
CNF+AgNW →AgNW 2 Layered	0.1 wt.%, 100mL CNF+ **0.08 vol.%,** 10mL, AgNW	**7.4 vol.%,** 10mL AgNW	95	CNF→**5.8** AgNW→64+64 **=128**
CNF+ AgNW 1 Layered	0.1 wt.%, 100mL CNF+ **7.4 vol.%**, 10mL, AgNW	-	75	CNF→**5.8** AgNW→**64**
CNF+AgNW 1 Layered	0.1 wt.%, 100mL CNF+ **33 vol.%,** 10mL, AgNW	-	80	CNF→ **5.8** AgNW→**400**

Conventional coating methods such as drop casting or spin coating often causes partial loss in the interconnection of the nanowires, resulting in low conductivity. Contradictorily, filtration coating has allowed uniformly distributed wire network as shown in figure 4.63. This helps in exploring the full potential of conductive substrates and incorporating them into various devices. Filtering AgNW solution is analogous to nanopaper fabrication through filtration which makes it easier to control its thickness. Table 34 represents values of nanowire and CNF grammage; $400mg/cm^2$ is the highest grammage of silver deposited in both one-layered and two-layered specimens. The experimental analysis follows a uniformity with increasing the quantity of AgNW solution or increasing the volume fraction of nanowire deposited on CNPs Song, (2015) ; Preston, (2014a).

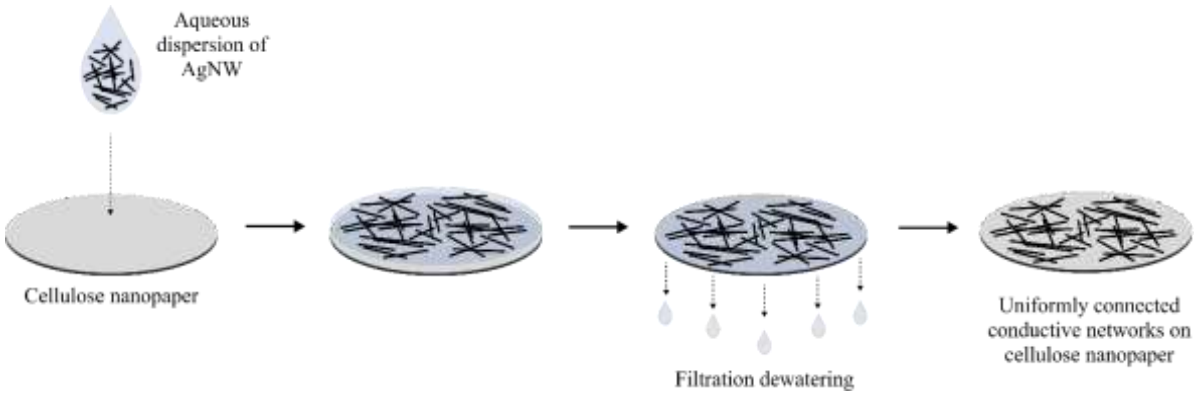


Figure 4.63. Putative process of formation of AgNW networks on nanopaper by filtration process

4.11.3. Electrical Conductivity

As discussed in section 2.10.1. the electrical conductivity largely depends on blending, filtration, and peeling. The percolation behaviour with increasing weight percent of AgNW was studied. Their respective values obtained through analysis are given in table 35 and 36.

The value of resistivity was calculated through:(ρ) = (R×A/L)/ = (R×L×t/L), as discussed in chapter 3.8. The conductance values were compared between 2 probe and 4 probe methods, and a constructive conclusion was drawn based on their values.

Table 35: 2 Probe Measurement show Varying values of resistivity (ρ) and conductivity (S/cm).

Composite	**Surface Density mg/cm^2**	**Resistance R (Ω)**	**Resistivity (ρ =R×L×t/L) = (R×t) (Ω .cm)**	**Conductivity (σ =1/ρ) (S/cm)**
CNF→AgNW PET Masked	CNF → **5.8** AgNW→ **415**	0.7 ±0.08	0.0077	130
CNF→ AgNW 2Layered	CNF→**5.8** AgNW→**32**	36.8±15.46	0.3495	0.002
CNF→AgNW 2 Layered	CNF→**5.8** AgNW→**400**	0.46±0.04	11.550	207
CNF + AgNW →AgNW 2 Layered	CNF→**5.8** AgNW→64+64 **=128**	3.76±0.75	0.3572	2.890

CNF+ AgNW 1 Layered	CNF→**5.8** AgNW→**64**	Infinite Resistance= Open circuit	0	0
CNF + AgNW 1 Layered	CNF→ **5.8** AgNW→**400**	Infinite Resistance= Open circuit	0	0

L= distance between the 2 probes, 0.5cm for each sample, as seen in figure 4.65.

Referring to table 35 the values of resistances were measured via 2 probe multimeters, with the probes at a distance of 0.5cm from each other for every measurement. An average of 5 readings at different positions were taken. The lowest conductivity was observed with a grammage of 32mg/cm^2 AgNW, the sample visibly showed a higher deviation due to the un-even distribution of nanowires and insufficient connection between them. The volume of nanowire added was low and they were too dispersed on the matrix, showing a conductivity as low as 0.002 S/cm and the conductivity for the highest grammage of nanowire, 400mg/cm^2 as a 2 layered structure was 207 S/cm as previously noticed by Koga, (2013) and Koga, (2014).

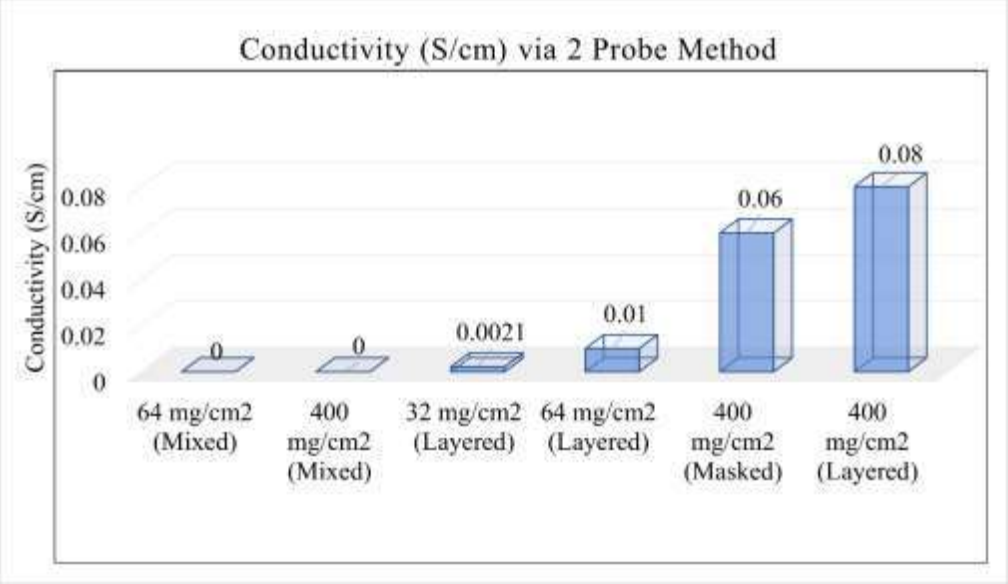


Figure 4.64. Graphical presentation of conductivity (S/cm) according to AgNW grammage (mg/cm^2)

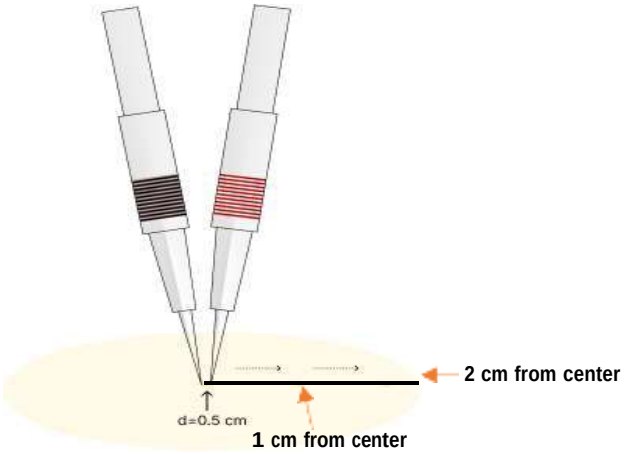


Figure 4.65. Demonstrating measurement of resistance via 2 Probe with probe distance d=0.5cm along the diameter of the nanopaper.

Advantage of Four Probe point method than Two Probe Point Method

The four-probe method is preferred over the two-point method as the contact and internal resistance were practically very large and the true value of resistivity cannot be measured by separating from the measured resistivity. In contrast, four probe method has 4 collinear probe heads among which two of the outer probes measure current (I) whereas, the inner probes measure voltage across the sample (V). Hence, the experimental resistances and their corresponding resistivities are more accurate and even lower.

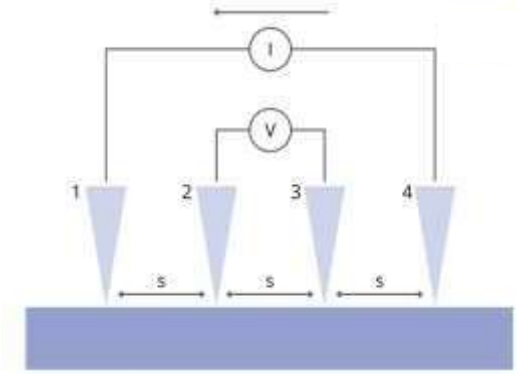


Figure 4.66. Demonstrating a typical 4 Probe Resistivity Measurement set-up adapted from Ossila Equipment.

The four-probe method is a widely recognised analysis to find resistivity among thin films. The probes are colinearly placed and equidistant at 1 mm distance from each other, as seen in schematic above in figure 4.66.

The correction factor is 1 here, as the diameter of the nanopaper is 40 times bigger than the probe gap. Table 36 shows a trend of increasing conductivity with a rise in silver nanowire volume fraction (Liu, 2022b).

Table 36- 4 Probe Measurement show Varying values of resistivity (ρ) and conductivity (S/cm)

Film Composite	**Thickness (µm)**	**ΔV/I (Experimental)**	**Sheet Resistance R_s (Ω)**	**Resistivity $\rho=R_s \times t$ (Ω.µm)**	**Conductivity (S/µm)**	**Conductivity (S/cm)**	**KiloS/cm**
CNF→AgNW PET Masked	110	0.11 ±0.01	0.5	55	0.020	200	0.2
CNF→ AgNW 2Layered	95	27.86±13.70	126.27	11995.65	0.0001	1	0.001
CNF→AgNW 2 Layered	105	0.02±0.001	0.09	9.45	0.105	1050	1.05
CNF + AgNW →AgNW 2 Layered	95	2.440±0.49	11.05	1049.75	0.001	10	0.01
CNF+ AgNW 1 Layered	75	Infinite Resistance= Open circuit	-	Open Circuit	0	-	-
CNF+AgNW 1 Layered	80	Infinite Resistance= Open circuit	-	Open Circuit	0	-	-

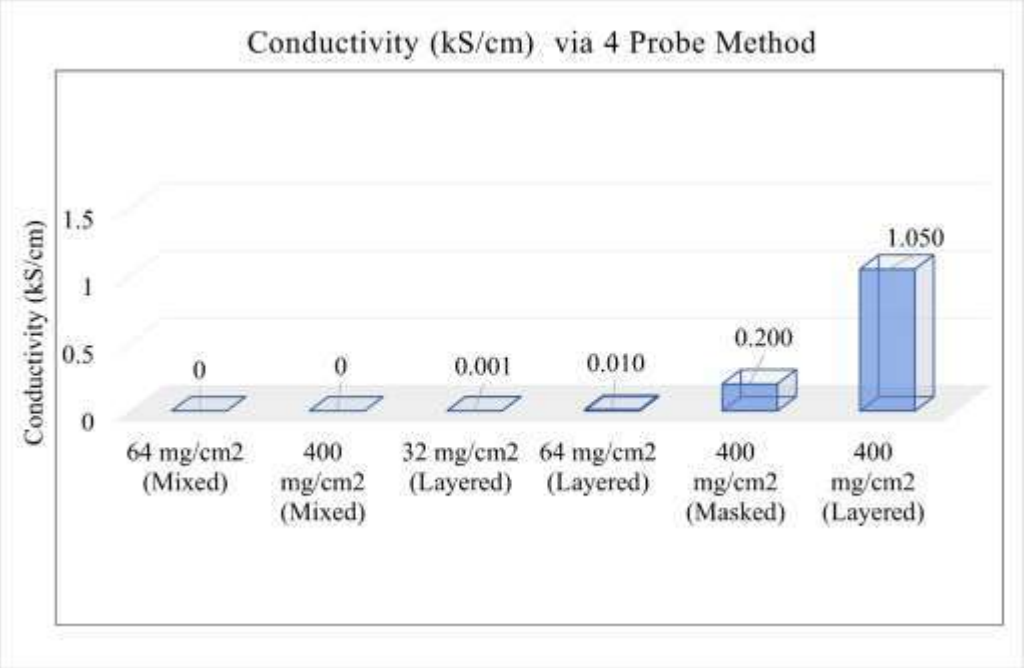


Figure 4.67. Graphical presentation of increasing conductance by increasing volume fraction of AgNWs.

Referring to the table 36, the V/I value were noted from the multimeter attached to the 4 probes. The formula to calculate the sheet resistance equation mentioned in the methodology section.

The substrate containing a 32mg/cm^2 grammage of nanowires once again, shows the highest conductivity 0.001 kS/cm on the contrary, a higher grammage around 400mg/cm^2 have high conductance around 1.05 kS/cm indicating an increase in the volume fraction of conductive wires show better percolation following power law relationship. A sharp contrast was observed between 2 probe and 4 probe results.

Comparing the results between 2 probe and 4 probe, it is apparent that the conductivity values are much higher without considering the contact resistance. Similar sheet resistances were mentioned by Koga, 2013 and Koga, 2014. Nanopapers produced through mixing the CNF and AgNWs resulted in no constructive conductivity as they lacked a percolating continuous pathway. This makes the layered structure more viable to be applied in electronics.

Surface and Cross-Sectional Morphology: FE-SEM

The morphological characteristic of silver embedded nanopapers were analysed under FE-SEM at a working frequency of 2kV. The surface of the nanopaper substrates were analysed for both 1

layered and 2 layered structures. Figure 4.68 (a) shows a few visible nanowires on the surface of the substrate even though no visible pathway or continuity can be noticed. This is due to the filtration of CNF and nanowire together which let the nanowires disperse and not bridge to promote the flow of electrons.

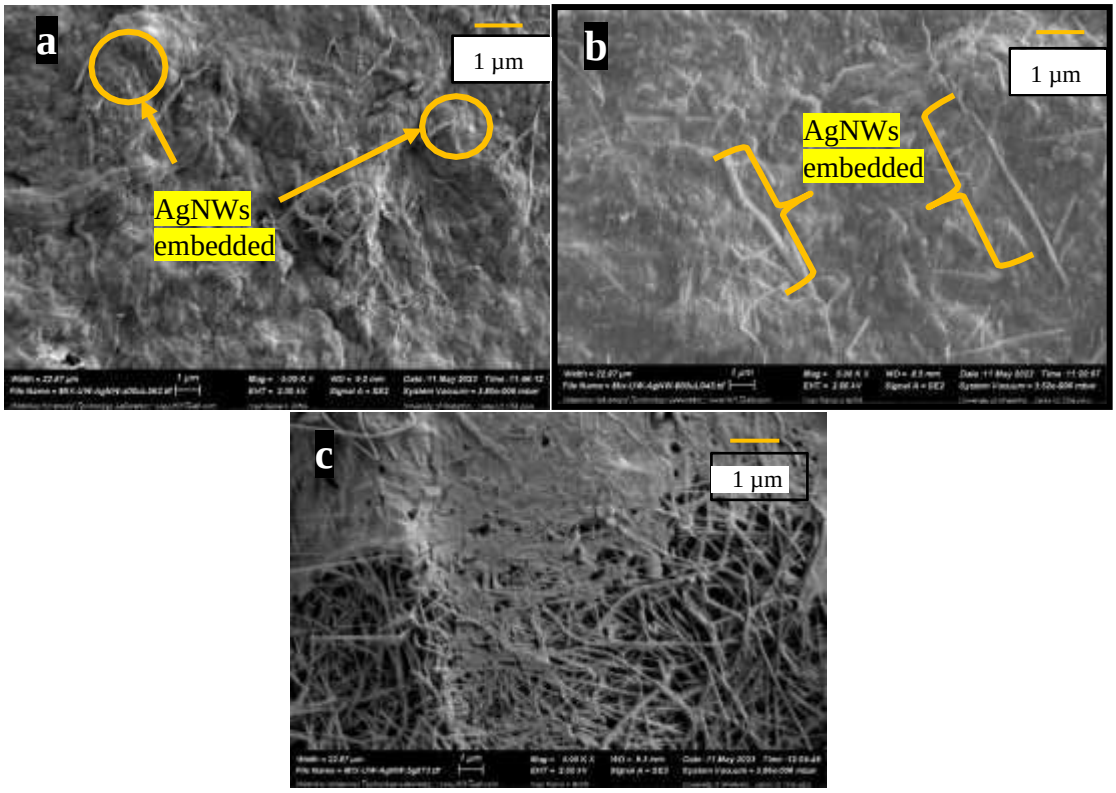


Figure 4.68. Top-view SEM micrographs of AgNW mixed nanopaper substrates for (a) 32mg/cm^2, (b)64mg/cm^2 (c) 400mg/cm^2 different grammage of nanowire

Micrograph 4.68. (a)-(c) show the increase in intensity of nanowires with more fraction of fillers but failed to produce any conductivity stating that mixing nanowires with nanocellulose would not give rise to electrical properties as CNF is an insulator. The SEM of bi-layered substrate displayed uniform distribution of nanowires that form percolated three-dimensional network enabling high electrical conductivity and excellent mechanical deformation ability. Figure 4.70. (c), exhibits the highest conductivity as the nanowire concentration is comparatively higher than the rest of the substrates, 400mg/cm^2 giving rise to a conductance as high as 1.05 kS/cm, even higher than pre-established results.



Figure 4.69. Network of AgNW rods well connected with each other (left) and the same network on nanopaper as a layered assembly (right).

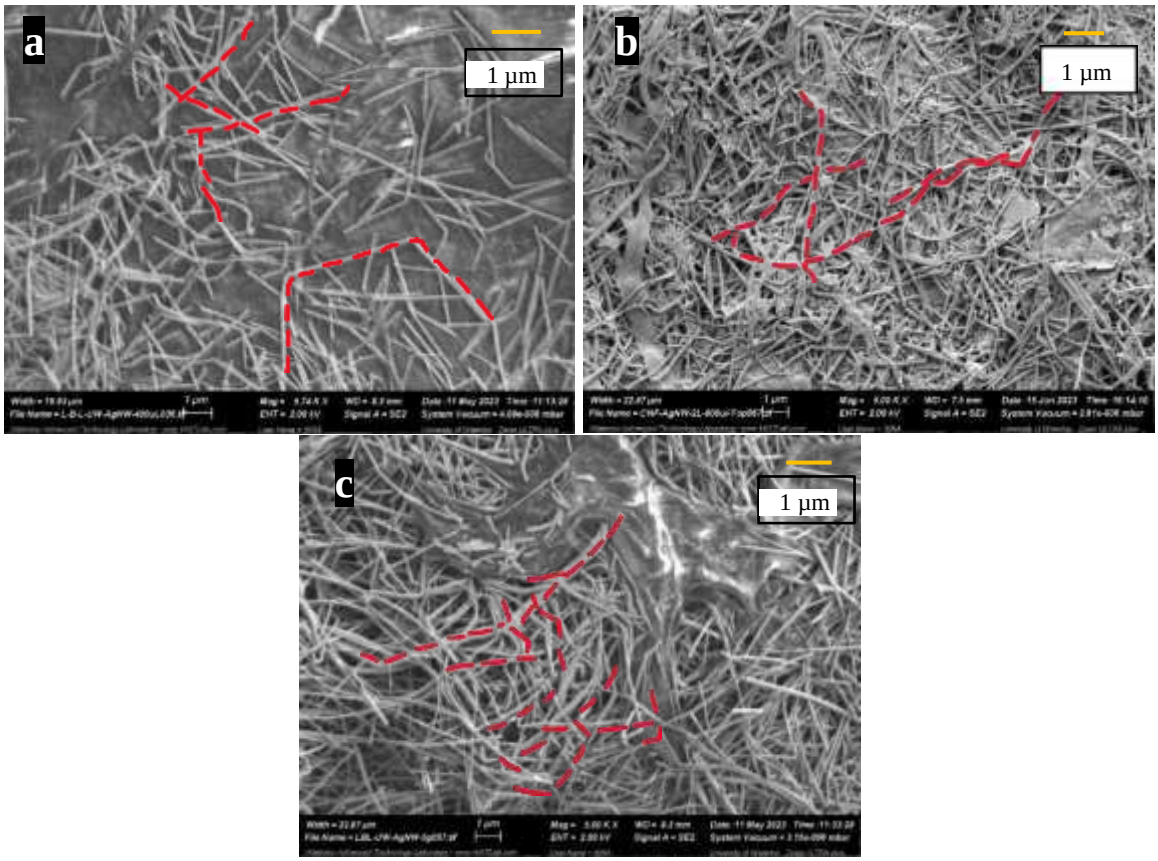


Figure 4.70. SEM image of AgNW films on nanopaper as bi-layered arrangement with grammage(mg/cm2) (a) 32mg/cm2, (b) 64mg/cm2 & (c) 400mg/cm2, respectively. Percolated nanowires are expressed in red dotted line.

The cross-sectional fractured surfaces of the constant three grammage were observed under the microscopy. The multi-layered structure showed the distinctive separation between nanowire layer and the CNF network.

The percolation theory suggests that when the conductive filler content is slowly increased then the composite undergoes changes from insulator to conductor.

The critical filler content is considered as the percolation threshold, here the conductivity jumps several folds indicating formation of continuous path described earlier in chapter 2, 2.10.1. In figures of bi-layered composite film figure 4.71., we see good interconnection at different 'sites' of nanowires. On contrary, when nanowires were mixed with CNF, the electrical properties are mostly controlled by insulating fillers. This defines the justification of percolation model evidently as noticed by author Deepalekshmi, (2018).

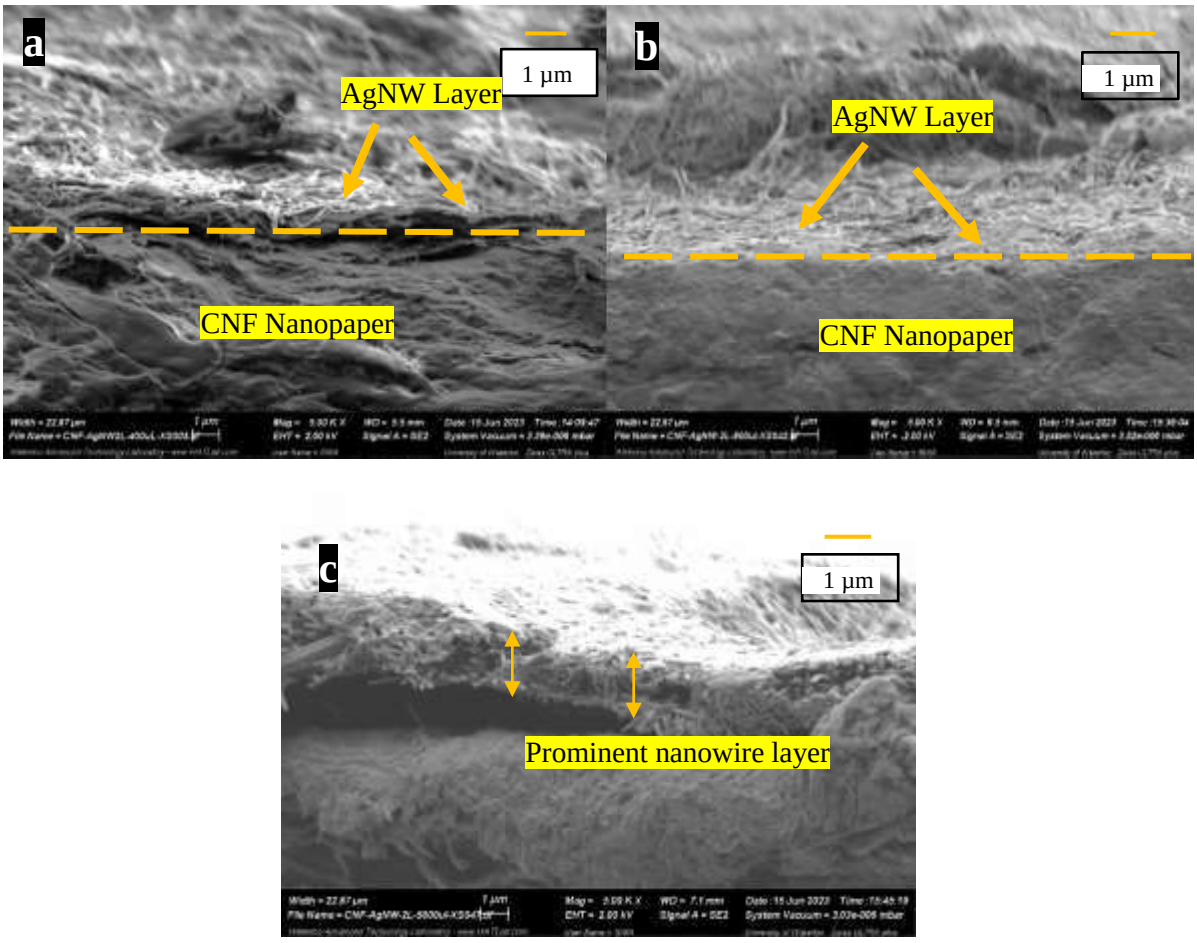


Figure 4.71. Cross-sectional SEM of bi-layered structure with AgNW and CNF with increasing volume of nanowire solution from (a) 32mg/cm2, (b) 64mg/cm2 & (c) 400mg/cm2.

Figures in 4.71. show the thickness of the silver nanowire layer increases with a rise in their volume. The layered structure suggests that the AgNW is well bonded amongst each other, and conductance is directly proportional to the volume of nanowire solution added during filtration. This is unlike mixing the two materials – AgNW and CNF together where CNF acts as the non-

conducting filler hindering the interlinkage of silver. Although the conductance is seen to be rising, there is a trade-off due to the lack of transmittance through the nanopaper impeding its optical properties.

Higher grammage of nanowire like 400mg/cm^2 also leads to the emergence of an independent layer of nanowire unlike lower grammage where the wires are embedded or distributed on the nanocellulose matrix to be observed in figure 4.71.(c).

Similar values of resistance or even higher for silver incorporated nanowire were observed by other authors (Preston, 2014b; Koga, 2014; Tao, 2020).

Chapter 5 Conclusion

5.1. Summary and Contributions

Nanopaper is an emerging ‘green’ alternative next generation substrate for electronics or energy devices. To mitigate electronic waste and to meet the growing demands of a modern society these individualised devices have found their needs.

Two different nanocellulose sources, including one of their extraction methods were explored to develop a new thin film for applications in conductive electronics such as electrodes or OLEDS. Specifically, the focus was on removal of impurities and extracting a niche quality cellulose nanofiber having uniform width and a web-like network bonded with hydrogen bonds at their intersections. They were individualized through a series of chemical treatments and ultra-sonication methods. Nanopaper was fabricated by two distinct methods, such as solution casting and filtration. The later was concluded to be a more efficient and less time-consuming methodology to fabricate these papers. Vacuum filtration allows for controlled deposition of nanofibrils onto the PVDF filter membrane. This results in a more aligned and anisotropic configuration of nanofibrils. The alignment of fibers in a particular direction contributes to efficient characteristic properties when compared to casted films. Even though nanopapers formed had considerable modulus but their optical properties were greatly compromised. To increase transmittance and to remold their visible appearance, CNF films were designed by adding some synthetic based polymers such as Polyvinyl Alcohol (PVA) which is a hydrophilic

additive and Acrylic Resin (AR) which was a hydrophobic pathway. The project also focused on applications and properties of AgNWs or silver nanowires networks by concentrating on their deposition method and interaction with CNF. The electrical characteristics such as conductivity (ʊ) and their properties directed by percolation has been examined.

5.2. Main Conclusion

The crucial aim of this research was to successfully obtain CNF from Bast fibers of hemp by IND Hemp and use CNF from University of Maine, USA to fabricate nanopaper of high quality. Nanopaper fabricating processes were developed from scratch based on mathematical calculation of required thickness and grammage of pulp.

1. **CNF Extraction -** The optimum conditions to extract cellulose and eventually nanocellulose (CNF) from hemp bast fibers were determined by subjecting fibers to repeated chemical treatments both acid and alkaline and rated with bleaching treatments. Hemp bast cellulose from two different sources were chosen as the cellulose source, due to its high cellulose content (>96%). The fibers were subjected to an alkaline treatment with 10wt.% and 5wt.% respectively. An intermediatory acid test was performed to get rid of hemicellulose, lignin and other non-cellulosic compounds. The hemp was noticed to lose its colour with each advancing step of treatment. Bleaching at lower temperature 70˚C produced a yellowish pulp than treating at higher temperatures at 80˚C promoting brightness and improving whiteness of the pulp. Thereafter, through multiple cycles of fibrillation, CNF was obtained by exposing the pulp to a Masuko Grinder. The CNF fibrils had high dispersity and under microscopy (TEM), the fibrils were noticed to have an average diameter around (50-75 nm). Similarly, freeze-dried CNF were also observed to range around 50 nm in diameters.

2. **CNPs were prepared via two broad classifications** – (i) Solution Casting (ii) Vacuum Filtration and the readers were given a clear distinction between their results; casting showed poorer results due to emergence of agglomeration owing to the absence of constant moisture supply during drying which led to extreme levels of shrinkage which also resulted in a higher deviation in their mechanical properties. This problem was slightly alleviated with the use of a plasticizer, Glycerol at just about (15-30) % was sufficient to improve the aspect of the films. But it resulted in a sharp decrease of mechanical properties such as modulus (MPa) from 495 MPa and 386 MPa for UM and UW films to 226 MPa and 198 MPa for UM and UW,

respectively. This phenomenon was undesirable as it negatively effected the physical characteristics of the nanopapers. Moreover, casting took longer periods of time to dry, inhibiting scale up.



Figure 5.1. Comparing nanopapers made from UM CNF (left) Casting (right) Filtration

Consequently, filtration proved to be a beneficial method to form nanopaper and scale-up production. Though, dewatering wet web and drying them at optimum temperature is still a complex process yet to be explored. The nanopapers were fabricated from dispersed CNF suspensions from UM and UW fibers at varied concentrations ranging between 0.05wt%-0.1wt% and effect of their interfibrillar interactions and structural development have been studied through various analyses. The study demonstrated that changing temperatures, resulting from drying nanopaper, has significance in contributing to mechanical and transmitting properties even though they were made from fibers of similar average diameter. Nanopapers dried at higher temperature around 110°C showed stronger mechanical properties for both UW and UM nanopapers made under same conditions. The high tensile values around 1345 MPa and 1174 for UM and UW CNPs were reported respectively. Owing to the higher rate of evaporation at elevated temperatures, causes irreversible “hornification” of nanofibers consolidation. This results in better intermolecular bonding and improves overall density of the specimen. Besides temperature, degree of fibrillation of nanocellulose fibers plays a vital role in defining its stability under high tension.

3. **Surface properties** – Hydrophilicity was measured through water contact angle (WCA) and mathematically finding out the surface energy of the films. A decrease in contact angle was noticed over a period of 30 seconds. The high hydrophilicity of neat CNPs arise from the

abundance of hydroxyl groups (OH^-) present on their surface. This makes the nanopaper suitable for printing and depositing conductive nanowires, usable as a substrate in electronics.

4. **Surface morphology** – Surface topography was determined for UM and UW CNPs processed at three different temperatures 25°C, 50°C and 110°C. The pore sizes were noticed to be decreasing with heat treatment from an average pore diameter of 70 nm to as small as 38 nm at elevated temperatures. This phenomenon can also be defined while calculating porosity of nanopapers by finding their densities. Nanopapers pressed at higher temperature reduced overall porosity enhancing structural properties.

5. **Addition of Polymers -** Additives such as PVA and PMMA were incorporated to improve optical transmittance of nanopapers. Even at room temperatures, CNPs showed some degree of light scattering due to its mesoporous nature. When 20% PVA was used, CNF films displayed smoother visual aspect and lesser corrugation and plain films. Increasing the composition to 50% resulted in significant change of nanopapers than simply casted films. Similarly, PMMA coated CNPs showed transmittance around >90% for both UM and UW papers. By the virtue of its hydrophobicity, it prevents the CNP from dissolving in polar solvents.

6. **Conductivity and CNP as a Conductive Substrate-** CNF nanopapers showed insulating properties and with a nanowire grammage of just $32mg/cm^2$ and upwards, CNPs exhibit conductive behaviour with a conductivity as high as 1.05 kS/cm. Increasing the grammage or volume fraction of AgNWs resulted in an exponential increase in nanopaper's conductivity which makes it suitable to form flexible electrodes with them. Subsequently, the transparency is decreased as the loading density is raised.

5.3. Recommendations and Future Work

It was concluded that nanopaper based conductive substrates have the potential to be combined in electronics due to their high mechanical strength and transparent properties. This being said, it still is yet to scale-up as their manufacturing processes are not ideal. Issues were faced while fabricating nanopapers due to variation of their aspect ratio (L/d) based on the treatments that were considered.

A list of recommendations has been enlisted below, that have been developed based on the current study:

1. To better understand the longitudinal dimension of the nanofibrils, TEM or AFM (Atomic Force Microscopy) could be performed by staining with a very dilute solution of nanofibrils. The aspect ratio solely depends on chemical treatments thus performed and fibrillation through grinding. Acid treatments such as HCl gives rise to lower degree of polymerization dissolving the amorphous domains of cellulose; a regulated quantity of acid hydrolysis and its effects at different dosage should be analysed for improved properties (Tibolla et al., 2014) (Benítez and Walther, 2017). Degree of polymerization (DP) of nanocellulose fibers depend widely on chemical treatment and origin. The intrinsic viscosity of the CNF suspensions could be measured and translated onto degree of polymerization according to TAPPI T 230 (Mazumder et al., 2000).
2. Bio-degradability test can be done to find the biodegradation rate over a period of time by inserting the nanopapers in a fixed quantity of soil and maintaining the relative humidity constantly, over a period of time. (Celano et al., 2016)
3. Porosity or total volume fraction of pores on nanopapers can be well measured by performing BET (Brunauer−Emmett−Teller) experiment by N_2 absorption, this would help delve deeper into the morphological characteristics to identify the variation in porosity with temperature. The lower the porosity of nanopaper, higher its mechanical strength (Sehaqui et al., 2011).
4. It would be interesting to oxidise hemp fibers through TEMPO (2,2,6,6-tetramethylpiperidine-N-oxyl) as it introduces carbonyl (C=O) and carboxyl (COOH) on cellulose nanofibers to improve delamination. These groups being more polar than hydroxyl (OH) groups would form a more transparent suspension with polar solvents and produce nanopapers with higher transparency. (Nechyporchuk et al., 2016).
5. Tuning the loading density of silver nanowires, their percolation threshold can be optimised and exactly calculated. This controls material usage by preventing waste. Adding higher density (mg/cm^3) of silver might compromise its mechanical flexibility.

References

Ahankari, S.S., Subhedar, A.R., Bhadauria, S.S., Dufresne, A., 2021. Nanocellulose in food packaging: A review. Carbohydr. Polym. 255, 117479-117483 https://doi.org/10.1016/j.carbpol.2020.117479

Andrzejewska, E., 2001. Photopolymerization kinetics of multifunctional monomers. Prog. Polym. Sci. 26, 605–665. https://doi.org/10.1016/S0079-6700(01)00004-1

Aulin, C., Gällstedt, M., Lindström, T., 2010. Oxygen and oil barrier properties of micro fibrillated cellulose films and coatings. Cellulose 17, 559–574. https://doi.org/10.1007/s10570-009-9393-y

Barr, M.C., Rowehl, J.A., Lunt, R.R., Xu, J., Wang, A., Boyce, C.M., Im, S.G., Bulović, V., Gleason, K.K., 2011. Direct monolithic integration of organic photovoltaic circuits on unmodified paper. Adv. Mater. 23, 3500–3505. https://doi.org/10.1002/adma.201101263

Benítez, A.J., Walther, A., 2017. Cellulose nanofibril nanopapers and bioinspired nanocomposites: a review to understand the mechanical property space. J. Mater. Chem. A 5, 16003–16024. https://doi.org/10.1039/C7TA02006F

Bhatnagar, A., Sain, M., 2005. Processing of cellulose nanofiber-reinforced composites. J. Reinf. Plast. Compos. 24, 1259–1268. https://doi.org/10.1177/0731684405049864

Celano, U., Nagashima, K., Koga, H., Nogi, M., Zhuge, F., Meng, G., He, Y., De Boeck, J., Jurczak, M., Vandervorst, W., Yanagida, T., 2016. All-nanocellulose nonvolatile resistive memory. NPG Asia Materials 8, e310–e310. https://doi.org/10.1038/am.2016.144

Stanley O., Esther I., 2017. Characterization of sulphated cellulose nanocrystals as stabilizer for magnetite nanoparticles synthesis with improved magnetic properties., Nigerian Journal of Materials Science and Technology (NJMSE), Vol. 7:21-30.

Chen, Z., 2001. A mechanical assessment of flexible optoelectronic devices. Thin Solid Films 394, 201–205. https://doi.org/10.1016/S0040-6090(01)01138-5

De Amorim, J.D.P., De Souza, K.C., Duarte, C.R., Da Silva Duarte, I., De Assis Sales Ribeiro, F., Silva, G.S., De Farias, P.M.A., Stingl, A., Costa, A.F.S., Vinhas, G.M., Sarubbo, L.A., 2020. Plant and bacterial nanocellulose: production, properties and applications in medicine, food,

cosmetics, electronics, and engineering. A review. Environ. Chem. Lett. 18, 851–869. https://doi.org/10.1007/s10311-020-00989-9
De Nooy, A.E.J., Besemer, A.C., Van Bekkum, H., 1995. Selective oxidation of primary alcohols mediated by nitroxyl radical in aqueous solution. Kinetics and mechanism. Tetrahedron 51, 8023–8032. https://doi.org/10.1016/0040-4020(95)00417-7
De, S., Higgins, T.M., Lyons, P.E., Doherty, E.M., Nirmalraj, P.N., Blau, W.J., Boland, J.J., Coleman, J.N., 2009. Silver Nanowire networks as flexible, transparent, conducting films: Extremely high DC to optical conductivity ratios. ACS Nano 3, 1767–1774. https://doi.org/10.1021/nn900348c
Dias, O.A.T., Konar, S., Leão, A.L., Yang, W., Tjong, J., Sain, M., 2020. Current state of applications of nanocellulose in flexible energy and electronic devices. Front. Chem. 8, 420. https://doi.org/10.3389/fchem.2020.00420
Dinesh, G., Kandasubramanian, B., 2022. Fabrication of transparent paper devices from nanocellulose fiber. Mater. Chem. Phys. 281, 125707. https://doi.org/10.1016/j.matchemphys.2022.125707
Dong, X.M, Revol, D.G., Effect of microcrystallite preparation conditions on the formation of colloid crystals of cellulose. Cellulose 5, 19–32 (1998). https://doi.org/10.1023/A:1009260511939
Dorris, A., Gray, D.G., 2012. Gelation of cellulose nanocrystal suspensions in glycerol. Cellulose 19, 687–694. https://doi.org/10.1007/s10570-012-9679-3
Du, L., Yu, H., Zhang, B., Tang, R., Zhang, Y., Qi, C., Wolcott, M.P., Yu, Z., Wang, J., 2021. Transparent oxygen barrier nanocellulose composite films with a sandwich structure. Carbohydr. Polym. 268, 118206. https://doi.org/10.1016/j.carbpol.2021.118206
Dufresne, A., 2013. Nanocellulose: a new ageless bionanomaterial. Mater. Today 16, 220–227. https://doi.org/10.1016/j.mattod.2013.06.004
Fang, Z., Zhu, H., Preston, C., Hu, L., 2014. Development, application and commercialization of transparent paper. Transl. Mater. Res. 1, 015004. https://doi.org/10.1088/2053-1613/1/1/015004
Fernandes Diniz, J.M.B., Gil, M.H., Castro, J.A.A.M., 2004. Hornification, its origin and interpretation in wood pulps. Wood Sci. Technol. 37, 489–494. https://doi.org/10.1007/s00226-003-0216-2

Gao, L., Chao, L., Hou, M., Liang, J., Chen, Y., Yu, H.-D., Huang, W., 2019a. Flexible, transparent nanocellulose paper-based perovskite solar cells. Npj Flex. Electron. 3, 4. https://doi.org/10.1038/s41528-019-0048-2

Ghanbarian, B., Male, F., 2021. Theoretical power-law relationship between permeability and formation factor. J. Pet. Sci. Eng. 198, 108249. https://doi.org/10.1016/j.petrol.2020.108249

Gupta, G.K., Shukla, P., 2020. Lignocellulosic Biomass for the Synthesis of Nanocellulose and its eco-friendly advanced applications. Front. Chem. 8, 601256. https://doi.org/10.3389/fchem.2020.601256

Ha, D., Fang, Z., Zhitenev, N.B., 2018. Paper in electronic and optoelectronic devices. Adv. Electron. Mater. 4, 1700593. https://doi.org/10.1002/aelm.201700593

Hisseine, O.A., Wilson, W., Sorelli, L., Tolnai, B., Tagnit-Hamou, A., 2019. Nanocellulose for improved concrete performance: A macro-to-micro investigation for disclosing the effects of cellulose filaments on strength of cement systems. Constr. Build. Mater. 206, 84–96. https://doi.org/10.1016/j.conbuildmat.2019.02.042

Hsieh, M.-C., Kim, C., Nogi, M., Suganuma, K., 2013. Electrically conductive lines on cellulose nanopaper for flexible electrical devices. Nanoscale 5, 9289-9294. https://doi.org/10.1039/c3nr01951a

Hu, L., Zheng, G., Yao, J., Liu, N., Weil, B., Eskilsson, M., Karabulut, E., Ruan, Z., Fan, S., Bloking, J.T., McGehee, M.D., Wågberg, L., Cui, Y., 2013. Transparent and conductive paper from nanocellulose fibers. Energy Env. Sci 6, 513–518. https://doi.org/10.1039/C2EE23635D

Irimia-Vladu, M., Głowacki, Eric.D., Voss, G., Bauer, S., Sariciftci, N.S., 2012. Green and biodegradable electronics. Mater. Today 15, 340–346. https://doi.org/10.1016/S1369-7021(12)70139-6

Isobe, N., Kasuga, T., Nogi, M., 2018. Clear transparent cellulose nanopaper prepared from a concentrated dispersion by high humidity drying. RSC Adv. 8, 1833–1837. https://doi.org/10.1039/C7RA12672G

Jain, N., Singh, V.K., Chauhan, S., 2017. A review on mechanical and water absorption properties of polyvinyl alcohol-based composites/films. J. Mech. Behav. Mater. 26, 213–222. https://doi.org/10.1515/jmbm-2017-0027

Jamaluddin, N., Hsu, Y.-I., Asoh, T.-A., Uyama, H., 2021. Optically transparent and toughened poly (methyl methacrylate) composite films with acylated cellulose nanofibers. ACS Omega 6, 10752–10758. https://doi.org/10.1021/acsomega.1c00325

Kafy, A., Kim, H.C., Zhai, L., Kim, J.W., Hai, L.V., Kang, T.J., Kim, J., 2017a. Cellulose long fibers fabricated from cellulose nanofibers and its strong and tough characteristics. Sci. Rep. 7, 17683. https://doi.org/10.1038/s41598-017-17713-3

Kafy, A., Kim, H.C., Zhai, L., Kim, J.W., Hai, L.V., Kang, T.J., Kim, J., 2017b. Cellulose long fibers fabricated from cellulose nanofibers and its strong and tough characteristics. Sci. Rep. 7, 17683. https://doi.org/10.1038/s41598-017-17713-3

Keiser, G., 2021. Fiber Optic Communications. Springer Singapore, Singapore. https://doi.org/10.1007/978-981-33-4665-9

Kim, T., Kim, Y.W., Lee, H.S., Kim, H., Yang, W.S., Suh, K.S., 2013. Uniformly interconnected silver-nanowire networks for transparent film heaters. Adv. Funct. Mater. 23, 1250–1255. https://doi.org/10.1002/adfm.201202013

Koga, H., Nogi, M., Komoda, N., Nge, T.T., Sugahara, T., Suganuma, K., 2014. Uniformly connected conductive networks on cellulose nanofiber paper for transparent paper electronics. NPG Asia Mater. 6, e93–e93. https://doi.org/10.1038/am.2014.9

Koga, H., Saito, T., Kitaoka, T., Nogi, M., Suganuma, K., Isogai, A., 2013. Transparent, conductive, and printable composites consisting of TEMPO-oxidized nanocellulose and carbon nanotube. Biomacromolecules 14, 1160–1165. https://doi.org/10.1021/bm400075f

Kulachenko, A., Denoyelle, T., Galland, S., Lindström, S.B., 2012. Elastic properties of cellulose nanopaper. Cellulose 19, 793–807. https://doi.org/10.1007/s10570-012-9685-5

Lee, K.-Y., Quero, F., Blaker, J.J., Hill, C.A.S., Eichhorn, S.J., Bismarck, A., 2011. Surface only modification of bacterial cellulose nanofibres with organic acids. Cellulose 18, 595–605. https://doi.org/10.1007/s10570-011-9525-z

Li, C., Kasuga, T., Uetani, K., Koga, H., Nogi, M., 2020. High-speed fabrication of clear transparent cellulose nanopaper by applying humidity-controlled multi-stage drying method. Nanomaterials 10, 2194. https://doi.org/10.3390/nano10112194

Li, J., Long, Y., Yang, F., Wei, H., Zhang, Z., Wang, Y., Wang, J., Li, C., Carlos, C., Dong, Y., Wu, Y., Cai, W., Wang, X., 2020. Multifunctional artificial artery from direct 3D printing with

built-in ferroelectricity and tissue-matching modulus for real-time sensing and occlusion monitoring. Adv. Funct. Mater. 30, 2002868-2002873. https://doi.org/10.1002/adfm.202002868
Li, L., Lee, S., Lee, H.L., Youn, H.J., 2011. Hydrogen peroxide bleaching of hardwood kraft pulp with adsorbed birch xylan and its effect on paper properties. BioResources 6, 721–736. https://doi.org/10.15376/biores.6.1.721-736
Liao, R., Wang, J., Gao, F., Yuan, Y., Xu, Z., 2016. Effects of aluminum nitride nanoparticles on the space charge behavior of cellulose paper. J. Mater. Sci. 51, 10701–10713. https://doi.org/10.1007/s10853-016-0196-x
Liu, K., Liu, W., Li, W., Duan, Y., Zhou, K., Zhang, S., Ni, S., Xu, T., Du, H., Si, C., 2022a. Strong and highly conductive cellulose nanofibril/silver nanowires nanopaper for high performance electromagnetic interference shielding. Adv. Compos. Hybrid Mater. 5, 1078–1089. https://doi.org/10.1007/s42114-022-00425-2
Liu, M., Thygesen, A., Summerscales, J., Meyer, A.S., 2017a. Targeted pre-treatment of hemp bast fibres for optimal performance in biocomposite materials: A review. Ind. Crops Prod. 108, 660–683. https://doi.org/10.1016/j.indcrop.2017.07.027
Mascheroni, E., Rampazzo, R., Ortenzi, M.A., Piva, G., Bonetti, S., Piergiovanni, L., 2016. Comparison of cellulose nanocrystals obtained by sulfuric acid hydrolysis and ammonium persulfate, to be used as coating on flexible food-packaging materials. Cellulose 23, 779–793. https://doi.org/10.1007/s10570-015-0853-2
Masłowski, M., Miedzianowska, J., Strzelec, K., 2018. Influence of peroxide modifications on the properties of cereal straw and natural rubber composites. Cellulose 25, 4711–4728. https://doi.org/10.1007/s10570-018-1880-6
Mattos, B.D., Tardy, B.L., Rojas, O.J., 2019. Accounting for substrate interactions in the measurement of the dimensions of cellulose nanofibrils. Biomacromolecules 20, 2657–2665. https://doi.org/10.1021/acs.biomac.9b00432
Mazumder, B.B., Ohtani, Y., Cheng, Z., Sameshima, K., 2000. Combination treatment of kenaf bast fiber for high viscosity pulp. J. Wood Sci. 46, 364–370. https://doi.org/10.1007/BF00776397
Meng, Q., Wang, T.J., 2019a. Mechanics of strong and tough cellulose nanopaper. Appl. Mech. Rev. 71, 040801-040808. https://doi.org/10.1115/1.4044018

Mercadante, M.A., Kelly, C.B., Bobbitt, J.M., Tilley, L.J., Leadbeater, N.E., 2013. Synthesis of 4-acetamido-2,2,6,6-tetramethylpiperidine-1-oxoammonium tetrafluoroborate and 4-acetamido-(2,2,6,6-tetramethyl-piperidin-1-yl)oxyl and their use in oxidative reactions. Nat. Protoc. 8, 666–676. https://doi.org/10.1038/nprot.2013.028

Ming Liu, PhD Thesis, 2018. Technical University of Denmark, Denmark

Mohammed, M.A., Basirun, W.J., Rahman, N.M.M.A., Salleh, N.M., 2021. Electrochemical applications of nanocellulose, in: Nanocellulose based composites for electronics. Elsevier, pp.313–335. https://doi.org/10.1016/B978-0-12-822350-5.00013-8

Moon, R.J., Hensdal, C.L., Beck, S., Fall, A., Costa, J., Kojima, E., Abitbol, T., Raghuwanshi, V., Walker, C., Batchelor, W., 2023. Setting priorities in CNF particle size measurement: What is needed vs. what is feasible. TAPPI J. 22, 116–137. https://doi.org/10.32964/TJ22.2.116

Moon, R.J., Martini, A., Nairn, J., Simonsen, J., Youngblood, J., 2011. Cellulose nanomaterials review: structure, properties and nanocomposites. Chem. Soc. Rev. 40, 3941. https://doi.org/10.1039/c0cs00108b

Mussatto, S.I., Rocha, G.J.M., Roberto, I.C., 2008. Hydrogen peroxide bleaching of cellulose pulps obtained from brewer's spent grain. Cellulose 15, 641–649. https://doi.org/10.1007/s10570-008-9198-4

Nasir, M., Hashim, R., Sulaiman, O., Asim, M., 2017. Nanocellulose, in: Cellulose-reinforced nanofibre composites. Elsevier, pp. 261–276. https://doi.org/10.1016/B978-0-08-100957-4.00011-5

Nechyporchuk, O., Belgacem, M.N., Bras, J., 2016. Production of cellulose nanofibrils: A review of recent advances. Ind. Crops Prod. 93, 2–25. https://doi.org/10.1016/j.indcrop.2016.02.016

Nguyen, T.H.L., Quiroga Cortes, L., Lonjon, A., Dantras, E., Lacabanne, C., 2014. High conductive Ag nanowire–polyimide composites: Charge transport mechanism in thermoplastic thermostable materials. J. non-cryst. Solids 385, 34–39. https://doi.org/10.1016/j.jnoncrysol.2013.11.008

Niskanen, I., Zhang, K., Karzarjeddi, M., Liimatainen, H., Shibata, S., Hagen, N., Heikkilä, R., Yoda, H., Otani, Y., 2022c. Optical properties of cellulose nanofibre films at high temperatures. J. Polym. Res. 29, 187. https://doi.org/10.1007/s10965-022-03019-0

Nogi, M., Iwamoto, S., Nakagaito, A.N., Yano, H., 2009a. Optically transparent nanofiber paper.

Adv. Mater. 21, 1595–1598. https://doi.org/10.1002/adma.200803174
Oliaei, E., Lindén, P.A., Wu, Q., Berthold, F., Berglund, L., Lindström, T., 2020. Microfibrillated lignocellulose (MFLC) and nanopaper films from unbleached kraft softwood pulp. Cellulose 27, 2325–2341. https://doi.org/10.1007/s10570-019-02934-8
Pääkkö, M., Ankerfors, M., Kosonen, H., Nykänen, A., Ahola, S., Österberg, M., Ruokolainen, J., Laine, J., Larsson, P.T., Ikkala, O., Lindström, T., 2007. Enzymatic hydrolysis combined with mechanical shearing and high-pressure homogenization for nanoscale cellulose fibrils and strong gels. Biomacromolecules 8, 1934–1941. https://doi.org/10.1021/bm061215p
Pacheco, G., De Mello, C.V., Chiari-Andréo, B.G., Isaac, V.L.B., Ribeiro, S.J.L., Pecoraro, É., Trovatti, E., 2018. Bacterial cellulose skin masks—Properties and sensory tests. J. Cosmet. Dermatol. 17, 840–847. https://doi.org/10.1111/jocd.12441
Peng, Y., Gardner, D.J., Han, Y., 2012. Drying cellulose nanofibrils: in search of a suitable method. Cellulose 19, 91–102. https://doi.org/10.1007/s10570-011-9630-z
Plotnikoff, R.C., Wright, M.-F., Karunamuni, N., 2004. Knowledge, attitudes, and behaviours related to climate change in Alberta, Canada: implications for public health policy and practice. Int. J. Environ. Health Res. 14, 223–229. https://doi.org/10.1080/0960312042000218633
Preston, C., Fang, Z., Murray, J., Zhu, H., Dai, J., Munday, J.N., Hu, L., 2014a. Silver nanowire transparent conducting paper-based electrode with high optical haze. J Mater Chem C 2, 1248–1254. https://doi.org/10.1039/C3TC31726A
Quero, F., 2018. Applications of nanocellulose as optically transparent papers and composites, in: Lee, K.-Y. (Ed.), Nanocellulose and Sustainability. CRC Press, Boca Raton: CRC Press, [2018] | Series: Sustainability contributions through science and technology, pp. 147–173. https://doi.org/10.1201/9781351262927-8
Ranalli, P., Venturi, G., 2004. Hemp as a raw material for industrial applications. Euphytica 140, 1–6. https://doi.org/10.1007/s10681-004-4749-8
Redondo, A., Mortensen, N., Djeghdi, K., Jang, D., Ortuso, R.D., Weder, C., Korley, L.T.J., Steiner, U., Gunkel, I., 2022. Comparing percolation and alignment of cellulose nanocrystals for the reinforcement of polyurethane nanocomposites. ACS Appl. Mater. Interfaces 14, 7270–7282. https://doi.org/10.1021/acsami.1c21656
Revol, J.-F., Bradford, H., Giasson, J., Marchessault, R.H., Gray, D.G., 1992. Helicoidal self-ordering of cellulose microfibrils in aqueous suspension. Int. J. Biol. Macromol. 14, 170–172. https://doi.org/10.1016/S0141-8130(05)80008-X

Roy, S., Ghosh, B.D., Goh, K.L., Muthoka, R.M., Kim, J., 2022. Modulation of interfacial interactions toward strong and tough cellulose nanofiber-based transparent thin films with anti-fogging feature. Carbohydr.Polym.278, 118974. https://doi.org/10.1016/j.carbpol.2021.118974

Rubentheren, V., Ward, T.A., Chee, C.Y., Nair, P., Salami, E., Fearday, C., 2016. Effects of heat treatment on chitosan nanocomposite film reinforced with nanocrystalline cellulose and tannic acid. Carbohydr. Polym. 140, 202–208. https://doi.org/10.1016/j.carbpol.2015.12.068

Sehaqui, H., Liu, A., Zhou, Q., Berglund, L.A., 2010. Fast preparation procedure for large, flat cellulose and cellulose/inorganic nanopaper structures. Biomacromolecules 11, 2195–2198. https://doi.org/10.1021/bm100490s

Shen, H., Peng, S., Luo, Q., Zhou, J., He, J., Zhou, G., Xu, X., 2023. Nanopaper electronics. Adv. Funct. Mater. 33, 2213820-2213825. https://doi.org/10.1002/adfm.202213820

Silva, F.A.G.S., Dourado, F., Gama, M., Poças, F., 2020. Nanocellulose bio-based composites for food packaging. Nanomaterials 10, 2041. https://doi.org/10.3390/nano10102041

Sinquefield, S., Ciesielski, P.N., Li, K., Gardner, D.J., Ozcan, S., 2020a. Nanocellulose dewatering and drying: Current state and future perspectives. ACS Sustain. Chem. Eng. 8, 9601– 9615. https://doi.org/10.1021/acssuschemeng.0c01797

Solhi, L., Guccini, V., Heise, K., Solala, I., Niinivaara, E., Xu, W., Mihhels, K., Kröger, M., Meng, Z., Wohlert, J., Tao, H., Cranston, E.D., Kontturi, E., 2023. Understanding nanocellulose– water interactions: turning a detriment into an Asset. Chem. Rev. 123, 1925–2015. https://doi.org/10.1021/acs.chemrev.2c00611

Song, X., Yang, S., Liu, X., Wu, M., Li, Y., Wang, S., 2018. Transparent and water-resistant composites prepared from acrylic resins ABPE-10 and acetylated nano-fibrillated cellulose as flexible organic light-emitting device substrate. Nanomaterials 8, 648-653. https://doi.org/10.3390/nano8090648

Song, Y., Jiang, Y., Shi, L., Cao, S., Feng, X., Miao, M., Fang, J., 2015. Solution-processed assembly of ultrathin transparent conductive cellulose nanopaper embedding AgNWs. Nanoscale 7, 13694–13701. https://doi.org/10.1039/C5NR03218K

Spence, K.L., Venditti, R.A., Rojas, O.J., Habibi, Y., Pawlak, J.J., 2011. A comparative study of energy consumption and physical properties of microfibrillated cellulose produced by different processing methods. Cellulose 18, 1097–1111. https://doi.org/10.1007/s10570-011-9533-z

Stamatelatou, K., Antonopoulou, G., Michailides, P., 2014. Biomethane and biohydrogen production via anaerobic digestion/fermentation, in: Advances in biorefineries. Elsevier, pp. 476–524. https://doi.org/10.1533/9780857097385.2.476

Stelte, W., Sanadi, A.R., 2009. Preparation and characterization of cellulose nanofibers from two commercial hardwood and softwood pulps. Ind. Eng. Chem. Res. 48, 11211–11219. https://doi.org/10.1021/ie9011672

Sulaiman, S., Mokhtar, M.N., Naim, M.N., Baharuddin, A.S., Mohd Salleh, M.A., Sulaiman, A., 2016. Development of cellulose nanofiber (CNF) derived from kenaf bast fiber and it's potential in enzyme immobilisation. Malays. J. Anal. Sci. 20, 309–317. https://doi.org/10.17576/mjas- 2016-2002-12

Tangnu, S.K., 1982. Process development for ethanol production based on enzymatic hydrolysis of cellulosic biomass, 36-49.

Taniguchi, T., Okamura, K., 1998. New films produced from microfibrillated natural fibres. Polym. Int. 47, 291–294. https://doi.org/10.1002/(SICI)1097-0126(199811)47:3<291:AID-PI11>3.0.CO;2-1

Tao, T., Liu, X., Islam, A., Wu, J., Ni, Y., Huang, L., Chen, L., Ouyang, X., Li, J., 2020. Flexible and conductive cellulose substrate by layered growth of silver nanowires and indium-doped tin oxide. BioResources 15, 4699–4710. https://doi.org/10.15376/biores.15.3.4699-4710

Tibolla, H., Pelissari, F.M., Menegalli, F.C., 2014. Cellulose nanofibers produced from banana peel by chemical and enzymatic treatment. LWT - Food Sci. Technol. 59, 1311–1318. https://doi.org/10.1016/j.lwt.2014.04.011

Tobjörk, D., Österbacka, R., 2011. Paper electronics. Adv. Mater. 23, 1935–1961. https://doi.org/10.1002/adma.201004692

Tomé, L.C., Freire, M.G., Rebelo, L.P.N., Silvestre, A.J.D., Neto, C.P., Marrucho, I.M., Freire, C.S.R., 2011. Surface hydrophobization of bacterial and vegetable cellulose fibers using ionic liquids as solvent media and catalysts. Green Chem. 13, 2464. https://doi.org/10.1039/c1gc15432j

Trache, D., Hussin, M.H., Haafiz, M.K.M., Thakur, V.K., 2017. Recent progress in cellulose nanocrystals: sources and production. Nanoscale 9, 1763–1786. https://doi.org/10.1039/C6NR09494E

Turbak, A.F., Snyder, F.W., 1981. US4374702A, Micro-fibrillated cellulose (Patent)

Walter B., Gallatin J., 1959. US3041246A, Enzymatic conversion of cellulosic fibers. Takashi K., Masahiro A., 1979. US4137046 (A),Transparent cellulosic paper making. Van De Groep, J., Spinelli, P., Polman, A., 2012. Transparent conducting silver nanowire networks. Nano Lett. 12, 3138–3144. https://doi.org/10.1021/nl301045a

Vartiainen, J., Vähä-Nissi, M., Harlin, A., 2014. Biopolymer films and coatings in packaging applications—A Review of Recent Developments. Mater. Sci. Appl. 05, 708–718. https://doi.org/10.4236/msa.2014.510072

Wang, B., Sain, M., 2007. Isolation of nanofibers from soybean source and their reinforcing capability on synthetic polymers. Compos. Sci. Technol. 67, 2521–2527. https://doi.org/10.1016/j.compscitech.2006.12.015

Wang, H., Li, D., Zhang, R., 2013. Preparation of ultralong cellulose nanofibers and optically transparent nanopapers derived from waste corrugated paper pulp. BioResources 8, 1374–1384. https://doi.org/10.15376/biores.8.1.1374-1384

Wang, M., Miao, X., Li, H., Chen, C., 2021. Effect of length of cellulose nanofibers on mechanical reinforcement of polyvinyl alcohol. Polymers 14, 128-135. https://doi.org/10.3390/polym14010128

Wang, X., Yao, C., Wang, F., Li, Z., 2017. Cellulose-based nanomaterials for energy applications. Small 13, 1702240. https://doi.org/10.1002/smll.201702240

Wetterling, J., Jonsson, S., Mattsson, T., Theliander, H., 2017. The influence of ionic strength on the electro assisted filtration of microcrystalline cellulose. Ind. Eng. Chem. Res. 56, 12789–12798. https://doi.org/10.1021/acs.iecr.7b03575

Wu, Q., Meng, Y., Concha, K., Wang, S., Li, Y., Ma, L., Fu, S., 2013. Influence of temperature and humidity on nano-mechanical properties of cellulose nanocrystal films made from switchgrass and cotton. Ind. Crops Prod. 48, 28–35. https://doi.org/10.1016/j.indcrop.2013.03.032

Wu, Y., Tang, Q., Yang, F., Xu, L., Wang, X., Zhang, J., 2019. Mechanical and thermal properties of rice straw cellulose nanofibrils-enhanced polyvinyl alcohol films using freezing-and-thawing cycle method. Cellulose 26,3193–3204.https://doi.org/10.1007/s10570-019-02310-6 Wulandari, W.T., Rochliadi, A., Arcana, I.M., 2016. Nanocellulose prepared by acid hydrolysis of isolated cellulose from sugarcane bagasse. IOP Conf. Ser. Mater. Sci. Eng. 107, 012045. https://doi.org/10.1088/1757-899X/107/1/012045

Yildirim, N., Shaler, S., 2017. A Study on thermal and nanomechanical performance of cellulose nanomaterials (CNs). Materials 10, 718-728. https://doi.org/10.3390/ma10070718

Zeng, J., Zeng, Z., Cheng, Z., Wang, Y., Wang, X., Wang, B., Gao, W., 2021. Cellulose nanofibrils manufactured by various methods with application as paper strength additives. Sci. Rep. 11, 11918-11925. https://doi.org/10.1038/s41598-021-91420-y

Zhu, H., Parvinian, S., Preston, C., Vaaland, O., Ruan, Z., Hu, L., 2013. Transparent nanopaper with tailored optical properties. Nanoscale 5, 3787-3799. https://doi.org/10.1039/c3nr00520h Zimmermann, T., Pöhler, E., Geiger, T., 2004. Cellulose fibrils for polymer reinforcement. Adv. Eng. Mater. 6, 754–761. https://doi.org/10.1002/adem.200400097

Zuo, X., Chang, K., Zhao, J., Xie, Z., Tang, H., Li, B., Chang, Z., 2016. Bubble-template-assisted synthesis of hollow fullerene-like MoS 2 nanocages as a lithium-ion battery anode material. J. Mater. Chem. A 4, 51–58. https://doi.org/10.1039/C5TA06869J

Deepalakshmi P., Neethu N., Sabu T., 2018. Carbon nanotube filled polymer composites, Ch13, 391-414, https://doi.org/10.1016/B978-0-08-101971-9.00014-4

Liu H., and Li H., 2017. Application and conversion of soybean hulls. Soybean - The basis of yield, Biomass and Productivity. InTech. doi-10.5772/66744.

ASTM Standards Used:

ASTM D882-12 - Standard Test Method for Tensile Properties of Thin Plastic Sheeting

ASTM E168, 1252- Fourier Transform Infrared Spectrometry ASTM E168, ASTM E1252

ASTM D5946 – Standard Test for Water Contact Angle for Polymer Films

ASTM D1003- Standard Test for Haze and Luminous Transmittance

Appendix A – Letter of Copyright Permission

1.1) Open Access

Front. Chem., 21 May 2020
Sec. Green and Sustainable Chemistry
Volume 8 - 2020 |
https://doi.org/10.3389/fchem.2020.00420

This article is part of the Research Topic
Recent Trends in Preparation, Characterization and Applications of Nanocellulose
View all 7 Articles >

Current State of Applications of Nanocellulose in Flexible Energy and Electronic Devices

Otavio Augusto Titton Dias[1*] Samir Konar[1,2] Alcides Lopes Leão[3] Weimin Yang[4]
Jimi Tjong[1,2] Mohini Sain[1,2]

[1] Centre for Biocomposites and Biomaterials Processing, University of Toronto, Toronto, ON, Canada
[2] Department of Mechanical and Industrial Engineering, University of Toronto, Toronto, ON, Canada
[3] College of Agricultural Sciences, São Paulo State University (Unesp), São Paulo, Brazil
[4] College of Mechanical and Electrical Engineering, Beijing University of Chemical Technology, Beijing, China

Received: 02 February 2020; **Accepted:** 21 April 2020;
Published: 21 May 2020.

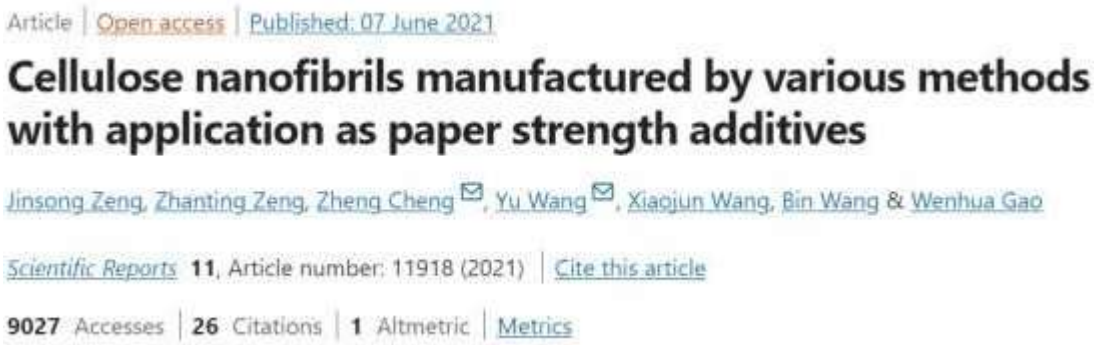
Edited by:
Djalal Trache, Ecole Militaire Polytechnique (EMP), Algeria

Reviewed by:
Gustav Nyström, Swiss Federal Laboratories for Materials Science and Technology, Switzerland
Dieter O. Klemm, Friedrich Schiller University Jena, Germany
Robin Zuluaga Gallego, Pontifical Bolivarian University, Colombia

Copyright © 2020 Dias, Konar, Leão, Yang, Tjong and Sain. This is an open-access article distributed under the terms of the Creative Commons Attribution License (CC BY). The use, distribution or reproduction in other forums is permitted, provided the original author(s) and the copyright owner(s) are credited and that the original publication in this journal is cited, in accordance with accepted academic practice. No use, distribution or reproduction is permitted which does not comply with these terms.

***Correspondence:** Otavio Augusto Titton Dias, otavio.dias@mail.utoronto.ca

1.2) Open Access



Article | Open access | Published: 07 June 2021

Cellulose nanofibrils manufactured by various methods with application as paper strength additives

Jinsong Zeng, Zhanting Zeng, Zheng Cheng ✉, Yu Wang ✉, Xiaojun Wang, Bin Wang & Wenhua Gao

Scientific Reports **11**, Article number: 11918 (2021) | Cite this article

9027 Accesses | **26** Citations | **1** Altmetric | Metrics

1.3) Open Access



Nanocellulose Market Research 2020-2024 | Industry Planning Structure for the New Normal | Technavio

Shape strategic responses through the phases of industry recovery

American Process International LLC, CelluComp Ltd., and Celluforce will emerge as major nanocellulose market participants during 2020-2024

1.4) Open Access



1.5) Open Access



Study of the properties of biomedical materials based on cellulose mesylates

Magomed Akhmedov [1,*], Shagabudin Khidirov[2], Saida Alimova[2], and Amina Akhmedova[2]

[1] Dagestan Federal Research Center RAS, Russia, Republic of Dagestan, Makhachkala, st. M.Gadzhieva, 45;
[2] FSBEI HE Dagestan State University, Russia, Republic of Dagestan, Makhachkala, st. M.Gadzhieva, 43-A.

1.6) Open Access

OPEN ACCESS PEER-REVIEWED CHAPTER

Cellulose Grafting by Atom Transfer Radical Polymerization Method

WRITTEN BY

Nevin Çankaya

Submitted: 17 February 2015 , Reviewed: 07 October 2015 , Published: 09 December 2015

DOI: 10.5772/61707

1.7) Open Access



1.8) Open Access



1.9) Open Access

Article | Full-text available

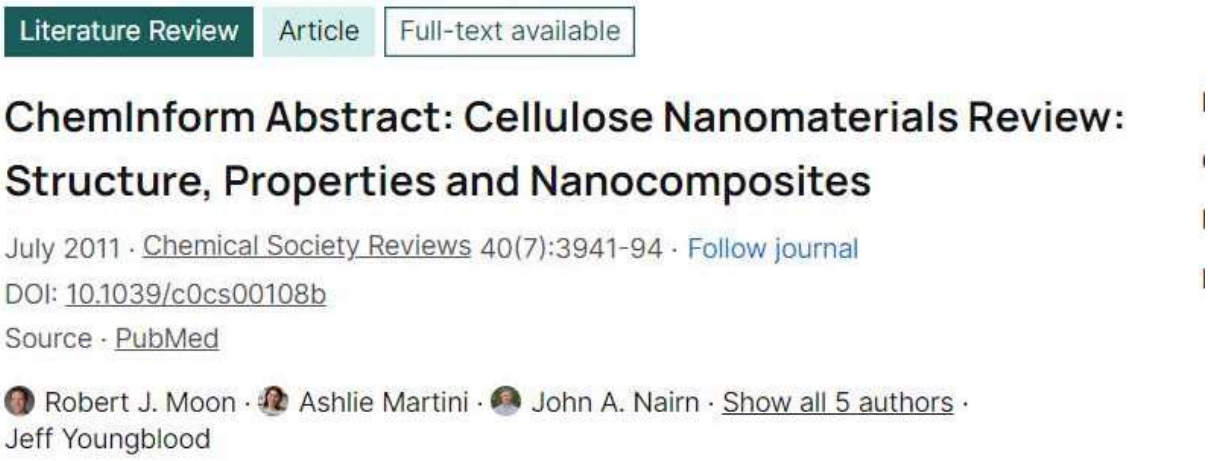
Cellulose nanofibril nanopapers and bioinspired nanocomposites: A review to understand the mechanical property space

April 2017 · Journal of Materials Chemistry A 5(31):16003-16024 · Follow journal
DOI: 10.1039/C7TA02006F

Lab: Walther Lab

Alejandro J Benitez · Andreas Walther

2.0) Open Access



2.1) Open Access


Article Full-text available

Processing nanocellulose to bulk materials: a review

September 2019 · Cellulose 26(13-14) · Follow journal

DOI: 10.1007/s10570-019-02642-3

Qianqian Wang · Qian Yao · Jun Liu · Show all 6 authors · Honglei Chen

2.2) Permission taken from Elsevier Licenses

ELSEVIER LICENSE TERMS AND CONDITIONS Oct 13, 2023

This Agreement between University of Waterloo, Canada -- Rajeswari Sen ("You") and Elsevier ("Elsevier") consists of your license details and the terms and conditions provided by Elsevier and Copyright Clearance Center.

License Number 5647110321563

License date Oct 13, 2023

Licensed Content Publisher Elsevier

Licensed Content Publication Carbohydrate Polymers

Licensed Content Title Nanocellulose in food packaging: A review

Licensed Content Author Sandeep S. Ahankari, Aditya R. Subhedar, Swarnim S. Bhadauria, Alain Dufresne

Licensed Content Date Mar 1, 2021

Licensed Content Volume 255

Licensed Content Issue n/a

Licensed Content Pages 1

Start Page 117479

End Page 0

Type of Use reuse in a thesis/dissertation

Portion figures/tables/illustrations

Number of

figures/tables/illustrations 1

Format electronic

Are you the author of this Elsevier article? No

Will you be translating? No

Title Fabrication of Transparent Nanopaper from Plant Sources for Energy Devices

Institution name University of Waterloo, Canada

Expected presentation date Dec 2023

Portions Fig. 2. Diagram showing the increase in diffusion path of the permeating molecule due to the presence of NC on Page 3

University of Waterloo, Canada

201 Erb Street West

A-5, Erb Court Apartments

Requestor Location

Waterloo, ON N2L 1V6 Canada

Attn: University of Waterloo, Canada

Publisher Tax ID GB 494 6272 12

Total 0.00 CAD

2.3) Open Access



Appendix B- Material Specification Sheet

1.1.) Freeze dried CNF specification sheet.

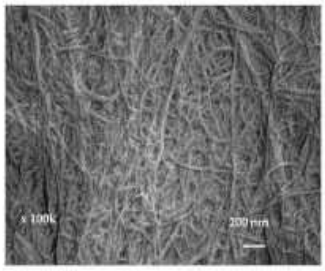
1865 THE UNIVERSITY OF MAINE
Process Development Center
5737 Jenness Hall, Orono, ME 04469

Product Specification

Material information

Name of product: **Cellulose nanofibers (CNF)**

CAS Number: 9004-34-6



Test	Specification
Appearance	White, odorless
Solids:	3.0 w% aqueous gel 98 w/% dry powder
Fiber dimensions:	nominal fiber width of 50 nm lengths of up to several hundred microns
Surface property:	Hydrophilic 31-33 m^2/g (BET)
Density:	1.0 g/cm^3 aqueous gel 1.5 g/cm^3 dry powder
Required storage conditions:	For the gel products, store under refrigeration. Do not freeze. For dry products, store in dry locale.
Expiry date:	If properly stored, > 1 year
Available Packaging: Gel (slurry) Dry	 5-gallon pails that contain 1.0 pound of product. Wide mouth plastic jars/ bags that contain 0.25 pounds of product

Name and address of original manufacturer:

Process Development Center
University of Maine
5737 Jenness Hall
Orono, ME 04469
Telephone: 207-581-2281
Fax: 207-581-4174
www.umaine.edu/pdc